UNIVERSIDADE FEDERAL DE SANTA MARIA
CENTRO DE CIÊNCIAS NATURAIS E EXATAS
PROGRAMA DE PÓS-GRADUAÇÃO EM BIODIVERSIDADE ANIMAL

Rodrigo Temp Müller

ORIGEM E IRRADIAÇÃO DOS SAUROPODOMORFOS: NOVOS ESPÉCIMES E SUAS IMPLICAÇÕES

Santa Maria, RS
2018

Rodrigo Temp Müller

ORIGEM E IRRADIAÇÃO DOS SAUROPODOMORFOS: NOVOS ESPÉCIMES E SUAS IMPLICAÇÕES

Tese de doutorado apresentado ao Programa de Pós-Graduação em Biodiversidade Animal da Universidade Federal de Santa Maria (UFSM), como requisito parcial para a obtenção do título de **Doutor em Ciências Biológicas - Área Biodiversidade Animal.**

Orientador: Dr. Sérgio Dias da Silva
Coorientador: Dr. Max Cardoso Langer

Müller, Rodrigo
Origem e irradiação dos sauropodomorfos: novos espécimes e suas implicações / Rodrigo Müller.- 2018.
180 p.; 30 cm

Orientador: Sérgio Dias da Silva
Coorientador: Max Langer
Tese (doutorado) - Universidade Federal de Santa Maria, Centro de Ciências Naturais e Exatas, Programa de Pós-Graduação em Biodiversidade Animal, RS, 2018

1. Paleontologia 2. Evolução 3. Dinossauros 4. Triássico 5. Sistemática filogenética I. Dias da Silva, Sérgio II. Langer, Max III. Título.

Sistema de geração automática de ficha catalográfica da UFSM. Dados fornecidos pelo autor(a). Sob supervisão da Direção da Divisão de Processos Técnicos da Biblioteca Central. Bibliotecária responsável Paula Schoenfeldt Patta CRB 10/1728.

Rodrigo Temp Müller

ORIGEM E IRRADIAÇÃO DOS SAUROPODOMORFOS: NOVOS ESPÉCIMES E SUAS IMPLICAÇÕES

Tese de doutorado apresentado ao Programa de Pós-Graduação em Biodiversidade Animal da Universidade Federal de Santa Maria (UFSM), como requisito parcial para a obtenção do título de **Doutor em Ciências Biológicas - Área Biodiversidade Animal.**

Aprovado em 11 de dezembro de 2018:

Sérgio Dias da Silva, Dr. (UFSM)
(Presidente/Orientador)

Jonathas de Souza Bittencourt Rodrigues, Dr. (UFMG)

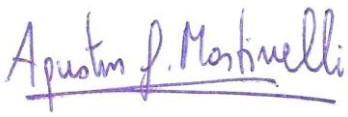

Agustin Guillermo Martinelli, Dr. (CONICET)

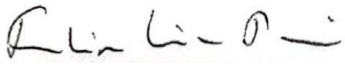

Felipe Lima Pinheiro, Dr. (UNIPAMPA)

Flávio Augusto Pretto, Dr. (UFSM)

Santa Maria, RS
2018

AGRADECIMENTOS

Não é por uma questão de conveniência que volto a agradecer meus pais, Estefânia Temp Müller e Gercides Müller. O apoio que sempre recebi de vocês para fazer o que me faz feliz é inestimável. Hoje preciso substituir as revistas com curiosidades de dinossauros que vocês me deram, por periódicos mais rigorosos, mas foram aquelas revistas à minha primeira fonte bibliográfica, antes de poder ler eu já havia me apaixonado pela forma dos dinossauros representados nelas. Obrigado! Eu também sou profundamente grato a Débora Gama de Barros, você fez as horas fora do laboratório serem muito agradáveis e foi meu refúgio sempre que precisei. Fico feliz em ver quantos nomes de dinossauros você já decorou nos últimos anos.

Agradeço ao professor Dr. Sérgio Dias da Silva pela orientação e ensinamentos, tanto durante os anos de graduação como também durante o mestrado e todo o doutorado. Também agradeço ao professor Dr. Max Cardoso Langer que tem atuado como meu co-orientador.

A descoberta dos espécimes estudados nessa tese teve influência de vários fatores. Assim, agradeço primeiramente aos proprietários dos sítios de onde os fósseis foram escavados, especialmente as famílias Wachholz e Buriol, as quais sempre nos receberam muito bem. Não posso deixar de ressaltar que a descoberta dos espécimes que compõem CAPPA/UFSM 0001 teve vários nomes envolvidos. Inicialmente os Senhores Dilo Wachholz e Olímpio Neu notaram algo incomum aflorando da rocha ao lado da casa da Família Wachholz. Os mesmos contataram as Senhoras Cladis Müller Kobs e Mariana Kobs, que foram até o local e fizeram algumas fotografias. As mesmas comunicaram aos meus pais, Estefânia Temp Müller e Gercides Müller, que por fim, enviaram-me uma fotografia de um centro vertebral caudal que estava isolado, o primeiro osso a ser descoberto de uma das mais importantes associações de fósseis de dinossauros já descobertas para o Triássico do mundo todo. São esses os nomes por trás dessa descoberta, por conta disso gostaria de deixar um agradecimento especial a cada um, talvez outra pessoa em qualquer uma das etapas dessa descoberta poderia ter deixado de lado o artefato incomum que aflorava, fazendo com que aqueles esqueletos se perdessem da história para sempre.

Lidar com formulários, papéis, datas e normas pode ser muito maçante. Por isso, gostaria de agradecer ao Secretário do PPGBA da UFSM, Senhor Sidnei Cruz, pela

Santa Maria, RS
2018

disposição e paciência em atender a todas as demandas que tive durante o período em que fui aluno do programa.

Agradeço ao Dr. César Leandro Schultz, Dr. Jonathas Bittencourt, Dr. Agustin Martinelli, Dr. Felipe Lima Pinheiro, Dr. Flávio Augusto Pretto e Dr. Leonardo Kerber por participarem como membros da banca examinadora da presente tese.

Durante os anos que passei estudando paleontologia pude conhecer mais do que esqueletos antigos, conheci várias pessoas que gostaria de manter próximas para a vida toda, colegas que compartilham tanto as mesmas dificuldades como também a paixão pelos fósseis. Portanto, sou grato aos colegas do PPGBA, aos membros do CAPPA/UFSM e do Laboratório de Palebiodiversidade Triássica da UFSM, e também aos conhecidos de outros laboratórios de paleontologia. Às vezes as coisas não podem ser resolvidas com adição de caracteres ou implementação de pesagem.

Os artigos publicados durante o doutorado foram avaliados por pesquisadores que desempenharam um ótimo papel como revisores. Assim, agradeço ao Dr. Diego Pol, Dr. Fernando Novas, Dr. Matthew Baron, Dr. Volkan Sarıgül e aqueles que exerceram o papel de revisores anonimamente. Também estendo meus agradecimentos aos editores dos periódicos *Acta Palaeontologica Polonica*, *Historical Biology*, *Zoological Journal of the Linnean Society*, *Journal of South American Earth Sciences* e *Biology Letters*, onde os manuscritos foram publicados.

Por fim, agradeço a Coordenação de Aperfeiçoamento de Pessoal de Nível Superior (CAPES) pela bolsa de estudos que recebi durante parte do doutorado.

Santa Maria, RS
2018

RESUMO

ORIGEM E IRRADIAÇÃO DOS SAUROPODOMORFOS: NOVOS ESPÉCIMES E SUAS IMPLICAÇÕES

AUTOR: Rodrigo Temp Müller
ORIENTADOR: Sérgio Dias da Silva
COORIENTADOR: Max Cardoso Langer

A origem e a irradiação inicial dos dinossauros sauropodomorfos tem recebido bastante atenção em virtude de novas descobertas realizadas em estratos fossilíferos da América do Sul. Porém, ainda restam muitas dúvidas a respeito de como foi a fase de transição entre o hábito alimentar carnívoro para uma dieta herbívora e também como foi a mudança ecológica que fez com que os sauropodomorfos passassem a ser, durante o Noriano, os animais de grande porte mais abundantes das faunas onde eles ocorrem. Somam-se ainda as disputas filogenéticas envolvendo sauropodomorfos triássicos. Deste modo, com o objetivo de levantar novas informações a respeito desses temas, nesta tese são estudados materiais coletados em unidades triássicas do Rio Grande do Sul. Dentre os principais resultados, observa-se que disparidade morfológica resultante de variação ontogenética é elevada em formas basais do grupo, podendo causar impacto sobre as topologias. Da mesma forma, notou-se que a codificação de caracteres morfológicos pode também ser influenciada por compressão sedimentar, resultando em estados de caracteres artificiais. O excelente grau de preservação de um dos espécimes estudados (CAPPA/UFSM 0035) possibilitou uma melhor compreensão a respeito da anatomia dos primeiros sauropodomorfos. Além disso, o espécime reforça a hipótese de que os sauropodomorfos tiveram origem a partir de um ancestral carnívoro e passaram a acumular traços dentários relacionados a uma dieta mais voltada à herbivoria apenas em um segundo momento da história evolutiva do grupo. A transição morfológica do clado pôde também ser acompanhada a partir das descobertas realizadas em estratos do Rio Grande do Sul, incluindo os esqueletos referentes a CAPPA/UFSM 0001 (outro dos espécimes estudados nesta tese). De fato, esses espécimes permitiram traçar alterações que ocorreram no plano corpóreo dos sauropodomorfos durante um intervalo de oito milhões de anos, revelando um cenário plausível de como o clado passou de formas pequenas e raras a animais grandes e abundantes. Além de corresponder a um novo táxon, CAPPA/UFSM 0001 também trouxe novos dados referentes à biologia dos sauropodomorfos, sugerindo a mais antiga evidencia de gregarismo para o clado. Por fim, uma análise filogenética adotando uma nova matriz de dados revelou uma rica diversidade de formas basais a Plateosauria que são ainda pouco investigadas. Essa nova hipótese ajuda a entender como foram os primeiros momentos de diversificação do grupo e como foi a dispersão dos sauropodomorfos durante sua fase inicial de irradiação.

Palavras-chave: Cladística. Dinosauria. Evolução. Saurischia. Triássico.

Santa Maria, RS
2018

ABSTRACT

ORIGEM AND IRRADIATION OF SAUROPODOMORPHS: NEW SPECIMENS AND ITS IMPLICATIONS

AUTHOR: Rodrigo Temp Müller
ADVISOR: Sérgio Dias da Silva
COADVISOR: Max Cardoso Langer

The origin and early irradiation of sauropodomorph dinosaurs received much attention in response of new discoveries from fossiliferous strata from South America. However, there are still doubts regarding the transitionary period from carnivorous to herbivorous feeding behaviour and the ecological shift in which sauropodomorphs became the most abundant large vertebrates from their faunas. Moreover, there are several disputes regarding the phylogenetic affinities of triassic sauropodomorphs. Thus, in the present thesis, some sauropodomorphs yielded from Triassic strata of Rio Grande do Sul are studied in order to produce new information on these issues. Among the main results, it was noted that the morphological disparity resulting from ontogenetic variation is high in basal forms, affecting the recovered topologies. Similarly, the sedimentary compression impacts character codification, resulting in artificial scores. The excellent preservation degree of one of the studied specimens (CAPPA/UFSM 0035) provides a better understanding of the anatomy of the earliest sauropodomorphs. In addition, the specimen reinforces the hypothesis that sauropodomorphs evolved from a carnivorous ancestor and accumulated traits related to an herbivorous diet during a second evolutionary moment. The morphological transition of the clade could also be tracked through findings from Rio Grande do Sul strata, including the skeletons that compose CAPPA/UFSM 0001 (another specimen studied in the present thesis). Indeed, these specimens allow to track the modifications on the body plan of sauropodomorphs during a time interval of eight million years, revealing a plausible scenario where the clade changes from small and rare to large and abundant animals. CAPPA/UFSM 0001, a new taxon, also brings new data regarding the biology of sauropodomorphs, suggesting the oldest evidence of gregarious behaviour for the clade. Finally, a new phylogenetic analysis employing a new data matrix revealed a rich diversity of non-plateosaurian sauropodomorphs, still poorly studied. This new hypothesis helps to understand how were the first moments of diversification of the group and how was their dispersion during their first phase of irradiation.

Keywords: Cladistics. Dinosauria. Evolution. Saurischia. Triassic.

Santa Maria, RS
2018

LISTA DE FIGURAS

LISTA DE ABREVIATURAS E SIGLAS

CAPPA/UFSM	Centro de Apoio à Pesquisa Paleontológica da Quarta Colônia
Ma	Milhões de anos

SUMÁRIO

1 INTRODUÇÃO

1.1 ANTES DOS “LAGARTOS TERRÍVEIS”

Antes dos primeiros dinossauros sauropodomorfos serem capazes de se elevar sobre suas patas posteriores e esticar seu longo pescoço em direção a um ramo de vegetação que lhes servisse de alimento, uma longa jornada foi trilhada por seus precursores avemetatarsalianos durante o Triássico Inicial e Médio. Abordagens filogenéticas indicam que a linhagem aviana separou-se da linhagem crocodiliana durante o Início do Triássico, há cerca de 252 milhões de anos atrás (NESBITT et al., 2017). Enquanto os pseudossúquios (arcossauros mais relacionados aos crocodilos do que às aves) alcançaram grande sucesso evolutivo durante o Triássico Médio e início do Triássico Superior, a linhagem avemetatarsaliana passou a exercer dominância ecológica sobre os ambientes continentais somente a partir da metade do Triássico Superior (BRUSATTE et al., 2008).

O clado mais basal de Avemetatarsalia é chamado de Aphanosauria (NESBITT et al., 2017) e inclui algumas formas quadrúpedes de aparência um tanto enigmática, já que esse clado retém características presentes em Pseudosuchia, como a morfologia geral do calcanhar e as proporções dos membros. Até o momento, o registro fóssil do grupo estende-se do início do Triássico Médio até o início do Triássico Superior, com representantes tanto no continente Gonduana como no Laurásia (NESBITT et al., 2017). Os afanossauros correspondem ao grupo irmão de Ornithodira, o clado que engloba pterossauros, dinossauros e as formas aparentadas (Figura 1). Enquanto Pterosauria não possui até o momento registros em rochas do Triássico Inferior e Médio, seu grupo irmão Dinosauromorpha (BENTON, 1985) é representado por vários esqueletos fósseis a partir do Triássico Médio (NESBITT et al., 2010), além de possíveis registros icnológicos em rochas do Triássico Inferior (BRUSATTE et al., 2011). As evidências filogenéticas apontam até o momento para a existência de três principais clados de dinossauromorfos. O mais basal, Lagerpetidae (ARCUCCI, 1986), inclui cerca de meia dúzia de espécies supostamente cursoriais, as quais se estendem temporalmente ao longo de quase todo o Triássico Superior (e.g., IRMIS et al., 2007).CABREIRA et al., 2016; MARTÍNEZ et al., 2016; MÜLLER et al., 2018). A biologia desse clado ainda é pouco compreendida em virtude da incompletude dos espécimes já descobertos. Por exemplo, o único material craniano atribuído a Lagerpetidae refere-se a uma caixa craniana (CABREIRA et al., 2016), de modo que até o momento nenhum elemento ósseo contendo dentes foi registrado, dificultando a investigação dos seus hábitos alimentares. Além disso, com exceção de um espécime descoberto na Argentina (MARTÍNEZ et al., 2016), todos outros espécimes indicam um tamanho corpóreo pequeno. Os fósseis mais antigos de lagerpetídeos são

registrados em rochas carnianas da América do Sul (ROMER, 1971; CABREIRA et al., 2016), enquanto que formas de idade noriana são também registradas na América do Norte (IRMIS et al., 2007; SARIGÜL, 2016). Embora pouco se conheça ainda sobre esse enigmático grupo, estudos investigando séries ontogenéticas de lagerpetídeos (e.g. NESBITT et al., 2009) têm servido como base para melhorar o entendimento a respeito da biologia do desenvolvimento de dinossauromorfos.

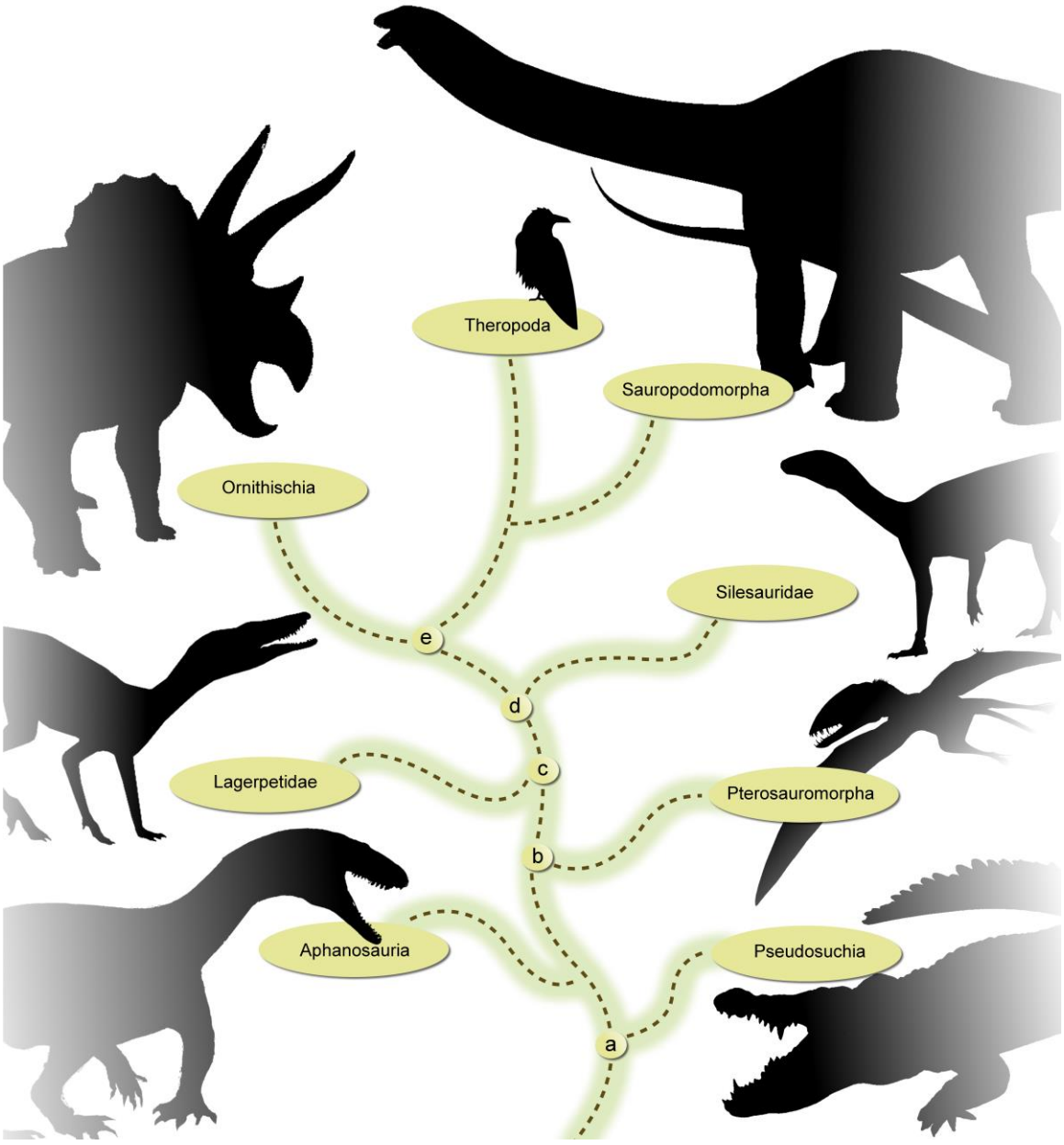

Figura 1 – Árvore filogenética representando as afinidades de dinossauros e grupos relacionados. a, Archosauria; b, Ornithodira; c, Dinosauromorpha; d, Dinosauriformes; e, Dinosauria. Fonte: Silhuetas construídas a partir de diversas fontes.

Com pouco mais de dez espécies válidas, o segundo ramo que compõe o clado dos dinossauromorfos é chamado de Silesauridae (LANGER et al., 2010; NESBITT et al., 2010). Tal ramo está mais próximo daquele que inclui os dinossauros, formando junto com eles e algumas poucas formas de posicionamento geralmente flutuante, o clado Dinosauriformes (NOVAS, 1992). Todavia, ainda existe uma linha de evidencias que pode sugerir um relacionamento ainda mais próximo entre silessaurídeos e dinossauros, onde os primeiros na verdade estariam inseridos em Ornithischia, um dos três principais grupos de dinossauros. Sendo assim, silessaurídeos poderiam na verdade ter sido dinossauros (e.g. LANGER e FERIGOLO, 2013; CABREIRA et al., 2016) ao invés de grupo-irmão dos mesmos (e.g. NESBITT et al. 2010). Temporalmente, os silessaurídeos estendem-se do Anisiano até próximo do final do Noriano (NESBITT et al. 2010), o que faz destes os dinossauromorfos com registros corpóreos mais antigos. De fato, o registro fóssil deste grupo é muito mais abrangente em comparação com o registro de afanossauros e lagerpetídeos, o que ajuda a entender diferentes aspectos da biologia do grupo, como, por exemplo, seu hábito alimentar, até o momento sugerido como herbívoro ou onívoro (NESBITT et al., 2010; CABREIRA et al., 2016). Além disso, os membros anteriores bastante alongados sugerem que este grupo foi formado por animais quadrúpedes, contrastando com o padrão bípede dos primeiros dinossauros. A maioria das formas não chegava a ultrapassar 1,5 metros de comprimento (e.g. FERIGOLO e LANGER, 2007), entretanto um possível espécime de silessaurídeo escavado em rochas da Tanzânia pode ter chegado a medir quase 3 metros de comprimento (BARRETT et al., 2015). Assim como os lagerpetídeos, seu padrão de distribuição geográfica aponta para uma origem gonduânica, posteriormente alcançando ampla distribuição geográfica também na Laurásia (DZIK, 2003). Tal como todos outros grupos de dinossauromorfos não-dinossaurianos, os silessaurídeos tornaram-se extintos pouco antes de alcançar o final do Triássico, porém o grupo coexistiu com seus parentes próximos dinossaurianos por cerca de 20 milhões de anos (IRMIS et al., 2007).

Por fim, o terceiro e esmagadoramente mais diverso ramo de dinossauromorfos, Dinosauria (OWEN, 1842), é agrupado em três principais clados menos inclusivos: Ornithischia, Theropoda e Sauropodomorpha. Por muito tempo, os dois últimos foram considerados filogeneticamente mais próximos, formando o grande clado Saurischia (SEELEY, 1887). No entanto, essa afinidade tem sido desafiada a partir de uma nova hipótese que sugere maior afinidade entre terópodes e ornitísquios (BARON et al., 2017). De qualquer forma, pode-se observar características distintas em cada um dos três clados, de modo que entender a evolução de cada um deles corresponde a um desafio à parte. Somam-se ainda a essa difícil tarefa a presença de algumas formas de posicionamento consideravelmente

instável, como os herrerasaurídeos, já classificados tanto quanto terópodes, como também como saurísquios basais à dicotomia Theropoda/Sauropodomorpha (LANGER et al., 2010). Em relação ao registro fóssil de dinossauros, as formas inequívocas mais antigas são reportadas a partir de rochas de idade Carniana da América do Sul, além de registros fragmentários da África e Índia (EZCURRA, 2012). Todavia, as três principais linhagens não são registradas de maneira equivalente em rochas dessa idade. Ornitísquios foram por muito tempo somente representados por *Pisanosaurus mertii* (CASAMIQUELA, 1967), da Formação Ischigualasto da Argentina. Entretanto, uma reavaliação filogenética apontou possíveis afinidades deste táxon com silessaurídeos (AGNOLÍN e ROZADILLA, 2017), fazendo assim com que ornitísquios não mais passassem ser representados em estratos do Carniano. Na verdade, esse posicionamento coloca o Período Jurássico como a época do registro mais antigo de ornitísquios, dado que nenhum outro espécime inequívoco é reconhecido para o Triássico até o momento (BARON, 2017). Entretanto cabe-se ressaltar que, se a hipótese que reconhece silessaurídeos como ornitísquios for considerada, o grupo passa a possuir um registro bastante amplo durante o Triássico (CABREIRA et al., 2016).

De forma semelhante ao exposto acima, se reconhecermos os herrerasaurídeos como terópodes, o registro desses últimos aumenta drasticamente para o Carniano. Contudo, terópodes registrados nesses estratos e que não façam supostamente parte do grupo dos herrerasaurídeos são extremamente raros e geralmente questionáveis. Um dos mais completos espécimes corresponde a *Eodromaeus murphi* (MARTÍNEZ et al., 2011), da Formação Ischigualasto da Argentina. Porém a inclusão desse táxon em Theropoda foi recentemente desafiada através de uma hipótese que sugere um posicionamento basal à dicotomia Theropoda/Sauropodomorpha (CABREIRA et al., 2016). Diferentemente do registro de Ornithischia, os terópodes passam a ser registrados mais frequentemente em rochas de idade Noriana e Retiana (PINHEIRO, 2016; EZCURRA, 2017; MARTÍNEZ e APALDETTI, 2017).

Finalmente, o registro de sauropodomorfos é, de longe, o mais abundante em comparação com outros clados dinossaurianos durante o Triássico. O mesmo é verdade para os estratos Carnianos, nos quais os sauropodomorfos alcançam a maior diversidade, com três espécies da Formação Ischigualasto da Argentina e quatro para a Formação Santa Maria (= porção inferior da Sequência Candelária) do Brasil. Embora possam apresentar maior diversidade taxonômica, a abundância desses animais ainda é pequena quando comparada com outros táxons recuperados nessas mesmas unidades (MARTÍNEZ et al., 2013), fato que se torna oposto quando examinados os registros a partir do final do Noriano (MÜLLER et al., 2017). De qualquer modo, independentemente da linhagem a qual pertençam, todos os principais registros de dinossauros de idade Carniana apontam para um plano corpóreo

bípede, com mãos livres, um pescoço não muito alongado e dentição não completamente especializada para uma dieta herbívora (CABREIRA et al., 2016), indicando possíveis traços do plano corporal ancestral do grupo.

1.2 A ASCENÇÃO DO "IMPÉRIO PROSAUROPODA"

Enquanto rochas de idade Carniana raramente revelam materiais de sauropodomorfos durante escavações, estratos mais recentes geralmente produzem registros muito abundantes desse clado em grande parte do mundo. Essa mudança abrupta no conteúdo fossilífero referente a sauropodomorfos parece refletir um importante câmbio biótico, onde estes passam de formas pequenas e "tímidas" para os vertebrados terrestres mais abundantes em seus ecossistemas. Esse evento é conhecido como o "Império Prosauropoda" (BENTON, 1983) e marca o primeiro momento em que os dinossauros efetivamente passam a exercer domínio sobre os ecossistemas terrestres. O principal fator intrínseco ligado a essa mudança parece estar relacionado à aquisição de uma dieta voltada à herbivoria. Enquanto formas mais basais apresentam características que indicam hábito alimentar faunívoro (CABREIRA et al., 2016; BRONZATI et al., 2017), as formas sucessivamente mais derivadas registradas próximo ao final do Triássico possuem diversas adaptações relacionadas a uma dieta herbívora. Somando-se ainda a essa tendência, outras mudanças ocorreram durante esse período de transição, como por exemplo o aumento do tamanho corpóreo e o alongamento do pescoço, ambos permitindo o forrageio de vegetação mais alta do que qualquer outro grupo de vertebrados era capaz de alcançar nessa época (PARRISH, 1998). Desta forma, parece que a adoção de um novo estilo de dieta em combinação com tais características, tenha sido um dos principais responsáveis pela ascensão do grupo. Porém, o tempo e modo em que essas características se estabeleceram ainda é mal compreendido, dada a escassez de restos fósseis de sauropodomorfos do exato momento de transição, o qual deve ter ocorrido possivelmente durante o início e a metade do Noriano (MÜLLER et al., 2017).

Diversas controvérsias filogenéticas também afetam as tentativas de estabelecer padrões mais complexos relacionados ao grupo. O mais conhecido desafio filogenético que envolve os sauropodomorfos está ligado à disputa entre dois cenários: (1) os "prossaurópodes" (sauropodomorfos de médio a grande porte, bípedes, com pescoço longo e crânio pequeno) comporiam um arranjo monofilético (UPCHURCH et al., 2007) e (2) seriam parafiléticos (YATES et al., 2007). O aumento na quantidade de espécimes que tem ocorrido ao longo dos últimos anos parece dar mais suporte ao último cenário, indicando que os

"prossaurópodes" formariam uma série com poucos táxons sucessivamente parafiléticos em relação aos saurópodes propriamente ditos (Figura 2). Neste ponto, outro desafio entra em cena. Este diz respeito à falta de consenso do que exatamente constitui um "verdadeiro" saurópode, muitas vezes relacionado à postura quadrúpede (MCPHEE e CHOINIERE, 2017). Evolução convergente também já foi apontada como responsável por produzir distintos sinais filogenéticos entre o crânio e o pós-crânio de alguns sauropodomorfos (APALDETTI et al., 2014). Finalmente, outra dificuldade que assola o estudo do grupo envolve a flutuabilidade de certos táxons, especialmente as formas mais basais e algumas formas norte americanas (ROWE et al., 2010; SERTICH e LOEWEN, 2010). Além de reduzir a robustez de ramos específicos, essa condição também interfere nas tentativas de estabelecer padrões biogeográficos e evolutivos.

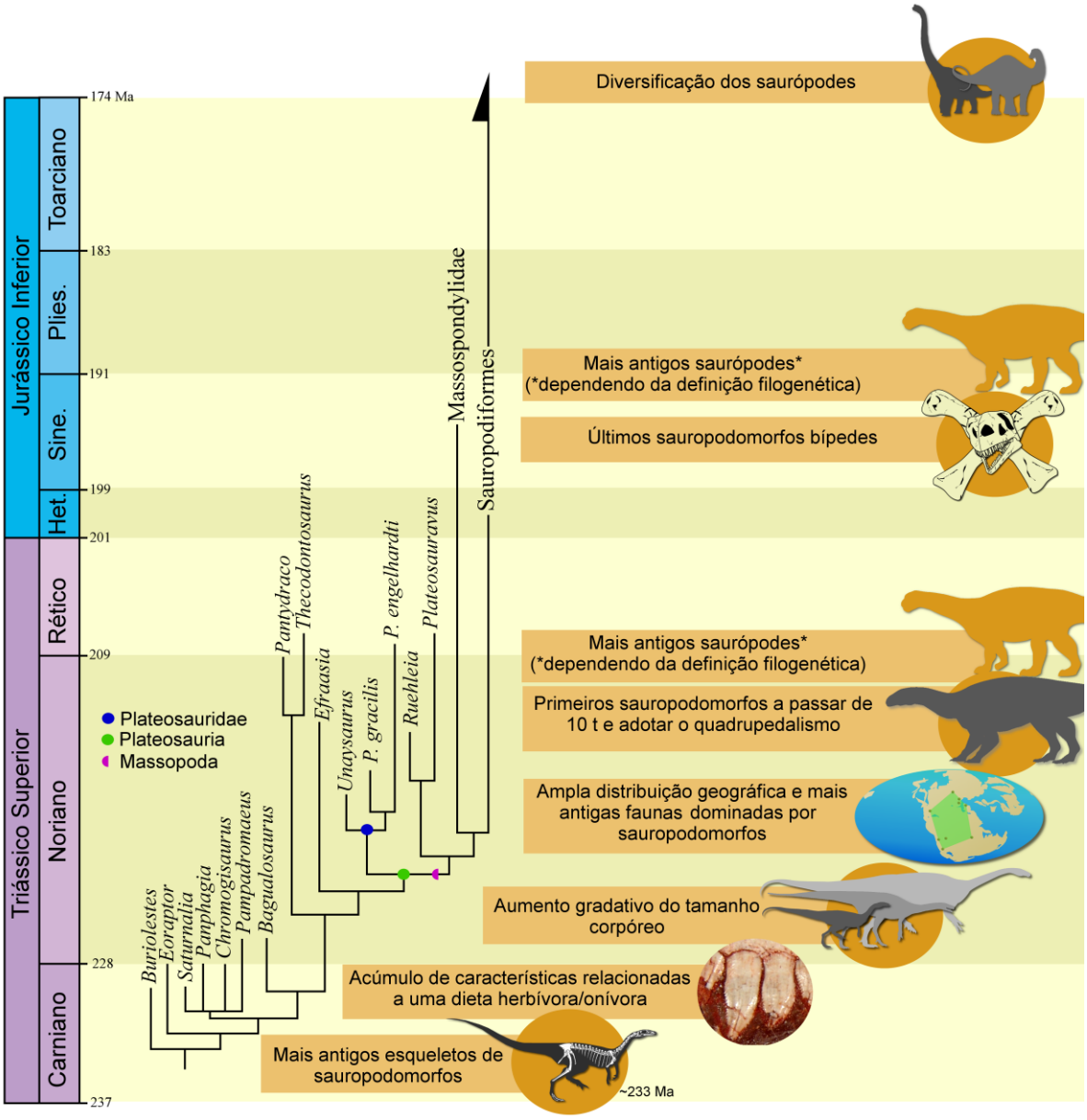

Figura 2 – Padrões macroevolutivos dos sauropodomorfos ao longo do Triássico Superior e Jurássico Inferior. Fonte: Compilação de dados obtidos de Cabreira et al. (2016), Müller et al. (2017; 2018), Apaldetti et al. (2018), McPhee et al. (2018) e Pretto et al. (2018).

Ainda que muitas controvérsias pairem sobre as afinidades internas de Sauropodomorpha, esforços de coleta ao redor do mundo tem contribuído na construção de um cenário promissor. Já é possível entender tanto a forma do esqueleto, como aspectos biológicos das formas mais basais do grupo (CABREIRA et al., 2016). Técnicas computacionais de reconstrução de tecidos moles têm possibilitado acesso a informações antes desconhecidas (e.g. BRONZATI et al., 2017) e estudos histológicos e ontogenéticos vem revelando padrões biológicos intrigantes (APALDETTI et al., 2018; MÜLLER et al., 2018). Entretanto, ainda resta muito a ser feito para que seja possível contar a história evolutiva dos sauropodomorfos com maior acuidade e riqueza de detalhes.

1.3 DEFININDO UM SAUROPODOMORFO

Ao se deparar com um esqueleto fóssil de um animal gigante, quadrúpede, de pescoço incrivelmente longo, cabeça pequena e dentição herbívora, não irão restar dúvidas, trata-se de um dinossauro sauropodomorfo. Mas e se esse esqueleto for de um dinossauro pequeno, bípede, cabeça proporcionalmente um pouco maior, com pescoço curto e dentes em forma de punhal? Seria um equívoco reconhecê-lo como um sauropodomorfo? Esse é um desafio que vem sendo enfrentado por aqueles que estudam as formas mais basais de sauropodomorfos. Por muitos anos, o pequeno saurísquio *Eoraptor lunensis* (SERENO et al., 1993), da Formação Ischigualasto da Argentina, foi reconhecido como um terópode, dado que apresentava todas essas características mencionadas acima e que, até então, eram reconhecidas somente em terópodes. Porém, a descoberta de um outro esqueleto que recebeu o nome de *Eodromaeus murphii* (MARTÍNEZ et al., 2011), trouxe alguns questionamentos à tona. Esse esqueleto também compartilhava todas essas características e ainda possuía outras feições comuns aos terópodes, enquanto que estas eram ausentes em *Eoraptor* (SERENO et al., 2013). Tal fato levou os pesquisadores a examinar com mais detalhes a anatomia de *Eoraptor*, o que por fim revelou vários traços compartilhados com os sauropodomorfos, como por exemplo, a abertura ampla da narina, o processo ventral do esquamosal delgado e o primeiro dente do dentário localizado posteriormente à extremidade anterior da mandíbula (MARTÍNEZ et al., 2011). Assim, quase duas décadas após a descrição original, *Eoraptor* passou a ser aninhado junto aos outros sauropodomorfos. Esse novo arranjo mudou em vários aspectos o modo de ver a origem do grupo, afinal, *Eoraptor* não parecia portar uma dentição típica de um animal herbívoro ou onívoro. Foi então que, em 2016, um novo sauropodomorfo de idade Carniana, da Formação Santa Maria (correspondente à porção inferior da Sequência Candelária) foi descrito. O táxon recebeu o nome de *Buriolestes schultzi* (CABREIRA et al.,

2016) e foi apontado como membro mais basal de Sauropodomorpha, de modo que apresentava um aspecto ainda menos parecido com as formas típicas de grupo, especialmente em relação à forma de sua dentição, claramente de um animal faunívoro. Apesar de bastante completo, o esqueleto que corresponde ao holótipo de *Buriolestes* carrega poucas sinapomorfias que servem para suportar seu parentesco com outros sauropodomorfos, sendo a extremidade anterior do dentário ventralmente direcionada uma das principais características (CABREIRA et al., 2016). Esse é, de fato, um cenário plausível quando se está lidando com as formas mais basais de um clado, especialmente quando se conhece pouco acerca da morfologia ancestral e das formas basais dos grupos relacionados. Como resultado, a retenção de características plesiomoórficas pode ser erroneamente interpretada como características compartilhadas por clados próximos. Por exemplo, a dentição zifodonte de *Buriolestes* aparentemente corresponde a condição plesiomórfica de dinossauros, no entanto, poderia ser equivocadamente identificada como uma sinapomorfia compartilhada com terópodes, uma vez que formas mais derivadas de sauropodomorfos não possuem tal padrão dentário (CABREIRA et al., 2016; MÜLLER et al., 2018).

Deste modo, ao se deparar com formas supostamente próximas da origem de um clado, em se tratando de Sauropodomorpha, torna-se particularmente difícil classificar seus integrantes através do uso de "caracteres-chave", especialmente se o espécime em questão for composto por poucos elementos ósseos. Sendo assim, identificar um sauropodomorfo pode ser mais razoável através de sua inclusão por meio de uma abordagem filogenética, seguindo a definição em vigência proposta para esse clado. A definição filogenética para Sauropodomorpha mais aceita atualmente foi proposta por Taylor et al. (2010) como "o clado mais inclusivo contendo *Saltasaurus* mas não *Tyrannosaurus rex*". Essa definição engloba também as formas mais basais, ao contrário da definição mais antiga proposta por Salgado et al. (1997) que excluía essas formas, uma vez que foi construída utilizando o grupo "Prosauropoda", que atualmente é considerado sinônimo de Plateosauridae de acordo com definição proposta para "Prosauropoda" por Galton e Upchurch (2007): "todos os táxons mais proximamente relacionados a *Plateosaurus* do que a Sauropoda". Uma outra definição mais recentemente proposta por Baron et al. (2017) considera sauropodomorpha como "o clado mais inclusivo que contém *Diplodocus carnegii* mas não *Triceratops horridus*, *Passer domesticus* ou *Herrerasaurus ischigualastensis*. Embora essa definição tenha sido proposta para um contexto onde sauropodomorfos estariam menos relacionados com terópodes (i.e. terópodes como grupo irmão de ornítsquios = Ornithoscelida), ela também serve para definir o grupo em esquemas filogenéticos tradicionais (i.e. Saurischia composto por terópodes e sauropodomorfos).

1.4 SAUROPODOMORFOS TRIÁSSICOS DO RIO GRANDE DO SUL

Sauropodomorfos são registrados em rochas triássicas da Sequência Candelária (*sensu* HORN et al., 2014) no Rio Grande do Sul (Figura 3). Essa Sequência faz parte da Supersequência Santa Maria, a qual abrange um intervalo temporal que vai do Triássico Médio até próximo do final do Triássico (ZERFASS et al., 2003). A Sequência Candelária, por sua vez, possui um alcance temporal que se inicia aproximadamente na metade do Carniano e vai até pouco antes da metade do Noriano (LANGER et al., 2018), e esta unidade vem produzindo os registros mais antigos de sauropodomorfos, permitindo o rastreio da evolução inicial do grupo. De fato, já são conhecidas quatro espécies provenientes da porção mais inferior dessa Sequência, além de pelo menos mais uma espécie da porção superior. Essa porção inferior corresponde a parte superior da Formação Santa Maria, que teve seu primeiro sauropodomorfo descrito em 1999, *Saturnalia tupiniquim* (LANGER et al., 1999). A espécie, oriunda do município de Santa Maria, é conhecida por uma série de esqueletos parciais escavados na localidade tipo. Mais de dez anos depois, foi descrito *Pampadromaeus barberenai* (CABREIRA et al., 2011), proveniente de um sítio localizado no município de Agudo. Além do holótipo, compreendendo um esqueleto incompleto, são também conhecidos alguns espécimes compostos por elementos isolados, todos da localidade tipo (MÜLLER et al., 2018). A espécie seguinte recebeu o nome de *Buriolestes schultzi* (CABREIRA et al., 2016) e foi descrita a partir de um esqueleto parcial e alguns elementos isolados de outros indivíduos descobertos no município de São João do Polêsine. Finalmente, a espécie mais recentemente apresentada, *Bagualosaurus agudoensis* (PRETTO et al., 2018), foi descrita a partir de um esqueleto parcial coletado na mesma localidade que revelou *Pampadromaeus barberenai*.

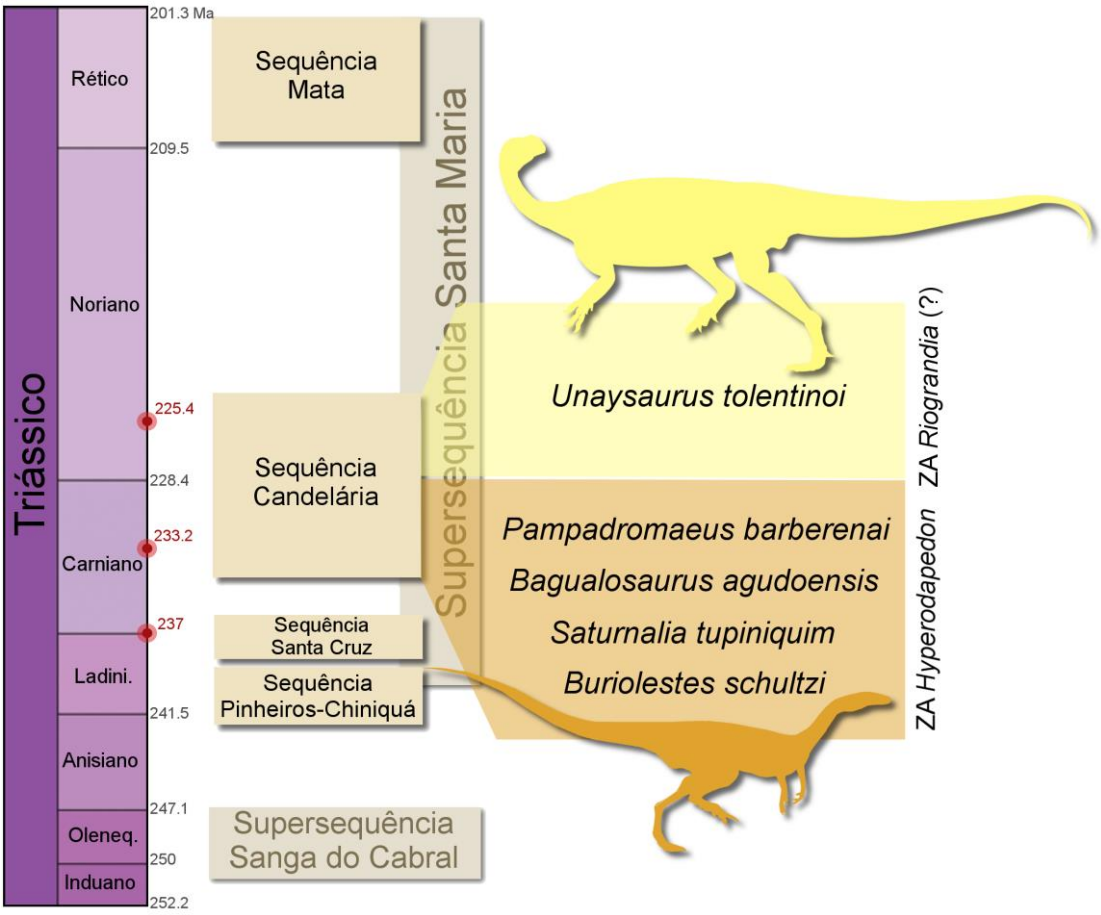

Figura 3 – Sauropodomorfos do Triássico do Rio Grande do Sul. Fonte: As idades absolutas seguem Langer et al. (2018) e Philipp et al. (2018).

Dado o exposto acima, pode-se observar um súbito aumento taxonômico de sauropodomorfos de idade Carniana para o Brasil nos últimos anos, possivelmente relacionado à ampliação numérica de equipes realizando trabalho de prospecção em rochas triássicas do Rio Grande do Sul, e também pelo aumento na frequência de expedições de prospecção e coleta na região. Esse acréscimo amostral não apenas tem expandido a diversidade do grupo, mas também incrementado a qualidade de seu registro. De fato, nunca antes tantos espécimes (muitos ainda em fase de preparação) oriundos desses estratos haviam sido registrados como nos últimos anos. Por conta disso, pode-se esperar que ao longo dos próximos anos, muitos estudos sejam realizados com enfoque em sauropodomorfos carnianos do Rio Grande do Sul. Por outro lado, a diversidade taxonômica desse clado a partir da porção superior da Sequência Candelária (correspondente à Formação Caturrita), não havia aumentado desde a descrição de *Unaysaurus tolentinoi* (LEAL et al., 2004), escavado no município de São Martinho da Serra. Além de representar a única espécie inequívoca de Sauropodomorpha para esses estratos, também é conhecida por um único esqueleto parcial. No entanto, vale ressaltar que esse não é único registro para esta unidade. De fato, até o momento já foram reportados pelo menos mais dez espécimes (e.g. BITTENCOURT et al.,

2012; 2013; MÜLLER et al., 2015) atribuídos a Sauropodomorpha, no entanto, seu estado em maioria fragmentário ou a incompleto torna a identificação em um nível menos inclusivo bastante incerta. Entretanto, isso não é regra para todos os espécimes, sendo alguns deles muito bem preservados e completos, os quais até pouco tempo atrás, encontravam-se em fase de preparação. Essa situação, também torna a porção superior da Sequência Candelária bastante promissora no que se refere ao estudo dos sauropodomorfos.

1.5 ESPÉCIMES ESTUDADOS

Dentre os diversos espécimes descobertos nos estratos mencionados anteriormente, alguns compõem o cerne da presente tese e estão tombados na coleção do Centro de Apoio à Pesquisa Paleontológica da Quarta Colônia (CAPPA/UFSM). Algumas informações referentes à coleta e integridade dos espécimes, bem como o código de cada espécime, são apresentadas neste item. O espécime CAPPA/UFSM 0028 corresponde a um fêmur esquerdo isolado com 113 mm de comprimento total. Este material foi coletado no afloramento conhecido como "Sítio Janner", no município de Agudo. O conteúdo fossilífero deste sítio, condizente com aquele da Zona de Associação de *Hyperodapedon*, sugere idade Carniana (LANGER et al., 2007). Apesar de ser composto por um único elemento ósseo, CAPPA/UFSM 0028 foi encontrado associado a um esqueleto parcial de *Exaeretodon*. O espécime é particularmente interessante por seu tamanho reduzido e também por apresentar feições que podem indicar grau de maturação menos avançado em relação aos outros dinossauros coevos.

O espécime seguinte também é composto por um elemento isolado. CAPPA/UFSM 0179 corresponde a um áxis parcial coletado no afloramento "Sítio Buriol", no município de São João do Polêsine. Assim como o "Sítio Janner", o conteúdo fossilífero deste afloramento também sugere idade Carniana em virtude da presença de rincossauros com morfologia condizente com *Hyperodapedon* (ROBERTO-DA-SILVA et al., 2014). Apesar de não se conhecer muito bem a morfologia do axis de sauropodomorfos de idade Carniana, a presença de *Buriolestes schultzi* no "Sítio Buriol" pode sugerir que CAPPA/UFSM 0179 tenha pertencido a um sauropodomorfo. Deste modo, o principal interesse por trás do estudo deste espécime é trazer novos dados a respeito da morfologia do axis em dinossauros basais.

Outro importante espécime deste estudo, tombado sob o código CAPPA/UFSM 0035, também exumado do "Sítio Buriol", corresponde a um esqueleto bastante completo, incluindo um crânio com todos os seus elementos. Enquanto os outros dois espécimes acima puderam ser coletados sem a necessidade de procedimentos mais refinados, CAPPA/UFSM 0035 demandou uma coleta que levou dois dias, onde um bloco de rocha circundante revestido com gesso foi inteiramente removido e transportado para o laboratório de preparação do

CAPPA/UFSM. Todos os elementos foram removidos da rocha matriz através de preparação mecânica. A única exceção foi uma série dorsal parcial (composta por vértebras anteriores e mediais, bem como suas respectivas costelas) que foi mantida em um bloco de rocha menor e revestido com gesso, com a finalidade de preservar as costelas articuladas às vértebras. A idade e o elevado grau de completude do espécime tornam este um dos principais materiais estudados nesta tese.

O último material recebe o código CAPPA/UFSM 0001, correspondendo a uma associação de pelo menos três esqueletos, sendo dois deles completos. Estes espécimes foram descobertos no município de Agudo, em um afloramento chamado de “Sítio Wachholz”. A ausência de marcadores bioestratigráficos dificulta a inclusão deste sítio em alguma das Zonas de Associação propostas para o Rio Grande do Sul, entretanto um estudo bioestratigráfico incluindo os sauropodomorfos deste sítio sugeriu correlação com sítios que pertencem a Zona de Associação de *Riograndia*, indicando idade Noriana inicial para o sítio (MÜLLER et al., 2017). A coleta de CAPPA/UFSM 0001 demandou maior esforço e logística, uma vez que, além de incluir animais de mais de 3 m de comprimento, os esqueletos estavam intimamente associados. Optou-se por coletar todos os espécimes em um único bloco de rocha, tarefa que demandou uma grande equipe e mais de 20 dias de trabalho de campo. Como resultado, foi extraído um bloco de rocha revestido com gesso e suportado por vigas de madeira, totalizando cerca de 5,2 toneladas. Os espécimes do bloco foram expostos através de preparação mecânica, onde os dois mais completos já foram totalmente removidos. Para facilitar os estudos envolvendo os espécimes deste bloco, cada um recebeu um complemento ao número tombo, por exemplo, CAPPA/UFSM 0001a. A importância desses espécimes está ligada principalmente ao estado de preservação excepcional. Além do mais, estes esqueletos podem corresponder a alguns dos poucos materiais de sauropodomorfos do momento seguinte ao “surgimento” do grupo.

2 OBJETIVOS

O objetivo geral da presente tese é tornar conhecida a anatomia óssea dos espécimes CAPPA/UFSM 0001, 0028, 0035 e 0179 e realizar sua identificação taxonômica no menor nível inclusivo possível.

2.1 OBJETIVOS ESPECÍFICOS

1- Testar as afinidades dos espécimes e suas potenciais implicações no contexto filogenético dos sauropodomorfos;

2- Avaliar a suposição de que CAPPA/UFSM 0028 corresponda a um indivíduo juvenil e levantar dados a respeito da ontogenia dos sauropodomorfos;

3- Acessar os sinais filogenéticos das diferentes regiões do esqueleto de CAPPA/UFSM 0035;

4- Avaliar as implicações da compressão sedimentar sobre a morfologia do ílio de sauropodomorfos primitivos, em especial de CAPPA/UFSM 0001b;

5- Refinar o entendimento do tempo e modo em que determinadas características evoluíram em Sauropodomorpha;

6- Por fim, construir uma nova matriz filogenética de sauropodomorfos que inclua, tanto os novos espécimes, bem como dados gerados por estudos recentes.

3 ARTIGO I

Título: On a dinosaur axis from one of the oldest dinosaur-bearing sites worldwide

Autores: Rodrigo Temp Müller, Flávio Agusto Pretto, Micheli Stefanello, Edurado Silva Neves e Sérgio Dias da Silva

Periódico: Acta Palaeontologica Polonica

Volume: 62

Páginas: 543-548

Ano: 2017

DOI: 10.4202/app.00369.2017

Brief report

Acta Palaeontologica Polonica 62 (3): 543–548, 2017

On a dinosaur axis from one of the oldest dinosaur-bearing sites worldwide

RODRIGO T. MÜLLER, FLÁVIO A. PRETTO, MICHELI STEFANELLO, EDUARDO SILVA-NEVES, and SÉRGIO DIAS-DA-SILVA

The axial skeleton is proportionally underrepresented in the fossil record of early dinosaurs, when compared to other skeletal parts (e.g., pelvic girdle and hindlimb). For instance, the axis is poorly known in early dinosaurs, which precludes a better understanding of this important anatomical structure. Therefore, the present contribution fills an important gap with a description of the axis of a new early dinosaur (CAPPA/UFSM 0179). The specimen was collected at the Buriol outcrop, a Triassic fossiliferous locality from southern Brazil (Candelária Sequence, Santa Maria Supersequence) biostratigraphically correlated to Carnian units, placing this specimen among the oldest dinosaurs worldwide. Notable features include the combination of a neural spine that bears an almost straight dorsal margin along its length and presence of an epipophysis. This axis arrangement is unique among Carnian dinosaurs, representing a new morphotype, though a similar morphology is observed in some early theropods. Indeed, a phylogenetic analysis nested the specimen within Theropoda. However, this outcome is probably biased by the large amount of missing data in CAPPA/UFSM 0179 and also due to the limited sampling of the axis in early dinosaurs, particularly among sauropodomorphs. As the specimen comes from the site that includes *Buriolestes schultzi* (an early sauropodomorph), it is quite plausible that CAPPA/UFSM 0179 might be referable to that taxon. If so, the specimen improves the anatomical knowledge of *Buriolestes schultzi*, given its axis is yet unknown. An alternative possibility to be considered is that the specimen would belong to a dinosaur not yet known in the Candelária Sequence, which would increase its dinosaur diversity for the outcrop, improving the Triassic dinosaurian record from Southern Brazil.

Introduction

The Buriol (Fig. 1A) and surrounding outcrops in the municipality of São João do Polêsine, Rio Grande do Sul, Brazil has yielded many fossil vertebrates. Its fossiliferous content includes fishes (Perez and Malabarba 2002), temnospondyls (Dias-da-Silva et al. 2011, 2012), aetosaurs and rhynchosaurs (Roberto-da-Silva et al. 2014), dinosauromorphs (Cabreira et al. 2016), and cynodonts (Pacheco et al. 2017). Its dinosauromorph fossil record is particularly interesting because it encompasses the oldest unequivocal members of Dinosauria, as well as exceptionally well preserved dinosaur relatives (Cabreira et al. 2016). Indeed, the presence of the hyperodapedontid rhynchosaurs supports a Carnian age (Martínez et al. 2011) for the outcrop. As widely known, so far Carnian strata record the oldest unambiguous dinosaurs worldwide (e.g., Sereno et al. 1993; Langer et al. 1999; Martinez and Alcober 2009). Dinosauromorph taxa from the Buriol outcrop include the lagerpetid *Ixalerpeton polesinensis* and the early sauropodomorph *Buriolestes schultzi* (Cabreira et al. 2016). These records have crucially enhanced the knowledge regarding both the anatomy and phylogenetic affinities of early dinosaurs and their close relatives. In spite of this, many skeletal parts of both taxa remain unknown. Indeed, this is the current condition of most Carnian dinosaurs, as a number of skeletal portions are far more represented than other ones in the fossil record. For instance, pelvic and/or hind limb elements are known from all described Carnian dinosaurs. In contrast, the axial skeleton is still poorly sampled, usually represented by a few isolated vertebrae (e.g., *Chromogisaurus novasi*, *Pampadromaeus barberenai*, *Panphagia protos*). The axis is poorly known in early dinosaurs, being preserved in a few Carnian specimens (e.g., Sereno and Novas 1993; Alcober and Martínez 2010; Sereno et al. 2013). The axis is an important anatomical structure as it provides the attachment site for muscles connecting the skull with the postcranial skeleton (e.g., Snively and Russell 2007). Hence, considering the scarce knowledge regarding this structure in early dinosaurs and their anatomical importance, herein we describe the anatomy of an early dinosaur axis from the abovementioned site, providing its comparison with some other Triassic dinosauromorphs.

Institutional abbreviations.—AMNH, American Museum of Natural History, New York, USA; CAPPA/UFSM, Centro de Apoio à Pesquisa Paleontológica da Quarta Colônia, São João do Polêsine, Rio Grande do Sul, Brazil; PULR, Universidad Nacional de La Rioja, La Rioja, Argentina; PVSJ, Instituto y Museo de Ciencias Naturales, San Juan, Argentina; SAM, Iziko South African Museum, Cape Town, South Africa; TMM, Texas Memorial Museum, Austin, USA; ULBRA, Universidade Luterana do Brasil, Coleção de Paleovertebrados, Canoas, Rio Grande do Sul, Brazil; ZPAL, Institute of Paleobiology, Polish Academy of Sciences, Warsaw, Poland.

 https://doi.org/10.4202/app.00369.2017

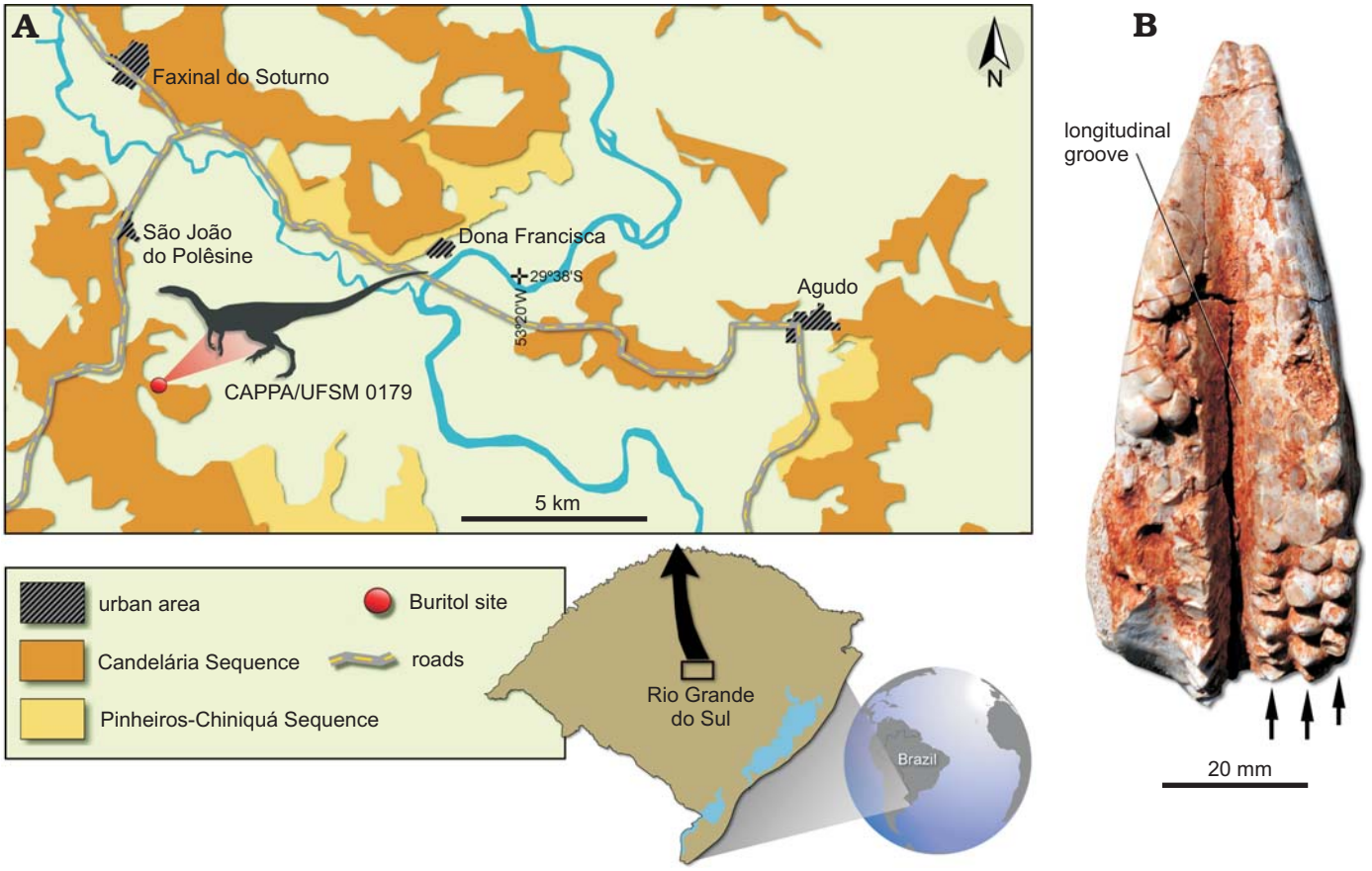

Fig. 1. **A**. Map of the São João do Polêsine área, Rio Grande do Sul, Brazil, showing the location of the Buriol outcrop (modified from Zerfass et al. 2007). **B**. CAPPA/UFSM 0044, a left maxilla of a Hyperodapedontinae from the Buriol ourcrop, Carnian, late Triassic, arrows point to the teeth rows.

Systematic palaeontology

Archosauria Cope, 1869

Dinosauromorpha Benton, 1985

Dinosauriformes Novas, 1992

Dinosauria Owen, 1842

Genus et species incertae sedis

Material.—CAPPA/UFSM 0179 (Fig. 2), an isolated and nearly complete axis including the caudal half of the centrum, the neural arch, and the neural spine. Bone surface is exceptionally well preserved. The specimen was recovered from the Buriol outcrop (Fig. 1A) (29°39'34.2" S; 53°25'47.4" W), in São João do Polêsine, Rio Grande do Sul, Brazil, in the same layer where the holotype (ULBRA-PVT280) of *Buriolestes schultzi* was excavated. This outcrop belongs to the Candelária Sequence (Horn et al. 2014), part of the Santa Maria Suspersequence of Zerfass et al. (2003). At least two rhynchosaur specimens collected at the site (Fig. 1B) may be referable to Hyperodapedontinae, and among these, more closely resemble *Hyperodapedon* sp. than other forms (Langer and Schultz 2000; Langer et al. 2000; Montefeltro et al. 2010; Schultz et al. 2016). They possess a characteristic longitudinal groove (Fig. 1B) between the lingual and buccal tooth rows. In both margins, the teeth cover a wide area, with as much as three rows of teeth that are more significantly worn towards the cranial portion of the series (Fig. 1B). Therefore, the fossil vertebrate content from this locality has been correlated with those from the Ischigualasto Formation, northwest Argentina (Langer et al. 2007), radioisotopically dated as 231.4 ± 0.3 Ma (Martínez et al. 2011).

Description.—The preserved portion of the axial centrum is 12.5 mm in length. It is constricted towards the mid-point (Fig. 2D), with 4 mm in width, while the caudal articular facet expands to 8.5 mm in width. This suggests that the centrum was spool-shaped. The dorsal surface of the centrum is excavated to form the floor of the neural canal, which also is transversely larger at the caudal extremity than in the mid-point. The lateral surface lacks any pneumatic features. The ventral surface bears a 1.85 mm wide longitudinal ventral keel that reaches the ventral margin of the caudal articular surface (Fig. 2A). A ventral keel is absent in some plateosaurian sauropodomorphs (e.g., *Plateosaurus*, *Riojasaurus*) but present in early dinosaurs and related groups (e.g., *Herrerasaurus*, *Lewisuchus*) (Yates 2003). The ventral extension of the keel is uncertain as the centrum is cranially fractured. The caudal articular surface is 8.8 mm in height and markedly concave (Fig. 2F). In lateral view, the ventral margin of this surface slightly extends more cau-

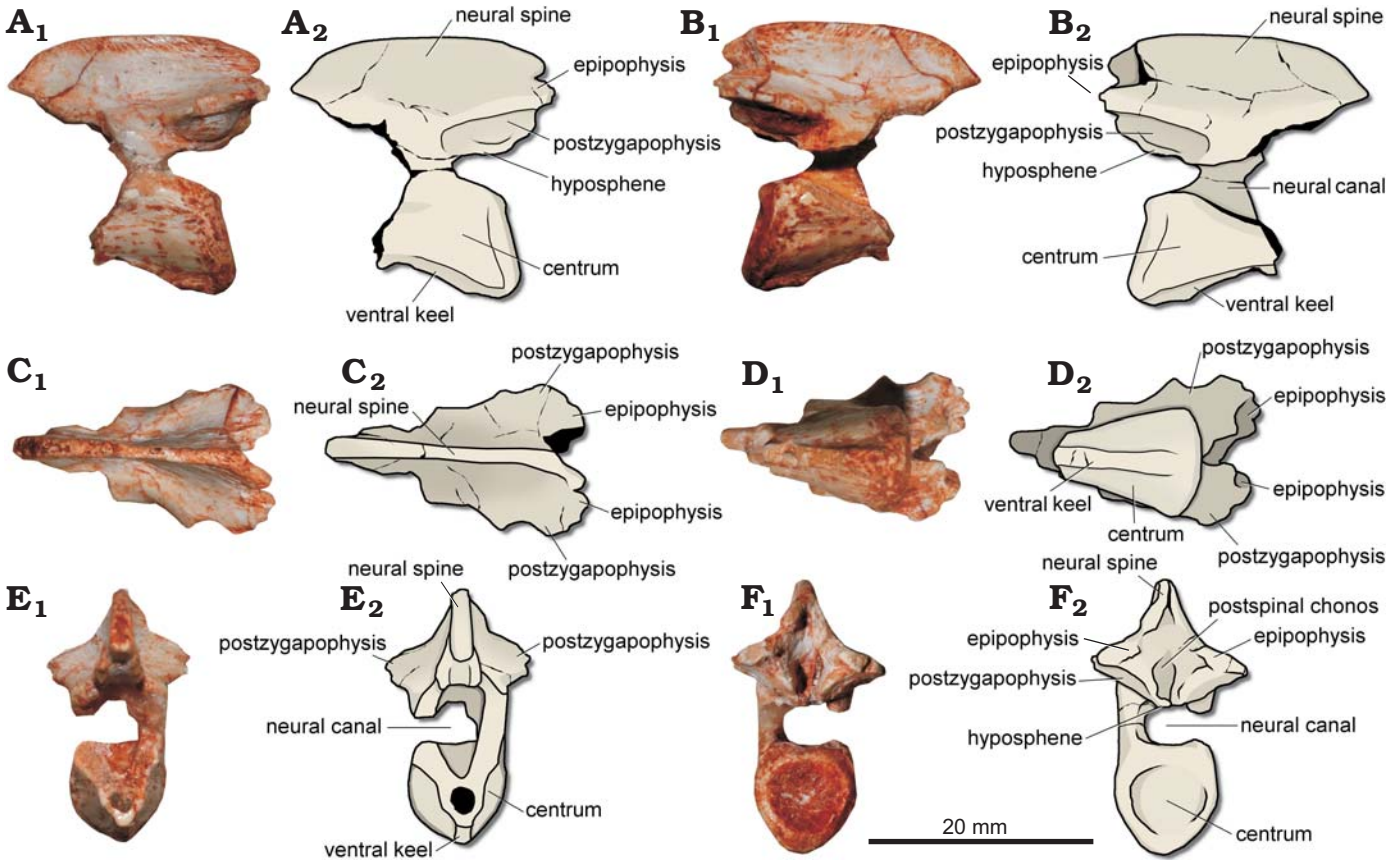

Fig. 2. Dinosauria gen. et sp. indet., CAPPA/UFSM 0179 from the Buriol outcrop, São João do Polêsine, Rio Grande do Sul, Brazil; Carnian, late Triassic. Photographs (A_1–F_1) and schematic drawings (A_2–F_2) of the axis in left (**A**) and right (**B**) lateral, dorsal (**C**), ventral (**D**), cranial (**E**), and caudal (**F**) views.

dally than the dorsal margin (Fig. 2A, B). At the mid-point of the centrum, the bone wall is approximately 0.8 mm in width.

The preserved portion of the neural arch is completely fused to the centrum, and there is no sign of a neurocentral suture. The dorsoventral height of the neural canal is approximately 3.5 mm, whereas the space between the dorsal tip of the postzygapophysis and the ventral margin of the neural canal is 7.6 mm. The lateral surface, ventral to the cranial margin of the postzygapophysis, is gently excavated. The postzygapophysis extends laterally to form a convex margin in dorsal view (Fig. 2C). On the ventral surface of the postzygapophysis there is a subovoid facet with 6 mm in length, which would receive the dorsomedial oriented facet of the prezygapophysis of the third cervical vertebra. Indeed, the articular facet of the postzygapophysis is ventromedially oriented (Fig. 2F). The medial margin of such structure folds ventrally to form a faint hyposphene (Fig. 2F), an accessory articulation. Its caudal tip extends caudally as far the caudal margin of the dorsal portion of the centrum. The caudal extension of the postzygapophysis reaches the caudal extension of the ventral margin of the centrum, as in *Silesaurus opolensis* (ZPAL AbIII/1930; Piechowski and Dzik 2010), whereas in *Herrerasaurus ischigualastensis* (PVSJ 407; Sereno and Novas 1993) the postzygapophysis projects more caudally than the caudal articular facet of the axial centrum. On the dorsal surface of the postzygapophysis there is a caudodorsal process that exceeds its caudal extension (Fig. 2B, F). Its structure corresponds to the epipophysis but the caudal tip of both epipophyses is not preserved. Nonetheless, this corresponds to the maximum caudal extension of the axis. Some dinosauriforms lack axial epipophyses, such as, *Silesaurus opolensis* (ZPAL AbIII/1930), and *Lewisuchus admixtus* (PULR 01). A cleft separates the dorsal surface of the epipophysis from the caudal margin of the neural spine (Fig. 2A).

The 21.4 mm long neural spine is entirely preserved (Fig. 2A, B). The structure is 1.4 mm in width at the mid-point. Its height is constant along its length. Therefore, as in *Lewisuchus admixtus* (PULR 01) and *Coelophysis bauri* (AMNH FR 7224), the dorsal margin of the cranial half and the caudal half runs almost in the same plane, resulting in a straight margin, excepting the cranial and caudal extremities that are gently curved ventrally. In contrast, the dorsal margin of the neural spine is caudodorsally angled in most archosauriforms (Nesbitt 2011). The laterodorsal margin is densely covered by striations (Fig. 2A, B) which could be related to the origin of the m. splenius capitis (e.g., Snively and Russell 2007), whereas ventrally, close to the dorsal surface of the postzygapophysis, a depressed surface could be related to the attachment of the m. complexus. The cranial tip of the spine tappers to a point (Fig. 2A, B), whereas the caudal extremity of the spine bifurcates to form a Y-shaped caudal portion in dorsal view (Fig. 2C). This condition resembles that from *Herrerasaurus ischigualastensis* (PVSJ 407), whereas

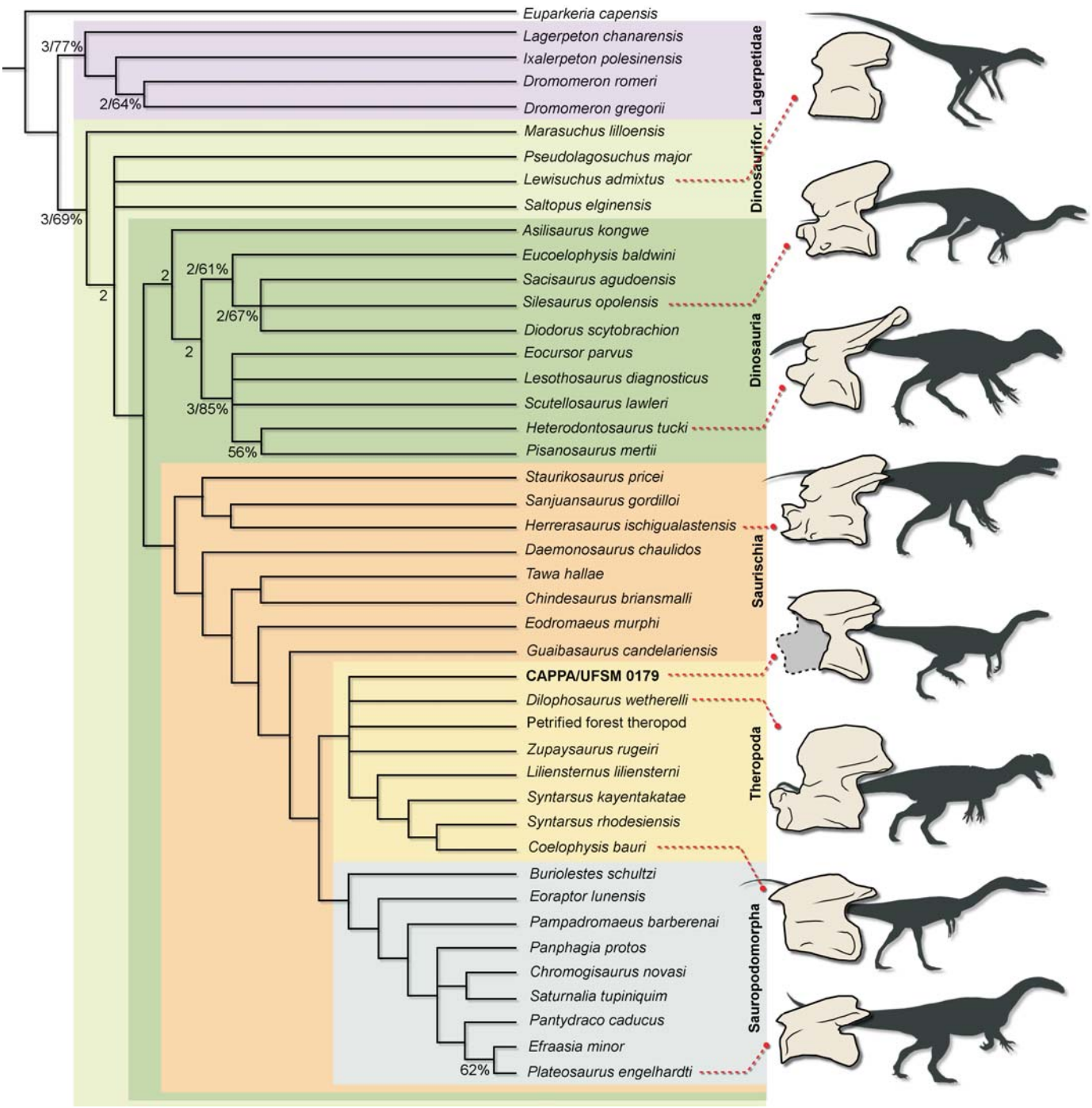

Fig. 3. Strict consensus tree depicting the phylogenetic position of CAPPA/UFSM 0179 and the schematic general morphology of the axis of some Triassic dinosauriforms. Numbers below nodes represent Bremer support values (left) higher than 1 and Bootstrap values (right) higher than 50%. Abbreviation: Dinosaurifor., Dinosauriformes.

in some dinosauriforms, such as *Silesaurus opolensis* (ZPAL AbIII/1930; Piechowski and Dzik 2010) and *Lewisuchus admixtus* (PULR 01; Bittencourt et al. 2014), the caudodorsal tip of the neural spine projects further caudally, precluding the bifurcation and forming the roof of the postspinal chonos. In addition, distinct from the caudally extended neural spine of *Heterodontosaurus tucki* (e.g., SAM-PK-K1332), the caudal margin of the neural spine only slightly exceeds the caudal margin of the axial centrum in CAPPA/UFSM 0179. On the other hand, the neural spine is caudally short in some sauropodomorphs, such as *Adeopapposaurus mognai* (PVSJ568) and *Sarahsaurus aurifontanalis* (TMM 43646-2).

Phylogenetic analysis

CAPPA/UFSM 0179 was scored in the data matrix of Cabreira et al. (2016), in order to test its phylogenetic affinities (Appendix 1). The data matrix totalizes 256 morphological characters

and 44 operational taxonomic units. It was processed with the software TNT v1.1 (Goloboff et al. 2008). All characters received the same weight and 31 (3, 4, 6, 11, 36, 60, 62, 64, 83, 115, 123, 139, 147, 148, 157, 160, 171, 173, 175, 178, 179, 182, 195, 200, 201, 202, 205, 216, 222, 240, and 248) were treated as ordered following the study of Cabreira et al. (2016). The most parsimonious trees (MPTs) were recovered via "traditional search" (random addition sequence + tree bisection reconnection) with 1000 replicates of Wagner trees (with random seed = 0), tree bisection reconnection (TBR) and branch swapping (holding 20 trees save per replicate).

The analysis recovered 242 MPTs of 846 steps (CI = 0.345; RI = 0.637). CAPPA/UFSM 0179 nests as an early diverging theropod in all trees. In the strict consensus tree (Fig. 3), the specimen is placed in a polytomy at the base of Theropoda, together with *Dilophosaurus wetherlli*, *Zupaysaurus rugeiri*, and the "Petrified Forest theropod". The only character state supporting CAPPA/UFSM 0179 as theropod is the dorsal margin of the axial neural spine that arcs dorsally, where the cranial portion height is equivalent to the caudal height (character 76, state 1). However, this character is not scored to other early diverging sauropodomorphs (e.g., *Buriolestes schultzi*, *Eoraptor lunensis*, *Pampadromaeus barberenai*). In addition, *Lewisuchus admixtus* presents the same condition of CAPPA/UFSM 0179. Therefore, this represents an ambiguous synapomorphy of theropods. So, the phylogenetic position of CAPPA/UFSM 0179 remains uncertain due to both the limited entries in the data matrix and the lack of the axis in other early diverging sauropodomorphs.

Discussion and conclusions

The incomplete and fragmentary condition of the specimen prevents a reliable taxonomic ascription. Nevertheless, CAPPA/UFSM 0179 supports a dinosaurian assignation due to its combination of features. As observed by Nesbitt (2011), the axial neural spine of most archosauriforms is craniocaudally slanted, with the caudodorsal corner much taller than the craniodorsal corner. In contrast, the inverse condition occurs in some early diapsids like *Araeoscelis gracilis* and *Petrolacosaurus kasensis* (Nesbitt et al. 2015). In addition, Nesbitt (2011) also observed that the craniodorsal height is equivalent to the caudodorsal height in the axial neural spine of some ornithodirans, as in CAPPA/UFSM 0179. Among ornithodirans that share this condition, only dinosaurs bear an epipophysis on the axis, as it is absent in *Lewisuchus admixtus* (Bittencourt et al. 2014). Assignation of CAPPA/UFSM 0179 to a less inclusive group within Ornithodira is currently precluded, as it lacks diagnostic information in order to do so. As already stated, the theropod affinities expressed in the phylogenetic analysis could reflect the poor sampling of axis among early dinosaurs and relatives, and the large amount of missing data for CAPPA/UFSM 0179. Indeed, despite the sauropodomorph affinities of *Buriolestes schultzi*, it shares some particular traits with theropods (see Cabreira et al. 2016). So, it is plausible that CAPPA/UFSM 0179 could represent an axis from this species, as both CAPPA/UFSM 0179 and the holotype (ULBRA-PVT280) of *Buriolestes schultzi* were excavated in the exact same layer of the outcrop. Moreover, the hypothesis that CAPPA/UFSM 0179 could belong to the lagerpetid species *Ixalerpeton polesinensis* (ULBRA-PVT059, also from the same outcrop), is not plausible, as ULBRA-PVT059 lacks epipophyses on the preserved cervical vertebrae.

The new specimen increases the fossil record of dinosaurs from the Candelária Sequence and announces a new axial morphotype for Carnian dinosaurs, previously known only for younger taxa. The two most plausible hypotheses and implications related to the taxonomic ascription of CAPPA/UFSM 0179 are: (i) it belongs to *Buriolestes schultzi*; or (ii) it belongs to an as yet unknown dinosaur from the Buriol outcrop. In the first hypothesis, CAPPA/UFSM 0179 increases the anatomical knowledge related to *Buriolestes schultzi*, as the axis is currently unknown to the taxon. In the second hypothesis, the specimen increases the early dinosaur diversity for the outcrop, contributing to a better knowledge of the Carnian dinosaurian fauna in South America. As a putative new, still undescribed specimen (CAPPA/UFSM 0035) of *Buriolestes schultzi* was recently discovered, the possibility to assign CAPPA/UFSM 0179 to this taxon will be addressed in detail. At this point, it is possible to observe that both elements present an overall morphological similarity. However, the axis of CAPPA/UFSM 0035 is 12% smaller than CAPPA/UFSM 0179 and the caudal half of the dorsal margin of the neural spine of CAPPA/UFSM 0035 is broken. Therefore, it is uncertain if *Buriolestes schultzi* possesses the same straight margin of CAPPA/UFSM 0179. Concluding, only the discovery of a more complete specimen with the same morphology of CAPPA/UFSM 0179 would solve if it belongs to *Buriolestes schultzi* or to a still unknown new early dinosaur in South America.

Acknowledgements.—We are grateful to the Buriol family (São João do Polêsine, Rio Grande do Sul, Brazil) for allowing access to their property to excavate the specimen herein described. The comments and suggestions of Matthew G. Baron (Department of Earth Sciences, University of Cambridge, UK) and an anonymous reviewer greatly improved the quality of this manuscript. We also thank the Coordenação de Aperfeiçoamento de Pessoal de Nivel Superior (CAPES) for the scholarship to RTM, ESN, and ME; the Conselho Nacional de Desenvolvimento Científco e Tecnológico (CNPq) for the research grant to SDS (process 306352/2016-8). We thank the Willi Henning Society, for the gratuity of TNT software.

References

Alcober, O.A. and Martínez, R.N. 2010. A new herrerasaurid (Dinosauria, Saurischia) from the Upper Triassic Ischigualasto Formation of northwestern Argentina. *ZooKeys* 63: 55–81.

Benton, M.J. 1985. Classification and phylogeny of diapsid reptiles. *Zoological Journal of the Linnean Society* 84: 97–164.

Bittencourt, J.S., Arcucci, A.B., Maricano, C.A., and Langer, M.C. 2014. Osteology of the Middle Triassic archosaur *Lewisuchus admixtus* Romer (Chañares Formation, Argentina), its inclusivity, and relationships amongst early dinosauromorphs. *Journal of Systematic Palaeontology* 13: 189–219.

Cabreira, S.F., Kellner, A.W.A., Dias-da-Silva, S., Roberto-da-Silva, L., Bronzati, M., Marsola, J.C., Müller, R.T., Bittencourt, J.S., Batista, B.J., Raugust. T., Carrilho, R., and Langer, M.C. 2016. A unique Late Trias-

sic dinosauromorph assemblage reveals dinosaur ancestral anatomy and diet. *Current Biology* 26: 3090–3095.

Cope, E.D. 1869. Synopsis of the extinct Batrachia, Reptilia, and Aves of North America. *Transactions of the American Philosophical Society (New Series)* 14: 1–252.

Dias-da-Silva, S., Cabreira, S.F., and Roberto-da-Silva, L. 2011. Occurrence of giant stereospondyl remains in the Santa Maria Formation (Middle⁄Upper Triassic of southern Brazil). *Alcheringa* 35: 11–19.

Dias-da-Silva, S., Sengupta, D.P., Cabreira, S.F., and Roberto-da-Silva, L. 2012. The presence of *Compsocerops* (Brachyopoidea: Chigutisauridae) (Late Triassic) in southern Brazil with comments on chigutisaurid palaeobiogeography. *Paleontology* 55: 163–172.

Goloboff, P.A., Farris, J.S., Nixon, and K.C.C. 2008. TNT, a free program for phylogenetic analysis. *Cladistics* 24: 774–786.

Horn, B.L.D., Melo, T.M., Schultz, C.L., Philipp, R.P., Kloss, H.P., and Goldberg, K. 2014. A new third-order sequence stratigraphic framework applied to the Triassic of the Paraná Basin, Rio Grande do Sul, Brazil, based on structural, stratigraphic and paleontological data. *Journal of South American Earth Sciences* 55: 123–132.

Langer, M.C. and Schultz, C.L. 2000. A new species of the Late Triassic rhynchosaur *Hyperodapedon* from the Santa Maria Formation of South Brazil. *Palaeontology* 43: 633–652.

Langer, M.C., Abdala, F., Richter, M., and Benton, M.J. 1999. A sauropodomorph dinosaur from the Upper Triassic (Carnian) of Southern Brazil. *Comptes Rendus de l'Academie des Sciences IIA* 329: 511–517.

Langer, M.C., Boniface, M., Cuny, G., and Barbieri, L. 2000. The phylogenetic position of *Isalorhynchus genovefae*, a Late Triassic rhynchosaur from Madagascar. *Annales de Paléontologie* 86: 101–127.

Langer, M.C., Ribeiro, A.M., Schultz, C.L., and Ferigolo, J. 2007. The continental tetrapod-bearing Triassic of South Brazil. *Bulletin of the American Museum of Natural History* 41: 201–218.

Martinez, R.N. and Alcober, O.A. 2009. A basal sauropodomorph (Dinosauria: Saurischia) from the Ischigualasto Formation (Triassic, Carnian) and the early evolution of Sauropodomorpha. *PLoS One* 4 (2): e4397.

Martínez, R.N., Sereno, P.C., Alcober, O.A., Colombi, C.E., Renne, P.R., Montañez, I.P., and Currie, B.S. 2011. A basal dinosaur from the dawn of the dinosaur era in southwestern Pangaea. *Science* 331: 201–210.

Montefeltro, F.C., Langer, M.C., and Schultz, C.L. 2010. Cranial anatomy of a new genus of hyperodapedontine rhynchosaur (Diapsida, Archosauromorpha) from the Upper Triassic of southern Brazil. *Earth and Environmental Science Transactions of the Royal Society of Edinburgh* 101: 27–52.

Nesbitt, S.J. 2011. The early evolution of archosaurs: Relationships and the origin of major clades. *Bulletin of the American Museum of Natural History* 352: 1–292.

Nesbitt, S.J., Flynn, J.J., Pritchard, A.C., Parrish, J.M., Ranivoharimanana, L., and Wyss, A.R. 2015. Postcranial anatomy and relationships of *Azendohsaurus madagaskarensis*. *Bulletin of the American Museum of Natural History* 398: 1–126.

Novas, F.E. 1992. Phylogenetic relationships of the basal dinosaurs, the Herrerasauridae. *Palaeontology* 35: 51–62.

Owen, R. 1842. Report on British fossil reptiles. Part II. *Reports of the British Association for the Advancement of Science* 11: 60–204.

Pacheco, C.P., Martinelli, A.G., Pavanatto, A.E., Soares, M.B., and Dias-da-Silva, S. 2017. *Prozostrodon brasiliensis*, a probainognathian cynodont from the Late Triassic of Brazil: second record and improvements on its dental anatomy. *Historical Biology* [published online].

Perez, P.A. and Malabarba, M.C. 2002. A Triassic freshwater fish fauna from the Paraná Basin in southern Brazil. *Revista Brasileira de Paleontologia* 4: 27–33.

Piechowski, R. and Dzik, J. 2010. The axial skeleton of *Silesaurus opolensis*. *Journal of Vertebrate Paleontology* 30: 1127–1141.

Roberto-da-Silva, L., Desojo, J.B., Cabreira, S.F., Aires, A.S.S., Müller, R.T., Pacheco, C.P., and Dias-da-Silva, S. 2014. A new aetosaur from the Upper Triassic of the Santa Maria Formation, southern Brasil. *Zootaxa* 3764: 240–278.

Schultz, C.L., Langer, M.C., and Montefeltro, F.C. 2016. A new rhynchosaur from south Brazil (Santa Maria Formation) and rhynchosaur diversity patterns across the Middle–Late Triassic boundary. *Paläontologische Zeitschrift* 90: 593–609.

Sereno, P.C. and Novas, F.E. 1993. The skull and neck of the basal theropod *Herrerasaurus ischigualastensis*. *Journal of Vertebrate Paleontology* 13: 451–476.

Sereno, P.C., Forster, C.A., Rogers, R.R., and Monetta, A.M. 1993. Primitive dinosaur skeleton from Argentina and the early evolution of Dinosauria. *Nature* 361: 64–66.

Sereno, P.C., Martínez, R.N., and Alcober, O.A. 2013. Osteology of Eoraptor lunensis (Dinosauria, Sauropodomorpha). *Journal of Vertebrate Paleontology* 32: 83–179.

Snively, E. and Russell, A. P. 2007. Functional variation of neck muscles and their relation to feeding style in Tyrannosauridae and other large theropod dinosaurs. *The Anatomical Record* 290: 934–957.

Yates, A.M. 2003. A new species of the primitive dinosaur, *Tecodontosaurus* (Saurischia: Sauropodomorpha) and its implications for the systematics of early dinosaurs. *Journal of Systematic Palaeontology* 1: 1–42.

Zerfass, H., Lavina, E.L., Schultz, C.L., Garcia, A.J.V., Faccini, U.F., and Chemale, F. 2003. Sequence stratigraphy of continental Triassic strata of Southernmost Brazil: a contribution to Southwestern Gondwana palaeogeography and palaeoclimate. *Sedimentary Geology* 161: 85–105.

Zerfass, H., Sander, A., and Flores, A.F. 2007. *Agudo, Folha SH.22-V.C.V, escala 1:100.000, Rio Grande do Sul*. Serviço Geológico do Brasil (CPRM), Brasília.

Rodrigo Temp Müller [rodrigotmuller@hotmail.com], Micheli Stefanello [michelistefanello@hotmail.com], and Eduardo Silva-Neves [edusneves90@gmail.com], Programa de Pós-Graduação em Biodiversidade Animal, Universidade Federal de Santa Maria, Av. Roraima, 1000, Bairro Camobi, 97105-900 Santa Maria, RS, Brasil.
Flávio Augusto Pretto [flavio_pretto@yahoo.com.br] and Sérgio Dias-da-Silva [paleosp@gmail.com], Centro de Apoio à Pesquisa da Quarta Colônia, Universidade Federal de Santa Maria, Rua Maximiliano Vizzotto, 598, 97230-000 São João do Polêsine, RS, Brasil.

Received 4 April 2017, accepted 11 May 2017, available online 12 July 2017.

Appendix 1

Codification for CAPPA/UFSM 0179 of the 256 characters of Cabreira et al. (2016).

???1?1????1??????????????????????????????????????
??
???????????

4 ARTIGO II

Título: The role of ontogeny on character polarization in early dinosaurs: a new specimen from the Late Triassic of southern Brazil and its implications

Autores: Rodrigo Temp Müller, Max Cardoso Langer, Cristian Pereira Pacheco e Sérgio Dias da Silva

Periódico: Historical Biology

Volume: Online-first

Páginas: 1-13

Ano: 2017

DOI: 10.1080/08912963.2017.1395421

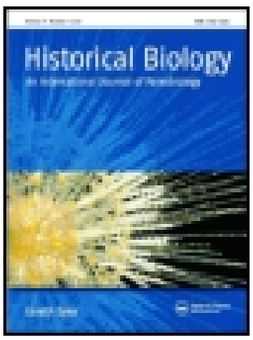

Historical Biology

An International Journal of Paleobiology

ISSN: 0891-2963 (Print) 1029-2381 (Online) Journal homepage: http://www.tandfonline.com/loi/ghbi20

The role of ontogeny on character polarization in early dinosaurs: a new specimen from the Late Triassic of southern Brazil and its implications

Rodrigo Temp Müller, Max Cardoso Langer, Cristian Pereira Pacheco & Sérgio Dias-da-Silva

To cite this article: Rodrigo Temp Müller, Max Cardoso Langer, Cristian Pereira Pacheco & Sérgio Dias-da-Silva (2017): The role of ontogeny on character polarization in early dinosaurs: a new specimen from the Late Triassic of southern Brazil and its implications, Historical Biology, DOI: 10.1080/08912963.2017.1395421

To link to this article: http://dx.doi.org/10.1080/08912963.2017.1395421

Published online: 27 Oct 2017.

HISTORICAL BIOLOGY, 2017
https://doi.org/10.1080/08912963.2017.1395421

Taylor & Francis
Taylor & Francis Group

The role of ontogeny on character polarization in early dinosaurs: a new specimen from the Late Triassic of southern Brazil and its implications

Rodrigo Temp Müller[a], Max Cardoso Langer[b], Cristian Pereira Pacheco[a] and Sérgio Dias-da-Silva[c]

[a]Programa de Pós Graduação em Biodiversidade Animal, Universidade Federal de Santa Maria, Santa Maria, Brazil; [b]Laboratório de Paleontologia de Ribeirão Preto, Universidade de São Paulo, Ribeirão Preto, Brazil; [c]Centro de Apoio à Pesquisa Paleontológica da Quarta Colônia, Universidade Federal de Santa Maria, Santa Maria, Brazil

ABSTRACT

Only recently, new ontogenetic series of early dinosaurs and related groups have been described. Here, we present an isolated immature dinosauriform femur from the Late Triassic of southern Brazil and investigate its influence on character polarization. Because the specimen shares a number of synapomorphies with *Pampadromaeus barberenai*, herein we postulate that it corresponds to a juvenile individual of that taxon. Accordingly, we investigate the morphological variation between juvenile and mature individuals of *P. barberenai*. Scoring these character states into a published phylogenetic data-set of Dinosauromorpha reveals that morphological variation is higher than that observed among closely-related taxa. Ontogenetic variation thus exerts influence on character polarization. In addition, modification of the scores affected by ontogeny produces different topologies, as noted by the reduction in both the number of most parsimonious trees and number of steps, and increased inclusivity of some clades and reduction of polytomies as well. Our study, together with other recent contributions, sheds light on the morphologic pathways seen during dinosauromorph ontogenetic development, which is crucial to more reliably assess phylogenetic reconstructions and macroevolutionary patterns of this widespread and successful group.

ARTICLE HISTORY
Received 31 August 2017
Accepted 18 October 2017

KEYWORDS
Dinosauria; Dinosauriformes; Sauropodomorpha; ontogeny; Carnian; Candelária Sequence

Introduction

Different causes may explain distinct morphologies in duplicated bones of purportedly the same fossil species: taphonomy (Holz and Schultz 1998), pathologies (Trotteyn and Martínez 2013), sexual dimorphism (Raath 1990), ontogeny (Hone et al. 2016), and independent individual variation. When fossil remains are scarce, deciding on these alternatives is difficult, which might lead to misinterpretations and misconceptions (e.g. Vega-Dias et al. 2005; Brusatte et al. 2016). As external morphology is usually the only available tool to infer phylogenetic relations of extinct taxa, the understanding of controlling factors that shape a given structure is crucial. As stated by Raath (1990) 'only once the limits of intraspecific variation have been established can the real taxonomic significance of morphological character suites be assessed'. Among these factors, ontogeny represents a powerful shape controller, requiring much effort in order to be properly recognized, as ontogenetic series of extinct taxa are rare. In spite of this, accessing ontogenetic information is quite important, as the identification of development pathways allows a better understanding of biological aspects, e.g. postural changes adopted throughout the life (Zhao et al. 2013). By disregarding distinct ontogenetic stages during phylogenetic studies, a given data-set can produce contradicting results, as character states are susceptible to change through the life of an individual (e.g. Steyer 2000). Although character states can also on occasion be stable, but this needs to be determined through an adequately sampled fossil record (Kear and Zammit 2014).

Brown and Schlaikjer (1940) were the first authors to drew attention to the ontogeny of dinosaurs. However, the ontogeny of early dinosaurs and related groups is still poorly understood. Pioneer contributions by Raath (1990) and Colbert (1990) started such investigations, and more recently, new ontogenetic series have been recognized and described (e.g. Nesbitt et al. 2009; Piechowski et al. 2014; Griffin and Nesbitt 2016a; Wang et al. 2017). These works have challenged the understanding of several anatomical structures extensively applied in phylogenetic analyses of dinosauromorphs (e.g. Nesbitt 2011), bringing to attention the need to discuss ontogenetic data. In addition, southern Brazil has recently yielded a considerable amount of new early dinosaur remains (e.g. Cabreira et al. 2011, 2016; Pretto et al. 2015; Müller et al. 2016), most of them still under preparation and study. Among these, an isolated femur is investigated here. Its small size suggests that it belonged to an immature individual, raising the opportunity to assess developmental patterns on an early dinosaur femur and to investigate their phylogenetic implications.

CONTACT Rodrigo Temp Müller rodrigotmuller@hotmail.com

Material and methods

The new specimen comes from the Janner site (*Hyperodapedon* Assemblage Zone), at the municipality of Agudo, Rio Grande do Sul, Brazil (Figure 1). It is housed at the Centro de Apoio à Pesquisa Paleontológica da Quarta Colônia (CAPPA/UFSM), São João do Polêsine, Brazil, under the code CAPPA/UFSM 0028. The Janner site is included in the Candelária Sequence (*sensu* Horn et al. 2014) of the Santa Maria Supersequence (Zerfass et al. 2003). Its dinosaurian content is among the oldest known worldwide, given that the *Hyperodapedon* Assemblage Zone) is dated as Carnian in coeval strata from Argentina (Martínez et al. 2011).

CAPPA/UFSM 0028 is a 113 mm long left femur (Figure 2) exhumed from the basal-most fossiliferous horizon of the Janner site sequence. It was associated with a partially articulated juvenile specimen of the traversodontid cynodont *Exaeretodon*, and occurred on the same bedding layer as the holotype of *Pampadromaeus barberenai* (ULBRA-PVT016), as well as an isolated left femur also referred to *P. barberenai* (CAPPA/UFSM 0027, see Müller et al. 2016). As typical of the site, sedimentary compression strongly affected the shape of CAPPA/UFSM 0028. The deformation was mainly mediolaterally oriented, resulting in a very thin femoral shaft in cranial and caudal views (Figure 2(A)). Despite the deformation, the bone has a well-preserved surface, allowing for recognition of even the most delicate structures. This was also supplemented by a 3D virtual model obtained by 3D scan using a ZScanner 700® with surface resolution of 0.2 mm (Figure 2).

As the first step in our attempt to identify the affinities of CAPPA/UFSM 0028, we assessed its degree of ossification by following two macroscopic, size independent criteria: (1) epiphysis development analysis according to the patterns observed by Bennett (1993) – note that we apply the term 'epiphysis' to the end of a long bone, not to independent ossification centers – (Watanabe and Matsuoka 2013); and (2) the bone surface texture analysis termed 'textural ageing' by Tumarkin-Deratzian et al. (2006). Those authors tested and applied this approach in various vertebrate groups (e.g. Johnson 1977; Tumarkin-Deratzian et al. 2006; Watanabe and Matsuoka 2013), including dinosaurs (e.g. Tumarkin-Deratzian 2009; Rauhut et al. 2012; Sekiya et al. 2014). In both methods, the bone surface of CAPPA/UFSM 0028 was examined under a stereomicroscope (with 10 × magnification).

The second step of our study includes a taxonomic evaluation of CAPPA/UFSM 0028 based upon its external morphology and attempting to identify synapomorphies usually considered diagnostic for dinosaurs and related groups (e.g. Nesbitt 2011). Direct comparisons with CAPPA/UFSM 0027 and ULBRA-PVT016, both ascribed to *P. barberenai* (Cabreira et al. 2011; Müller et al. 2016) were also undertaken. ULBRA-PVT016 is housed at the Museu de Ciências Naturais of Universidade Luterana do Brasil, Canoas, Brazil. Morphological differences among the specimens were evaluated from an ontogenetic perspective based on observations from previous studies of dinosauromorph femoral development (Raath 1990; Nesbitt et al. 2009a; Piechowski et al. 2014; Griffin and Nesbitt 2016a).

To assess the effects of ontogenetic variation on the polarization of femoral characters, we scored CAPPA/UFSM 0028 (Table 1) in the data-set of Bittencourt et al. (2015), computing the percentage of coding differences in relation to *P. barberenai* [considering the hypothesis that CAPPA/UFSM 0028 belongs to this taxon (see below)]. The femur of *P. barberenai* was rescored (Table 1) based on new data provided by Müller et al. (2016). We also computed the percentage of codification differences of femoral characters between *P. barberenai* (disregarding CAPPA/

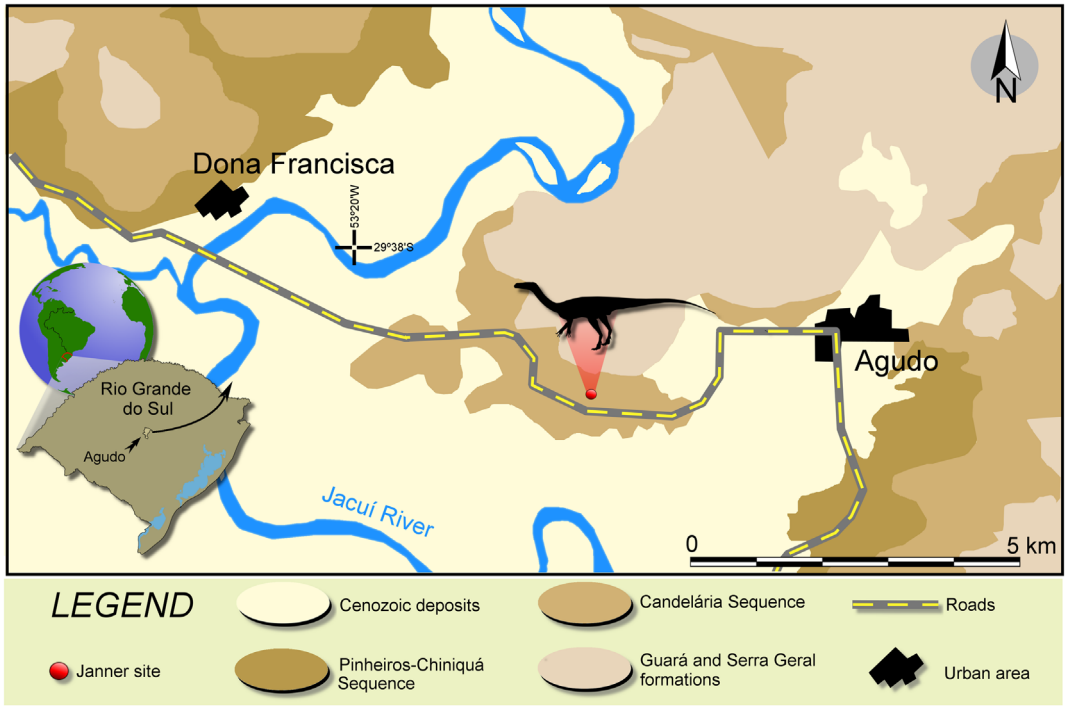

Figure 1. Map of the Agudo area, Rio Grande do Sul, Brazil, showing the location of the Janner site. Surface distribution of geological units according to Zerfass et al. (2007), names of the geological units updated according to Horn et al. (2014).

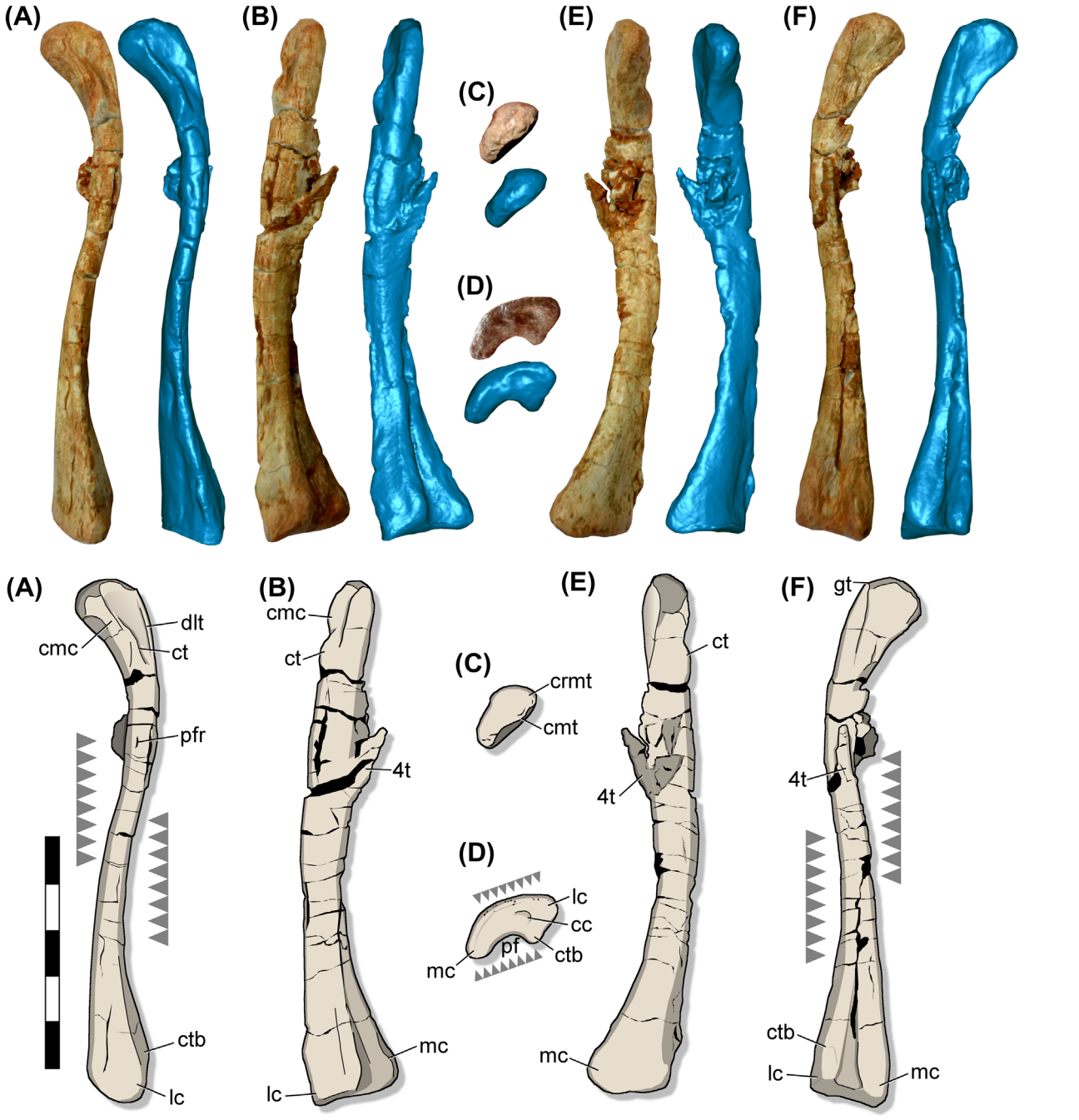

Figure 2. CAPPA/UFSM 0028, a left femur in: (A), cranial; (B), lateral; (C), proximal; (D), distal; (E), medial; and (F), caudal views. Note: the arrows in the drawings indicate the orientation of the sedimentary compaction.

Abbreviations: 4t, fourth trochanter, cc, concavity; cmc, craniomedial crst; cmt, caudomedial tuber; crmt, craniomedial tuber; ct, cranial trochanter; ctb, crista tibiofibularis; dlt, dorsolateral trochanter; gt, greater trochanter; lc, lateral condyle, mc, medial condyle; pf, popliteal fossa; pfr, perforating foramina. Scale bar = 50 mm.

UFSM 0028) and some coeval dinosaurs in order to compare divergent results (e.g. ontogeny versus taxonomy). Femoral character scores followed Bittencourt et al. (2015) for the following taxa: *Saturnalia tupiniquim* (Langer et al. 1999), *Eoraptor lunensis* (Sereno et al. 1993), *Eodromaeus murphi* (Martínez et al. 2011), *Herrerasaurus ischigualastensis* (Reig 1963), and *Staurikosaurus pricei* (Colbert 1970).

A quantitative morphospace analysis including only femoral characters from the data-set by Bittencourt et al. (2015) was also conducted. This analysis aimed to compare morphospace occupation by CAPPA/UFSM 0028, CAPPA/UFSM 0027, and ULBRA-PVT016. For such analysis, the operational taxonomic units (OTUs) that lack preserved femora were excluded (e.g. *Panphagia protos*, *Lewisuchus admixtus*). All polymorphic scores were modified to uncertain (?). First, a Euclidian distance matrix (EDMA) was calculated using the software MATRIX (Wills 1998). A Principal Coordinate Analysis (PCO) was then performed for the EDMA with the multivariate package GINKGO (Bouxin 2005). The parameters selected in GINKGO include the centroid of all OTUs as the origin of the multivariate axes and the Calliez method of negative eigenvalue correction. The PCO axes 1 and 2 were plotted in a bivariate graph with

Table 1. Codification of CAPPA/UFSM 0027 *plus* ULBRA-PVT 016 and CAPPA/UFSM 0028 to the 27 femoral characters of Bittencourt et al. (2015). ? = missing data.

Character number and abbreviated description	CAPPA/UFSM 0027 and ULBRA-PVT016	CAPPA/UFSM 0028
216: craniomedial tuber	(1) small and rounded	(1) small and rounded
217: caudomedial tuber	(0) present and small	(0) present and small
218: craniolateral tuber	(0) absent	(0) absent
219: medial articular surface of the head in dorsal view	(0) rounded	(0) rounded
220: ventral to the proximal head	(2) concave emargination	(?)
221: femoral head orientation angle with respect to the transverse axis through the femoral condyles	(1) craniomedial, 20–60 degrees	(1) craniomedial, 20–60 degrees
222: femoral head in medial and lateral views	(0) rounded	(0) rounded
223: dorsolateral margin of the proximal portion	(1) sharp ridge	(1) sharp ridge
224: cranial trochanter M. iliofemoralis cranialis insertion	(1) present and forms a steep margin with the shaft but is completely connected to the shaft	(1) present and forms a steep margin with the shaft but is completely connected to the shaft
225: medial articular facet of the proximal portion	(0) rounded	(0) rounded
226: craniolateral side of the femoral head	(0) smooth, featureless	(0) smooth, featureless
227: cranial trochanter shelf proximal to the fourth trochanter	(1) present	(?)
228: facies articularis antitrochanterica of the head	(1) level with 'greater trochanter'	(0) ventrally descended
229: 'greater trochanter' shape	(1) angled	(1) angled
230: extension of proximal articular surface of head	(0) extended distally	(0) extended distally
231: proximal surface	(1) transverse groove that is straight	(0) rounded and smooth
232: mediolateral positon of the cranial trochanter	(0) closer to the medial edge	(0) closer to the medial edge
233: dorsoventral position of the fourth trochanter	(0) distal end of fourth trochanter within proximal 30–40% of the femur length	(0) distal end of fourth trochanter within proximal 30–40% of the femur length
234: fourth trochanter shape	(1) a sharp flange	(1) a sharp flange
235: fourth trochanter symmetry	(1) asymmetrical with distal margin forming a steeper angle to the shaft	(?)
236: surface between the lateral condyle and crista tibiofibularis on the distal surface	(1) deep groove	(0) smooth
237: surface between the lateral condyle and crista tibiofibularis on the distal surface	(?)	(?)
238: distal condyles of the femur divided caudally	(0) less than 1/4 the length of the shaft	(?)
239: cranial surface of the distal portion	(0) smooth	(0) smooth
240: crista tibiofibularis	(0) smaller or equal in size to the medial condyle	(0) smaller or equal in size to the medial condyle
241: craniomedial corner of the distal end	(0) rounded	(0) rounded
242: tibiofibularis crest distal shape	(0) distally semicircular	(0) distally semicircular

the software *PAST* (Hammer et al. 2001). Convex hulls were drawn according the phylogenetic relationships recovered by Bittencourt et al. (2015).

Finally, in order to verify the putative influence of ontogeny on the phylogenetic relationships of early dinosaurs we conducted an exploratory analysis of the data matrix of Bittencourt et al. (2015) following the same parameters (except for 1000 rather than 10,000 random additional sequences), with modifications on femoral characters that we do not consider influenced by ontogenetic control. States '1' and '2' of character 223, related to the form of the dorsolateral trochanter (Nesbitt 2011), were collapsed into a single state ('presence' = 1), following the conclusions of Raath (1990) and Piechowski et al. (2014), which associated this variation to ontogeny and sexual dimorphism. In this case, immature individuals of both sexes may share the same morphology, but during development, sexual dimorphism becomes more evident. Another modification includes the rescore of character 227 (presence/absence of trochanteric shelf) for some OTUs. The presence of such structure has been exhaustively recognized as the effect of both ontogeny and sexual dimorphism (Raath 1990; Nesbitt 2011; Piechowski et al. 2014; Griffin and Nesbitt 2016a) making its phylogenetic signal doubtful. Accordingly, we rescored as 'missing data' ('?') all OTUs previously coded as 'absent' (0) in which there is no ontogenetic control, as these could be sampled only on immature specimens. This includes *Sacisaurus agudoensis* (Feirolgo and Langer 2007) and *Guaibasaurus candelariensis* (Bonaparte et al. 1999). The lagerpetid *Dromomeron gregorii* was coded as '0' in the data matrix of Bittencourt et al. (2015), but Nesbitt (2011) shows that the trochanteric shelf is present in the large individuals, thus it was rescored as '1'. The taxon was not scored as polymorphic because juvenile individuals of many OTUs are unknown and we avoid the combination of distinct ontogenetic stages in an OTU, preferring to score the mature condition. As such, the polymorphic condition of *Silesaurus opolensis* was rescored as 'present' (1), rather than 'absent' and 'present' (0/1). The analysis was carried out in TNT v1.1 (Goloboff et al. 2008).

Results

Degree of ossification

Regarding epiphyseal ossification, both articular surfaces of CAPPA/UFSM 0028 are rough and irregular (Figure 3(A, E–F)), suggesting that the epiphyseal cartilage was not yet completely ossified, a pattern observable in immature animals (Bennett 1993) but differing from the fully ossified smooth bone surfaces of mature animals (Bennett 1993; Holliday et al. 2010). In addition, an abrupt unevenness divides the proximal rough surface from the remaining bone (Figure 3(A)). According to Holliday et al. (2010), the long bones of non-avian adult dinosaurs have calcified cartilage laminae on their ends. When this develops, it should form a continuous, rather than uneven bone surface (Holliday et al. 2010). Therefore, the presence of that unevenness suggests that a fully calcified lamina on the specimen had not started growing.

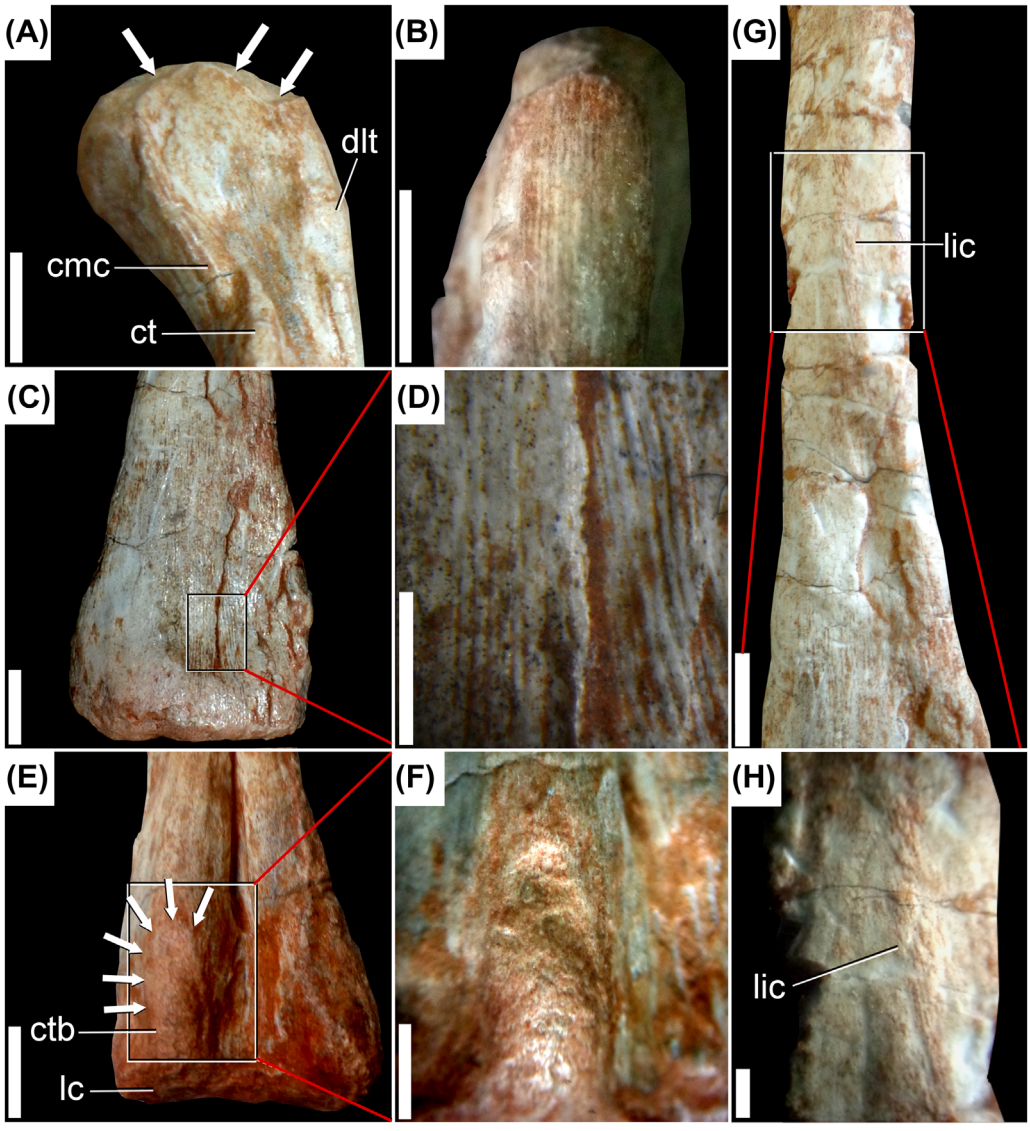

Figure 3. Ossification degree of the femur of CAPPA/UFSM 0028: (A), cranial view of the proximal portion, the arrows indicate unevenness; (B), lateral view of the proximal portion, note the longitudinal striation on the dorsolateral trochanter; (C), cranial view of the distal portion; (D), magnification of the cranial surface of the distal portion, note the longitudinal striations; (E), caudal view of the distal portion, the arrows point to rough surface; (F), magnification of the cristatibiofugularis in caudal view; (G), craniomedial view of the femoral shaft; (H), magnification of the the linea intermuscularis cranialis in craniomedial view.

Abbreviations: cmc, craniomedial crest; ct, cranial trochanter; ctb, crista tibiofibularis; dlt, dorsolateral trochanter; lc, lateral condyle; lic, linea intermuscularis cranialis. Scale bars = 5 mm in A, B, C, E, G, 2 mm in D, F, H.

The external surface of the entire bone reveals several patches of longitudinal parallel striations clustered on both proximal and distal portions (Figure 3(B–D)). These striations differ from typical rugosities or tuberosities of muscle scars (Bennett 2015), but resemble those observed in a wide range of immature vertebrates (Tumarkin-Deratzian et al. 2006; Rauhut et al. 2012; Watanabe and Matsuoka 2013). Striations are absent in the middle of the femoral shaft, where bone surface is smooth, except for a series of faint striations on its craniad surface that probably correspond to an early development stage of the *linea intermuscularis cranialis* (Figure 3(G–H)). Apart from this, there are no other areas with scars that could be related to soft tissue attachment. According to Raath (1969), the amount of muscle scarring is indicative of advanced age in dinosaurs, and their lack is an additional indicator of immaturity, a statement recently corroborated by Griffin and Nesbitt (2016a).

Taxonomic assignation

The presence and shape of several muscle attachment areas in CAPPA/ UFSM 0028 support its inclusion within Dinosauriformes: a small caudomedial tuber (Figure 2(C)); protruding cranial trochanter (Figure 2(A) and 3(A)); dorsolateral trochanter (Figure 2(A) and 3(A)); craniomedial crest (*sensu* Bittencourt and Kellner 2009) (Figures 2(A) and 3(A)); and sharply-flanged fourth trochanter (Figure 2(F)). CAPPA/ UFSM 0028 further differs from femora of non-dinosauriform dinosauromorphs because lacks a hook shaped head (Figure 3(A)), but possesses a craniolateral tuber (Figure 4(A)), reduced crista tibiofibularis (Figure 2(D)), and rounded craniomedial corner of the distal end (Figure 2(D)).

Among dinosauromorphs, transition from the femoral shaft to the ventral portion of the head may manifest a smooth transition, be notched, or have a concave emargination (Nesbitt 2011).

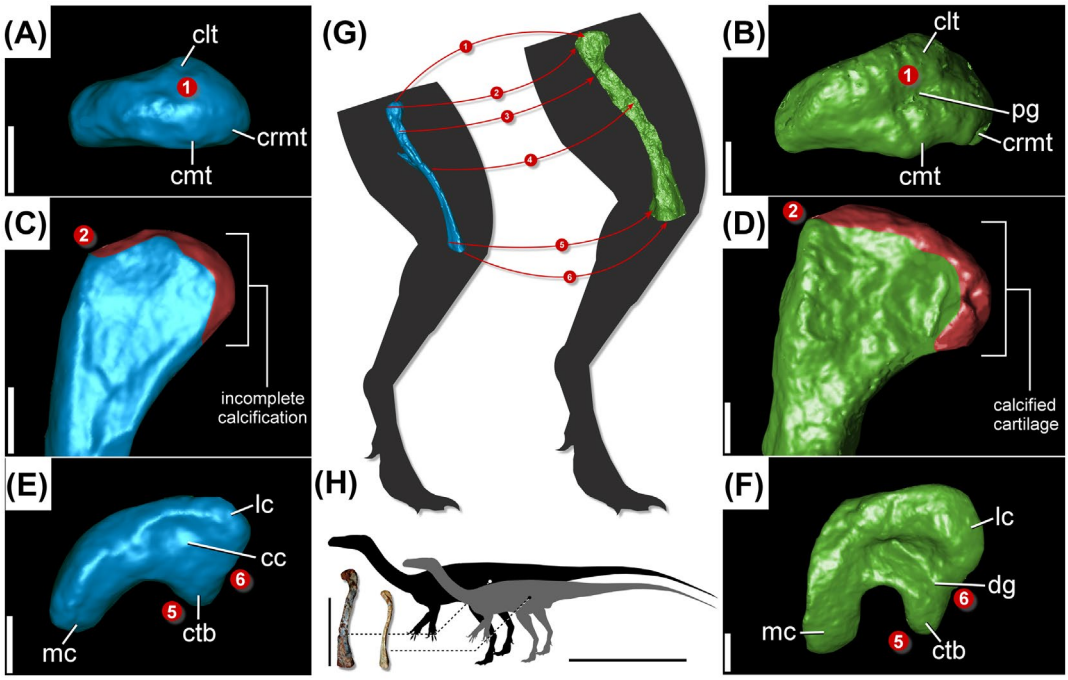

Figure 4. Comparison between 3D scan femora of CAPPA/UFSM 0028 and CAPPA/UFSM 0027: (A), proximal view of CAPPA/UFSM 0028; (B), proximal view of CAPPA/UFSM 0027; (C), caudal view of the proximal portion of CAPPA/UFMS 0028; (D), caudal view of the proximal portion of CAPPA/UFMS 0027; (E), distal view of CAPPA/UFSM 0028; (F), distal view of CAPPA/UFSM 0027; (G), illustrated summary of main modifications related to ontogeny between the specimens; (H), size comparison between CAPPA/UFSM 0028 (grey) and UFSM 0027 (black) based in femoral proportions.

Abbreviations: cc, concavity; clt, craniolateral truber; cmt, caudomedial tuber; crmt, craniomedial tuber; ctb, crista tibiofibularis; lc, lateral condyle; mc, medial condyle; dg, distal groove. Note: the number 1 indicates the change related to the proximal surface (proximal groove); 2 indicates the form of the greater trochanter; 3 indicates the caudolateral extension of the trochanteric shelf; 4 indicates the development degree of the linea intermuscularis cranialis; 5 indicates the development degree of the crista tibiofibularis; 6 indicates the formation of the distal groove. Scale bars = 5 mm in A, B, C, D, E, F, 100 mm in femora and 500 mm in silhouettes of H.

According to Langer and Ferigolo (2013), the difference between a notch and emargination reflects only greater expansion of the head. A smooth transition occurs in lagerpetids and *Marasuchus lilloensis*, whereas the notch is found in silesaurids, and a concave emargination in dinosaurs (Nesbitt 2011). CAPPA/UFSM 0028 bears a smooth transition, but more detailed observation indicates the presence of an arcuate line setting the shaft/head boundary (Figures 2(A) and 3(A)); this closely resembles the concave emargination diagnostic for dinosaurs but could also reflects ontogenetic immaturity. Indeed, the craniomedial portion of the femoral head is characterized by a rough and irregular surface, indicating that the epiphyseal cartilage was not yet ossified. This, together with the extreme mediolateral compression, affected the shape of the femoral head.

Although CAPPA/UFSM 0028 lacks obvious dinosaur synapomorphies, a combination of traits suggests affinities with *Pampadromaeus barberenai*. CAPPA/UFSM 0028 was derived from the same site that yielded both holotype and a referred femur of *P. barberenai* (Müller et al. 2016), thus it is plausible that all these elements represent the same taxon. Among coeval Brazilian dinosauriforms, CAPPA/UFSM 0028 shares some exclusive features with *P. barberenai*. (1) The 'sulcus for the *ligamentum capitis femoris*' is narrow due the position of the caudomedial tuber (Figure 4(A)), whereas all coeval saurischians bear a wider sulcus (Müller et al. 2016). (2) The proximal portion of the cranial trochanter is fully connected to the femoral shaft (Figure 2(B)), whereas a cleft is evident between the trochanter and the femoral shaft in *Saturnalia tupiniquim* (Langer 2003). (3) A well-developed craniomedial crest extends between the craniomedial tuber and the cranial trochanter (Figures 2(A) and 3(A)), whereas the homologous surface is less prominent in other coeval dinosauriforms, such as *Saturnalia tupiniquim*, *Staurikosaurus pricei*, and *Buriolestes schultzi* (Langer 2003; Bittencourt and Kellner 2009; Cabreira et al. 2016). (4) The crista tibiofibularis is reduced (Figure 4(E)), which represents a demonstrable autapomorphy of *P. barberenai* (Müller et al. 2016).

Ontogenetic patterns of Pampadromaeus barberenai

We interpret CAPPA/UFSM 0028 as an immature individual of *Pampadromaeus barberenai*. The holotype femora of this taxon (ULBRA-PVT016) are fractured but show similar proportions. The referred femur CAPPA/UFSM 0027 is about 142 mm long (comparable to ULBRA-PVT016). In contrast, CAPPA/UFSM 0028 is only 113 mm long and thus belongs to a substantially smaller individual. However, Griffin and Nesbitt (2016a) demonstrated that individuals of *Asilisaurus kongwe* reached maturity at different body sizes. ULBRA-PVT016 and CAPPA/UFSM 0027) are, nevertheless, still considered more mature than CAPPA/UFSM 0028 because both have fully ossified articular surfaces and well-developed muscle attachment structures (see comparison below). In addition, ULBRA-PVT016 also has well-formed bone surface texturing, which is not visible in CAPPA/UFSM 0027 because of poor preservation.

In contrast to the minor variation found in femoral head morphologies of *Dromomeron gregorii* (Nesbitt et al. 2009a), the craniomedial tuber of CAPPA/UFSM 0028 is reduced (Figure 4(A)) and lacks a medially descending bone wall (Figure 4(C))

otherwise present in CAPPA/UFSM 0027 (Figure 4(D)). In CAPPA/UFSM 0027, a shelf connects the craniomedial and caudomedial tuberosities (Figure 4(D)), but is absent in the proximal articular surface of CAPPA/UFSM 0028 (Figure 4(C)). The craniolateral tuber is also taller and more prominent in the osteologically more mature specimens. In contrast, the entire periphery of the proximal articular surface is poorly developed in CAPPA/UFSM 0028. This condition could explain weaker tuberosity development and the absence of a groove on the proximal end of the femur of CAPPA/UFSM 0028 (Figure 4(A)); this structure is likewise poorly developed in a small individuals (AbIII/457L) of *Silesaurus opolensis* (Dzik 2003), but well-incised in larger specimens [see the figure 9 of Piechowski et al. (2014)]. Finally, CAPPA/UFSM 0028 lacks a ventrally descended *facies articularis antitrochanterica* on the proximal portion of the femur (Figure 4(C)).

The greater trochanter of CAPPA/UFSM 0028 possesses a rounded shape (Figure 4(C)), unlike the more angular trochanters of the larger specimens (Figure 4(D)). All three share a 'sharply-ridged' dorsolateral trochanter. In contrast, Nesbitt (2011) and Piechowski et al. (2014) showed that only the smaller femora of *S. opolensis* conformed to this morphology, whereas larger femora of the same taxon have a rounded ridge. In addition, Griffin and Nesbitt (2016a) demonstrated that this ridge is absent in smaller femora attributed to *A. kongwe*, but becomes more developed, and also changes in shape and position with increasing body size.

The larger specimens of *P. barberenai* have a well-developed trochanteric shelf, but this structure is not visible on the smaller individual because the distal portion of the craniad trochanter is badly fractured (Figure 2(A)). Irrespectively, we suggest that the trochanteric shelf was probably poorly developed because it does not reach the preserved caudolateral corner of the femoral shaft. Indeed, Raath (1990) ascribed the presence of a trochanteric shelf to sexual dimorphism in *Syntarsus rhodensis*, while Nesbitt et al. (2009a) stated that it is present in larger, but not in smaller individuals of *D. gregorii*. Piechowski et al. (2014) argued that the trochanteric shelf appears only in larger specimens of *S. opolensis*, and followed Raath (1990) in concluding that this feature might be related to ontogeny and/or sexual dimorphism. Recently, Griffin and Nesbitt (2016a) recognized the absence of the trochanteric shelf in smaller specimens of *A. kongwe*.

Nesbitt et al. (2009a) identified the *linea intermuscularis cranialis* only in the largest specimen (TMM 31100-1306) of *D. gregorii*. A series of faint striations on the craniad surface of the mid-shaft in CAPPA/UFSM 0028 might correspond to an early developmental stage of this intermuscular line. Indeed, it is not as long as in the larger individuals, and does not form a raised process as in ULBRA-PVT016. Other intermuscular lines are absent in CAPPA/UFSM 0028. Like ULBRA-PVT016, CAPPA/UFSM 0028 bears a foramen on the craniad surface of the proximal half of the bone (Figure 2(A)).

The distal end of the crista tibiofibularis is slightly more caudally projected in the larger individuals (Figure 4(F)). This conforms with the observations of Nesbitt et al. (2009a), who suggested that an increase in the size of the distal condyles occurred with ontogeny in *D. gregorii*. The surface between the lateral condyle and the crista tibiofibularis also forms only a shallow concavity and does not extend to the caudolateral corner of the bone in CAPPA/UFSM 0028 (Figure 4(E)). In contrast, CAPPA/UFSM 0027 has a deep and well marked groove that extends to the caudolateral corner of the bone and separates the crista tibiofibularis from the lateral condyle (Figure 4(F)). Rough muscle scars are observable all over the outer surfaces of both femora of ULBRA-PVT016, and include the cranial trochanter, trochanteric shelf, dorsolateral trochanter, and the lateral surface on the distal end of the femur. On the other hand, CAPPA/UFSM 0028 does not show any muscle scars in these areas.

Ontogenetic implications on character polarization

The Bittencourt et al. (2015) data-set includes 291 morphological characters, of which 27 (about 9% of the total character number) are related to the femur. Of these, characters 228, 231, and 236 score differently for CAPPA/UFSM 0028 vs. CAPPA/UFSM 0027 and ULBRA-PVT016. For example, the ventrally descended 'facies articularis antitrochanterica' on the femoral head (character 228) is absent in CAPPA/UFSM 0028 (Figure 4(C)), but present in the other specimens referred to *Pampadromaeus barberenai* (Figure 4(D)). The transverse groove on the proximal surface of the femoral head (character 231) is likewise absent in CAPPA/UFSM 0028 (Figure 4(A); compare with Figure 4(B)). The groove between the lateral condyle and crista tibiofibularis on the distal surface of the femur (character 236) is shallow and does not divide the lateral condyle and crista tiobiofibularis in CAPPA/UFSM 0028 (Figure 4(E)); it is alternatively deep in *P. barberenai* (Figure 4(F)). Finally, a trochanteric shelf (character 227) is present in *P. barberenai* but may be absent in CAPPA/UFSM 0028 (see above). These differences correspond to 13.63% of the comparable femoral scores (17.39% if the trochanteric shelf character is considered). All these features are located in bone portions usually affected by the maturation degree of the individual (e.g. Holliday et al. 2010; Griffin and Nesbitt 2016b). Therefore is possible that they are related to ontogeny.

Amongst the 26 femoral characters coded for *P. barberenai* (CAPPA/UFSM 0027 and ULBRA-PVT016) and *Saturnalia tupiniquim*, only two (= 7.69%) have substantially different scores. The same percentage is recovered in comparison to *Eoraptor lunensis*, with 1 differently and 12 identical character scores. To *Eodromaeus murphi* 18 characters are equally coded, and 1 (= 5.26%) differently scored. The difference with *Herrerasaurus lunensis* is 11.53%, with 3 distinct entries out of 26 scored characters. This contrasts with the 4% of difference recovered in the comparison with *Staurikosaurus pricei*, where 1 coding out of 25 is distinct from those of *P. barberenai*. Accordingly, the highest difference in scoring occurs between the two ontogenetic stages of *P. barberenai* (13.63%) (Figure 5). On the other hand, the 11 comparable characters between *E. lunensis* and CAPPA/UFSM 0028 are equally scored. From the 16 comparable characters between *E. murphi* and CAPPA/UFSM 0028, only 1 (6%) is scored differently. *Staurikosaurus pricei* differs in 2 (10%) of the 20 comparable characters, while *H. ischigualastensis* has 18% difference (4 of the 22 comparable characters) scored for this specimen. Finally, the difference with *S. tupiniquim* is 22% (5 of the 22 comparable characters).

The results of the disparity analysis place CAPPA/UFSM 0028 within the morphospace of saurischian dinosaurs (Figure 6). However, CAPPA/UFSM 0028 lies outside of sauropodomorph morphospace, and is distant from *P. barberenai* as opposed to *Eoraptor lunensis* and *Eodromaeus murphi*.

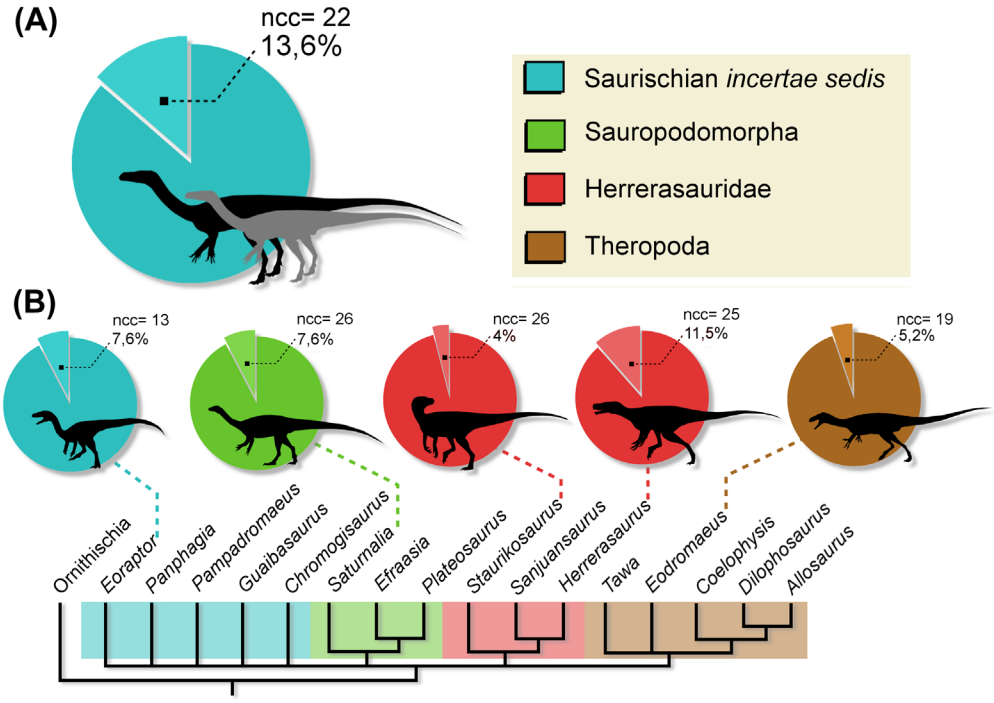

Figure 5 Ontogenetic influence on the polarization of femoral characters: (A), percentage of difference between *Pampadromaeus barberenai* and the immature individual (CAPPA/UFSM 0028); (B), percentage of difference between *Pampadromaeus barberenai* and related basal saurischians plotted in a simplified strict consensus tree from Bittencourt et al. (2015).
Abbreviation: ncc, number of comparable characters.

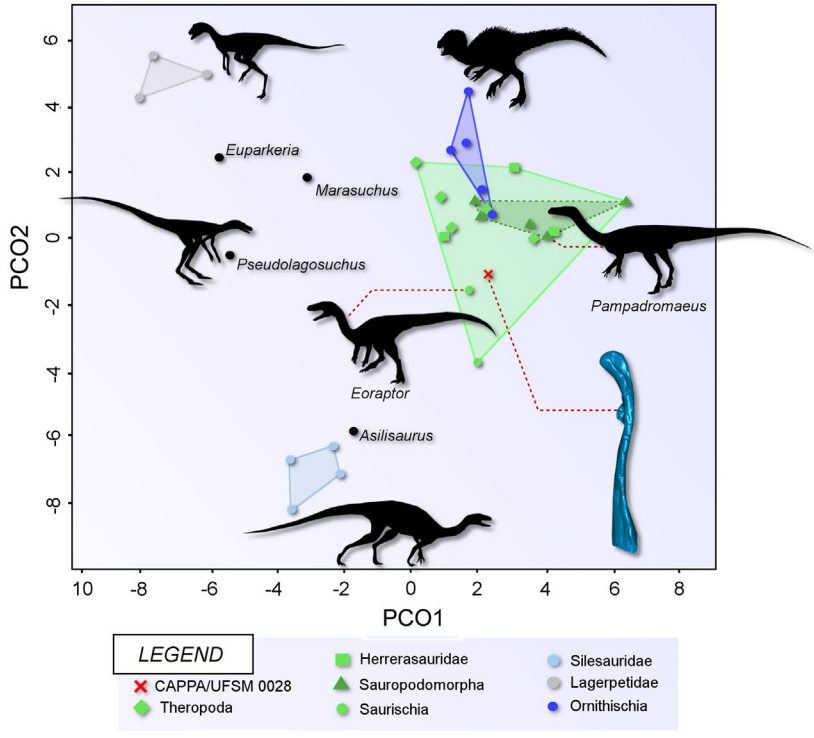

Figure 6. Bivariate plot showing the results of the morphospace occupation analysis.
Note: light green polygon, saurischians; dark green, sauropodomorphs; light blue, silesaurids; dark blue, ornithischians; grey, lagerpetids.

Ontogenetic influence on the phylogenetic relationships

A heuristic search on the modified data matrix resulted in six most parsimonious trees (MPTs) of 778 steps (Consistency Index = 0.43; Retention Index = 0.60), while the original analysis resulted in 27 MPTs of 781 steps (Bittencourt et al. 2015). In contrast to Bittencourt et al. (2015), the saurischian branch does not include an initial polytomy (Figure 7). *Pampadromaeus barberenai* is placed as the sister taxon of all other sauropodomorphs (Figure 7(B)), as proposed by Cabreira et al. (2011). *Guaibasaurus candelariensis*, *Panphagia protos* (Martinez & Alcober, 2009), and *Chromogisaurus novasi* (Ezcurra 2010) are also recovered within Sauropodomorpha (Figure 7(B)). Herrerasauridae and *Eoraptor lunensis* are nested within Theropoda (Figure 7(B)). Another difference is the position of *Asilisaurus kongwe* (Nesbitt et al. 2010), which was found here as the sister-group of all other Silesauridae (Figure 7(B)). In the original analysis the dorsolateral trochanter formed by a sharp ridge (state '1' of character 223) corresponds to one of the synapomorphies that support a dinosauriform clade more derived than *Marasuchus liloensis*. This does not correspond to a synapomorphy for the same group in the new analysis. Another synapomorphy from the original study that was not recovered here includes the dorsolateral trochanter formed by a rounded ridge (state '2' of character 223). This provides support to Sauropodomorpha, which includes *Saturnalia tupiniquim*, *Efraasia minor*, and *Plateosaurus* sp. in the analysis of Bittencourt et al. (2016), while our analysis recovered a more inclusive Sauropodomorpha (Figure 7(B)). The absence of a trochanteric shelf (state '0' of character 227) is not a synapomorphy to the node supporting *Plateosaurus* sp. and *Efraasia minor* in the former analysis, contrasting with the present results. In addition, the presence of a trochanteric shelf on the femur (state '1' of character 227) supports Dinosauriformes in this new analysis but not in the first one.

Discussion

Morphological features of CAPPA/UFSM 0028, including the shape of the proximal and distal ends of the femur, match those of immature individuals, such as *Struthio camelus*, *Megapnosaurus rhodesiensis*, and *Pteranodon* sp. (Bennett 1993; Holliday et al. 2010; Griffin and Nesbitt 2016b). As such, the ossification degree might explain conflicting osteological features, although sexual dimorphism and intraspecific variation could also influence shape (see Raath 1990; Piechowski et al. 2014). Indeed, features such as the absence of grooves on the proximal and distal ends of the femur and the lack of a ventrally descended 'facies articularis antitrochanterica' can be assigned to the incomplete calcification of cartilage around the articulations. In any case, our analyses suggest that femoral traits in an osteologically immature individual contrast with ontogenetically mature conspecifics more than with other phylogenetically distinct taxa. Actually, Müller (2017) obtained percentages similar to those recovered here, gathered from small and large specimens of two species of dinosauromorphs (16% to *Dromomeron gregorii* and 13% to *Silesaurus opolensis*). Curiously, in our study, femoral scores were identical to *Eoraptor lunensis* and only manifest 6% difference relative to *E. murphi*. However, both species share few common characters with CAPPA/UFSM 0028. Based on the data presented here and previous contributions (Nesbitt et al. 2009a; Nesbitt 2011; Piechowski et al. 2014) it is possible to conclude that at

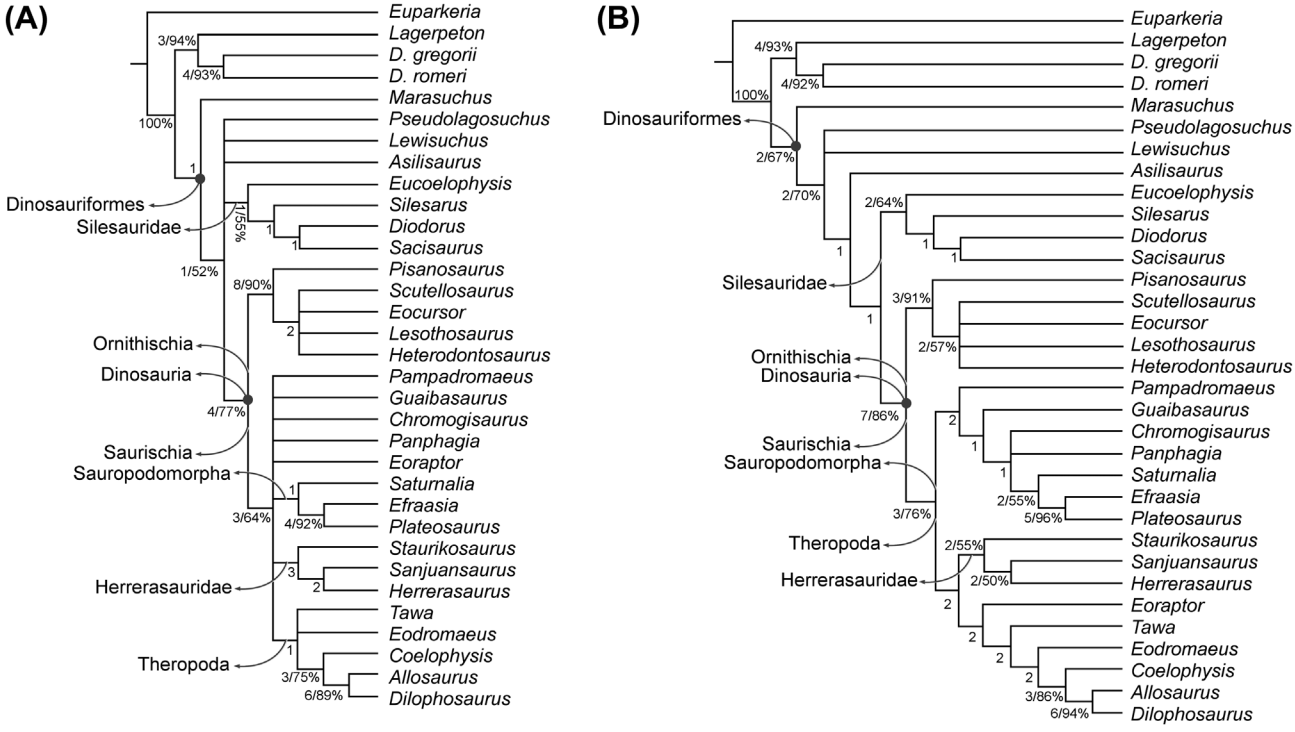

Figure 7. Comparison between the strict consensus tree of 27 most parsimonious trees of Bittencourt et al. (2015) (A) and the strict consensus tree of the 6 most parsimonious trees recovered here (B).

Note: values associated with nodes correspond to Bremer support and bootstrap proportions (above 50%).

least 27% of the femoral characters codified in the data matrix of Bittencourt et al. (2015) are susceptible to misinterpretation as a result of ontogenetic variation.

Although most phylogenetic studies on early dinosaurs and related groups comprise rigorous cladistics methodologies (Benton et al. 2014), their relationships are still controversial (Langer 2014). We consider that the lack of ontogenetic control might partially explain this situation, as ontogenetic series are still extremely scarce for most taxa (Nesbitt et al. 2009a). Indeed, there is evidence that some valid early dinosaur taxa comprise immature individuals. This is the case for *Guaibasaurus candelariensis* (Bonaparte et al. 1999), in which both the holotype (MCN PV2355) and the referred specimen (UFRGS PV0725T) possess unfused neurocentral sutures on the dorsal and caudal vertebrae; see Brochu (1996) and Irmis (2007) for discussions on the significance of these traits. Similarly, the epiphyses of the holotype and the metatarsal ends of the paratype (MCN PV2356) are either incompletely ossified or damaged by preparation (Langer et al. 2011). *Staurikosaurus pricei* (Colbert 1970; Bittencourt and Kellner 2009; Ezcurra 2010; Nesbitt 2011) also displays features suggesting that the only known specimen (MCZ 1669) is less ontogenetically developed than other herrerasaurids including *Herrerasurus ischigualastensis* (Reig 1963) and *Sanjuansaurus gordilloi* (Alcober and Martínez 2010). These two taxa exhibit a well-developed trochanteric shelf on the femur, which is absent or considerably reduced in the holotype of *S. pricei* (Bittencourt and Kellner 2009). Also, the lack of a deep groove dividing the lateral condyle from the crista tibiofibularis on the distal end of the femur may be related to incomplete ossification. This accords with the small size of the specimen relative to other herrerasaurids: the femoral length of MCZ 1669 is 220 mm (Carrano 2006), compared to 482 mm in *H. ischigualastensis* (Carrano 2006) and 395 mm in *S. gordilloi* (Alcober and Martínez 2010).

Recently, Barrett et al. (2015) described a large sized silesaurid femur estimated at 345.8 ± 50 mm in length. Until then, the largest femur recorded in the group belonged to *Silesaurus opolensis*, reaching about 210 mm (Piechowski et al. 2014). All known femora of *Sacisaurus agudoensis* from southern Brazil (Feirolgo and Langer 2007) are approximately half the length of those recovered for *S. opolensis* (Langer and Ferigolo 2013). This could imply that the holotype of *S. agudoensis* is osteologically immature. Actually, Piechowski et al. (2014) suggested that a distinct tuberosity and lack of a trochanteric shelf on the femora of *S. agudoensis* were indicative juvenile or male individuals. In addition, Langer and Ferigolo (2013) recognized the presence of a striated area on the distal portion of some femora of *S. agudoensis*. This resembles the condition found in the osteologically immature remains described here.

The aforementioned cases are examples of the scarcity of ontogenetic control on early dinosaurs and related groups, generally occurring in response to limited sampling. However, ontogenetic markers as body size, opening of neurocentral sutures, and robustness of the trochanteric shelf are not unambiguous. Therefore, new specimens, as well as future studies based on bone histology will probably help this matter. Fortunately, recent contributions (e.g. Nesbitt et al. 2009a; Piechowski et al. 2014; Griffin and Nesbitt 2016a, 2016b) are shedding light on the morphologic pathways of dinosauromorphs along their development, which is crucial to access reliable phylogenetic affinities and macroevolutionary patterns (e.g. Brusatte et al. 2008a, 2008b). Among these studies, that of Griffin and Nesbitt (2016b) particular demonstrates that an extremely high amount of intraspecific variation was evident in early dinosaurs and their relatives. In addition, Wang et al. (2017) noted that inclusion of osteologically immature specimens compromises topological resolution, and corroborates Sharma et al. (2016) who found that the inclusion of distinct developmental stages as terminal taxa does not provide reliable phylogenetic information. On the other hand, Sharma et al. (2016) also argued that phylogenetic trees with fossil taxa are valid if ontogenetic stages are easy to detect. Ontogenetic variation can otherwise be accommodated by scoring polymorphisms for 'juvenile' versus 'adult' states; however, we advocate caution and suggest that ontogenetic variation should be continuously revaluated as new fossils come to light.

Conclusions

CAPPA/UFM 0028 derived from an osteologically immature dinosauriform consistent with *Pampadromaeus barberenai*. Comparisons with other specimens reveals reduced tuberi, the absence of a transverse groove on the proximal end of the femur, and a ventrally descended 'facies articularis antitrochanterica'; features that are alternatively present in more osteologically mature individuals. The trochanteric shelf is absent or badly developed in CAPPA/UFM 0028, but alternatively prominent in 'adults', in which the linea intermuscularis cranialis forms a raised process. Furthermore, the deep groove separating the lateral condyle from the crista tiobiofibularis on the distal end of the femur is only observed in 'adult' examples. The dorsolateral, cranial, and fourth trochanters are present in all evaluated specimens.

Analyses of morphological variation using a published phylogenetic detatset of Bittencourt et al. (2015) found considerable disparity between the putative 'juvenile' and 'adult' specimens of *P. barberenai*, and more so relative to indirectly related taxa. Modifications to the scoring of femoral characters influenced by ontogeny returned conflicting topologies. We therefore conclude that ontogenetic assessment of additional skeletal elements might improve the current understanding of early dinosaur relationships.

Acknowledgements

The authors thank Leonardo R. Kerber (CAPPA/UFSM) and Flávio A. Pretto (CAPPA/UFSM) for the 3D scans of the specimen studied here. We are grateful to Matthew Wills (University of Bath) for the software MATRIX. We thank the Willi Henning Society, for the gratuity of TNT software.

Disclosure statement

The authors have no financial interests relating to this paper.

Funding

This work was supported by a Coordenação de Aperfeiçoamento de Pessoal de Nível Superior (CAPES) scholarship for RTM and CPP, by Fundação de Amparo à Pesquisado Estado de São Paulo FAPESP [grant number 2014/03825-3 to MCL], and by Conselho Nacional de Desenvolvimento Científco e Tecnológico CNPq [research grant to SDS, process number 306352/2016-8].

ORCID

Rodrigo Temp Müller http://orcid.org/0000-0001-8894-9875
Max Cardoso Langer http://orcid.org/0000-0003-1009-4605

References

Alcober OA, Martínez RN. 2010. A new herrerasaurid (Dinosauria, Saurischia) from the Upper Triassic Ischigualasto formation of northwestern Argentina. ZooKeys. 63:55–81.
Barrett PM, Nesbitt SJ, Peecook BR. 2015. A large-bodied silesaurid from the Lifua member of the Manda beds (Middle Triassic) of Tanzania and its implications for body-size evolution in Dinosauromorpha. Gondwana Research. 27:925–931.
Bennett SC. 1993. The ontogeny in *Pteranodon* and other pterosaurs. Paleobiology. 19:92–106.
Bennett SC. 2015. An external mandibular fenestra and other archosauriform characters in basal pterosaurs re-examined. Historical Biology. 27:796–814.
Benton MJ, Forth J, Langer MC. 2014. Models for the rise of the dinosaurs. Current Biology. 24:87–95.
Bittencourt JS, Kellner AWA. 2009. The anatomy and phylogenetic position of the Triassic dinosaur *Staurikosaurus pricei* Colbert, 1970. Zootaxa. 2079:1–56.
Bittencourt JS, Arcucci AB, Marscicano CA, Langer MC. 2015. Osteology of the Middle Triassic archosaur *Lewisuchus admixtus* Romer (Chañares Formation, Argentina), its inclusivity, and relationships amongst early dinosauromorphs. J Syst Palaeontol. 13:189–219.
Bonaparte JF, Ferigolo J, Ribeiro AM. 1999. A new early Late Triassic saurischian dinosaur from Rio Grande do Sul State, Brazil. National Sci Museum Monographs. 15:89–109.
Bouxin G. 2005. Ginkgo, a multivariate analysis package. J Vegetation Sci. 16:355–359.
Brochu CA. 1996. Closure of neurocentral sutures during crocodilian ontogeny: Implications for maturity assessment in fossil archosaurs. J Vertebr Paleontol. 16:49–62.
Brown B, Schlaikjer EM. 1940. The structure and relationships of *Protoceratops*. Ann NY Acad Sci. 40:133–265.
Brusatte SL, Benton MJ, Ruta M, Lloyd GT. 2008a. Superiority, competition, and opportunism in the evolutionary radiation of dinosaurs. Science. 321:1485–1488.
Brusatte SL, Benton MJ, Ruta M, Lloyd GT. 2008b. The first 50 Myr of dinosaur evolution: macroevolutionary pattern and morphological disparity. Biol Lett. 4:733–736.
Brusatte SL, Carr TD, Williamson TE, Holtz TR, Hone DW, Williams SA. Dentary groove morphology does not distinguish 'Nanotyrannus' as a valid taxon of tyrannosauroid dinosaur. Comment on: "Distribution of the dentary groove of theropod dinosaurs: Implications for theropod phylogeny and the validity of the genus Nanotyrannus Bakker et al, 2016. Cretaceous Res. 65:232–237.
Cabreira SF, Schualtz CL, Bittencourt JS, Soares MB, Fortier DC, Silva LR, Langer MC. 2011. New stem-sauropodomorph (Dinosauria, Saurischia) from the Triassic of Brazil. Naturwissenschafte. 98:1035–1040.
Cabreira SF, Kellner AWA, Dias-da-Silva S, Silva LC, Bronzati M, Marsola JC, Müller RT, Bittencourt JS, Batista BJ, Raugust T, et al. 2016. A unique Late Triassic dinosauromorph assemblage reveals dinosaur ancestral anatomy and diet. Curr Biol. 26:3090–3095.
Carrano MT. 2006. Body-size evolution in the Dinosauria. In: Carrano MT, Gaudin TJ, Blob RW, Wible JR, editors. Amniote paleobiology: perspectives on the evolution of mammals, birds, and reptiles. Chicago (IL): University of Chicago Press; p. 225–268.
Colbert EH. 1970. A saurischian dinosaur from the Triassic of Brazil. Am Museum Novitates. 2405:1–39.
Colbert EH. 1990. Variation in *Coelophysis bauri*. In: Carpenter K, Currie PJ, editors. Dinosaur systematics: approaches and perspectives. Cambridge: Cambridge University Press; p. 81–90.
Dzik J. 2003. A beaked herbivorous archosaur with dinosaur affinities from the early Late Triassic of Poland. J Vertebr Paleontol. 23:556–574.
Ezcurra MD. 2010. A new early dinosaur (Saurischia: Sauropodomorpha) from the Late Triassic of Argentina: a reassessment of dinosaur origin and phylogeny. J Syst Palaeontol. 8:371–425.
Feirolgo J, Langer MC. 2007. A late triassic dinosauriform from south brazil and the origin of the ornithischian predentary bone. Historical Biol. 19:23–33.
Goloboff PA, Farris JS, Nixon KC. 2008. TNT, a free program for phylogenetic analysis. Cladistics. 24:774–786.
Griffin CT, Nesbitt SJ. 2016a. The femoral ontogeny and long bone histology of the Middle Triassic (?late Anisian) dinosauriform *Asilisaurus kongwe* and implications for the growth of early dinosaurs. J Vertebrate Paleontol. 36:e1111224.
Griffin CT, Nesbitt SJ. 2016b. Anomalously high variation in postnatal development is ancestral for dinosaurs but lost in birds. Proc Nat Acad Sci. 113:14757–14762.
Hammer Ø, Harper DAT, Ryan PD. 2001. PAST: paleontological statistics software package for education and data analysis. Palaeontologica Electronica. 4:1–9.
Holliday CM, Ridgely RC, Sedlmayr JC, Witmer LM. 2010. Cartilaginous epiphyses in extant archosaurs and their implications for reconstructing limb function in dinosaurs. PLoS One. 5(9):e13120.
Holz M, Schultz CL. 1998. Taphonomy of the Brazilian Triassic paleoherpetofauna: fossilization mode and implications for morphological studies. Lethaia. 31:335–345.
Hone DWE, Farke AA, Wedel MJ. 2016. Ontogeny and the fossil record: what, if anything, is an adult dinosaur? Biol Lett. 12:20150947.
Horn BLZ, Melo TM, Schultz CL, Philipp RP, Kloss HP, Goldber K. 2014. A new third-order sequence stratigraphic framework applied to the Triassic of the Paraná Basin, Rio Grande do Sul, Brazil, based on structural, stratigraphic and paleontological data. J South Amer Earth Sci. 55:123–132.
Randall B. Irmis. Axial skeleton ontogeny in the Parasuchia (Archosauria: Pseudosuchia) and its implications for ontogenetic determination in archosaurs. Journal of Vertebrate Paleontology. 2007; 27(2) 350-361.
Johnson R. 1977. Size independent criteria for estimating relative age and the relationships among growth parameters in a group of fossil reptiles (Reptilia: Ichthyosauria). Can J Earth Sci. 14:1916–1924.
Kear BP, Zammit M. 2014. In utero foetal remains of the Cretaceous ichthyosaurian *Platypterygius*: ontogenetic implications for character state efficacy. Geol Mag. 151:71–86.
Langer MC. 2003. The pelvic and hind limb anatomy of the stem-sauropodomorph *Saturnalia tupiniquim* (Late Triassic, Brazil). PaleoBios. 23:1–30.
Langer MC. 2014. The origins of Dinosauria: much ado about nothing. Palaeontology. 57:469–478.
Langer MC, Abdala F, Richter M, Benton MJ. 1999. A sauropodomorph dinosaur from the Upper Triassic (Carnian) of Southern Brazil. Comptes Rendus de l'Académie des Sciences-Series IIA-Earth and Planetary Sci. 329:511–517.
Langer MC, Bittencourt JS, Schultz CL. 2011. A reassessment of the basal dinosaur *Guaibasaurus candelariensis*, from the Late Triassic Caturrita Formation of south Brazil. Earth Environ Sci Trans R Soc Edinburgh. 101:301–332.
Langer MC, Ferigolo J. 2013. The Late Triassic dinosauromorph *Sacisaurus agudoensis* (Caturrita Formation; Rio Grande do Sul, Brazil): anatomy and affinities. Geol Soc, London, Spec Publ. 379:353–392.
Martínez RN, Sereno PC, Alcober OA, Colombi CE, Renne PR, Montañez IP, Currie BS. 2011. A basal dinosaur from the dawn of the dinosaur era in southwestern Pangaea. Science. 331:201–210.
Müller RT. 2017. Are the dinosauromorph femora from the Upper Triassic of Hayden Quarry (New Mexico) three stages in a growth series of a single taxon? Anais da Academia Brasileira de Ciências. 82:835–839.
Müller RT, Langer MC, Cabreira SF, Dias-da-Silva S. 2016. The femoral anatomy of *Pampadromaeus barberenai* based on a new specimen from the Upper Triassic of Brazil. Historical Biol. 28:656–665.
Nesbitt SJ. 2011. The early evolution of archosaurs: relationships and the origin of major clades. Bull Am Museum Nat History. 352:1–292.
Nesbitt SJ, Irmis RB, Parker WG, Smith ND, Turner AH, Rowe T. 2009. Hindlimb osteology and distribution of basal dinosauromorphs from the Late Triassic of North America. J Vertebrate Paleontol. 29:498–516.

Nesbitt SJ, Sidor CA, Irmis RB, Angielzcyk KD, Smith RM, Tsuji LA. 2010. Ecologically distinct dinosaurian sister group shows early diversification of Ornithodira. Nature. 464:95–98.

Piechowski R, Tałanda M, Dzik J. 2014. Skeletal variation and ontogeny of the Late Triassic Dinosauriform *Silesaurus opolensis*. J Vertebrate Paleontol. 34:1383–1393.

Pretto FA, Schultz CL, Langer MC. 2015. New dinosaur remains from the Late Triassic of southern Brazil (Candelária Sequence, *Hyperodapedon* Assemblage Zone). Alcheringa. 39:264–273.

Raath MA. 1990. Morphological variation in small theropods and its meaning in systematics: evidence from *Syntarsus rhodesiensis*. In: Carpenter K, Currie PJ, editors. Dinosaur systematics: approaches and perspectives. Cambridge: Cambridge University Press; p. 91–106.

Raath MA. 1969. A new coelurosaurian dinosaur from the Forest Sandstone of Rhodesia. Arnoldia Rhodesia. 4:1–25.

Rauhut OW, Foth C, Tischlinger H, Norell MA. 2012. Exceptionally preserved juvenile megalosauroid theropod dinosaur with filamentous integument from the Late Jurassic of Germany. Proc Nat Acad Sci. 109:11746–11751.

Reig OA. 1963. La presencia de dinosaurios saurisquios en los "Estratos de Ischigualasto" (Mesotriásico Superior) de las provincias de San Juan y La Rioja (Republica Argentina). Ameghiniana. 3:3–20.

Sekiya T, Jin X, Zheng W, Shibata M, Azuma Y. 2014. A new juvenile specimen of *Yunnanosaurus robustus* (Dinosauria: Sauropodomorpha) from Early to Middle Jurassic of Chuxiong Autonomous Prefecture, Yunnan Province. China Historical Biol. 26:252–277.

Sereno PC, Forster CA, Robers RR, Monetta AM. 1993. Primitive dinosaur skeleton from Argentina and the early evolution of the Dinosauria. Nature. 361:64–66.

Sharma PP, Clouse RM, Wheller WC. 2016. Hennig's semaphoront concept and the use of ontogenetic stages in phylogenetic reconstruction. Cladistics. 33:93–108.

Steyer JS. 2000. Ontogeny and phylogeny in temnospondyls: a new method of analysis. Zool J Linn Soc. 130:449–467.

Trotteyn MJ, Martínez RN. 2013. First record of coxofemoral dysplasia in a Late Triassic rynchosaur. Ameghiniana. 50:217–226.

Tumarkin-Deratzian AR. 2009. Evaluation of long bone surface textures as ontogenetic indicators in centrosaurine ceratopsids. Anatomical Record. 292:1485–1500.

Tumarkin-Deratzian AR, Vann DR, Dodson P. 2006. Bone surface texture as an ontogenetic indicator in long bones of the Canada goose *Branta canadensis* (Anseriformes: Anatidae). Zool J Linn Soc. 148:133–168.

Vega-Dias C, Maisch MW, Schwanke C. 2005. The taxonomic status of *Stahleckeria impotens* (Therapsida, Dicynodontia): redescription and discussion of its phylogenetic position. Revista Brasileira de Paleontologia. 8:221–228.

Wang S, Stiegler J, Amiot R, Wang X, Du G, Clark JM, Xu X. 2017. Extreme ontogenetic changes in a ceratosaurian theropod. Curr Biol. 27:1–5.

Watanabe J, Matsuoka H. 2013. Ontogenetic change of morphology and surface texture of long bones in the *Gray heron* (Ardea cinerea, Ardeidae). In: Gohlich UB, Kroh A, editors. Proc 8th Int Meeting Soc Avian Paleontol Evol. Vienna: Verlag Naturhistorisches Museum; p. 279–306.

Wills MA. 1998. Cambrian and recent disparity: the picture from priapulids. Paleobiology. 24:177–199.

Zerfass H, Lavina EL, Schultz CL, Garcia AJV, Faccini UF, Chemale FJr. 2003. Sequence stratigraphy of continental Triassic strata of Southernmost Brazil: a contribution to Southwestern Gondwana palaeogeography and palaeoclimate. Sedimentary Geol. 161:85–105.

Zerfass H, Sander A, Flores AF. 2007. Agudo, Folha SH22-VCV, escala 1:100000, Rio Grande do Sul. Brasília: Serviço Geológico do Brasil (CPRM).

Zhao Q, Benton MJ, Sullivan C, Sander PM, Xu X. 2013. Histology and postural change during the growth of the ceratopsian dinosaur *Psittacosaurus lujiatunensis*. Nat Commun. 4:2079.

5 ARTIGO III

Título: Under pressure: Effect of sedimentary compression on the iliac morphology of early sauropodomorphs

Autores: Rodrigo Temp Müller, Maurício Silva Garcia, Átila Augusto Stock da Rosa e Sérgio Dias da Silva

Periódico: Journal of South American Earth Sciences

Volume: 88

Páginas: 345-351

Ano: 2018

DOI: 10.1016/j.jsames.2018.09.005

Journal of South American Earth Sciences 88 (2018) 345–351

Contents lists available at ScienceDirect

Journal of South American Earth Sciences

journal homepage: www.elsevier.com/locate/jsames

Under pressure: Effect of sedimentary compression on the iliac morphology of early sauropodomorphs

Rodrigo Temp Müller[a,b,*], Maurício Silva Garcia[c], Átila Augusto Stock Da-Rosa[d], Sérgio Dias-da-Silva[b]

[a] Programa de Pós-Graduação em Biodiversidade Animal, Universidade Federal de Santa Maria, Av. Roraima, 1000, Bairro Camobi, 97105-900, Santa Maria, RS, Brazil
[b] Centro de Apoio à Pesquisa da Quarta Colônia, Universidade Federal de Santa Maria, Rua Maximiliano Vizzotto, 598, 97230-000, São João do Polêsine, RS, Brazil
[c] Curso de Ciências Biológicas, Centro de Ciências Naturais e Exatas, Universidade Federal de Santa Maria, Av. Roraima, 1000, Bairro Camobi, 97105-900, Santa Maria, RS, Brazil
[d] Laboratório de Estratigrafia e Paleobiologia, Universidade Federal de Santa Maria, 97105-900, Santa Maria, RS, Brazil

ARTICLE INFO

Keywords:
Brazil
Dinosauria
Saurischia
Taphonomy
Triassic
Western Gondwana

ABSTRACT

Sedimentary compression can produce deep changes in the organismal morphology during fossil diagenesis, so that intrinsic biological aspects (e.g. internal architecture of bones) could also generate non-natural traits when determinate bone element suffers sedimentary compression. Here we report a particular taphonomic case, in which the mode of preservation of a basal sauropodomorph from the Late Triassic of Brazil offers a valuable opportunity to examine the effects of sedimentary compression on a specific doubled body part of a single individual. The specimen is associated with two other almost complete and articulated individuals, comprising a monotypic association. The specimen herein studied presents the left ilium and hindlimb disarticulated from its body, where the right ilium was preserved with its ventral surface ventrally directed, and, conversely, the lateral surface of the left one was ventrally directed. Thus, their distinct placement in the substrate resulted in two distinct taphonomic histories reflected in their dissimilar shapes. This corresponds to a particular case of taphomorphic differences expressed in a single individual. Indeed, some of the peculiar traits of each ilium also occur in other specimens of close related taxa that experienced similar taphonomic histories. Sedimentary compression may produce dissimilar shapes in different portions of the skeleton, and incorrect observations generate what we call "taphoanatomical features", traits shared among close phylogenetic taxa/specimens resulting from similar taphonomic processes in response to specific biological aspects of the skeleton, not necessarily expressing phylogeny. Failing to recognize these trends could affect anatomical interpretations, especially regarding their role in a phylogenetic context.

1. Introduction

The establishment of a reliable alpha taxonomy demands great sampling efforts in order to minimize biases caused by morphological variation. Often related to intrinsic biological aspects (e.g. ontogeny, sexual dimorphism – Piechowski et al., 2014; Griffin and Nesbitt, 2016), anatomical variation in bone parts are also originated by extrinsic processes (e.g. diseases, predation – Trotteyn and Martínez, 2013). Moreover, non-biological factors also affect the shape of fossilized bones. Actually, taphonomic processes can produce drastic changes in the original morphology of any bone. For instance, Holz and Schultz (1998) demonstrated that cementation by calcite and hematite can produce conspicuous morphological and volumetric differences among specimens from the same taxonomic group, both affecting their internal and external structures. Similarly, White (2003) suggested expanding matrix distortion as the cause of putative misinterpretations regarding diversity of early hominids. Swelling, brittle (fractures, joints, and faults) or plastic deformation (folds) can distort bones during fossilization, depending on temperature, confining pressure, and strain rate (Arbour and Currie, 2012). Indeed, these alterations are so usual that a large number of fossilized organisms affected by these in various degrees. There are several examples of fossils from diverse taxonomic groups that present deformation by sedimentary compression (e.g. Ponce de León, 2002; Langer and Ferigolo, 2013; Pacheco et al., 2017). Nevertheless, it is also possible that in some cases non-natural traits formed by sedimentary compression may appear like intrinsic

* Corresponding author. Programa de Pós-Graduação em Biodiversidade Animal, Universidade Federal de Santa Maria, Av. Roraima, 1000, Bairro Camobi, 97105-900, Santa Maria, RS, Brazil.
E-mail address: rodrigotmuller@hotmail.com (R.T. Müller).

https://doi.org/10.1016/j.jsames.2018.09.005
Received 29 July 2018; Received in revised form 14 September 2018; Accepted 15 September 2018
Available online 18 September 2018
0895-9811/

biological aspects. For instance, does a peculiar skeletal feature shared between distinct but phylogenetically close taxa produce similar artificial traits when undergo a similar taphonomic history? Thus, the aim of this contribution is to report a particular taphonomic case in which, in which the mode of preservation of a basal sauropodomorph from the Late Triassic of Brazil offers a valuable opportunity to examine the effect of sedimentary compression on a single individual.

1.1. Institutional abbreviations

CAPPA/UFSM, Centro de Apoio à Pesquisa Paleontológica da Quarta Colônia da Universidade Federal de Santa Maria, São João do Polêsine, Brazil; **MCN**, Museu de Ciências Naturais, Fundação Zoobotânica do Rio Grande do Sul, Porto Alegre, Brazil; **NMMNH**, New Mexico Museum of Natural History and Science, Albuquerque, USA; **PVSJ**, Museo de Ciencias Naturales, Universidad Nacional de San Juan, San Juan Province, Argentina; **UFRGS**, Instituto de Geociências, Universidade Federal do Rio Grande do Sul, Porto Alegre, Brazil; **UFSM**, Coleção de Paleontologia, Laboratório de Estratigrafia e Paleobiologia, Universidade Federal de Santa Maria, Santa Maria, Brazil; **ULBRA**, Universidade Luterana do Brasil, Coleção de Paleovertebrados, Canoas, Brazil; **UMMP**, University of Michigan Museum of Paleontology, Ann Arbor, USA; **ZPAL**, Institute of Paleobiology of the Polish Academy of Sciences, Warsaw, Poland.

2. Material and methods

The specimen herein examined was quarried from the Wachholz site (Müller et al., 2015), at the municipality of Agudo, Rio Grande do Sul, Brazil (Fig. 1). This fossiliferous locality belongs to the upper portion of the Candelária Sequence (Horn et al., 2014) from the Santa Maria Supersequence (Zerfass et al., 2003), considered Norian (Late Triassic) in age (Müller et al., 2017; Langer et al., 2018). The specimen is housed at the Centro de Apoio à Pesquisa Paleontológica da Quarta Colônia (CAPPA/UFSM), São João do Polêsine, Brazil, under the code CAPPA/UFSM 0001b. It comprises an almost complete skeleton of a basal sauropodomorph dinosaur closely related to *Unaysaurus tolentinoi* (Leal et al., 2004; Müller et al., 2017). CAPPA/UFSM 0001b is associated with other two almost complete sauropodomorph specimens, comprising a monotypic association (Müller et al., 2015). Articulation is almost complete in these three individuals, but the left ilium and hindlimb of CAPPA/UFSM 0001b are disarticulated (Fig. 2), where the right ilium was preserved with its ventral surface ventrally directed, and, conversely, the lateral surface of the left one rested was ventrally directed. The elements from this association lack any signals of preburial abrasion, weathering, and breakage, which suggests a short timespan before the final burial.

As Müller et al. (2015) already pointed out that sedimentary compression deformed some bones from the Wachholz site, we observed that both ilia display distinct deformations as they rested in distinct positions. In order to evaluate this assumption in detail, distinct measurements (Fig. 3) and comparisons were performed in both elements, as follows: maximum height from the ventral margin of the peduncles to the dorsal margin of the iliac dorsal blade (i); maximum length from the cranial tip of the pubic peduncle to the caudal margin of the postacetabular ala (ii); acetabular height from the ventral margin of the ischiadic peduncle to the roof of the supra-acetabular crest (ii); iliac blade height from the roof of the supra-acetabular crest to the dorsal margin of the blade (iv); pubic peduncle width (v); and ischiadic peduncle width (vi). We also obtained the height of both ilia from two other specimens: CAPPA/UFSM 0001a and CAPPA/UFSM 0035, as both specimens do not present any sign of sedimentary compression in distinct angles, in an attempt to use them as "control samples" regarding CAPPA/UFSM 0001b. Moreover, we employed a comparative approach in order to list distinct discrete traits between both ilia from CAPPA/UFSM 0001b, possibly caused by taphonomic deformation. Thus, a 3D virtual model obtained by 3D scan using a ZScanner 700® with surface resolution of 0.2 mm was produced for each ilium. The features considered as taphonomic artifacts are those characterized by fractures, joints, and faults (Arbour and Currie, 2012), rather than a smooth bone surface. Finally, these features served as a model to find putative influence of sedimentary compression on the ilia from other specimens, in order to find a reliable tool help avoiding further perpetuation of misinterpretations due to taphonomic biases.

3. Geological setting

CAPPA/UFSM 0001b was preserved in alluvial sediments, in fluvial channels, below a 2–3 m package of overbank facies, constituted by fine sandstones deposited in a crevasse splay (Müller et al., 2015). There is no clear separation on the crevasse splays, to ensure that deposition took place immediately above the fluvial facies, such as paleosol

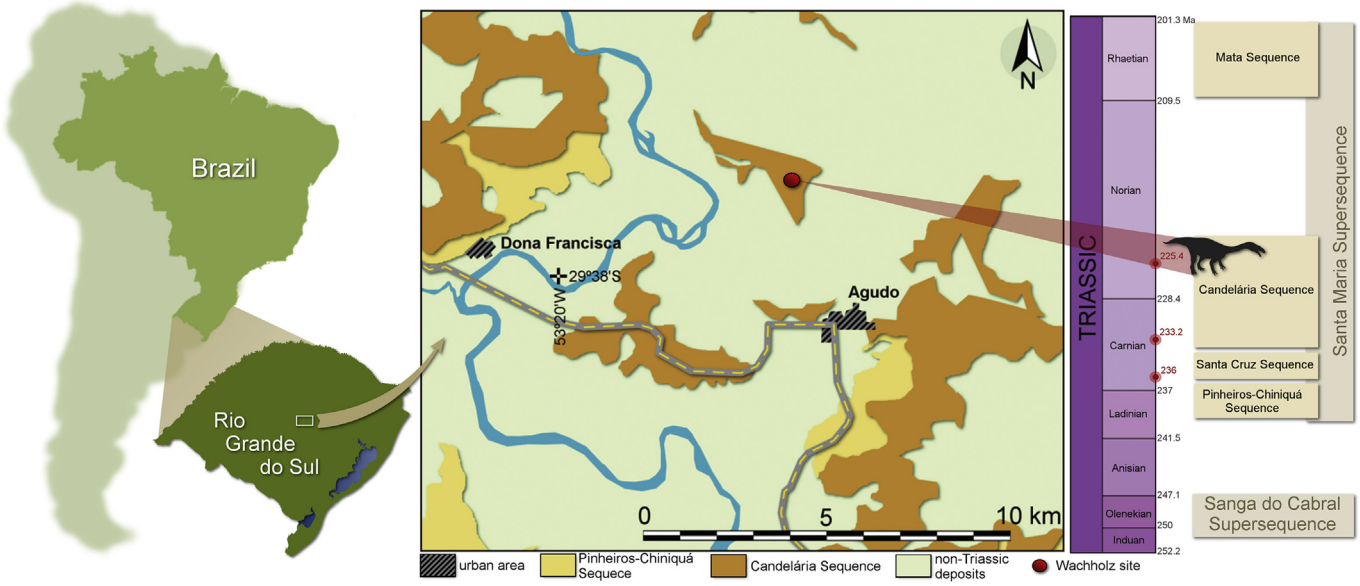

Fig. 1. Location of the Wachholz site and the Chronostratigraphy of the Triassic units from Southern Brazil, showing the level of CAPPA/UFSM 0001. Modified from Müller et al. (2018). The radiometric dating of 236, 233.2, and 225.4 Mya according to Philipp et al. (2013) and Langer et al. (2018).

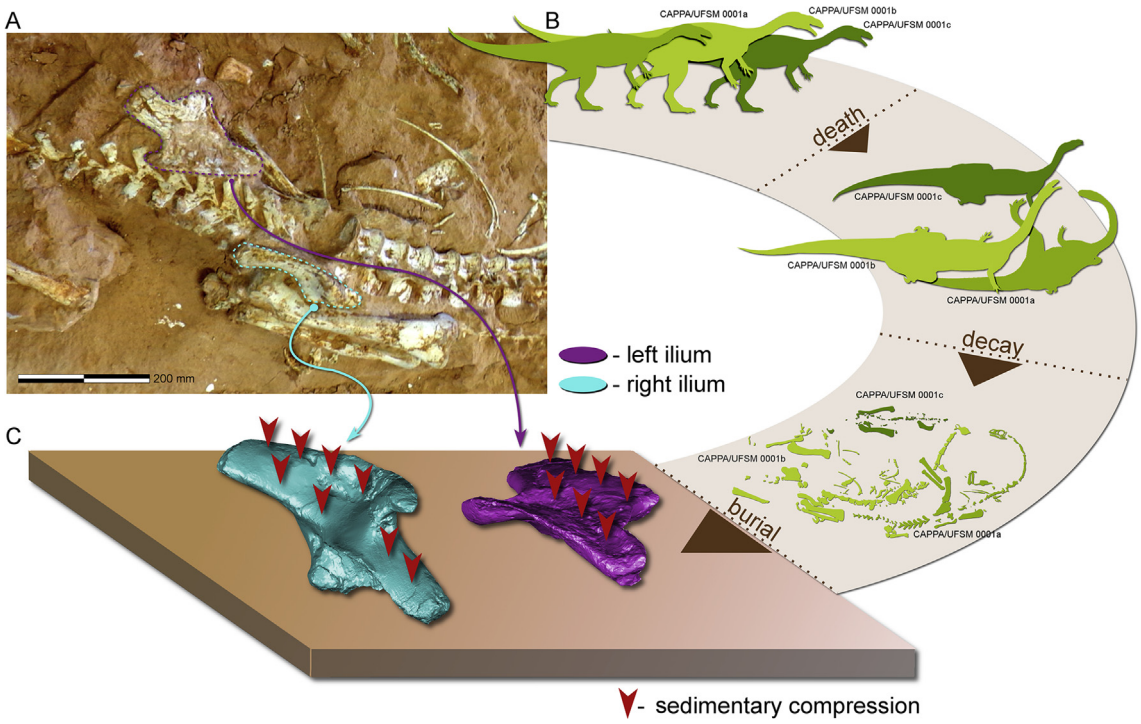

Fig. 2. Schematic taphonomic model for CAPPA/UFSM 0001. (**A**) pelvic girdle of CAPPA/UFSM 0001b in situ. (**B**) taphonomic stages experienced by specimens. (**C**) position of the ilia of CAPPA/UFSM 0001b in the matrix.

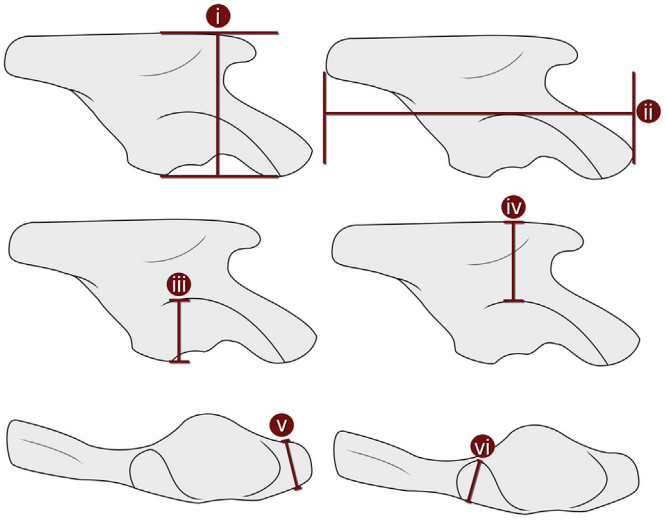

Fig. 3. Schematic linedrawing of a hypothetical dinosaur ilium illustrating the measurements that were taken for comparisons.

surfaces, carbonate concretions or mottling, being these features most common on the upper part of the outcrop.

The vertebrate-bearing fine sandstones are highly cemented, as observed in the "hard-to-collect" block, suggesting that early diagenesis occurred prior to compaction. In fact, a carbonatic level, composed of erratic carbonate nodules up to 10 cm in diameter occurs few centimeters below the fossiliferous level at the outcrop, also suggesting the presence of vadose-phreatic boundary, in which carbonate precipitation took place.

4. Results

4.1. Measurements

(i) Maximum height: the left ilium of CAPPA/UFSM 0001b is 12.5 cm in height, whereas the right element is 10.3 cm. On the other hand, the left ilium of CAPPA/UFSM 0001a is 7.9 cm and the right one is 7.55 cm. For CAPPA/UFSM 0035 the left element is 4 cm in height and the right is 3.95 cm.

(ii) Maximum length: the left ilium of CAPPA/UFSM 0001b is 21.8 cm in length and the right one is 22.1 cm. As expected by the mode of preservation, both elements are almost equal in length. The preservation status of the two other specimens hampers the acquisition of the accurate lengths.

(iii) Acetabular height: the acetabular height of the left element of CAPPA/UFSM 0001b is 5.5 cm, whereas for the right ilium is just 4.2 cm. In CAPPA/UFSM 0001a the same structure is 3.45 cm for the left element and 3.3 cm for the right one. For CAPPA/UFSM 0035 the measurement is 1 cm for the left bone and 1.05 cm for the right element.

(iv) Iliac blade height: the left iliac blade of CAPPA/UFSM 0001b is 7 cm in height, whereas for the right ilium this structure is 6.1 cm. For CAPPA/UFSM 0001a the height are 4.45 cm and 4.25 cm, respectively and for CAPPA/UFSM 0035 are 3 cm and 2.9 cm.

(v) Pubic peduncle width: the left pubic peduncle of CAPPA/UFSM 0001b is 2.7 cm in width, while the right element is 3.45 cm. The left pubic peduncle of CAPPA/UFSM 0035 is 1.05 mm in width, whereas the right is 1.08 mm. The preservation status of CAPPA/UFSM 0001a hampers the acquisition of the accurate lengths.

(vi) Ischiadic peduncle width: the left ischiadic peduncle of CAPPA/UFSM 0001b is 2.15 cm in width, while the right is 2.95 cm. The left ischiadic peduncle of CAPPA/UFSM 0035 is 0.82 mm, while the right element is 0.85 mm. The preservation status of CAPPA/UFSM 0001a hampers the acquisition of the accurate lengths.

The discrepancy between these measurements corroborates the

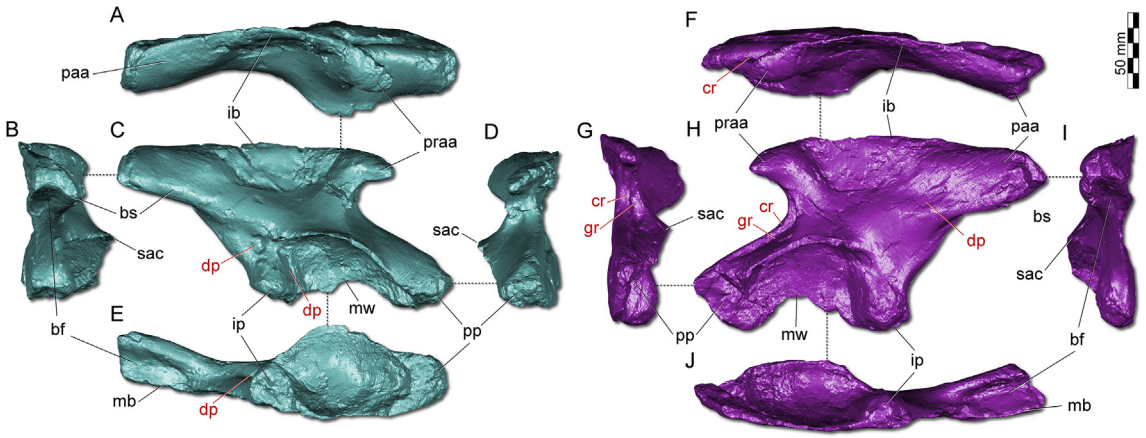

Fig. 4. 3D scan ilia of CAPPA/UFSM 0001b. Right ilium in (**A**) dorsal, (**B**) caudal, (**C**) lateral, (**D**) cranial, and (**E**) ventral views. Left ilium in (**F**) dorsal, (**G**) cranial, (**H**) lateral, (**I**) caudal, and (**J**) ventral views. Abbreviations: bf, brevis fossa; bs, brevis shelf; cr, crest; dp, depression; gr, groove; ib, iliac blade; ip, ischiadic peduncle; md, medial blade; mw, medial wall; paa, postacetabular ala; pp, pubic peduncle; praa, preacetabular ala; sac, supracetabular crest. Red abbreviations correspond to taphonomic traits. (For interpretation of the references to colour in this figure legend, the reader is referred to the Web version of this article.)

proposition by Müller et al. (2015) that sedimentary compression plays a role on the shape of fossils from the Wachholz site.

4.2. Discrete traits

The left ilium bears a deep depression on the dorsal surface of the pubic peduncle that extends until the ventral surface of the preacetabular ala, which forms a groove medially bounded by a crest (Fig. 4G and H). Conversely, the homologous surface is smooth in the right element. Such surface possibly receive the *Musculus puboischiofemoralis internus* (Fechner, 2009). The distal end of the pubic peduncle of the right ilium is semi-circular in shape, whereas it is triangular in the opposite element.

On the lateral surface, dorsal to the ischiadic peduncle, there is a deep depression in the right ilium (Fig. 4C), almost connecting to the brevis fossa. This depression is absent in the homologous surface of the left bone. The antitrochanteric surface of the right element also shows a slight depression that does not occur in the left one (Fig. 4C).

The caudal portions of the supraacetabular crest of the right ilium form a right angle with the pubic peduncle in caudal view and merge abruptly with the peduncle (Fig. 4B). On the other hand, the supraacetabular crest of the opposite element merges smoothly with the pubic peduncle and forms a wider angle. In ventral view, the acetabular area is semi-circular in the right ilium (Fig. 4E) and ovoid in the left one (Fig. 4J).

On the postacetabular ala, both elements present distinct morphologies as well, the most accentuated is the degree of ventral orientation of the brevis shelf and medial blade of the left element, which results in a brevis fossa quite deeper in comparison to the right bone. A shallow depression also is present in the lateral surface of the postacetabular ala of the left element, at the craniocaudal level of the ischiadic peduncle (Fig. 4H). In the right ilium, this surface is plane. This area was suggested as comprising the point of origin of the *Musculus iliofibularis* for saurischians (Carrano and Hutchinson, 2002; Fechner, 2009).

5. Discussion

The present chapter is dedicated to (i) the morphological variation in response to taphonomy, (ii) the negative effects of taphonomic distortion and non-preservation that may obscure the phylogenetic position of the specimens, and (iii) this situation is explained in detail mainly on the Late Triassic dinosaurs of Brazil.

According to Antcliffe et al. (2015), "taphomorphy is morphological variation in a suite of fossils caused by their different taphonomic histories, even when the specimens are in close proximity to each other". The association of over thirty femora of *Sacisaurus agudoensis* (Ferigolo and Langer, 2007), a dinosauriform silesaurid from the Late Triassic of southern Brazil, is a compelling example of taphomorphy. Despite the fact that all elements have been quarried from a small area, Langer and Ferigolo (2013) demonstrated that both proximal and distal ends of these femora present a high degree of morphological variation in response to taphonomic processes. Thus, the specimen analyzed here configures an interesting occurrence of taphomorphy in a single individual, where sedimentary compression played an important role distorting the shape of iliac elements. In this particular case, although both ilia were found in close association (side by side), their distinct placement on the substrate resulted in two distinct taphonomic histories reflected by their dissimilar shapes. Indeed, the difference in the height of the elements is about 17.6% (Fig. 5). For comparison, the specimen CAPPA/UFSM 0001a, which bears both ilia with the ventral surface directed ventrally, reveals just 4.4% of difference in height. The specimen CAPPA/UFSM 0035, which is ascribed to the early sauropodomorph *Buriolestes schultzi* (Cabreira et al., 2016; Müller et al., 2018), present just 1.2% of difference. In this case, the animal was buried with the sacrum articulated, where the lateral surface of the left

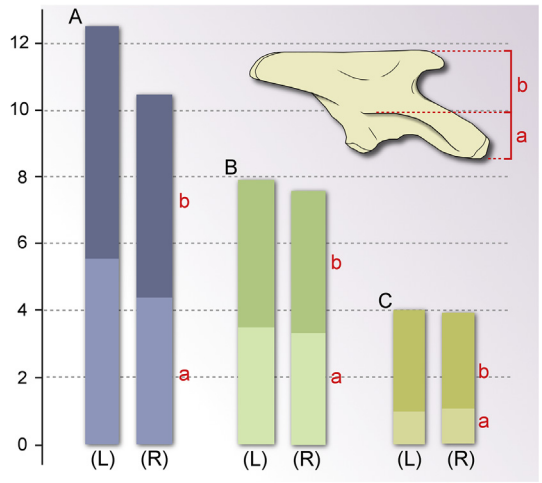

Fig. 5. Size comparison (in centimeters) between left (L) and right (R) ilia of (A) CAPPA/UFSM 0001b (blue), (B) CAPPA/UFSM 0001a (green), and (C) CAPPA/UFSM 0035 (yellow). (For interpretation of the references to colour in this figure legend, the reader is referred to the Web version of this article.)

ilium and the medial surface of the right one directs ventrally.

Another interesting point observed is the disparity of proportions in distinct regions of these ilia. For instance, the dorsal iliac blade of both elements is about to 12.8% different in height (Rb/Lb for Fig. 5A), whereas the acetabulum of the left element is about 19.6% taller (Fig. 5). This suggests that distinct regions of the bone respond differently when submitted to compression, rather than maintaining a proportion for the whole element. Therefore, the specific architecture of a determinate bone is also a determinant factor regarding the effects of compression. These results should be taken into account, once that several former phylogenetic studies aiming the investigation of the affinities of early dinosaurs employed characters based upon proportions of distinct regions of the ilium (e.g. Nesbitt, 2011; Cabreira et al., 2016; Baron et al., 2017).

In addition to the size variation, both iliac elements of CAPPA/UFSM 0001b also carry a distinct combination of traits that should result from their different patterns of preservation. These taphonomic traits are distinguishable, as they exhibit a cracked arrangement, resulting from the rupture of the cortical bone. Moreover, the origin of these traits to paleopathology is discarded because there is no sign of bone reshuffle (Waldron, 2009). Similar situations have already been reported for early dinosaurs, such as the case of the femora of *Chromogisaurus novasi* (Ezcurra, 2010) and *Eodromaeus murphi* (Martínez et al., 2011), both show evidence of postmortem transverse compression. The elements bear an elliptical fossa ventral to the trochanteric shelf that was pointed by Martínez et al. (2013a) as a result of crushing and collapse of the internal lumen of the femoral shaft. Actually, in several specimens of early dinosaurs the femoral shaft presents a similar condition, such as specimens of *Pampadromaeus barberenai* (CAPPA/USFM 0027; CAPPA/UFSM 0028) and the specimen herein studied (CAPPA/UFSM 0001b). Therefore, it is possible to recognize a sort of taphonomic trend related to the preservational mode of the femora of early dinosaurs. Indeed, dinosaurs are known for possessing a thin bone wall, reaching an extreme condition of this trait in theropods (Nesbitt, 2011). Therefore, the nature of internal structure of the bones makes them susceptible to break up. In fact, these femoral “taphonomic features” might in some degree be mistakenly considered as synapomorphies shared among early dinosaurs, as these taxa are close related to each other (e.g. *Pampadromaeus barberenai* and *Chromogisaurus novasi* are two early diverging sauropodomorphs). Similarly, we extend the observations regarding the taphonomic traits of both ilia of CAPPA/UFSM 0001b to other specimens, in order to recognize “taphoanatomical features” (i.e. a trait shared among close phylogenetic taxa/specimens resulting from similar taphonomic processes in response to specific biological aspects of the organism, not necessarily expressing phylogenetic affinities – Fig. 6E). For instance, Sereno et al. (2013) describes the distal articular surface of the pubic peduncle of the ilium of *Eoraptor lunensis* (Sereno et al., 1993 - PVSJ 512) as subtriangular in shape, a condition that is unusual in early dinosaurs. They generally have a semicircular distal end of the pubic peduncle, such as *Panphagia protos* (Martínez and Alcober, 2009 - PVSJ 874) and *Buriolestes schultzi* (Cabreira et al., 2016 - ULBRA-PVT280; CAPPA/UFSM 0035). Nevertheless, the holotype (ULBRA-PVT016) of *Pampadromaeus barberenai* (Cabreira et al., 2011) shares the condition of PVSJ 512. However, the left ilium of ULBRA-PVT016 also bears the groove bounded medially by a ridge on the dorsal surface of the pubic peduncle (Fig. 6B), the same as in the left ilium of CAPPA/UFSM 0001b (Fig. 6A) and MCP 3945-PV (a specimen referenced to *Saturnalia tupiniquim* Langer et al., 1999). Moreover, the left ilium of ULBRA-PVT016 was preserved with its medial surface directed ventrally. Therefore, it suffered transverse compression, as in the equivalent element of CAPPA/UFSM 0001b. Finally, the same is apparently true for PVSJ 512. Therefore, it is possible that the subtriangular outline of the distal end of the pubic peduncle of all these specimens, as well as the ridge on the dorsal surface of the pubic peduncle of CAPPA/UFSM 0001b and ULBRA-PVT016 result from similar taphonomic histories, not reflecting the natural shape of the structure.

The ruptured area on the antitrochanteric surface of the right ilium of CAPPA/UFSM 0001b also could provide insights about taphonomic trends. If this region is more susceptible to collapse, similar to the case of the femoral diaphysis of early dinosaurs, is plausible to hypothesize that the unusual morphology in other dinosaurs could also be controlled/affected by sedimentary compression. For instance, Langer et al. (2011) point to the presence of an elongated groove excavating the cranial portion of the antitrochanter of the right ilium of the holotype (MCN PV2355) of *Guaibasaurus candelariensis* (Bonaparte et al., 1999). The same authors also recognize an equivalent, but less developed groove, on the homologous portion of the right ilium of UFRGS PV0725T, a specimen ascribed to the same species (Bonaparte et al., 2007). Therefore, in their study, such trait is suggested to be a putative autapomorphy of *Guaibasaurus candelariensis*, although Langer et al. (2011) recognizes that such condition in MCN PV2355 may have been enhanced by overpreparation. Then, an alternative hypothesis for the condition observed in MCN PV2355 and UFRGS PV0725T is that the groove comprises a taphonomic artifact, rather than an autapomorphic feature, as a similar condition is present in the right ilium of CAPPA/UFSM 0001b.

The supraacetabular crest of both ilia of CAPPA/UFSM 0001b shows slightly variation regarding the angle formed with the main body of the bone. On the other hand, an apparently usual trait resultant from sedimentary compression is the displacement of this crest. The specimen referred to *Buriolestes schultzi* (CAPPA/UFSM 0035) possesses a pair of ilia strongly affected by transverse compression, where the supracetabular crest is overly directed ventrally (Fig. 6C). This condition seems clearly to be a taphonomic artifact, once the femoral head does not fit correctly on the acetabular portion of the ilium of the specimen. A left ilium (CAPPA/UFSM 0200) of an indeterminate sauropodomorph from a fossiliferous site (Piche site) close to the type-locality (Buriol site) of *Buriolestes schultzi* also bears a similar condition to the supracetabular crest. Indeed, CAPPA/UFSM 0035 and CAPPA/UFSM 0200 are extremely cracked, especially on the supracetabular crest. This kind of deformation could affect the interpretation of phylogenetic characters (Fig. 6E), such as those describing the projected angle of the supracetabular crest (generally varying from laterally to ventrally, e.g. Gauthier, 1986; Nesbitt, 2011). Therefore, when the supracebatular crest is associated with cracks and fractures, it is mandatory to choose carefully the state of such characters. The medial blade of both ilia of CAPPA/UFSM 0035 also could be displaced ventrally, affecting the deepness of the brevis fossa, similar to the condition of the left ilium of CAPPA/UFSM 0001b. In contrast, the medial blade of CAPPA/UFSM 0200 is almost horizontally oriented, resulting in a quite shallow fossa. This is also problematic in a phylogenetic context as the arrangement of the fossa brevis is another character extensively applied in phylogenetic studies of archosaurs (e.g. Novas, 1996; Nesbitt, 2011; Cabreira et al., 2016).

Additionally, the iliac blade appears to be greatly affected by sedimentary compression, once several specimens present a series of fragmentations in this structure. For instance, while CAPPA/UFSM 0001b and CAPPA/UFSM 0001a preserve the complete iliac blade in both ilia, CAPPA/UFSM 0200 does not preserve the mid portion of this structure. Another case occurs in CAPPA/UFSM 0035, which had a displacement in the position of the iliac blade (Fig. 6C), in both ilia, due to the fragmentation of the structure. Specimens of the early diverging sauropodomorph *Saturnalia tupiniquim* (Langer et al., 1999; Langer, 2003), also demonstrate that the iliac blade is one of the structures in the ilium that is most taphonomically affected. Although MCP 3845-PV preserves both ilia, the right element suffered fragmentation in the mid portion of the iliac blade, similar to CAPPA/UFSM 0200, but in MCP 3845-PV the pre-acetabular ala was also lost. Accordingly, MCP 3844-PV and MCP 3846-PV present fragmentation in the iliac blade as well. Moreover, the holotype specimens of *Panphagia protos* (PVSJ 874) and *Chromogisaurus novasi* (PVSJ 845), two early diverging sauropodomorphs from

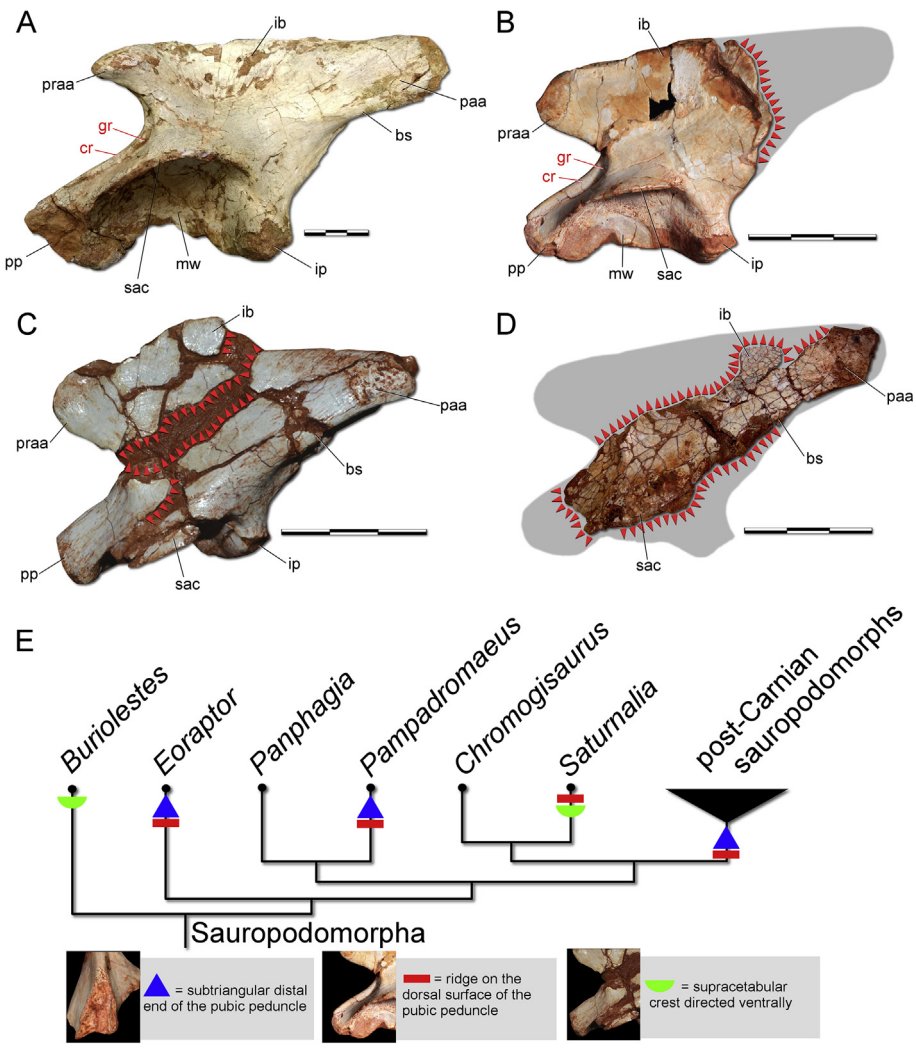

Fig. 6. Features produced by taphonomic processes in some early sauropodomorphs. Lateral view of selected sauropodomorphs left ilium of the Candelária Sequence: (**A**) CAPPA/UFSM 0001b; (**B**) *Pampadromaeus barberenai* (ULBRA-PVT016); (**C**) *Buriolestes schultzi* (CAPPA/UFSM 0035); and (**D**) UFSM 11612. (**E**) Distribution of some "taphoanatomial features" in the reduced phylogenetic tree of early sauropodomorphs by Müller et al. (2018). Abbreviations: bs, brevis shelf; cr, crest; gr, groove; ib, iliac blade; ip, ischiadic peduncle; mw, medial wall; paa, postacetabular ala; pp, pubic peduncle; praa, preacetabular ala; sac, supracetabular crest. Red abbreviations correspond to taphonomic traits and arrows correspond to fractured portions. The scale bar = 30 mm. (For interpretation of the references to colour in this figure legend, the reader is referred to the Web version of this article.)

Argentina (Martínez and Alcober, 2009; Ezcurra, 2010), share these similarities in the preservation (or lack of preservation) of the iliac blade. While both specimens lack the preacetabular ala, PVSJ 874 also did not preserve the cranialmost portion of the iliac blade. *Guaibasaurus candelariensis* can also be included in this assortment, while the holotype (MCN PV2355) and a referred specimen (UFRGS PV0725T) preserved both ilia, their elements did not preserve part of the iliac blade (and the preacetabular ala in both elements of the holotype) (Langer et al., 2011). In this case, the loss of the iliac blade obscures a reliable iliac morphology of *Guaibasaurus candelariensis*, once this dinosaur has a floating phylogenetic position (e.g. Ezcurra, 2010; Langer et al., 2011; Cabreira et al., 2016). All these examples are maximally elevated in the specimen UFSM 11612 (a saurischian dinosaur tentatively attributed to Sauropodomorpha), which did not preserve most of the iliac blade and part of the peduncles, keeping only a partial postacetabular ala, part of the pubic peduncle and the "main body" of the ilium (Fig. 6D).

Nonetheless, other dinosauriforms such as herrerasaurians and silesaurids retain this pattern of preservation in the iliac blade even that at least the herrerasaurians tend to have a more robust ilium than silesaurids or Carnian sauropodomorphs. The holotype specimen (MCZ 1669) of *Staurikosaurus pricei* preserves both ilia, although the right element bears a fragmented iliac blade (Colbert, 1970; Bittencourt and Kellner, 2009). Similarly, specimens of *Caseosaurus crosbyensis* (UMMP 8870; NMMNH P-35995) did not preserve the iliac blade (Baron and Williams, 2018). Indeed, NMMNH P-35995 is much more fragmented than UMMP 8870, while the former lacks the iliac blade and the postacetabular ala, the latter lacks only part of the iliac blade, similar to the case of CAPPA/UFSM 0200 the aforementioned specimens alike it. In silesaurids, MCN PV10100, a specimen of *Sacisaurus agudoensis* (Ferigolo and Langer, 2007), has a preservation of the ilium that is quite similar to that of UFSM 11612, where virtually all the iliac blade was lost during the preservation of the individual. ZPAL AbIII404/1 and ZPAL AbIII 907/6, both specimens of *Silesaurus opolensis* (Dzik, 2003; Langer et al., 2011) and PVSJ 884, the holotype of *Ignotosaurus fragilis* (Martínez et al., 2013b) also have fragmented iliac blades. This series of aforementioned cases exemplify how taphonomic processes affect the iliac blade and consequently the preacetabular ala in several cases. This structure is one of the most gracile portions of the ilium, where the bone is delicate and thin, providing a more fragile structure that is easily broken and lost during fossilization history or even along the collecting phases.

All the above cases are good examples of what we call as "taphoanatomical features" expressed in ilia of early dinosaurs and related groups. Thus, the identification of these patterns together with a deeper knowledge on the whole anatomy of early dinosaurs and the mechanisms that rule their morphological variation (e.g. ontogeny, sexual dimorphism) may offer a reliable solution to the disputed scenario regarding phylogenetic affinities of such group. Actually, the vertebrate paleontology still demands far more specimens of early dinosaurs from "critical" evolutionary moments. Nevertheless, a satisfactory number of newly discovered dinosauromorph-bearing localities have been documented in the last decade (e.g. Nesbitt et al., 2010; Müller et al., 2015; Cabreira et al., 2016). The specimens yielded from these hotspots, associated with new materials from classical formations have already

incorporated an expressive amount of data that hints to an increasingly rigorous phylogenetic framework.

6. Conclusions

The specimen presented here reveals distinct morphologies between its ilia, reflecting distinct modes of preservation in each element. This corresponds, therefore, to a particular case of taphomorphy expressed in a single individual, permitting its use as a model to be considered in further studies in fossil vertebrates. Indeed, some of the peculiar traits of each ilium also occur in other specimens of related taxa, revealing putative taphonomic patterns. Therefore, traits originated in response to taphonomic processes are not exclusively of a single specimen, they could be shared between elements that experience similar taphonomic histories. Failing to recognize these trends could affect anatomical interpretations, especially regarding the phylogenetic context.

Acknowledgements

The authors thank Leonardo R. Kerber (CAPPA/UFSM) for help with the 3D scans of the specimen studied here. We are also grateful to Sérgio F. Cabreira (ULBRA) for allowing the use of photographs of ULBRA-PVT016. We also extends our gratitude to Dr. Volkan Sarıgül and two anonymous reviewers for their comments and suggestions, which helped us to improve the manuscript. This work was supported by a Fundação de Amparo à Pesquisa do Estado do Rio Grande do Sul (FAPERGS) scholarship for MSG and by Conselho Nacional de Desenvolvimento Científico e Tecnológico CNPq [research grant to SDS, process number 306352/2016-8].

References

Antcliffe, J.B., Hancy, A.D., Brasier, M.D., 2015. A new ecological model for the ~ 565 ma ediacaran biota of mistaken point, newfoundland. Precambrian Res. 268, 227–242.
Arbour, V.M., Currie, P.J., 2012. Analyzing taphonomic deformation of ankylosaur skulls using retrodeformation and finite element analysis. PLoS One 1–13.
Baron, M.G., Williams, M., 2018. A re-evaluation of the enigmatic dinosauriform *Caseosaurus crosbyensis* from the Late Triassic of Texas, USA and its implications for early dinosaur evolution. Acta Palaeontol. Pol. 63, 129–145.
Baron, M.G., Norman, D.B., Barrett, P.M., 2017. A new hypothesis of dinosaur relationships and early dinosaur evolution. Nature 543, 501–506.
Bittencourt, J.S., Kellner, A.W.A., 2009. The anatomy and phylogenetic position of the Triassic dinosaur *Staurikosaurus pricei* Colbert, 1970. Zootaxa 2079, 1–56.
Bonaparte, J.F., Brea, G., Schultz, C.L., Martinelli, A.G., 2007. A new specimen of *Guaibasaurus candelariensis* (basal saurischia) from the late triassic caturrita formation of southern Brazil. Hist. Biol. 19, 73–82.
Bonaparte, J.F., Ferigolo, J., Ribeiro, A.M., 1999. A new early late triassic saurischian dinosaur from Rio Grande do Sul state, Brazil. Natl. Sci. Mus. Monogr. 15, 89–109.
Cabreira, S.F., Kellner, A.W.A., Dias-da-Silva, S., Roberto-da-Silva, L., Bronzati, M., Marsola, J.C., Müller, R.T., Bittencourt, J.S., Batista, B.J., Raugust, T., Carrilho, R., Langer, M.C., 2016. A unique Late Triassic dinosauromorph assemblage reveals dinosaur ancestral anatomy and diet. Curr. Biol. 26, 3090–3095.
Cabreira, S.F., Schultz, C.L., Bittencourt, J.S., Soares, M.B., Fortier, D.C., Silva, L.R., Langer, M.C., 2011. New stem-sauropodomorph (dinosauria, saurischia) from the triassic of Brazil. Naturwissenschaften 98, 1035–1040.
Carrano, M.T., Hutchinson, J.R., 2002. Pelvic and hindlimb musculature of *Tyrannosaurus rex* (dinosauria: theropoda). J. Morphol. 253, 207–228.
Colbert, E.H., 1970. A saurischian dinosaur from the Triassic of Brazil. Am. Mus. Novit. 2405, 1–39.
Dzik, J., 2003. A beaked herbivorous archosaur with dinosaur affinities from the early Late Triassic of Poland. J. Vertebr. Paleontol. 23, 556–574.
Ezcurra, M.D., 2010. A new early dinosaur (Saurischia: Sauropodomorpha) from the Late Triassic of Argentina: a reassessment of dinosaur origin and phylogeny. J. Syst. Palaeontol. 8, 371–425.
Fechner, R., 2009. Morphofunctional Evolution of the Pelvic Girdle and Hindlimb of Dinosauromorpha on the Lineage to Sauropoda. Ph.D. Dissertation. Fakultät für Geowissenschaften, Ludwig-Maximilians-Universität, Munich, pp. 197.
Ferigolo, J., Langer, M.C., 2007. A Late Triassic dinosauriform from South Brazil and the origin of the ornithischian predentary bone. Hist. Biol. 19, 23–33.
Gauthier, J., 1986. Saurischian monophyly and the origin of birds. Memoir. Calif. Acad. Sci. 8, 1–55.
Griffin, C.T., Nesbitt, S.J., 2016. The femoral ontogeny and long bone histology of the Middle Triassic (? late Anisian) dinosauriform *Asilisaurus kongwe* and implications for the growth of early dinosaurs. J. Vertebr. Paleontol. 36, e1111224.
Holz, M., Schultz, C.L., 1998. Taphonomy of the south Brazilian Triassic herpetofauna: fossilization mode and implications for morphological studies. Lethaia 31, 335–345.
Horn, B.L.D., Melo, T.M., Schultz, C.L., Philipp, R.P., Kloss, H.P., Goldberg, K., 2014. A new third-order sequence stratigraphic framework applied to the Triassic of the Paraná Basin, Rio Grande do Sul, Brazil, based on structural, stratigraphic and paleontological data. J. S. Am. Earth Sci. 55, 123–132.
Langer, M.C., 2003. The pelvic and hind limb anatomy of the stem-sauropodomorph *Saturnalia tupiniquim* (Late Triassic, Brazil). PaleoBios 23, 1–30.
Langer, M.C., Abdala, F., Richter, M., Benton, M.J., 1999. A sauropodomorph dinosaur from the upper triassic (carnian) of southern Brazil. Comptes Rendus Acad. Sci. - Ser. IIA Earth Planet. Sci. 329, 511–517.
Langer, M.C., Bittencourt, J.S., Schultz, C.L., 2011. A reassessment of the basal dinosaur *Guaibasaurus candelariensis*, from the Late Triassic Caturrita Formation of south Brazil. Earth Environ. Sci. Trans. R. Soc. Edinburgh 101, 301–332.
Langer, M.C., Ferigolo, J., 2013. The late triassic dinosauromorph *Sacisaurus agudoensis* (caturrita formation: Rio Grande do Sul, Brazil): anatomy and affinities. Geol. Soc. London Special Publ. 379, 353–392.
Langer, M.C., Ramezani, J., Da-Rosa, A.S.S., 2018. Upb age constraints on dinosaur rise from south Brazil. Gondwana Res. 57, 133–140.
Leal, L.A., Azevedo, S.A., Kellner, A.W., Da Rosa, A.A.S., 2004. A new early dinosaur (Sauropodomorpha) from the caturrita formation (late triassic), paraná basin, Brazil. Zootaxa 690, 1–24.
Martínez, R.N., Alcober, O.A., 2009. A basal sauropodomorph (dinosauria: saurischia) from the ischigualasto formation (triassic, carnian) and the early evolution of Sauropodomorpha. PLoS One 1–12.
Martínez, R.N., Apaldetti, C., Abelin, D., 2013a. Basal sauropodomorphs from the ischigualasto formation. J. Vertebr. Paleontol. 32, 51–69.
Martínez, R.N., Apaldetti, C., Alcober, O.A., Colombi, C.E., Sereno, P.C., Fernandez, E., Santi Malnis, P., Correa, G.A., Abelin, D., 2013b. Vertebrate succession in the ischigualasto formation. J. Vertebr. Paleontol. 32, 10–30.
Martínez, R.N., Sereno, P.C., Alcober, O.A., Colombi, C.E., Renne, P.R., Montañez, I.P., Currie, B.S., 2011. A basal dinosaur from the dawn of the dinosaur era in southwestern Pangaea. Science 331, 201–210.
Müller, R.T., Da-Rosa, A.A.S., Roberto-da-Silva, L., Aires, A.S.S., Pacheco, C.P., Pavanatto, A.E., Dias-da-Silva, S., 2015. Wachholz, a new exquisite dinosaur-bearing fossiliferous site from the Upper Triassic of southern Brazil. J. S. Am. Earth Sci. 61, 120–128.
Müller, R.T., Langer, M.C., Dias-da-Silva, S., 2017. Biostratigraphic significance of a new early sauropodomorph specimen from the Upper Triassic of southern Brazil. Hist. Biol. 29, 187–202.
Müller, R.T., Langer, M.C., Bronzati, M., Pacheco, C.P., Cabreira, S.F., Dias-Da-Silva, S., 2018. Early evolution of sauropodomorphs: anatomy and phylogenetic relationships of a remarkably well-preserved dinosaur from the Upper Triassic of southern Brazil. Zool. J. Linn. Soc. 1–62.
Nesbitt, S.J., 2011. The early evolution of archosaurs: relationships and the origin of major clades. Bull. Am. Mus. Nat. Hist. 352, 1–292.
Nesbitt, S.J., Sidor, C.A., Irmis, R.B., Angielzcyk, K.D., Smith, R.M., Tsuji, L.A., 2010. Ecologically distinct dinosaurian sister group shows early diversification of Ornithodira. Nature 464, 95–98.
Novas, F.E., 1996. Dinosaur monophyly. J. Vertebr. Paleontol. 16, 723–741.
Pacheco, C.P., Eltink, E., Müller, R.T., Dias-da-Silva, S., 2017. A new Permian temnospondyl with Russian affinities from South America, the new family Konzhukoviidae, and the phylogenetic status of Archegosauroidea. J. Syst. Palaeontol. 15, 241–256.
Philipp, R.P., Closs, H., Schultz, C.L., Basei, M.B., Horn, L.D., Soares, M.B., 2013. Proveniência por U-Pb LA-ICP-MS em zircão detrítico e idade de deposição da Formação Santa Maria, Triássico da Bacia do Paraná, RS: evidências da estruturação do Arco do Rio Grande. In: Anais do VIII Symposium International on Tectonics and XIV Simpsio Nacional de Estudos Tectônicos. vol. 1. pp. 154–157.
Piechowski, R., Tałanda, M., Dzik, J., 2014. Skeletal variation and ontogeny of the late triassic dinosauriform *Silesaurus opolensis*. J. Vertebr. Paleontol. 34, 1383–1393.
Ponce de León, M.S., 2002. Computerized paleoanthropology and neanderthals: the case of le moustier 1. Evol. Anthropol. 68–72 Suppl. 1.
Sereno, P.C., Forster, C.A., Rogers, R.R., Monetta, A.M., 1993. Primitive dinosaur skeleton from Argentina and the early evolution of the Dinosauria. Nature 361, 64–66.
Sereno, P.C., Martínez, R.N.m, Alcober, O.A., 2013. Osteology of *Eoraptor lunensis* (dinosauria, Sauropodomorpha). J. Vertebr. Paleontol. 32, 83–179.
Trotteyn, M.J., Martínez, R.N., 2013. Primer registro de displasia coxofemoral en un rincosaurio del Triásico superior. Ameghiniana 50, 217–226.
Waldron, T., 2009. Palaeopathology. Cambridge University Press, Cambridge.
White, T., 2003. Early hominids – diversity or distortion? Science 299, 1994–1997.
Zerfass, H., Lavina, E.L., Schultz, C.L., Garcia, A.J.V., Faccini, U.F., Chemale, F., 2003. Sequence stratigraphy of continental Triassic strata of Southernmost Brazil: a contribution to Southwestern Gondwana palaeogeography and palaeoclimate. Sediment. Geol. 161, 85–105.

6 ARTIGO IV

Título: Early evolution of sauropodomorphs: anatomy and phylogenetic relationships of a remarkably well-preserved dinosaur from the Upper Triassic of southern Brazil

Autores: Rodrigo Temp Müller, Max Cardoso Langer, Mario Bronzati, Cristian Pereira Pacheco, Sérgio Furtado Cabreira e Sérgio Dias da Silva

Periódico: Zoological Journal of the Linnean Society

Volume: 184

Páginas: 1187-12483

Ano: 2018

DOI: 10.1093/zoolinnean/zly009/4996397

Zoological Journal of the Linnean Society, 2018, **184**, 1187–1248. With 45 figures.

Early evolution of sauropodomorphs: anatomy and phylogenetic relationships of a remarkably well-preserved dinosaur from the Upper Triassic of southern Brazil

RODRIGO T. MÜLLER[1,2*], MAX C. LANGER[3], MARIO BRONZATI[4], CRISTIAN P. PACHECO[2], SÉRGIO F. CABREIRA[5] AND SÉRGIO DIAS-DA-SILVA[1]

[1]*Centro de Apoio à Pesquisa Paleontológica, Universidade Federal de Santa Maria, Santa Maria, RS 97105-900, Brazil*
[2]*Programa de Pós Graduação em Biodiversidade Animal, Universidade Federal de Santa Maria, Santa Maria, RS 97105-900, Brazil*
[3]*Laboratório de Paleontologia, Faculdade de Filosofia, Ciências e Letras de Ribeirão Preto, Universidade de São Paulo, Ribeirão Preto, SP 14040-901, Brazil*
[4]*Ludwig-Maximilians-Universität and Bayerische Staatssammlung für Paläontologie und Geologie, Munich 80333, Germany*
[5]*Museu de Ciências Naturais, Universidade Luterana do Brasil, Canoas, RS 92425-900, Brazil*

Received 4 August 2017; revised 23 December 2017; accepted for publication 31 January 2018

An exceptional new specimen (CAPPA/UFSM 0035) of *Buriolestes schultzi* was discovered during recent fieldwork at the type locality of the taxon, which is Carnian in age (Late Triassic). This early sauropodomorph is peculiar owing to its faunivorous feeding habits, unusual amongst the members of this large omnivorous/herbivorous clade. The specimen incorporates new data on skeletal portions that have so far been unknown for *B. schultzi*, particularly regarding the skull and axial skeleton. As such, *B. schultzi* is now as complete as the best-known early dinosaurs, such as *Eoraptor lunensis* and *Herrerasaurus ischigualastensis*. A phylogenetic investigation fully supports *B. schultzi* as a sauropodomorph, corroborating the previous assignation. Despite the presence of traits found in Theropoda, distinct skeletal portions of *B. schultzi* do not share its morphospace in a morphological disparity analysis. We also propose an alternative evolutionary scenario for the first members of Sauropodomorpha: some Carnian taxa from South America form a monophyletic group instead of a series of low-diversity lineages paraphyletic with respect to Plateosauria.

ADDITIONAL KEYWORDS: Dinosauria – Gondwana – osteology – phylogenetics – Sauropodomorpha – South America.

INTRODUCTION

There is general agreement that the oldest dinosaurs are those quarried from Carnian strata of southwestern Pangea (e.g. Reig, 1963; Casamiquela, 1967; Colbert, 1970; Sereno *et al.*, 1993; Cabreira *et al.*, 2016), mainly represented by the Santa Maria Supersequence and the Ischigualasto Formation, respectively from Brazil and Argentina (but see Nesbitt *et al.*, 2012; Baron, Norman & Barrett, 2017a). These units yield Saurischian dinosaurs, represented by several well-preserved herrerasaurids (Reig, 1963; Colbert, 1970; Alcober & Martínez, 2010), sauropodomorphs (Sereno *et al.*, 1993; Langer *et al.*, 1999; Martínez & Alcober, 2009; Ezcurra, 2010; Cabreira *et al.*, 2011, 2016) and possible theropods (Martínez *et al.*, 2011; Müller *et al.*, 2017). In contrast, ornithischians are poorly known, so far represented only by *Pisanosaurus mertii* (Casamiquela, 1967). In any case, the taxonomic diversity recorded from both Argentina and Brazil suggests that the three main dinosaurian groups were already present in land ecosystems during the Carnian.

*Corresponding author. E-mail: rodrigotmuller@hotmail.com

In recent years, however, new findings and diverse/alternative methodological approaches are challenging and/or complementing those previously proposed evolutionary scenarios. For instance, Nesbitt *et al.* (2012) described a putative dinosaur from the Anisian of southern Tanzania, implying that dinosaurs arose 15 Myr earlier than previously thought. Langer & Ferigolo (2013) proposed that Silesauridae had ornithischian affinities, increasing their Triassic record. Cabreira *et al.* (2016) supported this scenario in a recent comprehensive phylogenetic study on Triassic dinosauromorphs, in which several taxa were, for the first time, placed in alternative positions in the dinosaur tree. For instance, *Eodromaeus murphi* (Martínez *et al.*, 2011) and *Tawa hallae* (Nesbitt *et al.*, 2009) were originally described as members of Theropoda, being recovered as basal saurischians outside the theropod–sauropodomorph dichotomy (Cabreira *et al.* 2016). In addition, *P. mertii* has recently been suggested to represent a silesaurid in two independent studies (Agnolín & Rozadilla, 2017; Baron, Norman & Barrett, 2017b). Even more unexpectedly, Baron *et al.* (2017a) proposed that theropods are closely related to ornithischians instead of sauropodomorphs. At the same time, new data regarding dinosaur relatives came to light, including the description of several new non-dinosaur dinosauromorphs (e.g. Irmis *et al.*, 2007; Cabreira *et al.*, 2016; Martínez *et al.*, 2016) and also the proposal of an entire new clade of early diverging avemetatarsalians (Nesbitt *et al.*, 2017).

Among these new findings, the Carnian *Buriolestes schultzi* was recovered as the basalmost member of Sauropodomorpha (Cabreira *et al.*, 2016), a group largely known for encompassing giant quadrupedal and herbivorous forms. This new taxon was a small biped and, outstandingly, the only strictly faunivorous sauropodomorph so far described, therefore being a key taxon to understand both biological and ecological trends in sauropodomorph early evolution.

During recent fieldwork at the type locality of *B. schultzi*, we discovered an exceptionally well-preserved new specimen (CAPPA/UFSM 0035), which revealed several skeletal structures so far unknown in *B. schultzi* and even in any other coeval dinosaurs. In the present study, we describe the anatomy of this new specimen in detail and investigate its implications for early dinosaur phylogeny.

MATERIAL AND METHODS

Intitutional abbreviations

CAPPA/UFSM, Centro de Apoio à Pesquisa Paleontológica da Quarta Colônia da Universidade Federal de Santa Maria, São João do Polêsine, Brazil; MCP, Museu de Ciências e Tecnologia Pontifícia Universidade Católica do Rio Grande do Sul, Porto Alegre, Brazil; NMT, National Museum of Tanzania, Dar es Salaam, Tanzania; PVSJ, Museo de Ciencias Naturales, Universidad Nacional de San Juan, San Juan Province, Argentina; ULBRA, Universidade Luterana do Brasil, Coleção de Paleovertebrados, Canoas, Brazil; ZPAL, Institute of Paleobiology of the Polish Academy of Sciences, Warsaw, Poland.

Phylogenetic analysis

Owing to its completeness, CAPPA/UFSM 0035 allowed the inclusion of many additional scores for *B. schultzi*, as several features are unavailable in the holotype. Accordingly, we performed a series of analyses to assess the relationships of CAPPA/UFSM 0035 and its possible implications for early dinosaurian evolution.

Firstly, it was simply scored in the data matrix by Cabreira *et al.* (2016), in order to test its taxonomic assignment to *B. schultzi*. In order to do so, CAPPA/UFSM 0035 and ULBRA-PVT280 (the holotype of *B. schultzi*) were coded as two distinct operational taxonomic units (OTUs). All parameters of the original analysis were replicated, and the data matrix was processed with the software TNT v1.1 (Goloboff, Farris & Nixon, 2008), with the most parsimonious trees (MPTs) recovered via 'traditional search' [random addition sequence + tree bisection reconnection (TBR)] with 1000 replicates of Wagner trees (with random seed = 0), TBR and branch swapping (holding 20 trees saved per replicate). Decay indices (Bremer support values) and bootstrap values (1000 replicates) were also obtained with TNT v1.1.

In the second analysis, CAPPA/UFSM 0035 and ULBRA-PVT280 were merged into a single OTU, keeping the computational parameters unchanged.

The third and fourth analyses used a modified version of the data matrix of Cabreira *et al.* (2016), in which *B. schultzi* was scored by combining its original entries with CAPPA/UFSM 0035, as follows. Character 36, originally with three states related to the median recess in the parabasisphenoid, had one deleted, and now reads: '0' shallow depression; '1' fossa or deep depression. Character 37, regarding the outline of the caudal margin of the parabasisphenoid in ventral view, was rescored for several taxa. Character 41, which describes the presence of a rugose ridge on the craniolateral edge of the supraoccipital (Nesbitt, 2011), was redefined as 'supraoccipital, dorsal surface: rugose ridge along exoccipital contact', with two states: '0' absent; '1' present. Several OTUs were rescored for character 42, which is related to the foramen for the trigeminal nerve and middle cerebral vein. *Panphagia protos* was rescored from '1' to '0/1' in character 63, which is associated with the shape of the caudal edge of the caudal half of the maxilla/dentary teeth.

Dentition of this dinosaur shows both proposed morphologies: 'concave or straight' and 'convex'. For character 246, which describes the presence of serrations in the mesial margin of the premaxillary teeth, *P. protos* was changed from '1' to '?', because there are no premaxillary teeth preserved for this dinosaur. Three additional characters were included in the data matrix. The first one (257) is modified from Nesbitt (2011) and defined as 'blind pit in the basioccipital'. Three states are proposed: '0' absent; '1' one pit; '2' two pits. The second character (258) is based upon the observations by Cabreira *et al.* (2011) on the prefrontal shape in early dinosaurs and defined as 'bone sheet between the rostral and ventral processes of the prefrontal'. Two states are proposed: '0' present; '1' absent. The third character (259) was proposed by Ezcurra (2006) as 'angle between ascending process and caudal process of jugal', with two states: '0' right or obtuse; '1' acute, with an ascending process strongly dorsocaudally oriented. This modified data matrix (which comprises 259 characters and 43 OTUs) was analysed following the same parameters as the first two analyses, with the three new characters treated as non-additive. The scores for all OTUs are included in the Appendix.

In the fourth analysis, the dataset was run using implied character weighting, with the value of the concavity constant (k) ranging between three and nine. According to Legg, Sutton & Edgecombe (2013), equal character weighting is only appropriate in analyses with no potential homoplasy, which is not the case for early dinosaurs (Langer, 2014). In addition, Goloboff *et al.* (2008) concluded that implied character weighting against homoplasy could improve phylogenetic analysis of morphological data matrices. Therefore, in this last analysis, we used implied character weighting in an attempt to minimize the effect of homoplasy. Nodal support was measured using symmetric resampling (Goloboff *et al.*, 2003), performed with 1000 replicates, each with a 33% of change probability.

In addition, a fifth analysis was carried out using the data matrix of Langer *et al.* (2017), which is a modified version of that of Baron *et al.* (2017a). In this analysis, the new information gathered from CAPPA/UFSM 0035 was added to *B. schultzi*. All the characters received the same weight, and the same parameters as for the previous analysis were used to recover the MPTs.

Morphological disparity analysis

In spite of its sauropodomorph affinity, *B. schultzi* shares several morphological features with theropods. Therefore, in order to explore both phylogenetic signals and putative convergences within distinct skeletal portions of this dinosaur, we conducted a morphological disparity analysis. Our analysis follows that of Novas *et al.* (2015), which aimed to investigate different homoplastic signals in distinct body parts of *Chilesaurus diegosuarezi*. We used a modified version of the dataset from the third and fourth phylogenetic analyses, with the polymorphic scores changed to 'missing entries' (Novas *et al.*, 2015). Then, six skeletal parts were isolated in the data matrix: skull; skull excluding dentition; postcranium; axial skeleton; pectoral girdle/forelimb; and pelvic girdle/hindlimb. Taxa with missing entries for a given skeletal part were excluded from the partitioned matrices. Next, seven Euclidian distance matrices (EDMA) were calculated using the software MATRIX (Will, 1998). The matrices were calculated from the six partitioned and one data matrix with all the characters. A principal coordinate analysis (PCoA) was then performed for each EDMA with the multivariate package GINKGO (Bouxin, 2005). At this point, we followed the parameters applied by Butler *et al.* (2012), in which the centroid of all OTUs is taken as the origin of multivariate axes, also using the Calliez method of negative eigenvalue correction. Finally, a bivariate graph with axes 1 and 2 of each PCoA was constructed using the software PAST (Hammer, Haper & Ryan, 2001). Convex hulls were drawn from the results of the third phylogenetic analysis performed here.

SYSTEMATIC PALAEONTOLOGY

DINOSAURIA OWEN, 1842

SAURISCHIA SEELEY, 1887

SAUROPODOMORPHA HUENE, 1932

BURIOLESTES SCHULTZI CABREIRA *ET AL.*, 2016

Holotype

ULBRA-PVT280, articulated partial skeleton, including partial skull with both lower jaws; few presacral, three sacral and 42 tail vertebrae; left scapula and forelimb lacking most of the manus; paired ilia and ischia; partial left pubis; and a nearly complete left hindlimb (Cabreira *et al.*, 2016).

Referred specimen

CAPPA/UFSM 0035, a nearly complete and articulated skeleton (Fig. 1A, C). The skull is almost entirely preserved, including both lower jaws. The axial skeleton includes the complete cervical and trunk series but lacks the last sacral vertebra and the caudal series. Pectoral elements include a partial left scapula and coracoid and a fragmentary left humerus. Pelvic elements include both ilia, the proximal portion of both pubes, the proximal portion of the right ischium, an almost complete right femur, a fragmentary left femur and partial right tibia and fibula. There are also some phalanges from the right pedal digits III and IV.

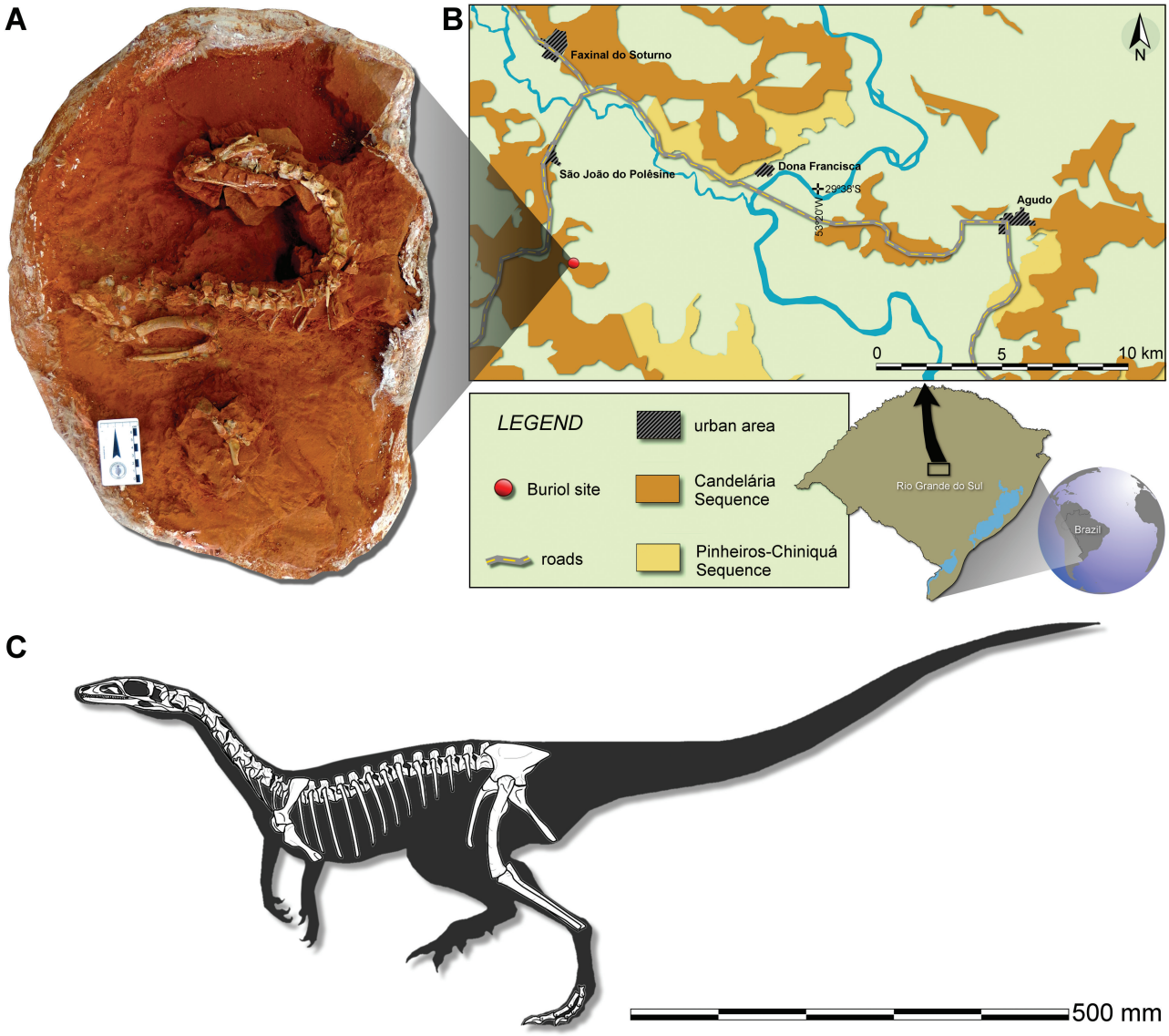

Figure 1. CAPPA/UFSM 0035 and the location of the study area. A, CAPPA/UFSM 0035 in the rock block before the final preparation. B, map of the São João do Polêsine area, Rio Grande do Sul, Brazil, showing the location of the Buriol outcrop (modified from Müller *et al.*, 2017). C, reconstruction of the preserved portions of the skeleton of CAPPA/UFSM 0035.

Locality and horizon

The new specimen was excavated from the Buriol outcrop (29°39′34.2″S; 53°25′47.4″W), in São João do Polêsine, Rio Grande do Sul, Brazil (Fig. 1B). This outcrop corresponds to the type locality of *B. schultzi* (Cabreira *et al.*, 2016). CAPPA/UFSM 0035 comes from the same layer that yielded the holotype (ULBRA-PVT280). Site strata belong to the lower portion of the Candelária Sequence (Horn *et al.*, 2014), which is part of the Santa Maria Suspersequence of Zerfass *et al.* (2003) (Fig. 2). The presence of specimens ascribed to the rhynchosaur *Hyperodapedon* (Dias-da-Silva, Cabreira & Roberto-da-Silva, 2011; Roberto-da-Silva *et al.*, 2014; Müller *et al.*, 2017) allows the correlation with the Ischigualasto Formation, in northwest Argentina, radioisotopically dated as 231.4 ± 0.3 Mya (Martínez *et al.*, 2011). In addition to *B. schultzi* and *Hyperodapedon* sp., the Buriol outcrop has also yielded the lagepetid *Ixalerpeton polesinensis* (Cabreira *et al.*, 2016), whereas fishes (dipnoi plate, hybodontiform shark spine and actinopterygian remains), aetosaurs, temnospondyls and cynodonts were found in close surrounding outcrops (Perez & Malabarba, 2002; Toledo & Bertini, 2005; Richter & Toledo, 2008; Dias-da-Silva *et al.*, 2011, 2012; Roberto-da-Silva *et al.*, 2014; Pacheco *et al.*, 2017).

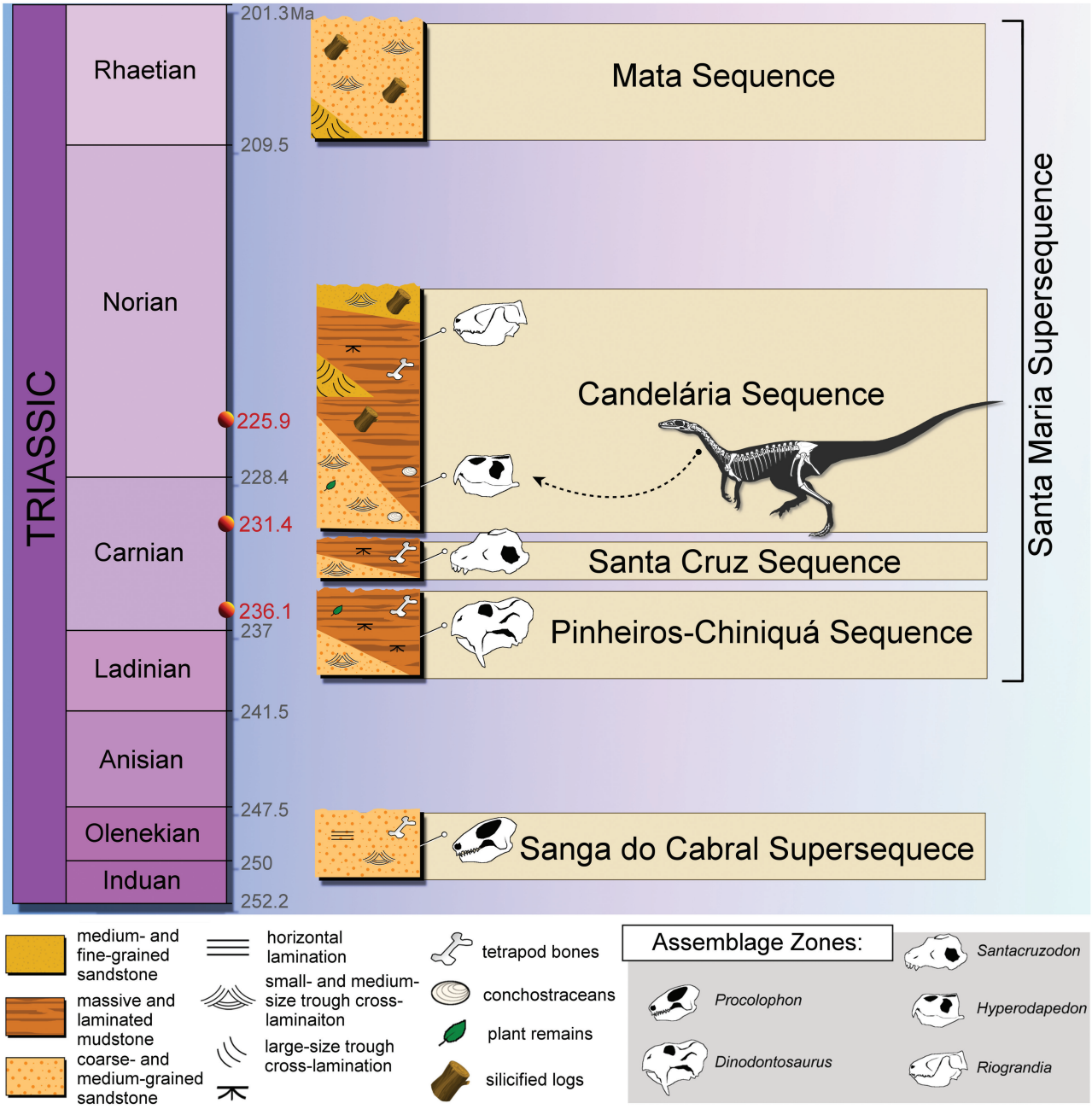

Figure 2. Chrono- and biostratigraphy of the Triassic units from southern Brazil, showing the level of CAPPA/UFSM 0035. Scheme based on Zerfass *et al.* (2003) and Horn *et al.* (2014). Geological time scale follows Gradstein *et al.* (2012). The radiometric dating of 236.1, 231.4 and 225.9 Mya corresponds to the first half of the Chañares Formation (Marsicano *et al.*, 2016) and the base of the Ischigualasto Formation (Martínez *et al.*, 2011), respectively.

DESCRIPTION

CRANIAL SKELETON

The skull preserves most bones in articulation (Figs 3–5), but some of them are almost entirely covered by matrix or other bones, for instance, the prootic, coronoid and intercoronoid. In addition, a few elements were displaced from their original position. Indeed, part of the skull roof suffered dorsoventral compression during fossil diagenesis. Hence, despite the excellent preservation, its height does not reflect the original condition. The skull length, from the preserved rostral tip of the premaxilla to the caudal margin of the occipital condyle, is 108.5 mm, but only the caudal

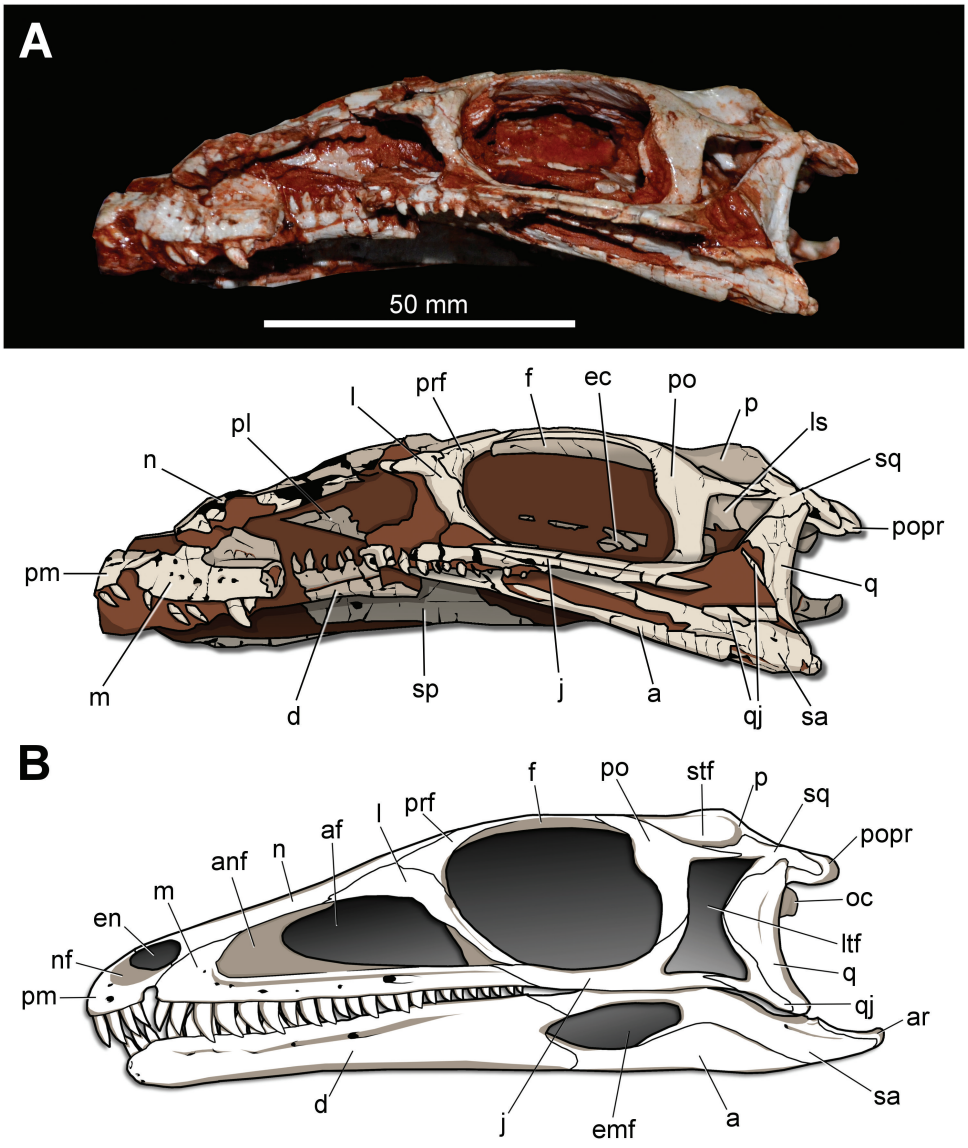

Figure 3. Skull of CAPPA/UFSM 0035 in left lateral view. A, photograph and interpretative drawing. B, reconstruction of the skull of *Buriolestes schultzi* (ULBRA-PVT280 plus CAPPA/UFSM 0035). Abbreviations: a, angular; af, antorbital fenestra; anf, antorbital fossa; ar, articular; ec, ectopterygoid; emf, external mandibular fenestra; f, frontal; j, jugal; l, lacrimal; ls, laterosphenoid; ltf, laterotemporal fenestra; m, maxilla; n, nasal; nf, narial fossa; oc, occipital condyle; p, parietal; pl, palatine; pm, premaxilla; po, postorbital; popr, paraoccipital process; prf, prefrontal; q, quadrate; qj, quadratojugal; sa, surangular; sp, splenial; sq, squamosal.

half of the premaxilla is preserved. This corresponds to ~80% of the femoral length. In contrast, the right lower jaw is entirely preserved, with a total length of 111.75 mm from the rostral tip of the dentary to the caudal extremity of the retroarticular process. The rostrocaudal length of the orbit is 25 mm; the internal antorbital fenestra is 24 mm long and has a maximal height of 10 mm. The external naris was probably low, given the dorsoventral space (3.5 mm) between the dorsal surface of the premaxilla and the ventral margin of the nasal (on the right side).

Premaxilla

Only the caudal portions of both premaxillae are preserved (Fig. 6). The left element, measuring 9 mm long and 4.75 mm wide (at the transversely wider portion) is more complete. Despite the poor preservation of the rostral region, it is clear that the premaxilla is slightly sloped, with its rostral portion projecting more ventrally than the caudal portio. Based on the preserved portion, it is possible to observe a shallow narial fossa. The rostral edge of the bone, as preserved, bears the caudal half of a foramen located at the rostrocaudal

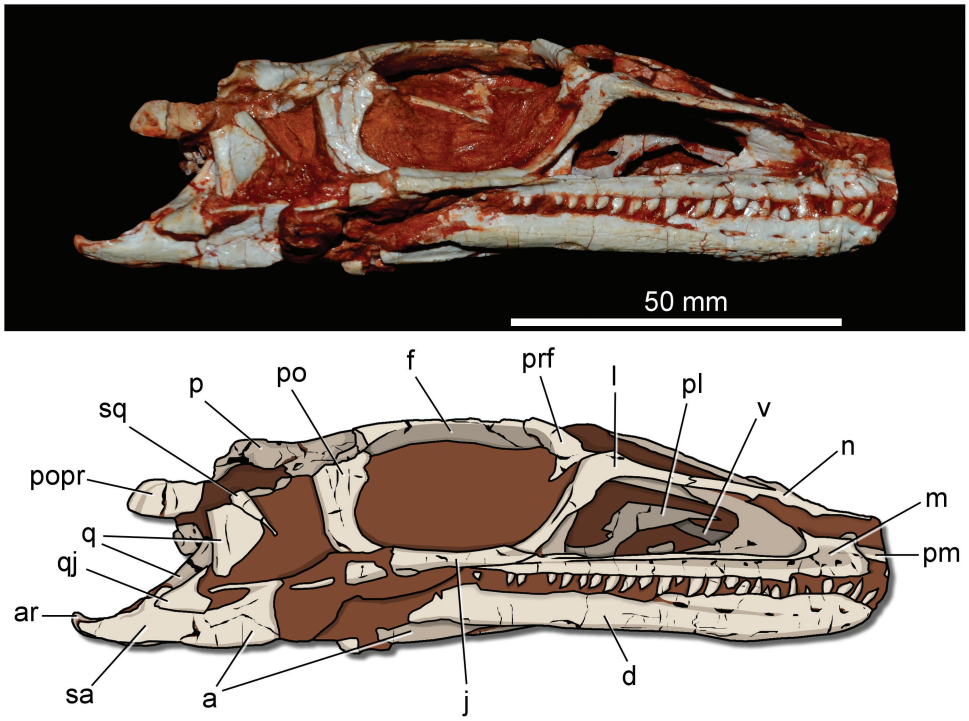

Figure 4. Photograph and interpretative drawing of the skull of CAPPA/UFSM 0035 in right lateral view. Abbreviations: a, angular; ar, articular; f, frontal; j, jugal; l, lacrimal; m, maxilla; n, nasal; p, parietal; pl, palatine; pm, premaxilla; po, postorbital; popr, paraoccipital process; prf, prefrontal; q, quadrate; qj, quadratojugal; sa, surangular; sq, squamosal; v, vomer.

level of the last premaxillary tooth. The caudolateral process tapers to a point caudally and does not project dorsally, although it contacts the rostroventral process of the nasal, excluding the maxilla from the caudal portion of the narial fenestra. In dorsal view, the caudomedial premaxillary margin is rounded in response to the lateral direction of the caudolateral process. The caudal margin of this process rests on the rostral process of the maxilla. Below it, a 3.5-mm-long subnarial gap marks the contact between the premaxillary and maxillary alveolar margins (Fig. 6A). The premaxilla contributes to the convex rostrodorsal margin of the gap, resulting in a semicircular gap.

Maxilla

Both maxillae are almost entirely preserved (Fig. 7). The bone is ~60 mm long, corresponding to ~55% of the total skull length. The rostral process is short (~12% of the total rostrocaudal length of the bone), with the dorsal margin (which receives the premaxilla) oblique to the main axis of the maxilla. Its ventral/alveolar margin is slightly upturned at the rostral half but aligned to that of the rest of the maxilla in the caudal half. The rostral margin of the rostral process is excavated (Fig. 7A, B), forming the caudal border of the subnarial foramen, as in the holotype (ULBRA-PVT280) of *B. schultzi*. This condition is unique among early dinosaurs, with the subnarial foramen totally confluent with the subnarial gap. In addition, several other foramina pierce the lateral surface of the rostral process. The dorsal process of the maxilla is not well expanded, and its dorsal margin is almost parallel to that of the caudal process of the maxilla, resulting in a dorsoventrally low rostrum. The caudal tip of the dorsal process reaches the middle of the antorbital fenestra, and its dorsal surface receives the ventral surface of the nasal. The height of the facial maxillary surface, between the alveolar margin and the ventral limit of the dorsal process, corresponds to about one-third of the height of the dorsal process.

The caudal process of the maxilla is elongated (~90% of the total craniocaudal length of the bone) and tapers caudally along its distal tenth. A longitudinal ridge divides the lateral and dorsal surfaces of the caudal process, bordered ventrally by a row of neurovascular foramina, the caudalmost of which is associated with a 4-mm-long caudal fossa. The alveolar margin of the caudal process is straight along its entire length. The process extends until the midhalf of the ventral border of the orbit, where the jugal articulates to the dorsal surface of the bone. The ventral portion of the medial surface of the maxilla is dorsoventrally convex, where the maxillary dentition is separated by lanceolate interdental plates (Fig. 7C). The palatine is

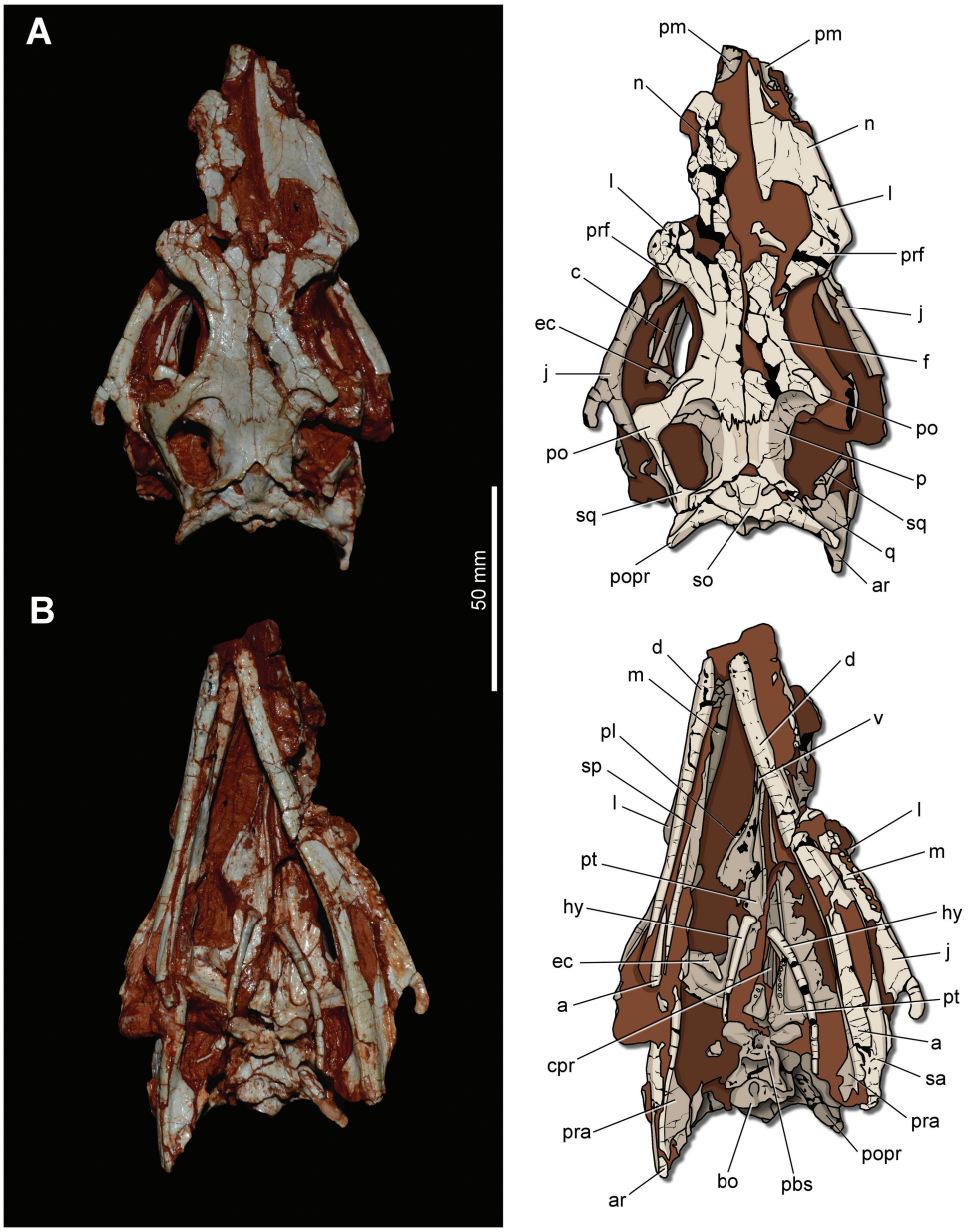

Figure 5. Skull of CAPPA/UFSM 0035. A, photograph and interpretative drawing in dorsal view. B, photograph and interpretative drawing in ventral view. Abbreviations: a, angular; ar, articular; bo, basicoccipital; c, coronoid; cpr, cultriform process; d, dentary; ec, ectopterygoid; f, frontal; hy, hyoid; j, jugal; l, lacrimal; n, nasal; p, parietal; pbs, parabasisphenoid; pl, palatine; pm, premaxilla; po, postorbital; popr, paraoccipital process; pra, prearticular; prf, prefrontal; pt, pterygoid; q, quadrate; sa, surangular; so, supraoccipital; sp, splenial; sq, squamosal; v, vomer.

disarticulated from the maxilla, but it probably contacted the medial surface of the main body of the bone on the caudal half of the antorbital fenestra.

The maxillary antorbital fossa is slightly longer rostrocaudally than dorsoventrally deep and restricted to the rostral portion of the antorbital fenestra. There is no promaxillary fossa at the rostral extremity of the antorbital fossa. The ventral portion of the antorbital fossa extends caudally for half the total craniocaudal length of the caudal process of the maxilla.

Nasal

The rostral portion of both nasals is not preserved (Fig. 7). Yet, based on premaxillary and maxillary morphology, it is reasonable to assume that the original nasal length is ~0.35 of the total skull length. The

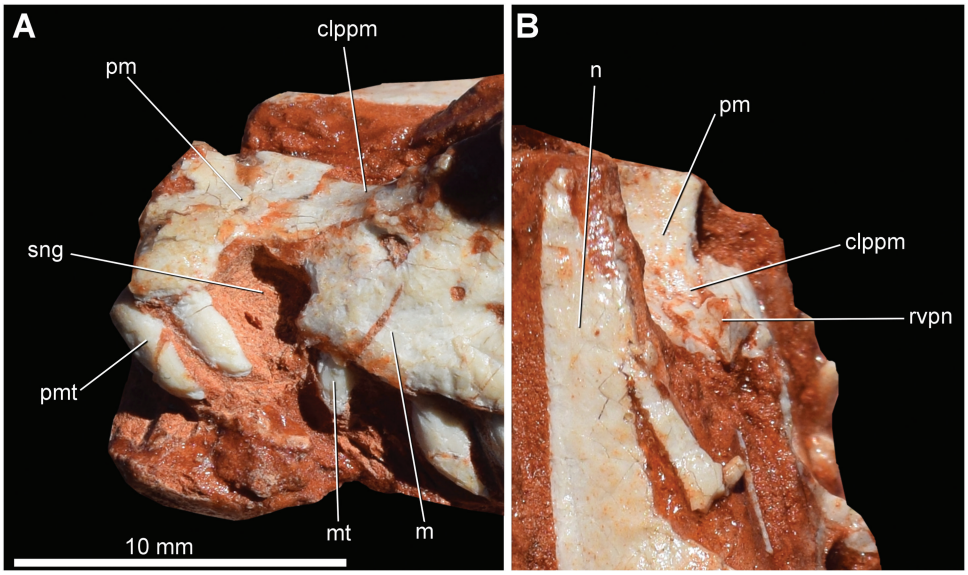

Figure 6. Cranial end of the skull of CAPPA/UFSM 0035. A, left lateral view. B, dorsal view. Abbreviations: clppm, caudolateral process of the premaxilla; m, maxilla; mt, maxillar tooth; n, nasal; pm, premaxilla; pmt, premaxillar tooth; rvpn, rostroventral process of the nasal; sng, subnarial gap.

nasal is dorsoventrally flat and 16 mm broad at the point of maximal transverse extension. Its rostral portion slopes ventrally, so that the bone is gently inclined. Its dorsal surface is mostly smooth, but slightly excavated along the internasal suture. The nasal rests on the dorsal surface of the dorsal process of the maxilla, forming a laterally expanded bone shelf and the dorsal roof of the antorbital fenestra (Fig. 8A). The ventral edge of the shelf is lateromedially concave and projects further laterally than the maxilla, so that the nasal is also observed in palatal view. The caudolateral process envelops the rostral process of the lacrimal, covering a small portion of the latter in lateral view. The nasal contact with the prefrontal and frontal is obscured by the fragmentary condition of the caudal portion of the nasals. The tip of the rostroventral process of the right nasal is preserved, being laterally covered by the maxilla and resting on the dorsal surface of the caudolateral process of the premaxilla, forming the caudal margin of the external naris (Fig. 8).

Lacrimal

The right lacrimal is completely preserved (Fig. 8A), whereas part of the rostral process is missing in the left one. The ventral and dorsal portions of the lacrimal are strongly offset, with the dorsal portion projecting laterally. The lacrimal separates the antorbital fenestra from the orbit, its height corresponding to two-thirds that of the fenestra. Its caudal margin forms an angle of ~45° with the caudal process of the maxilla. The rostral process is rostrocaudally longer (16 mm) than the ventral process (14 mm), folding over the caudodorsal part of the antorbital fenestra and forming a rostral notch that fits the nasal. At the point of its maximal transverse extension, the rostral process is 9.5 mm broad. This portion also corresponds to the broadest part of the preorbital portion of the skull. The lateral and medial edges of the rostral process expand ventrally, forming a slightly concave ventral surface or invagination. Part of the rostral and medial edges of the rostral process articulates with the nasal. The caudally concave caudomedial margin of the lacrimal receives the prefrontal, which extends ventrally along its medial margin.

The rostral and ventral processes of the lacrimal form a right angle. A lateral flange extends over the dorsal half of the ventral process (Fig. 8A). The dorsal portion of this flange merges rostrally with the ventral ridge of the rostral process. On the medial portion of the lacrimal, a marked ridge forms the caudal part of the antorbital fossa, corresponding to the rostral portion of the ventral process of the lacrimal. On the caudal surface of that process, the lacrimal foramen is visible (Fig. 9B), caudoventrally bordered by a shallow excavation. The contact with the jugal occurs at the level of the ventral margin of the orbit, where the ventral surface of the lacrimal overlaps the dorsal surface of the rostral tip of the jugal. The displaced condition of both lacrimals precludes the observation of a putative contact with the maxilla.

Prefrontal

The left prefrontal is nearly complete (Fig. 9), whereas the right one lacks the ventral process (Fig. 8A). This

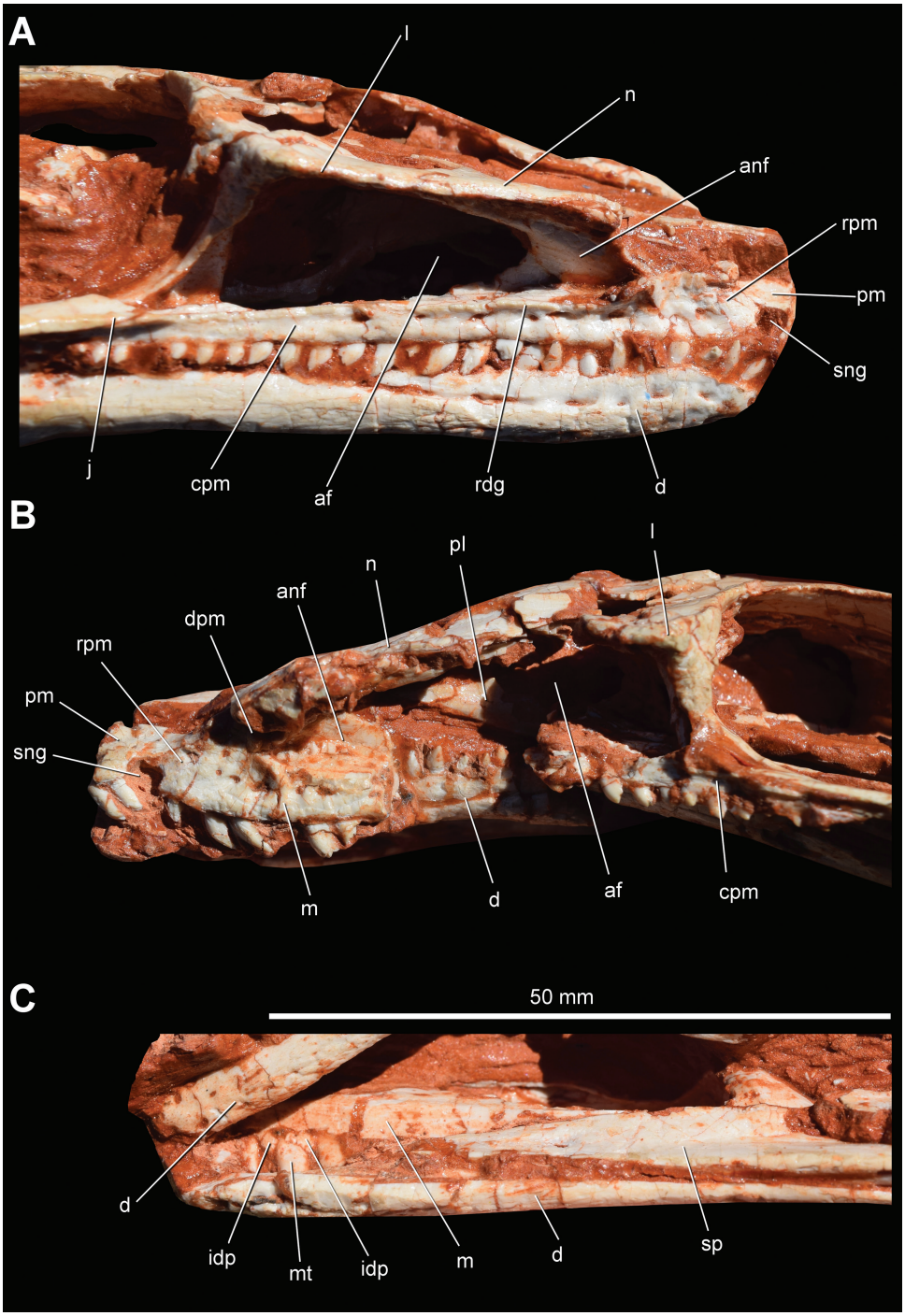

Figure 7. Snout of the skull of CAPPA/UFSM 0035. A, right lateral view. B, left lateral view. C, medial view of the right maxilla. Abbreviations: af, antorbital fenestra; anf, antorbital fossa; cpm, caudal process of the maxilla; d, dentary; dpm, dorsal process of the maxilla; idp, interdental plate; j, jugal; l, lacrimal; mt, maxillary tooth; n, nasal; pl, palatine; pm, premaxilla; rdg, ridge; rpm, rostral process of the maxilla; sng, subnarial gap; sp, splenial.

bone has a concave caudal margin that forms the rostrodorsal part of the orbital rim. The prefrontal articulates with the nasal rostrally, the lacrimal rostrolaterally, and the caudal process expands somewhat to fit medially an excavation on the frontal. In dorsal view, the caudal process is leaf shaped, with its tip tapering to a point (Fig. 9A). The process is 20 mm long and restricted to the rostral half of the orbit. Its medial

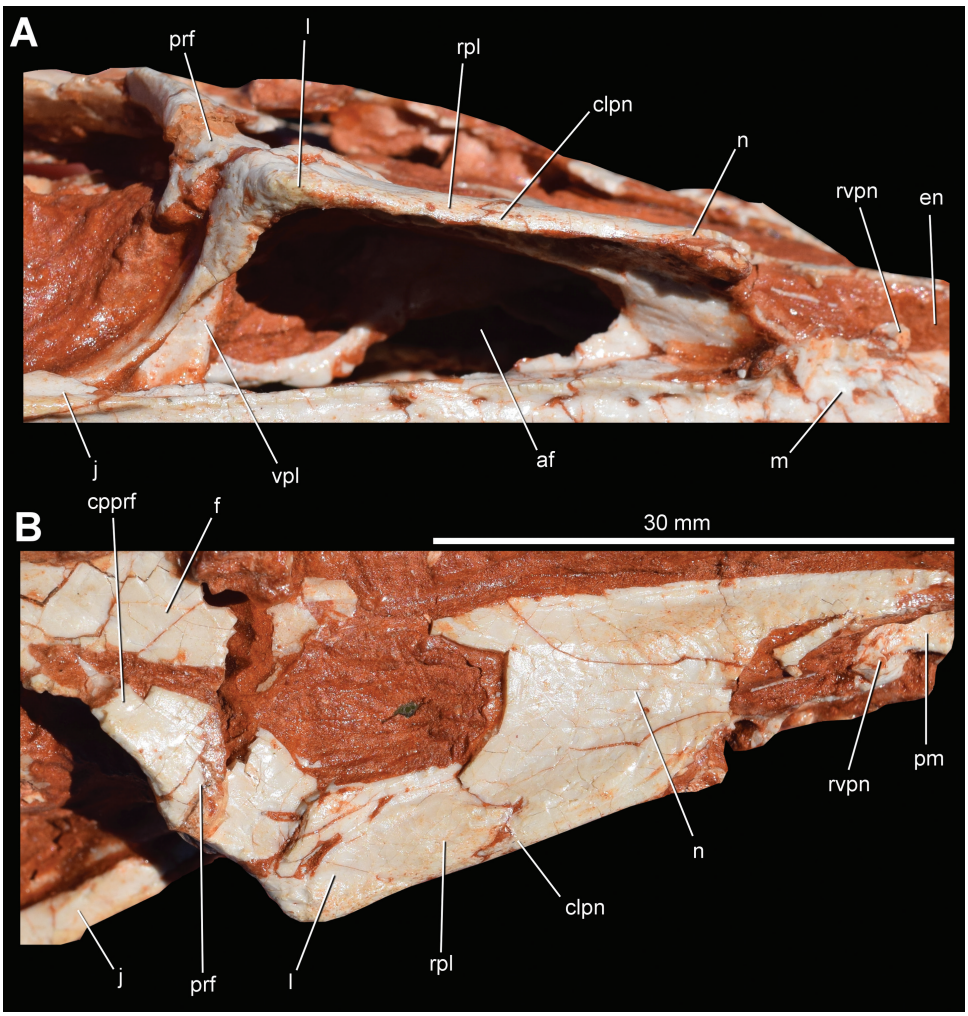

Figure 8. Right antorbital region of the skull of CAPPA/UFSM 0035. A, lateral view. B, dorsal view. Abbreviations: af, antorbital fenestra; clpn, caudolateral process of the nasal; cpprf, caudal process of the prefrontal; en, external nares; f, frontal; j, jugal; l, lacrimal; m, maxilla; m, nasal; prf, prefrontal; prf, rpl, rostral process of the lacrimal; rvpn, rostroventral process of the nasal; vpl, ventral process of the lacrimal.

margin is straight, becoming gently convex rostrocaudally. In the caudolateral margin, a bony sheet connects the dorsal process to the ventral one (Fig. 9B). In addition, it covers the caudodorsal portion of the main body of the lacrimal. The ventral process of the prefrontal is narrow (~1.5 mm in width) and articulates with the lacrimal laterally.

Frontal

In this paired element, the rostral margin is fractured (Fig. 9A). The bone is longer (38 mm) than wide (17 mm in the caudal portion), and the caudal margin is slightly wider than the rostral one (10.5 mm). Their respective lateral projections give a concave aspect to the lateral margin of the frontal in dorsal/ventral view, where it forms the entire dorsal margin of the orbital rim. At the middle of the orbital rim, the lateral and the medial edges are slightly elevated in comparison with the surface between them. The lateral margin of the frontal is as not as dorsoventrally deep (i.e. 1 mm in height) as the medial margin (5.5 mm in height). The interfrontal suture is straight and occupies the entire medial margin of the bones (Fig. 8A). Rostrally, the frontal articulates with the nasal, and a V-shaped notch on the lateral region corresponds to the articulation with the prefrontal. On the dorsal surface of the caudolateral process, there is a sigmoid excavation for the articulation with the postorbital, which tapers medially. Mediocaudally, the frontal contacts the parietal via a well-marked interdigitating suture. On the lateral portion of the caudal part of the frontal, an 8-mm-broad depression corresponds to the rostral extension of the supratemporal fossa. This surface probably received the m. pseudotemporalis

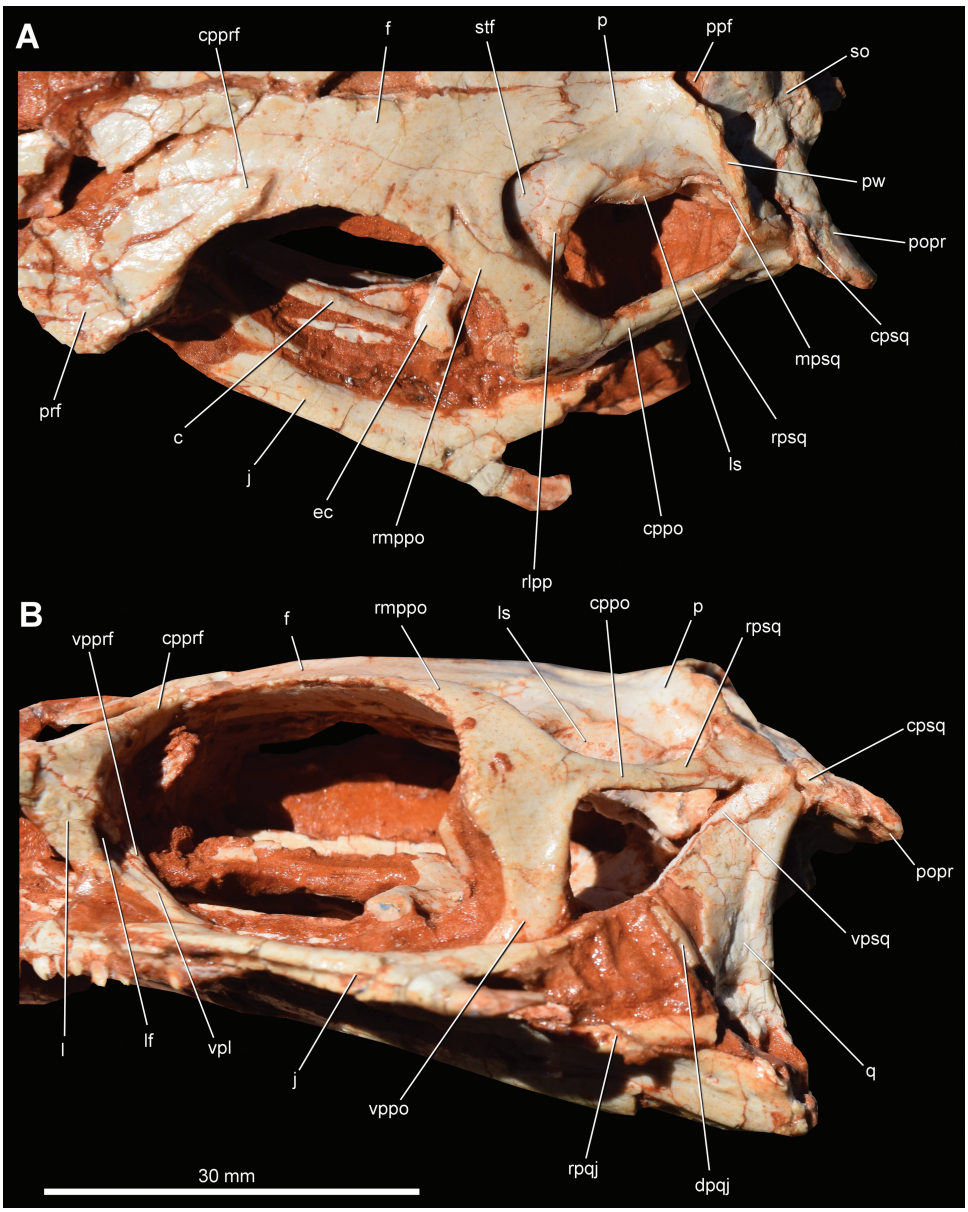

Figure 9. Left orbital region of the skull of CAPPA/UFSM 0035. A, dorsal view. B, lateral view. Abbreviations: c, coronoid; cppo, caudal process of the postorbital; cpprf, caudal process of the prefrontal; cpsq, caudal process of the squamosal; dpqj, dorsal process of the quadratojugal; ec, ectopterygoid; f, frontal; j, jugal; l, lacrimal; lf, lacrimal foramen; ls, laterosphenoid; mpsq, medial process of the squamosal; p, parietal; popr, paraoccipital process; ppf, postparietal fenestra; prf, prefrontal; pw, parietal wing; q, quadrate; rlpp; rostrolateral process of the parietal; rmppo, rostromedial process of the postorbital; rpqj, rostral process of the quadratojugal; rpsq, rostral process of the squamosal; so, supraoccipital; stf, supratemporal fossa; vpl, ventral process of the lacrimal; vppo, ventral process of the postorbital; vpprf, ventral process of the prefrontal; vpsq, ventral process of the squamosal.

superficialis (Button, Barrett & Rayfield, 2016), and its rostral margin forms a shallow rostral invagination. Although the frontal has an extensive participation in the supratemporal fossa, it is excluded from the internal supratemporal fenestra by the parietal–laterosphenoid contact.

Parietal

The specimen preserves both parietals, with the left one being better preserved (Fig. 9). The bone is 20 mm long, 14 mm wide at the rostral edge and 13 mm wide at the caudal edge. In dorsal/ventral view, the lateral margin of the parietal is concave and the medial is

straight. The interparietal suture indicates that the parietals are not fused, but there is no clear evidence of a foramen between them. The rostral margin of the parietal contacts the frontal via a serrated suture. The rostrolateral process articulates with the postorbital dorsally and with the laterosphenoid ventrally. The dorsal surface of the parietal possesses a medial depression bounded laterally by a low longitudinal ridge (Fig. 9A). This ridge delimits the medial margin of the supratemporal fossa, which housed the m. adductor mandibulae externus profundus (see Dilkes *et al.*, 2012; Sereno, 2012). The parietal wings diverge from one another caudolaterally, forming an angle of ~60° with the caudomedial border of the supratemporal fossa. In this region, the parietal contacts the squamosal laterally, the supraoccipital rostromedially and the paroccipital process of the opisthotic caudomedially. In dorsal/ventral view, the rostral surface of the parietal wing is convex, whereas the caudal is concave; the latter probably related to the m. transversospinalis capitis (Snively & Russell, 2007). A large triangular-shaped postparietal fenestra occurs between the caudal margin of these wings and the rostral end of the supraoccipital (Fig. 9A).

Postorbital

The postorbital comprises a triradiate bone with rostromedial, ventral and caudal processes. The left postorbital is complete (Fig. 9B), whereas the right one lacks the caudal process. The rostromedial process articulates with the frontal medially, forming the caudodorsal portion of the orbital rim. The caudal half of the rostromedial process contacts the parietal and the laterosphenoid medially. In dorsal view, the process is sigmoid, with its tip tapering to a point. The caudal surface of the process forms the rostrolateral margin of the supratemporal fenestra. The ventral process is slightly displaced, but *in vivo* it would have been articulated with the jugal, forming part of the caudal margin of the orbital rim. The tip of the ventral process is pointed and directed rostroventrally. Part of the caudal margin of the ventral process forms the dorsalmost portion of the rostral margin of the laterotemporal fenestra. The rostral margin of the bone, between the rostromedial and ventral processes, bears a rostrally oriented orbital flange (Fig. 9B). It invades the caudal rim of the orbit and has a rough rostral edge. The caudal process is 11.5 mm long and slender in comparison with the other two processes of the bone. It becomes dorsoventrally narrower rostrocaudally, where it tapers to a point. The process fits into the lateral surface of the rostral process of the squamosal, almost reaching the caudodorsal corner of the laterotemporal fenestra. A faint longitudinal ridge extends on the lateral surface of the caudal process, and it could be related to the attachment of m. adductor mandibulae externus superficialis.

Squamosal

Only the ventral process of the right squamosal is preserved, whereas the left element is complete (Fig. 9B). The squamosal is composed of four distinct processes: rostral, medial, ventral and caudal. The rostral process is ~12 mm long, with a gently rostrocaudally convex medial surface that delimits the lateral margin of the supratemporal fenestra. Its ventral surface is straight and forms the dorsal margin of the laterotemporal fenestra. The lateral surface accommodates the caudal process of the postorbital in a V-shaped notch. A thin ridge rises from the caudal portion of the dorsal surface of the rostral process, folding medially. This leads to the medial process, which is 5 mm wide. The dorsal surface of this process receives the parietal wing.

The ventral process forms an angle of ~45° with the rostral process. It extends rostroventrally and tapers to a point. The caudal surface is concave in lateral view and articulates with the rostral surface of the quadrate. Its ventral tip contacts the dorsal tip of the quadratojugal, extending until the rostralmost portion of the lateral quadrate flange. The ventral process is rostrocaudally short and does not wrap the quadrate shaft medially. The caudal process is 6.75 mm long. It articulates against the quadrate ventrally and with the paroccipital process caudally. The process bears a caudal projection that extends 5 mm over the articulation with the quadrate. It is plate like and slightly laterally oriented, following the orientation of the paroccipital process. Together with the paroccipital process, this projection might have supported m. depressor mandibulae (Sereno, 2012).

Jugal

The left jugal is better preserved than the right one (Fig. 10), but both elements are fractured and displaced from their original position, as their ventral surfaces are visible in lateral view. The jugal is Y shaped, including three main processes. The rostral process is 22 mm long, contributes to the ventral margin of the orbit, and is subparalel to the caudal ramus of the maxilla. Both ventral and dorsal margins of the rostral process are parallel along almost their entire length, but it tapers rostrally. Its tip rests in a slot on the caudal portion of the maxilla and receives the ventral margin of the lacrimal dorsally. On the right side, the tip of the process contributes minimally to the caudoventral corner of the external antorbital fenestra. On the lateroventral surface of the rostral process, a longitudinal ridge marks the lateral margin of a longitudinal fossa. Sereno (2012) speculated that a putative homologous surface in *Heterodontosaurus tucki* could support the origin of the m. adductor mandibulae externus ventralis.

The dorsal process of the jugal extends dorsocaudally, forming an angle of 45° with the caudal process.

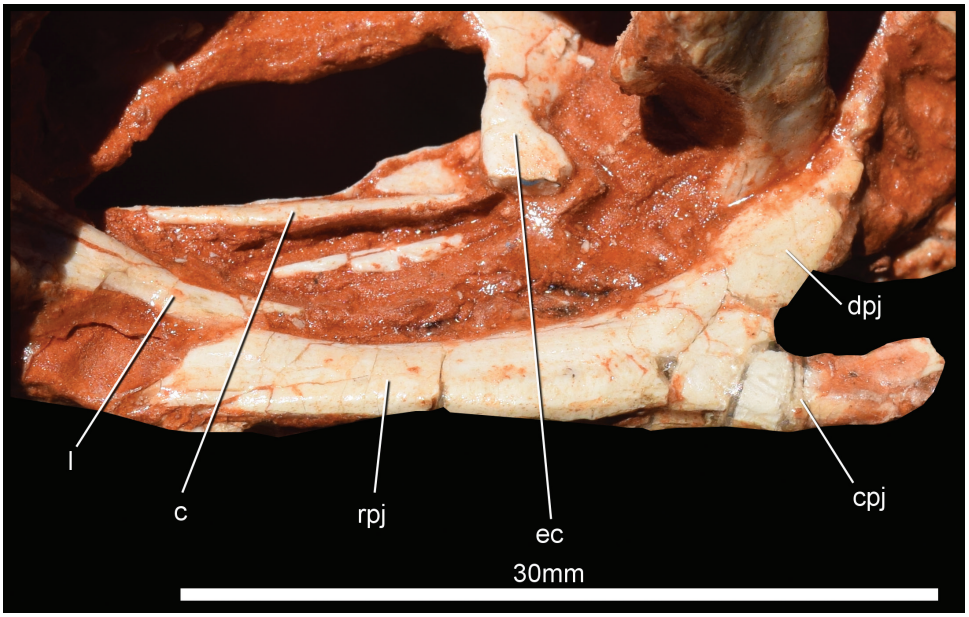

Figure 10. Jugal of CAPPA/UFSM 0035 in lateral view. Abbreviations: c, coronoid; cpj, caudal process of the jugal; dpj, dorsal process of the jugal; ec, ectopterygoid; l, lacrimal; rpj, rostral process of the jugal.

Its tip tapers to a point. The rostral margin articulates against the ventral process of the postorbital, whereas the caudal surface forms the ventral half of the rostral margin of the laterotemporal fenestra. The caudal process is poorly preserved in both elements. Nonetheless, it is possible to observe that they do not fork close to their rostral portion (Fig. 10), but a pedicel is present between the base and the caudal bifurcation of the caudal process.

Quadratojugal

Only the caudal portion of the right quadratojugal is preserved (Fig. 4), whereas for the left one part of the dorsal and cranial processes is preserved (Fig. 9B). The bone would exhibit the typical inverted L shape, but as the length of the processes is uncertain, this cannot be stated with certainty. The dorsal process articulates with the ventral part of the rostral surface of the quadrate, forming the ventrocaudal margin of the laterotemporal fenestra. The dorsal portion of the dorsal process is caudally concave in lateral view, and its tip contacts the ventral tip of the squamosal.

The rostral process seems to be longer (or at least subequal in length) and more robust than the dorsal process. Both processes form an almost right angle, tapering to a point at their tips. The articulation with the jugal is not well preserved, but the caudal portion of the quadratojugal is triangular in lateral view. Its lateral surface is convex, and the ventral margin is straight (Fig. 4). Indeed, the notch on the ventral margin of the caudalmost portion of the bone, present in *Eoraptor lunensis* (Sereno, Martínez & Alcober, 2013), is absent in CAPPA/UFSM 0035, as well as in the holotype of *B. schultzi*. The quadratojugal has a limited contribution to the craniomandibular joint, contacting only a restricted portion of the dorsolateral surface of the surangular.

Quadrate

Both quadrates are preserved in the specimen. The right element is broken into two pieces (Fig. 11), dorsal and ventral, whereas the left one lacks the condyles (Fig. 11A). In lateral view, the quadrate is arched (e.g. with convex cranial and concave caudal margins). The quadrate head is rounded, and it rests in a socket on the ventral surface of the squamosal (Fig. 9B). Ventral to that, the quadrate shaft bears two longitudinal bone flanges (Fig. 11A). The lateral one is rostrolaterally oriented, articulating dorsally with the ventral process of the squamosal and ventrally with the dorsal process of the quadratojugal. The ventral margin of the lateral flange connects smoothly onto the shaft, whereas that contact is more abrupt at the dorsal margin. There is no clear evidence of a quadrate foramen in the specimen. The other flange rises from the quadrate shaft (i.e. the pterygoid ramus). It is rostromedially directed, and its lateral surface has been considered the origin of the m. adductor mandibulae posterior (Button *et al.*, 2016). There is a dorsoventrally oriented groove on the medial surface of the bone, between its shaft and the pterygoid ramus. Ventral to that, a horizontal shelf is visible, but fractured and incomplete in both elements.

The quadrate shaft is transversely expanded (9 mm in width) in its ventral portion, where both mandibular

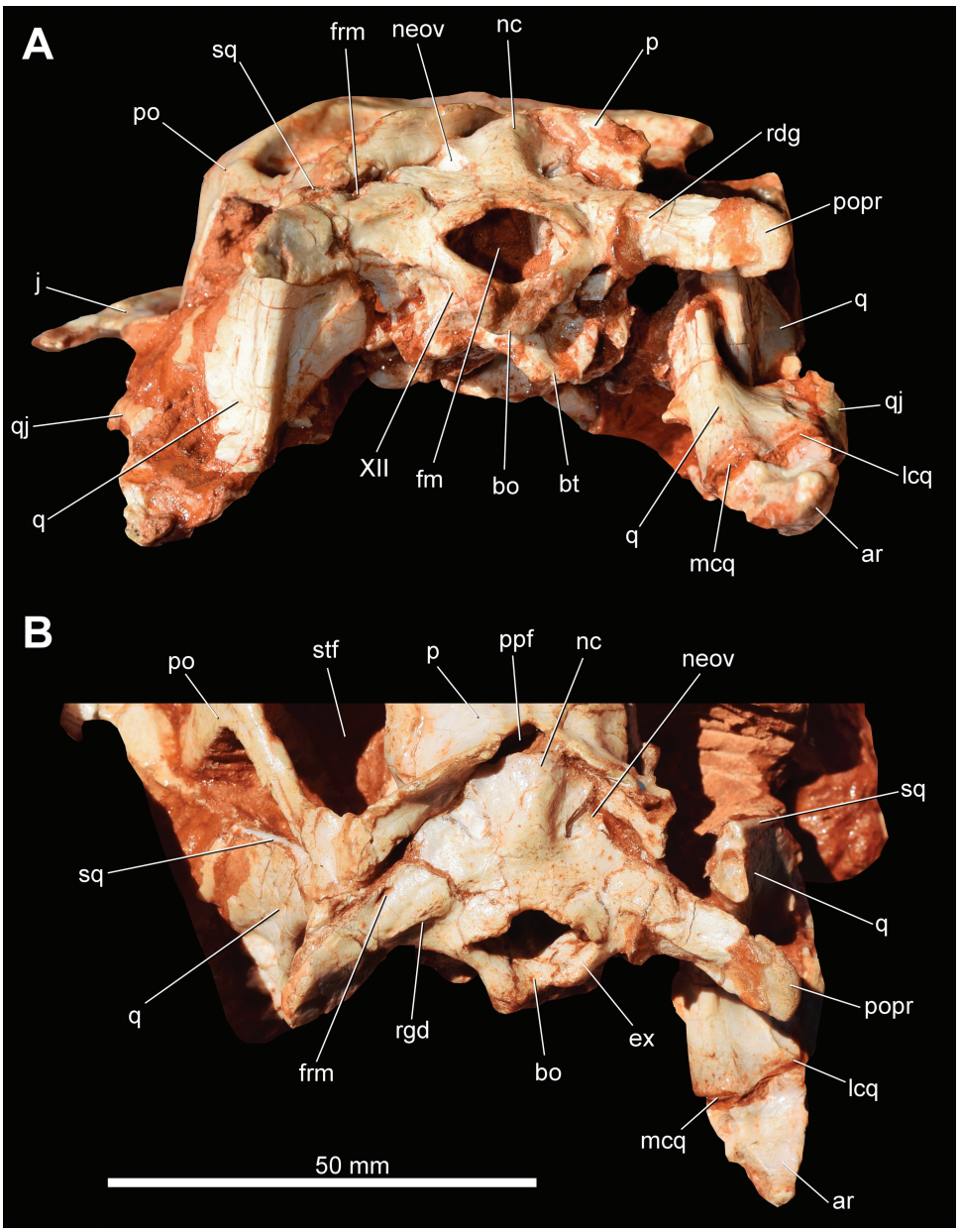

Figure 11. Caudal portion of the skull of CAPPA/UFSM 0035. A, occipital view. B, dorsal view. Abbreviations: ar, articular; bo, basioccipital; bt, basal tubera; ex, exoccipital; fm, foramen magnum; frm, foramen; j, jugal; lcp, lateral condyle of the quadrate; mcq, medial condyle of the quadrate; nc, nuchal crest; neov, notch for the external occipital vein; p, parietal; po, postorbital; popr, paraocciptal process; ppf, postparietal fenestra; q, quadrate; qj, quadratojugal; rdg, ridge; sq, squamosal; stf, supratemporal fenestra; XII, foramen for hypoglossal nerve.

condyles are located (Fig. 11). The medial condyle exceeds the caudal expansion of the lateral and articulates with both articular and prearticular. Close to the contact with the lower jaw, the caudal surface of the bone bears a transverse protuberance, and a shallow groove divides the medial and lateral condyles. The latter is laterally covered by the quadratojugal and articulates ventrally with the articular and surangular.

Pterygoid

Both pterygoids are preserved, but only their palatal view is exposed (Fig. 12). The left pterygoid is almost complete. It is ~70 mm long, comprising more than one-half of the total skull length. Each element contacts its opposite medially via a caudomedial process in the caudal portion. Along the rostral length, the pterygoids are separated from one another by the

interperygoid vacuity, in which the caudal half of the parasphenoid is observable.

The rostral ramus of the pterygoid is long, reaching the rostral half of the antorbital fenestra. Laterally, the rostral ramus articulates with the palatine, but a small part of its lateral edge participates in the caudomedial margin of the postpalatine fenestra, precluding the contact between the palatine and ectopterygoid. The caudal portion of the rostral ramus forms a subtriangular lamina, whereas the rostral part becomes transversely narrower, with a marked ventral ridge forming its medial edge. This ridge extends along the entire

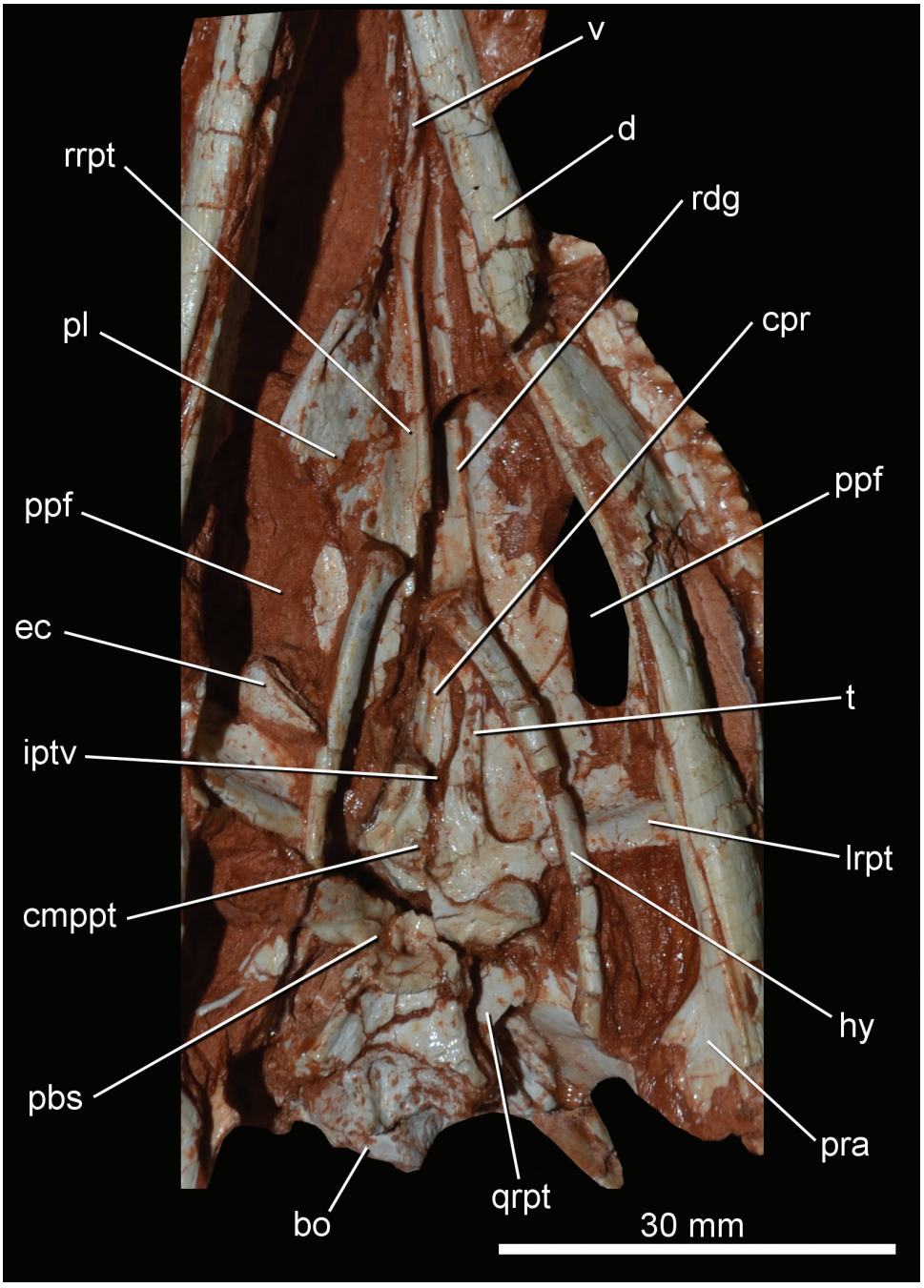

Figure 12. Ventral view of the palate of CAPPA/UFSM 0035. Abbreviations: bo, basioccipital; cmppt, caudomedial process of the pterygoid; cpr, cultriform process; d, dentary; ec, ectopterygoid; hy, hyoid; iptv, interpterygoid vacuity; lrpt, lateral ramus of the pterygoid; pbs, parabasisphenoid; pl, palatine; ppf, postpalatine fenestra; pra, prearticular; qrpt, quadrate ramus of the pterygoid; rdg, ridge; rrpt, rostral ramus of the pterygoid; t, tooth; v, vomer.

length of the rostral ramus. It is more conspicuous on the rostral half, where it meets the caudal part of the vomer. The ridge is wider in its caudal half, supporting a row of small palatal teeth. The ridge then turns laterally at its caudal part, extending along the lateral ramus, which forms a right angle with the rostral ramus. The lateral ramus is thicker dorsoventrally and extends laterally in the direction of the adductor fossa of the lower jaw. The quadrate ramus of the pterygoid projects caudally, forming a thin bony sheet with a concave lateral margin in palatal view. This structure articulates to the shelf on the medial surface of the quadrate. In palatal view, the basipterygoid process of the basisphenoid overlaps the quadrate ramus of the pterygoid, being overlapped by its caudal process, the latter simply corresponding to a caudal projection with a rounded margin.

Palatine

Both palatines are preserved in the specimen, with the right exposed in lateral (Fig. 4) and palatal views (Fig. 12), whereas the left is visible only in lateral view (Fig. 3A). The palatine is longer (31 mm) than wide (10 mm), with the medial margin of the rostral process, which is thin transversely, articulating against the caudal part of the vomer. In lateral view, the rostral portion of the palatine becomes shallower from the caudal to the rostral pointed tip. Its dorsal margin is straight, whereas the ventral is comparatively oblique. The caudal half of the palatine is dorsoventrally compressed and transversely broader than the rostral half. Its medial margin is longer than the lateral and lacks projections (i.e. peg-like structures). In palatal view, the pterygoid overlaps the thin medial lamina medially along its entire length. The lateral margin of the palatine is transversely flat, with a ventral lamina that articulates against the medial surfaces of the maxilla and the lacrimal. The caudolateral edge of the palatine forms the rostromedial margin of the postpalatine fenestra (Fig. 12), which is slightly shorter (19 mm in length) than the orbit.

Ectopterygoid

Both ectopterygoids are preserved (Figs 9, 12), but some parts are fractured and/or covered by rock matrix. The ectopterygoid rests on the dorsal surface of the transverse flange of pterygoid (Fig. 12) and connects the medial surface of the jugal to the palatal complex. The main body of the ectopterygoid is dorsoventrally compressed and longitudinally short, as observed in the preserved portion of the left element, which is 8 mm long. The lateral process is elongated, with the lateral extremity expanding caudally to contact the jugal. In ventral/dorsal view, the rostral margin of this process is convex and the caudal is concave. The bone lacks any ventral pneumatic recess, but a 9 mm dorsoventrally deep flange projects ventrally from the shaft of the lateral process. The flange is arched, with the concave margin facing medially. In addition, its rostral margin is convex, whereas the caudal is straight. The flange may articulate along the lateral margin of the pterygoid flange, as described by Sereno *et al.* (2013) for *E. lunensis* (PVSJ 512). However, both ectopterygoids are displaced from their original position, so the pterygoid–ectopterygoid suture is unclear.

Vomer

Only the caudal part of the right vomer is exposed (Figs 4, 12). It includes a transversely compressed lamina (~1 mm in width), which is longer than deep. The caudal end of that lamina rests in a groove bounded medially by the pterygoid and laterally by the palatine (Fig. 12). The caudal end of the bone extends until the middle of the antorbital fenestra and is caudodorsally oriented. Its caudal tip is slightly laterally oriented.

Supraoccipital

The supraoccipital is completely preserved (Fig. 11), with the following measurements: 12 mm long, 16 mm wide and 9 mm high. It contacts the parietal rostrally, the exoccipital–opisthotic ventrolaterally and, probably, the prootic rostroventrally. A low broad ridge on the medial portion of the cranial half of the bone corresponds to the nuchal crest. This structure seems to be related to the nuchal ligaments (Sereno & Novas, 1994). The tip of the rostral margin of the supraoccipital is almost straight.

The notch for the external occipital vein (= midcerebral vein; Sampson & Witmer, 2007) is visible on the dorsal surface of the supraoccipital, lateral to the nuchal crest, forming an angle of 45° with the longitudinal axis of the bone (Fig. 11). This indicates that the vein would exit the skull between the parietal and the supraoccipital. The dorsal surface of the supraoccipital is smooth immediately ventral to the notch. The caudal margin of the bone forms part of the dorsal margin of the foramen magnum, which is wider than deep (Fig. 11A). In addition, the caudal margin of the supraoccipital bears a medial notch, resulting in a concave outline (Fig. 11B).

Prootic

Both elements are preserved in the specimen, but the right one is badly fractured. The left is well preserved but covered by other bones, preventing a detailed observation (Fig. 13). The cranial half of the dorsal margin receives the laterosphenoid, whereas the caudal half contacts the parietal and the supraoccipital. Caudally, the bone articulates against the opisthotic. The ventral margin of the prootic rests on the dorsal surface of the parabasisphenoid. A caudoventrally oriented notch that corresponds to the opening for cranial nerve V (trigeminal) excavates the rostral margin of

the bone, dividing it into two regions. The dorsal one is dorsoventrally larger and tapers to a point rostrally, whereas the ventral is mostly covered by the laterosphenoid. There is a wide depression on the dorsal portion of the lateral surface, which is usually related to the tympanic recess (Fig. 13). The rostral portion of the bone, ventral to the notch for cranial nerve V, corresponds to the clinoid process. It bears an oblique crest extending at the lateral surface. The caudolateral portion of the prootic extends almost as caudally as the caudal margin of the quadrate.

Exoccipital–opisthotic

Usually, both elements are co-ossified in dinosaurs, forming the otoccipital (Sampson & Witmer, 2007), but this does not seem to be the case in the specimen described here, because a putative exoccipital–opisthotic suture is visible on the left side of the braincase (Fig. 14A). It starts dorsally on the lateral corner of the foramen magnum and extends ventrally. The opisthotic articulates laterally against the caudoventral margin of the supraoccipital and forms the ventral half of the lateral margin of the foramen magnum. Part of the rostral surface of the bone contacts the prootic and may also contact the caudal surface of the parietal. More dorsally, the bone receives both the squamosal and the quadrate.

The paraoccipital process is caudolaterally directed (Fig. 11B), and its caudal surface bears a transverse rugose ridge, which extends from the medial portion of the bone and merges on its lateral half. The surface ventral to the medial portion of that ridge is gently concave and possibly related to the insertion of m. iliocostalis capitis (Snively & Russell, 2007). A perforating foramen is present dorsal to the ridge, close to the dorsal margin of the bone. The ventral and dorsal margins of the paroccipital process are parallel along their length, so that the process does not expand distally (Fig. 11A). The distal tip of the process is rounded, with a rough texture, which resembles the area related to the insertion of m. longissimus capitis superficialis in some theropods (Snively & Russell, 2007). In caudal view, the ventral ramus of the opisthotic extends further laterally than the lateralmost edge of the exoccipital. On its dorsocaudal surface, the opisthotic bears a pair of depressions for the articulation of the proatlas.

The rostralmost of the two exits for the hypoglossal nerve (XII) is rostroventrally positioned relative to the caudal exit (Fig. 14A). The fenestra ovalis is separated from the more caudally located metotic foramen by the descending process of the opisthotic. However, a subvertical and crest-like strut separates the exits for cranial nerve XII from the metotic foramen, which is rostrally located relative to the exits. The exoccipitals do not articulate against one another on the floor of the endocranial cavity. Ventrally, the exoccipital rests on the dorsal surface of the basioccipital, forming the lateral and part of the ventral margins of the foramen magnum. In addition, the exoccipital participates in the dorsolateral portion of the occipital condyle (Fig. 11B).

Basioccipital

The basioccipital is entirely preserved, measuring 14 mm in width. Its dorsal surface forms the floor of the endocranial cavity (Fig. 11B), and the caudal portion

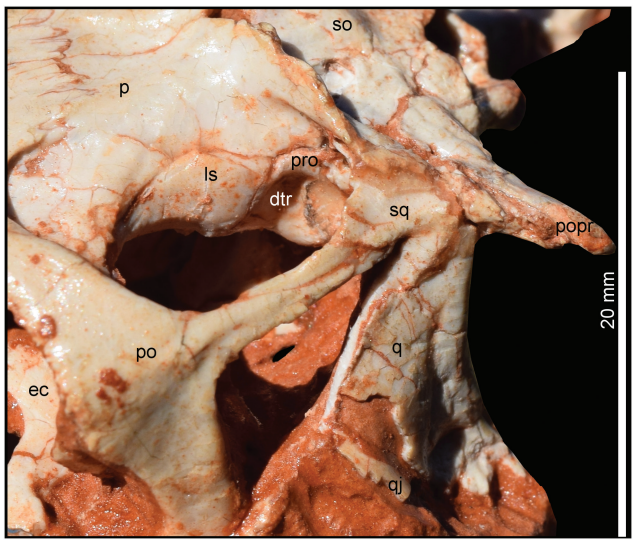

Figure 13. Left temporal region of the skull of CAPPA/UFSM 0035 in dorsolateral view. Abbreviations: dtr, dorsal tympanic recess; ec, ectopterygoid; ls, laterosphenoid; p, parietal; po, postorbital; popr, paraoccipital process; pro, prootic; q, quadrate; qj, quadratojugal; so, supraoccipital; sq, squamosal.

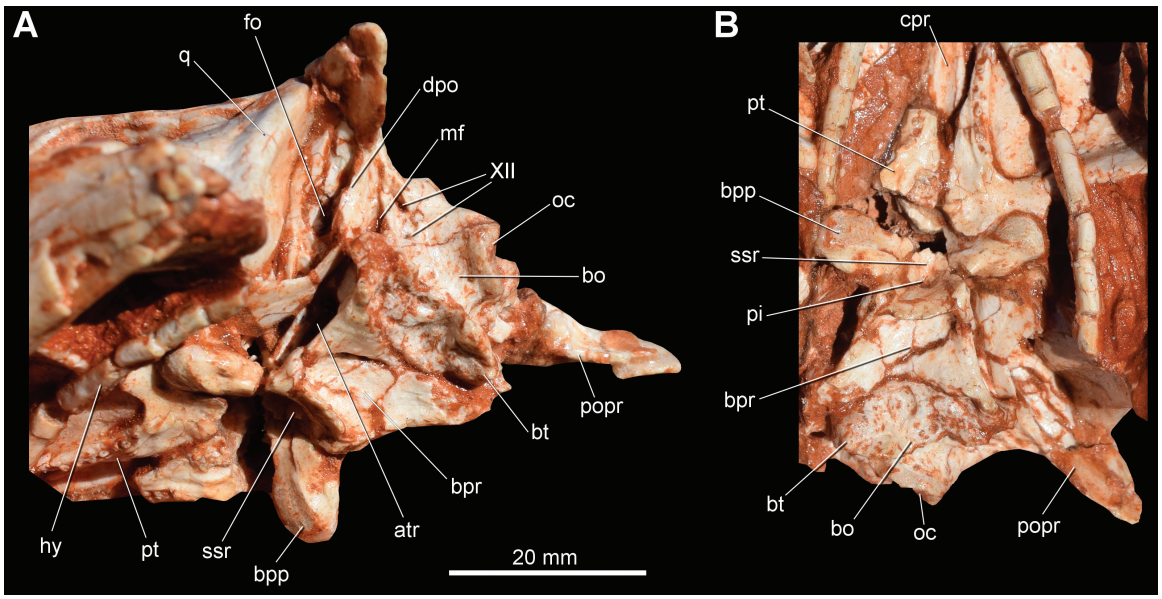

Figure 14. Caudal region of the skull of CAPPA/UFSM 0035. A, left lateroventral view. B, ventral view. Abbreviations: atr, anterior tympanic recess; bo, basioccipital; bpp, basipterygoid process; bpr, basisphenoid recess; bt, basal tubera; cpr, cultriform process; dpo, descending process of the opisthotic; hy, hyoid; mf, metodic foramen; oc, occipital condyle; pi, pit; popr, paraoccipital process; pt, pterygoid; q, quadrate; ssr, subsellar recess; XII, foramen for hypoglossal nerve.

contributes to the ventral margin of the foramen magnum. Together with the exoccipitals, the basioccipital forms the occipital condyle, which is heart shaped in occipital view (Fig. 11A). The occipital condyle is transversely narrower (7.5 mm) than the foramen magnum (9.5 mm). Ventrally, a subcondylar recess extends from the proximal margin of the occipital condyle to the basioccipital component of the basal tubera (Fig. 14). As in some other sauropodomorphs (Bronzati & Rauhut, 2017), the basioccipital component of the basal tubera corresponds to multiple protuberances on the ventrolateral surface of the bone, caudal to its rostromedial projection. A pair of protuberances occurs on each side of the basioccipital, medially separated by a U-shaped gap in occipital view. The lateralmost protuberances are located immediately dorsolateral to the medial ones and are smaller. The rostromedial projection of the basioccipital extends between those two caudolateral projections of the parabasisphenoid, carrying the basisphenoidal component of the tubera. This gives a U/V-shaped aspect to the contact between these two bones in ventral view. Within the rostromedial projection, a circular blind pit excavates the medial portion of the ventral surface of the basioccipital (Fig. 12). Inside the cranial cavity, a medial ridge occurs on the rostral portion of the dorsal surface of the basioccipital.

Parabasisphenoid

This 43-mm-long bone is almost entirely preserved (Fig. 12). It articulates rostrally with the pterygoid and caudally with the basioccipital. Its contact with the prootic is covered by matrix. Both the parasphenoid and the basisphenoid are co-ossified, as in other dinosaurs (Sampson & Witmer, 2007). A portion of the ventral surface of the bone, corresponding to the cultriform process of the basisphenoid, is visible in palatal view, within the interpterygoid vacuity. It is ~26 mm long and bears a ventral longitudinal groove, bounded by laminae on each side. The ventral surface of the process is set below the ventral surface of the occipital condyle.

On the caudal portion of the parabasisphenoid, two caudolateral projections, separated by the rostromedial process of the basioccipital, support the basisphenoidal component of the basal tubera. More rostrally, the basipterygoid processes project ventrolaterally. Together, these four projections give an X shape to the main body of the parabasisphenoid in ventral view (Fig. 14B). Central to these, a shallow depression corresponds to the basisphenoid recess (Witmer, 1997), which is not as developed as in neotheropods (Rauhut, 2004). The lateral surface of the braincase bears another 6-mm-long recess, which corresponds to the anterior tympanic recess. A well-developed (~6-mm-broad) crest extends transversely between the proximal portions of the basipterygoid processes, forming the separation between the basisphenoid recess caudally and the subsellar recess rostrally. The crest expands caudoventrally, forming a convex caudal surface. A circular foramen is present within the subsellar

recess. The basipterygoid processes are rounded and robust, and their caudal surface bears a rugose ridge. A faint, transversely oriented ridge divides their ventral surface.

Laterosphenoid

The specimen preserves both laterosphenoids. The bone is 10 mm long, corresponding to approximately one-third of the length of the supratemporal fenestra. Indeed, the laterosphenoid contributes to the medial half of the rostral margin of that fenestra, also forming almost its entire medial margin (Fig. 13). The lateral surface of the bone is concave in dorsal view, except for a gently convex mid-length projection. The tip of the rostrolateral process contacts the postorbital (Fig. 9A). At this point, the laterosphenoid is dorsoventrally narrower (~1.5 mm deep) than in its caudal part (9 mm deep at the maximal dorsoventral extension). The parietal fits on the straight dorsal surface of the bone. The prootic articulates against its caudoventral margin, where a notch is present, corresponding to the laterosphenoid portion of the trigeminal nerve (V) foramen (Fig. 7B). Rostrally, a groove extends from the notch.

Dentary

Both elements are well preserved, except for their caudalmost ends. They are not fused together in the symphysis, which occupies only their rostral margin. Indeed, the elements are preserved with the rostral portions separated from one another. The preserved portion of the right dentary is 65 mm long (Fig. 15A), whereas the left one is 61 mm long. At the level of the sixth tooth, the bone is ~6 mm in height. As such, the long and slender dentary comprises most of the lower jaw, and contact with other bones is restricted to the medial surface, where it meets the splenial more rostrally, the surangular on the caudodorsal portion, and the angular in the caudoventral portion. The tip of the dentary is rounded and lacks a ventral projection, but has a ventrally bent dorsal surface (Fig. 15A). This surface accommodates the first two teeth and, ventrally along its lateral surface, two large foramina are present. In addition, a set of neurovascular foramina pierces the lateral surface of the dentary along its length. These are located inside a groove that extends parallel to the long axis of the bone at its rostral part, being dorsally directed in the caudal portion.

Except for the longitudinal groove, the lateral surface of the dentary is convex dorsoventrally, lacking any other prominent feature. The bone lacks a dorsally expanded coronoid process at its caudal portion, where both ventral and dorsal margins extend parallel to one another. Also in its caudal half, the dentary gradually becomes transversely narrower, so it is quite thin and fragile in the caudal third. As a result, both caudal processes are fractured and incomplete. Nonetheless, a slot in the lateral surface of the angular suggests that the ventral process was ~8 mm long, with the caudal extremity exceeding the midlength of the mandibular fenestra. The splenial mostly covers the medial surface of the dentary, but the rostral part of the Meckelian groove is still exposed (Fig. 15B), extending along the ventral edge of that surface.

Surangular

The rostral portion of the right surangular is covered by matrix (Fig. 15C), whereas the left element lacks part of its caudal portion (Fig. 15D). This bone forms the dorsal portion of the caudal part of the lower jaw. At 52 mm in length, it measures less than half of the total length of the jaw (111.5 mm). The rostral process contacts the dentary laterally. It is ~17 mm long and becomes dorsoventrally narrow from the caudal to the rostral portion. The lateroventral part of the bone bears a slot that receives the angular. On its medial surface, the surangular articulates with the prearticular. In addition, the articular rests on the dorsal surface of the caudal end of the bone. As the surangular contributes to the jaw articulation, it also articulates to both the quadratojugal and the quadrate. The bone also contributes to the dorsal and caudal margins of the external mandibular fenestra. In lateral/medial view, the dorsal surface of the surangular, usually recognized as the insertion area for m. adductor mandibulae externus superficialis (e.g. Dilkes *et al.*, 2012; Button *et al.*, 2016), is flat to gently convex. Close to the dorsal edge, the lateral surface bears a rostrocaudally oriented ridge, which extends from the caudal portion of the rostral process and does not reach the retroarticular process. There is a small surangular foramen between the ridge and the glenoid. The surangular portion of the retroarticular process is elongated and tapers caudally.

Angular

Both elements are preserved but fractured. The right angular is 45 mm long, and the entire length of the bone is preserved (Fig. 15C), whereas the left one lacks its caudal part (Fig. 15D). The angular forms most of the ventral part of the caudal portion of the lower jaw. Its rostral portion articulates with the dentary laterally, where a slot excavates the bone. On the opposite side, the angular also bears a slot to receive the splenial. The contact with the surangular occurs dorsomedially in the caudal half of the angular, whereas the prearticular articulates along the caudal half of its medial surface, ventral to the contact with the surangular. The dorsal margin of the rostral half of the angular forms the ventral margin of the external mandibular fenestra, and its ventrolateral surface could be related to the insertion of m. pterygoideus ventralis (Button *et al.*, 2016).

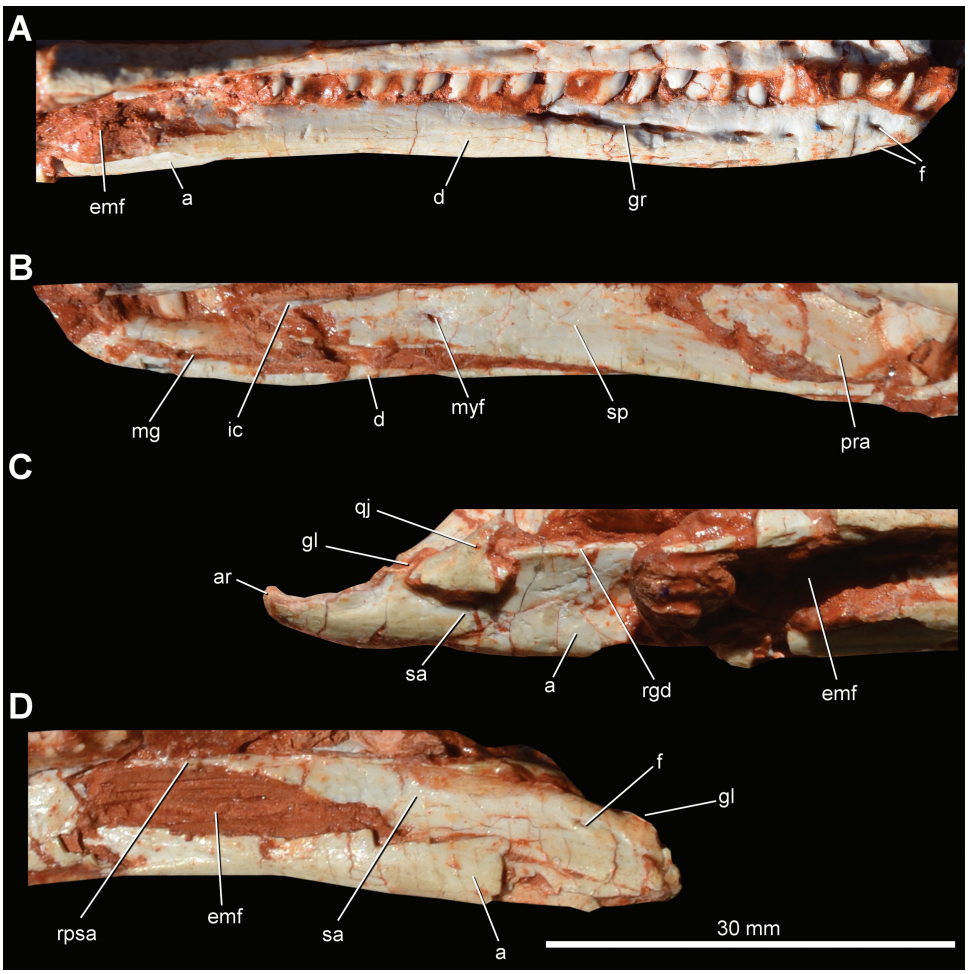

Figure 15. Lower jaws of CAPPA/UFSM 0035. A, details of the right dentary in lateral view. B, right dentary and splenial in medial view. C, caudal portion of the right lower jaw in lateral view. D, caudal portion of the left lower jaw in lateral view. Abbreviations: a, angular; ar, articular; d, dentary; emf, external mandibular fenestra; f, foramen; gl, glenoid; gr, groove; ic, intercoronoid; mg, Meckelian groove; myf, mylohyoid foramen; pra, prearticular; qj, quadratojugal; rgd, ridge; rpsa, rostral process of the surangular; sa, surangular; sp, splenial.

Splenial

Both elements are preserved in CAPPA/UFSM 0035. The splenial is elongated (55.5 mm) and transversely flat. Medially, it articulates with the dentary, covering the caudal part of the Meckelian groove (Fig. 15B). The dorsolateral surface receives the intercoronoid. The caudal part of the splenial articulates laterally with both the angular and the prearticular. There is no internal mandibular fenestra between the splenial and prearticular. The rostral portion of the bone is divided into two processes, with the ventral process extending more rostrally than the dorsal. A mylohyoid foramen is present on the rostral third of the splenial, located on its dorsoventral midpoint. Caudally, the splenial becomes dorsoventrally narrow, tapering to a point.

Coronoid

Only the dorsal portion of the left coronoid is exposed (Fig. 10), which is 13 mm long and 2 mm dorsoventrally deep. The bone rests against the dorsal margin of the prearticular. There is a gap between the rostral tip of the coronoid and the splenial. Its caudoventral process is overlapped by the prearticular. Rock matrix covers other bone contacts.

Intercoronoid

Only the right element is visible (Fig. 15B). The bone lies between the dorsomedial margin of the dentary and the dorsolateral margin of the splenial. The rostral tip extends until the rostral end of the rostroventral process of the right splenial. The caudal extension of the bone and its sutures are covered by the matrix.

The visible portion is rod like, slender, and ≤ 1 mm in height. The lateral border of the bone contributes to the boundary of the alveolar margin of the dentary.

Prearticular

Both elements are preserved in CAPPA/UFSM 0035. The bone forms part of the medial portion of the caudal half of the lower jaw. Its total length is ~55 mm. The rostral portion of the prearticular is transversely narrow (Fig. 16A) and articulates with the coronoid dorsally and the splenial ventrally. This portion is connected to the caudal part of the bone by an elongated shaft that extends along the ventral portion of the lower jaw. The ventrolateral surface of the shaft bears a longitudinal ridge that bounds the slot for the articulation with the angular. A medial lip occurs on the dorsal margin of the caudal third of the bone (Fig. 16B), which probably received the insertion of m. pterygoideus dorsalis on its ventral surface (Button *et al.*, 2016). In contrast, the dorsal surface of the lip contributes to the articular surface for the medial condyle of the quadrate (Fig. 15A). In addition, the caudal third of the bone articulates with the surangular laterally and with the articular dorsally, forming the retroarticular process.

Articular

Only the right articular is preserved in CAPPA/UFSM 0035, but its caudomedial portion is missing (Fig. 11). The bone forms the dorsal surface of the caudalmost portion of lower jaw and most of the jaw joint, receiving the quadrate condyles in two corresponding condylar surfaces, the medialmost of which is bounded by a caudal depression. In addition, the dorsal surface of the articular part of the retroarticular process receives the m. depressor mandibulae, contributing to the jaw abduction (Dilkes *et al.*, 2012). The surangular covers the lateral surface of the articular, whereas the prearticular fits in the ventral surface of the bone. The retroarticular process has a mostly caudal orientation, but its caudal tip is upturned (Fig. 15C). A large, 1.5-mm-long foramen, bounded ventrally by a medial ridge, is present on the medial surface of the articular (Fig. 16A).

Dentition

Two premaxillary teeth are preserved in the caudal half of the left premaxilla (Fig. 17A), corresponding to the two caudalmost of the four premaxillary teeth present in the holotype of *B. schultzi*. The apicobasal length of their crowns is ~3.5 mm, and the crown lacks a basal constriction. These dental elements are cylindrical along their length, but taper to a point at the tip. The main axes of the teeth are perpendicular to the premaxillary alveolar margin and oblique in relationship to that of the maxilla. Serrations are lacking in their mesial margins, whereas the distal margin of the

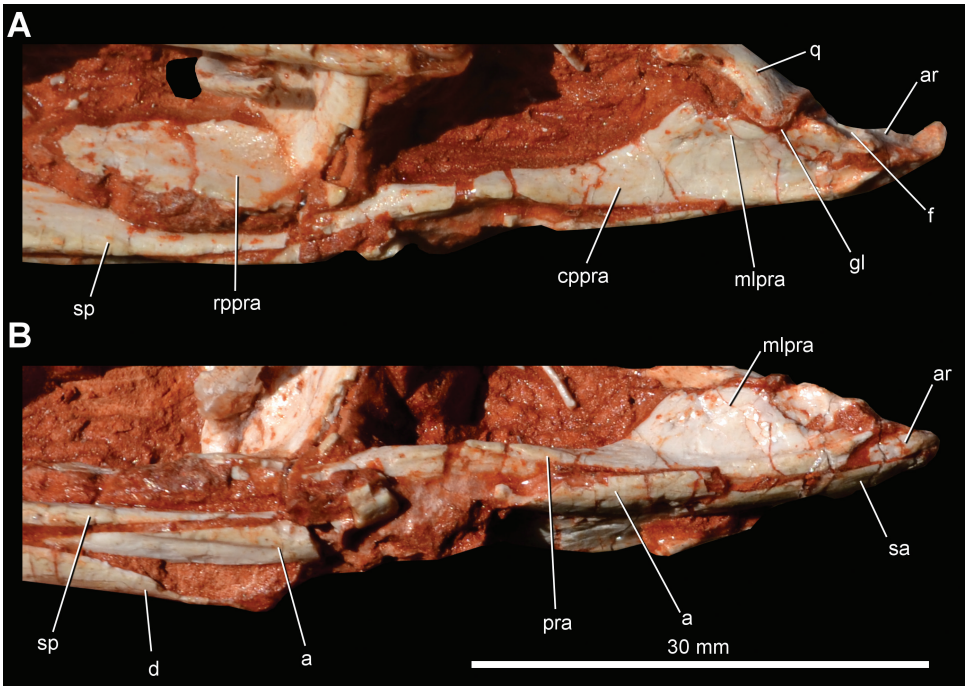

Figure 16. Caudal region of the lower jaw of CAPPA/UFSM 0035. A, medial view. B, ventral view. Abbreviations: a, angular; cppra, caudal portion of the prearticular; d, dentary; f, foramen; gl, glenoid; mlpra, medial lip of the prearticular; q, quadrate; rppra, rostral portion of the prearticular; sa, surangular; sp, splenial.

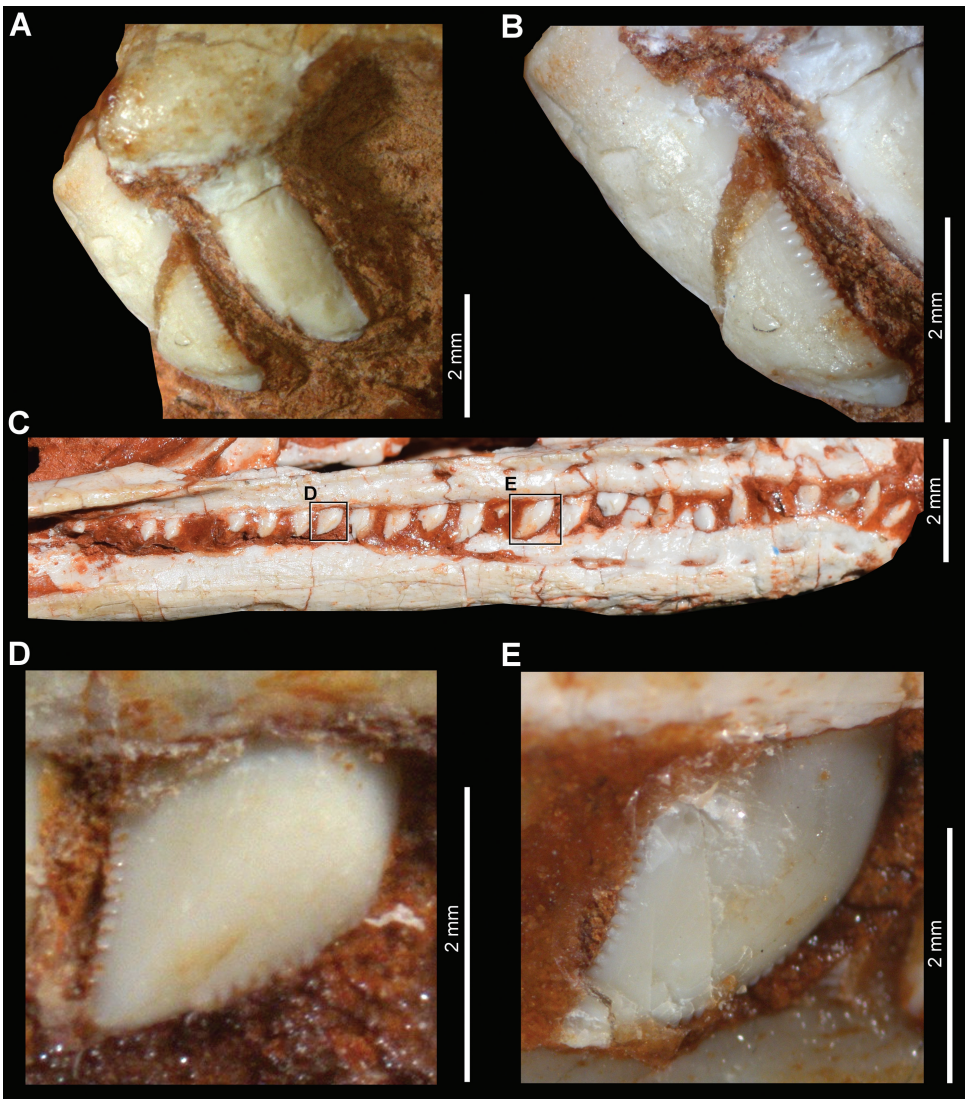

Figure 17. Teeth of CAPPA/UFSM 0035. A, last two premaxillary teeth in labial view. B, detail of the first preserved premaxillary tooth in labial view. C, maxillary teeth in labial view. D, labial view of a caudal maxillary tooth. E, labial view of a rostral maxillary tooth.

rostralmost tooth bears ~11 serrations per millimetre (Fig. 17B). These very small serrations bear convex tips and form right angles with the tooth margin.

The right maxilla bears ~24 tooth positions (Fig. 17C). They become gradually smaller caudally. For instance, the apicobasal lengths of the second and third preserved tooth crowns of the left maxilla are 4.5 and 5.0 mm, respectively, whereas the last two preserved teeth are slightly shorter than 2 mm. The maxillary tooth crowns are blade like, strongly caudally curved and labiolingually compressed. The mesial carina is convex, whereas the distal is concave to straight (Fig. 17D, E). Both mesial and distal margins bear fine serrations (approximately eight per millimetre) that form right angles to the tooth margin.

The number of dentary teeth cannot be estimated. The first three teeth lie on the dorsal, ventrally bent surface of the dentary, with the first tooth located slightly caudal to the rostral tip of the bone (Fig. 17C). Either matrix or other teeth generally cover the mesial margin of all crowns, so that the presence of serrations on this margin is uncertain. However, all teeth bear serrations on their distal margins. Teeth from the middle portion of the dentary are typically ziphodont, resembling the general morphology of the maxillary teeth (Fig. 7B).

Palatal dentition

There is a row of small teeth on the palatal process of the pterygoid (Fig. 18). The left process, better

preserved, bears at least 11 teeth aligned parasagittally, but the overlapped hyoid precludes a more precise quantification. The cross-sectional diameter and the apicobasal length of these teeth do not exceed 1 mm. The basal portion of the crowns is cylindrical, and their preserved portions lack serrations.

Hyoids

The hyoid apparatus comprises a pair of elongated bones preserved ventral to the palate, between the hemimandibles (Fig. 12). Both are broken, with their caudal portions missing. The preserved portion of the right element is 24 mm long, whereas the left one is 34 mm long. The hyoid shaft is rod like (2 mm broad), whereas the rostral portion is expanded (3 mm broad), forming a convex rostral margin. As preserved, their shafts are laterally bowed, although when completely preserved, the hyoid elements are generally sigmoid in other dinosaurs.

AXIAL SKELETON

Preserved axial elements include the cervical and trunk series, both complete and articulated, with sacral vertebrae and some ribs (Fig. 19). The tail was lost, possibly owing to erosion of the bearing rock. Nine cervical, 16 trunk and two primordial sacral vertebrae are preserved in the specimen.

Proatlas

Both proatlantal elements are preserved and articulate to one another rostrally (Fig. 20A). They are plate like (dorsoventrally compressed), and their total length is ~10 mm (Fig. 20B). Each element is bow like in dorsal view, with the concave margin facing medially. The cranial tip articulates against the occiput, covering part of the foramen magnum. The tips are medially directed, with each touching its opposite at a rostrocaudally straight margin. Each entire element forms a 2 mm dorsolateral wall over the foramen magnum. The midpoint of their lateral surfaces bears a ventrally facing protuberance (Fig. 20B). The caudal tip rests on the dorsal surface of the atlantal prezygapophysis, forming the roof of the neural canal. It tapers to a point and does not invade a large area between the dorsal margins of the atlantal neural arches.

Atlas

The atlas complex comprises the odontoid process (atlantal centrum), the intercentrum and paired neural arches (Fig. 20A, B). The odontoid process is coossified with the axis (Fig. 21A–E). Its dorsal surface is transversely concave, forming the floor of the neural canal. The cranial surface is smooth, 5 mm wide, and convex in dorsal/ventral views, articulating against the caudal surface of the occipital condyle. In addition, it is more cranially placed than the cranial margin of the axial intercentrum. On the lateral surface, an oblique sulcus is present, which starts cranially from the ventral margin of the odontoid process and reaches the caudodorsal border of that element (Fig. 21A). As a result, the ventral margin of the cranial portion of the odontoid process is transversely narrower than the dorsal margin. The caudal part of the process expands transversely towards the ventral portion, reaching 9.5 mm in width at the base.

The antlantal intercentrum is a small structure, 4.5 mm in length and 8 mm in width. It is subrectangular in dorsal/ventral views (Fig. 20C), U shaped in cranial/caudal views (Fig. 20D) and subtriangular in lateral view (Fig. 20B). The dorsal surface lacks a transverse ridge between its cranial and caudal portions, which are cranially and caudodorsally oriented, respectively. The cranial surface is larger and articulates with the ventral surface of

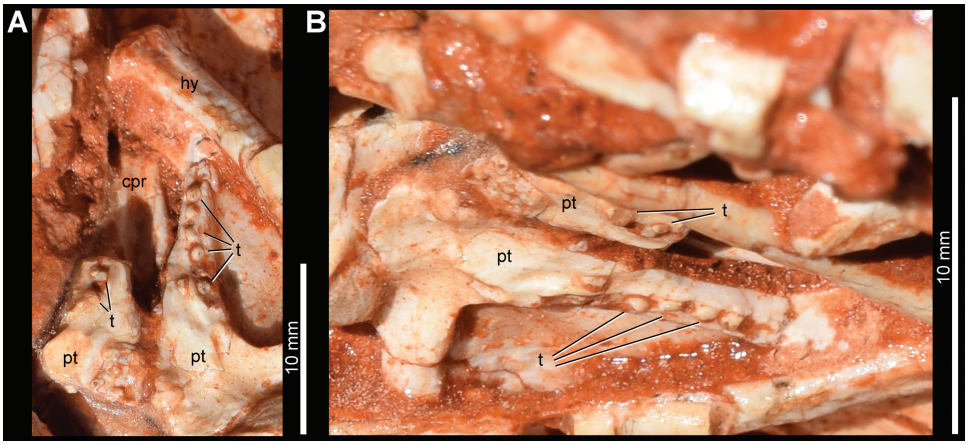

Figure 18. Palatal teeth of CAPPA/UFSM 0035. A, ventral view. B, ventrolateral view. Abbreviations: cpr, cultriform process; hy, hyoid; pt, pterygoid; t, tooth.

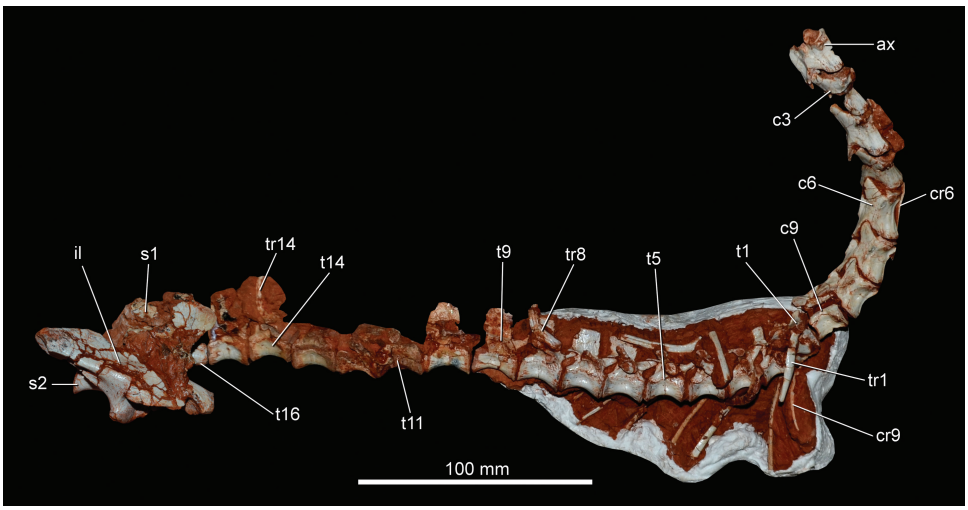

Figure 19. Axial skeleton of CAPPA/UFSM 0035. Abbreviations: ax, axis; c, cervical vertebra; cr, cervical rib; il, ilium; s, sacral vertebra; t, trunk vertebra; tr, trunk rib.

the occipital condyle. The caudal surface meets the sulcus on the cranioventral surface of the odontoid process. In addition, each dorsolateral margin bears an ovoid depression for the pedicle of the atlantal neural arch. The cranioventral surface of the bone is bumpy, contrasting with the opposite (caudoventral) surface, which is smooth, except for a U-shaped sulcus that receives the cranial projection of the ventral margin of the axial intercentrum. This sulcus divides the caudal surface into two regions; a dorsoventrally deeper and convex dorsal portion and a flat ventral portion (Fig. 20D).

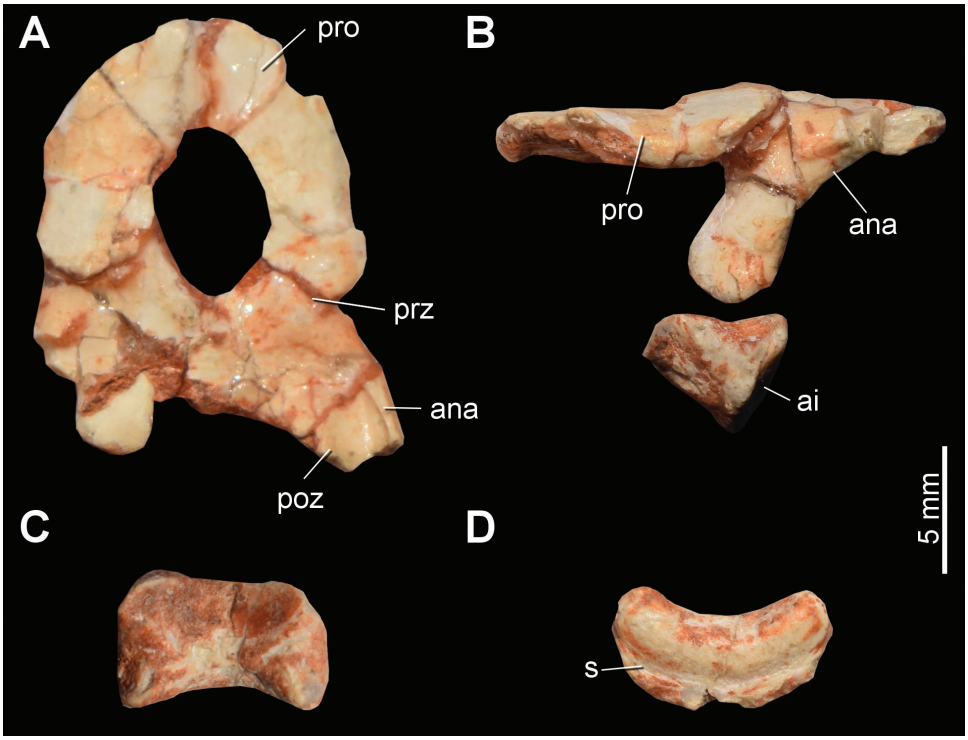

Figure 20. Proatlas and atlas of CAPPA/UFSM 0035. A, dorsal view. B, lateral view. C, dorsal view of the atlantal intercentrum. D, caudal view of the atlantal intercentrum. Abbreviations: ai, atlantal intercentrum; ana, atlantal neural arch; poz, postzygapophysis; pro, proatlas; prz, prezygapophysis; s, sulcus.

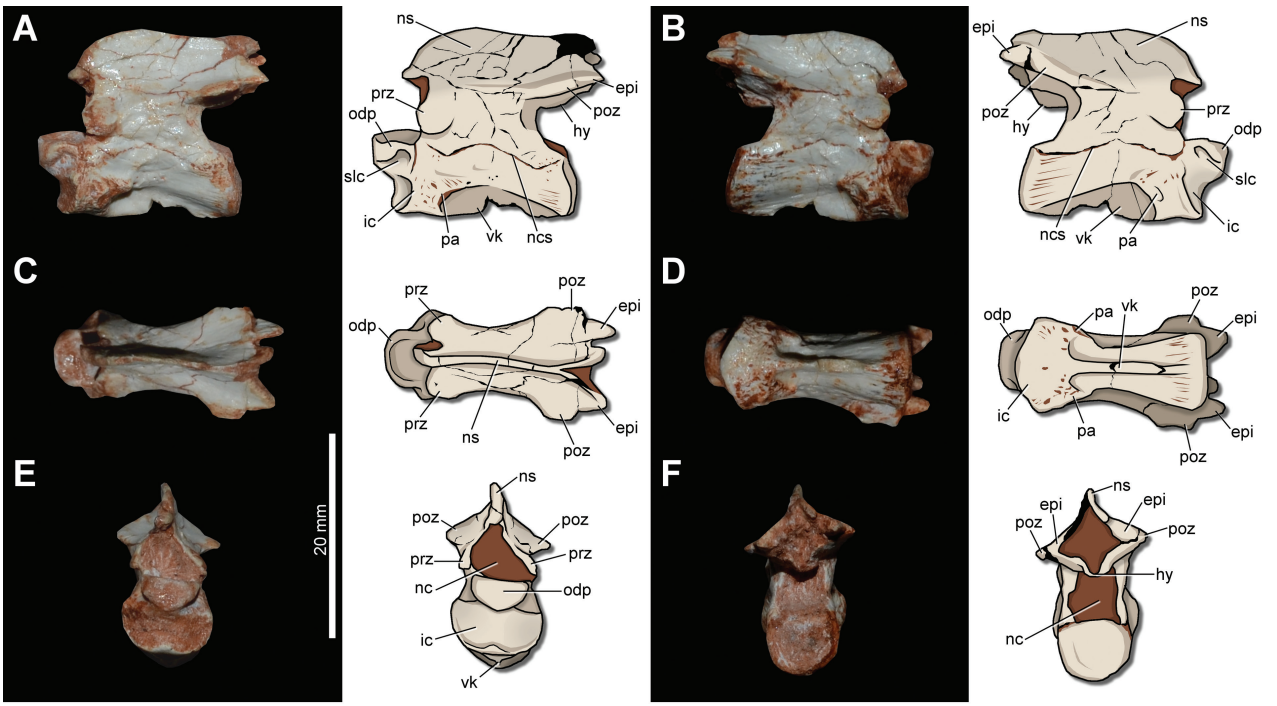

Figure 21. Axis of CAPPA/UFSM 0035. A, photograph and interpretative drawing in left lateral view. B, photograph and interpretative drawing in right lateral view. C, photograph and interpretative drawing in dorsal view. D, photograph and interpretative drawing in ventral view. E, photograph and interpretative drawing in cranial view. F, photograph and interpretative drawing in caudal view. Abbreviations: epi, epipophysis; hy, hyposphene; ic, axial intercentrum; nc, neural canal; ncs, neurocentral suture; ns, neural spine; odp, odontoid process; pa, parapophysis; poz, postzygapophysis; prz, prezygapophysis; slc, sulcus; vk, ventral keel.

Both atlantal neural arches are almost entirely preserved, except for the caudal part of the postzygapophyses (Fig. 20A). They form the roof and the lateral walls of the neural canal. Each prezygapophysis is short and receives the caudal tip of the proatlas. The cranial margin between the prezygapophyses is concave. More caudally, the medial margin of the atlantal neural arch, which has a flattened dorsal portion, contacts its counterpart. Although the caudal portions of the postzygapophyses are lacking, it is possible to recognize a lateral keel on the dorsal surface of this dorsoventrally compressed structure. In addition, the dorsal and the ventral surfaces of the postzygapophyses bear a longitudinal groove. The cranioventrally oriented pedicles (Fig. 20B) of the neural arch contact the intercentrum ventrally and the occipital condyle cranially. The lateral surface of the pedicle extends further ventrally than the medial, producing an oblique ventral surface in cranial or caudal views. In lateral view, its ventral margin is rounded.

Axis

The axis is composed of the intercentrum, centrum and neural arch and is fused to the atlantal centrum (Fig. 21). The intercentrum is fused to the centrum and, together, they form an 18-mm-long element. The intercentrum (Fig. 21A) is slightly shorter craniocaudally than the atlantal intercentrum, but transversely broader (9 mm in width). Its cranial surface bears two craniolaterally oriented articular facets that receive the atlantal intercentrum. The ventromedial margin of its cranial surface is cranially projected, and the caudolateral margin reaches the parapophysis of the axial centrum. The entire lateral surface of the intercentrum is rough.

The axial centrum is long, but shorter than the interzygapophyseal distance. Its cranial and caudal ends are subequal in height. The oval-shaped parapophysis is located on a rugose and raised subtriangular surface on the cranioventral portion of its lateral surface (Fig. 21A). There is no evident sign of a diapophysis above the parapophysis. At the dorsoventral level of the parapophysis, on the lateral surface, a series of small foramina pierce the centrum. Its ventral surface bears a 1-mm-thick (lateromedially) ventral keel. It is deeper than the concave ventral keel of the postaxial cervical vertebrae; in the axis, the keel is ventrally straight in lateral view.

The axial neural arch is almost entirely preserved. It rests on the centrum, with a clear suture between

both structures. The cranial opening of the neural canal is subtriangular (Fig. 21E), whereas the caudal is squared (Fig. 21F). The prezygapophysis is located in the cranial portion of the neural arch, below the level of the postzygapophysis. Indeed, the ventral margin of the prezygapophysis almost reaches the level of the ventral border of the neural canal. The prezygapophysis faces laterodorsally and is reduced in comparison with those of the postaxial cervical vertebrae. Its cranial margin is rounded in lateral view and slightly exceeds the cranial margin of the neural canal. The postzygapophysis is located higher in the neural arch than the prezygapophysis and reaches as caudally as the caudal margin of the centrum. The medial margin of the postzygapophysis projects ventrally, contacting its opposite. This arrangement forms a vertically oriented hyposphene, which has a flat ventral surface (Fig. 21F). The epipophysis rises from the caudodorsal margin of the postzygapophysis (Fig. 21C). It tapers caudally to a point, resulting in a triangular shape in dorsal or ventral views. The caudal tip of the epipophysis projects more caudally than the caudal margin of the centrum. The epipophysis has the cranial part of its dorsal surface crossed by a ridge that extends from the caudal bifurcation of the neural spine, which forms a Y-shaped structure in dorsal view. Except in this caudal portion, the neural spine is transversely compressed. Its cranial margin forms a pointed cranial projection, which extends cranially beyond the prezygapophyses (Fig. 21B). The dorsal margin of the neural spine is similar in height along the entire length, but the cranialmost margin is downturned, resulting in a rounded lateral view.

Postaxial cervical vertebrae

Although the complete series is preserved (Fig. 22), some vertebrae are incomplete. Their length generally decreases from the first to the last element, both for the length of the centrum and for the interzygapophyseal space. Yet, some adjacent elements are equivalent in size. The centrum of the third cervical vertebra (first postaxial element) is 23 mm in length, whereas the ninth cervical centrum is 15 mm long. Except for the caudalmost cervical vertebra, which has a centrum of similar length to that of the axis, all the others possess a more elongated centrum. The height of the centra is almost constant along the series. Other anatomical aspects of cervical centra include their transverse compression and the presence of a midline ventral keel, which is, however, reduced in the middle cervical vertebrae (fifth and sixth). Yet, the centrum of these two elements presents a longitudinal accessory lamina on each lateroventral surface (Fig. 22A). Both articular facets of the cervical centra are concave. The cranial articulation of the third to seventh elements is elevated in comparison with those of the eighth and ninth cervical vertebrae. This arrangement gives a parallelogram shape to those vertebrae. In contrast, the caudal cervical centra (eighth and ninth) are subrectangular. The lateral surface of all cervical centra is concave, lacking pleurocoels. However, there are piercing foramina on the lateral surface of some centra (e.g. six, eight and nine). The parapophysis is located on the cranial border of the lateral surface of the centrum in the entire cervical series. In the third, fourth and fifth vertebrae, the parapohypsis is triangular, whereas from the sixth to the ninth vertebrae it varies from circular to ovoid in shape. Indeed, there is a longitudinal ridge rising from the caudal edge of the parapophysis, which extends caudally and merges smoothly into the centrum in the cervical vertebrae with a triangular parapophysis. CAPPA/UFSM 0035 lacks the oval scars on the lateral surface of the caudal border of the cervical centra present in the holotype of *P. protos* (PVSJ 874; Martinez & Alcober, 2009), but there are several craniocaudally oriented striations on their entire lateral surface.

The cervical neural arches are longer than their respective centra, because the zygapophysis projects beyond the cranial and caudal margins of the latter elements. The neurocentral suture is present in only some of them (i.e. fourth, seventh, eighth and ninth). In dorsal view, the divergence of the pre- and postzygapophyses gives to the neural arch an X shape. In cranial view, the neural canal of the postaxial cervical vertebrae is subcircular. The cranial part of the neural canal of the third cervical vertebra is 4 mm in height and 4.5 mm in width. Below the prezygapophysis, the cranial face of the neural canal is laterally concave, lacking any recess on this region. The prezygapophyses are significantly more cranially expanded than that of the axis, but they decrease in size from the sixth to ninth cervical elements. The cranial tip of the prezygapophysis of the third cervical vertebra is 4.5 mm more cranially projected than the cranial margin of its respective centrum. In contrast, in the ninth cervical vertebra, that projection is only 1 mm. The articular facet of the prezygapophysis is smooth and oblique, facing dorsomedially. In contrast, the ventromedial surface of the cranialmost portion of the prezygapophysis is marked by a rough texture. At the dorsolateral surface of the prezygapophysis, a ridge extends from the cranial tip of that structure to merge on the surface lateral to the middle of the neural spine, producing a triangular cross-section to the base of the prezygapophysis. Unlike *E. lunensis* (Sereno *et al.*, 2013), the specimen lacks an accessory prezygapophyseal process on the middle surface of the prezygapophysis.

The diapophysis of the cranial (third and fourth) cervical vertebrae does not project much laterally and is located near the parapophysis. However, it gradually increases in size and moves upwards from the more

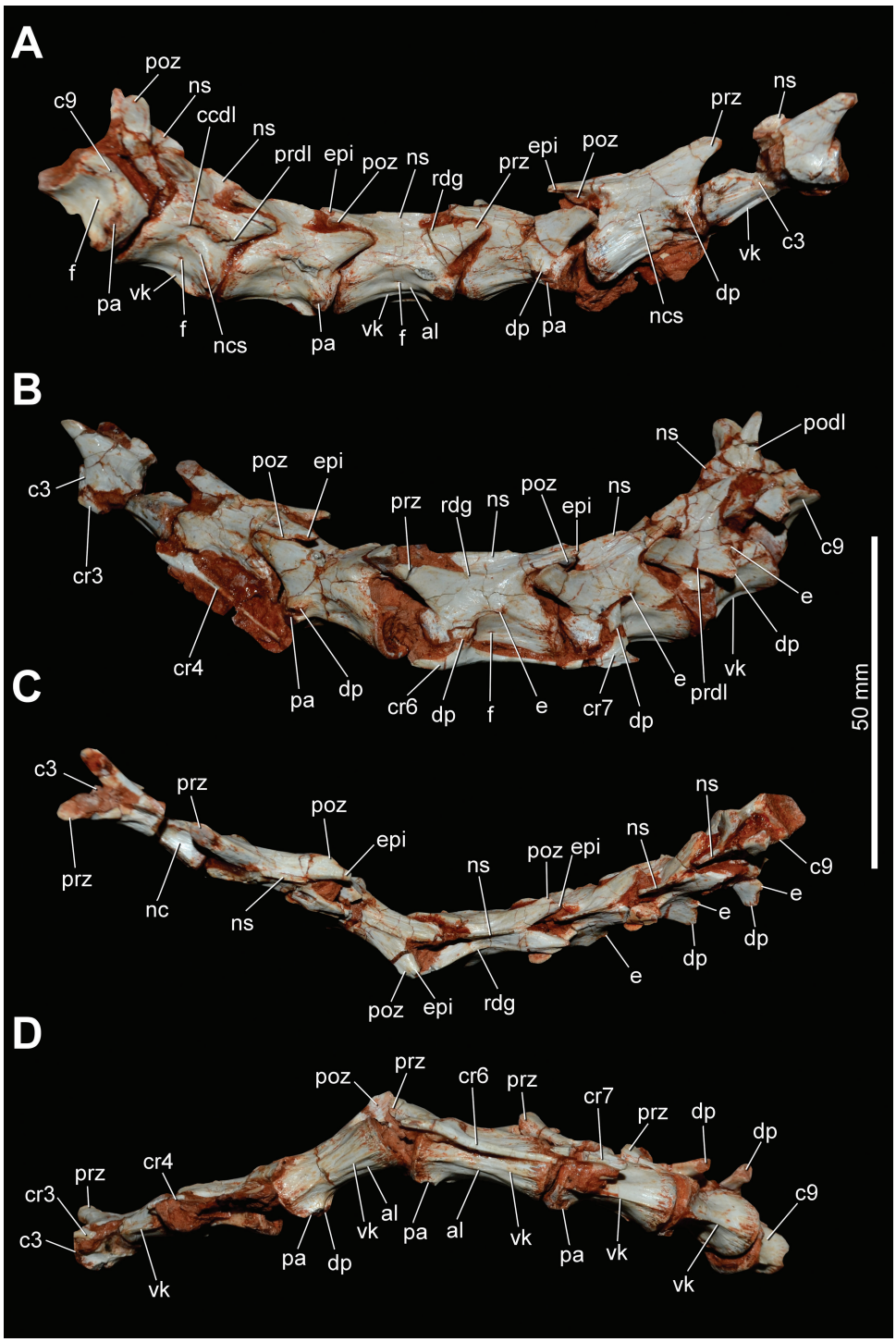

Figure 22. Postaxial cervical vertebrae and ribs of CAPPA/UFSM 0035. A, right lateral view. B, left lateral view. C, dorsal view. D, ventral view. Abbreviations: al, accessory lamina; c, cervical vertebra; ccdl, caudal centrodiapophyseal lamina; cr, cervical rib; dp, diapophysis; e, eminence; epi, epipophysis; f, foramen; ncs, neurocentral suture; ns, neural spine; pa, parapophysis; podl, postzygodiapophyseal lamina; poz, postzygapophysis; prdl, postzygodiapophyseal lamina; rdg, ridge; vk, ventral keel.

cranial to the more caudal cervical vertebrae, remaining close to the parapophysis until the middle caudal (fifth to seventh) cervical elements. In contrast, in the eighth and ninth vertebrae, both articular facets are well separated. The diapophysis is triangular in dorsal view and has articular facets that face lateroventrally (Fig. 22C). It bears an unusual protuberance that first appears on the sixth vertebra as a gentle eminence on the lateral surface of the neural arch and gradually increases in size in more caudal elements. In the sixth vertebra, the eminence is caudal to the diapophysis, but in the seventh and subsequent vertebrae, it merges into that element (Fig. 22B). Martinez & Alcober (2009) reported a similar feature in *P. protos*. Dorsal to the articular facet of the diapophysis in the middle to caudal (sixth to ninth) vertebrae, there is a rough surface that might relate to the m. longissimus capitis superficialis. A rudimentary prezygodiapophyseal lamina is present in the seventh cervical vertebra, which is well developed in the eighth element. Both eighth and ninth vertebrae present centrodiapophyseal and postzygodiapophyseal laminae.

The postzygapophysis of the cervical vertebrae forms a ventrolaterally directed oval facet. Cranioventral to each postzygapophysis, a C-shaped sulcus excavates the caudal margin of the pedicle and receives the tip of the prezygapophysis of the following vertebra. The tip of the postzygapophysis is as caudally projected as the caudal margin of the centrum. However, the epipophysis exceeds that margin in the cranial (fourth) and middle (fifth to sixth) cervical vertebrae. In the fourth cervical vertebra, the epipohypsis is well developed caudally. Its caudal tip tapers to a point, so that the structure is triangular in dorsal view. In contrast, in the last three cervical elements, the epipophysis reduces significantly. Indeed, there is only a faint eminence over the postzygapophysis of the ninth cervical vertebra.

The neural spines of the third, fourth and fifth cervical vertebrae are not completely preserved. The remaining cervical neural spines are transversely compressed and longer than tall. The dorsal margin of the neural spine of the sixth, seventh and eighth cervical vertebrae is straight (Fig. 22A, B). In the ninth element, the cranial half of the neural spine is slightly directed dorsally. The dorsal portion of the spines is longer than the ventral, as its cranial margin projects more cranially than the base. In contrast, the caudal portion merges smoothly into the neural arch. The spines become craniocaudally shorter from the sixth (12 mm in length) to the ninth (8 mm in length) elements.

Trunk vertebrae

As with the cervical series, the trunk vertebrae are also articulated along the entire series, which contains 16 vertebrae. In order to protect the integrity of the first nine elements, their left side was kept imbedded in the matrix (Fig. 23). Almost all vertebrae are well preserved, except from the 11nth to the 15nth element, which have damaged neural arches (Fig. 24). The general morphology of the centra approaches that from other early dinosaurs, because they are spool shaped and amphicoelous. The neurocentral suture is visible along all trunk elements. The first one is 15 mm long and 9.5 mm high (measured at the cranial articular facet), whereas the last is approximately 18 mm long and 13 mm high. The length of the seventh element is subequal to that of the last one, and so are the remaining between them, whereas the more cranial centra are craniocaudally shorter (e.g. fifth = 17 mm; sixth = 17.5 mm). All cranial trunk centra (first to fifth elements) are longer than deep, with cranial or caudal articular facets that are circular and similar in height. Conversely, the more caudal elements become significantly wider. In general, trunk centra lack pneumatic openings, but there is a shallow depression on each lateral surface. In contrast, in cross-section the centra are extremely hollowed internally. Only the first trunk centrum has a longitudinal ventral keel, whereas the others have a smooth ventral surface that is concave in lateral view. The contact of the ventral margin of the cranial articular facet of the first trunk centrum with its ventral keel does not form a hypapophysis.

The parapophysis is located at least partly in the centrum in the first three trunk vertebrae (Fig. 23A). In the first element, the parapophysis is ovoid and restricted to the centrum. In the second, the neurocentral suture traverses the middle of the parapophysis, resulting in an hourglass-shaped articulation. Only the ventral part of the parapophysis contacts the centrum of the third trunk vertebra. In the fourth, the parapophysis is completely restricted to the neural arch and subcircular in shape. In the subsequent elements, the parapophysis gradually moves upwards, reaching the transverse process and contacting the diapophysis in the caudalmost (fourteenth to fifteenth) elements.

The neural arch is not as dorsoventrally deep (disregarding the neural spine) as the respective centrum, but longer instead (considering the pre- to postzygapophyseal distance). In the first three trunk elements, the subretangular transverse process is horizontal and laterally directed, whereas from the fourth to the eighth elements it is slightly dorsocaudally directed. The transverse process of the last trunk vertebra is, however, craniolaterally oriented. The articular facet of the diapophysis is concave and located in the tip of the transverse process of all vertebrae in which the structure is preserved. In contrast to the same articular facet of the cervical vertebrae, those from the trunk are drastically larger and do not face ventrally. The prezygapophysis in the first three elements is more

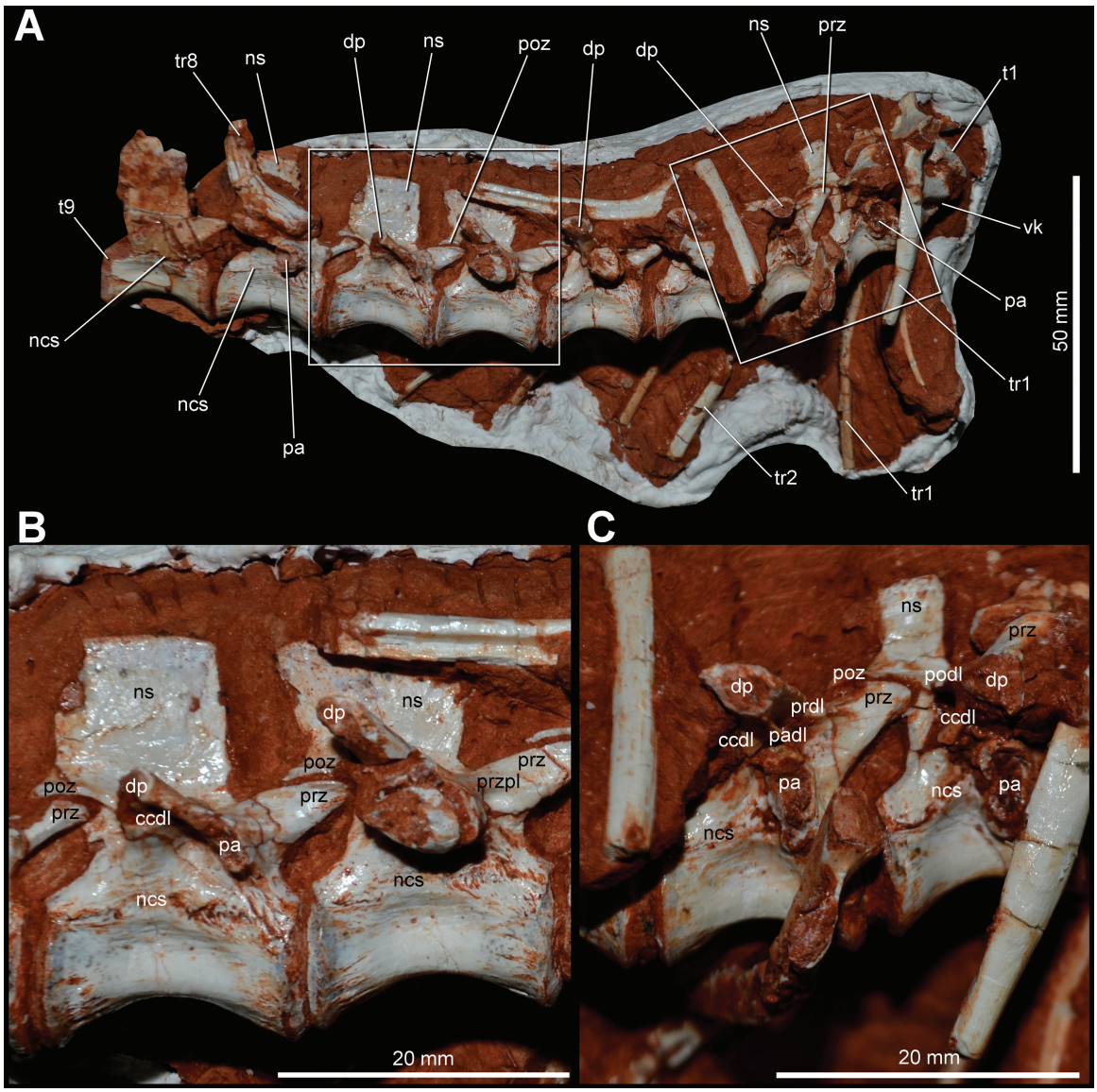

Figure 23. First nine trunk vertebrae of CAPPA/UFSM 0035. A, right lateral view. B, vertebrae six and seven in right lateral view. C, vertebrae two and three in right lateral view. Abbreviations: ccdl, centrodiapophyseal lamina; dp, diapophysis; ncs, neurocentral suture; ns, neural spine; pa, parapophysis; padl, parapodiapohyseal lamina; podl, postzygodiapophyseal; poz, postzygapophysis; prdl, prezygodiapophyseal lamina; prz, prezygapophysis; przpl, prezygoparapophyseal lamina; t, trunk vertebra; tr, trunk rib; vk, ventral keel.

dorsally directed than in the subsequent ones (i.e. from fourth to 16th). Hence, the prezygapophysis projects slightly cranial to the cranial margin of the respective centrum, whereas that limit is further surpassed from the third to tenth elements. The articular facet of the prezygapophysis is oblique (forming a 45° angle) to the neural spine in cranial view. On the medial surface of the prezygapophysis, a ventrally oriented facet is observed, forming an accessory joint, which corresponds to the hypantrum. Correspondingly, the hyposphene originates from a small ventral projection of the medial portion of the postzygapophysis. The tips of the preserved postzygapophyses reach the caudal margin of the respective centrum.

Several laminae are present on the lateral surface of the trunk vertebrae (Fig. 23B, C), and their arrangement changes along this series. A prezygodiapophyseal lamina is present from the first to the fifth element. In the sixth, this lamina connects the prezygapophysis with the parapophysis, forming a prezygoparapophyseal lamina. From the seventh vertebra onwards, this lamina is absent owing to the high placement of

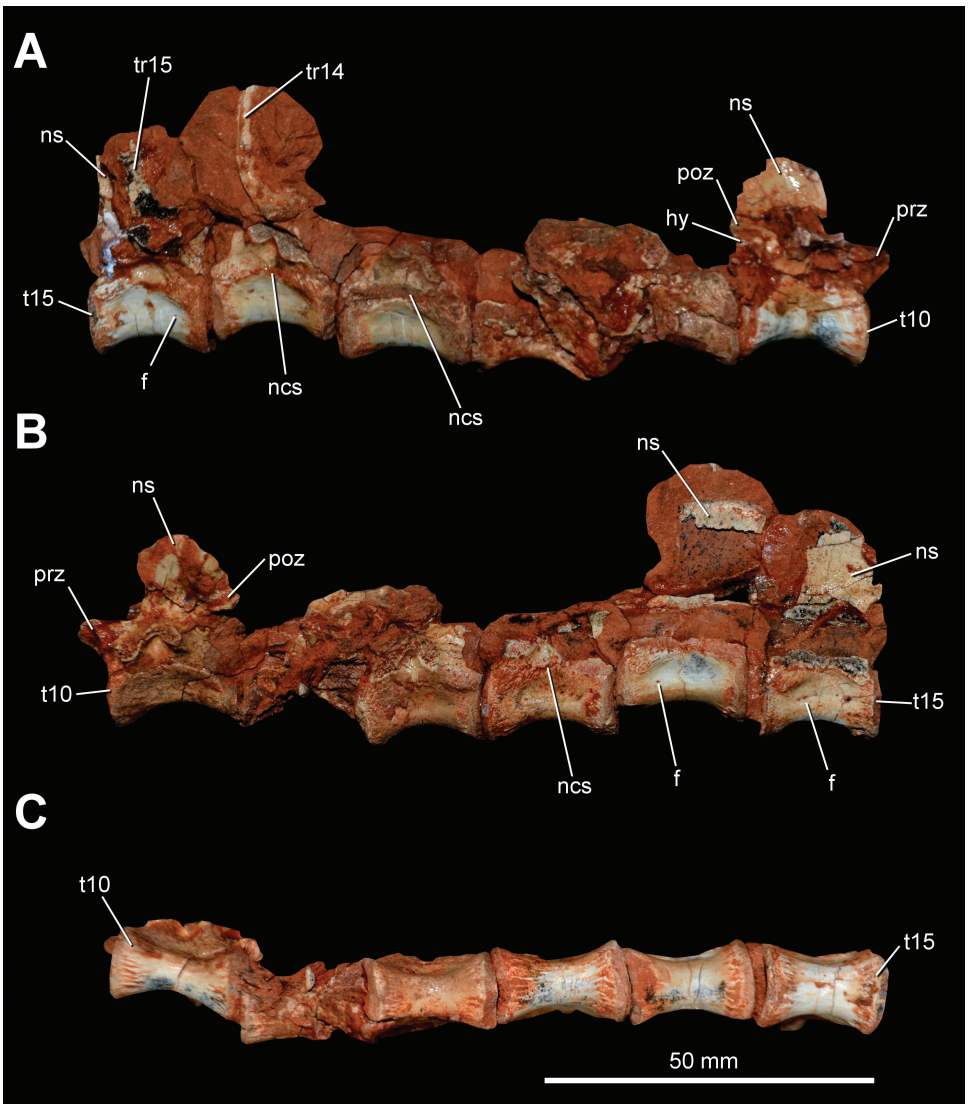

Figure 24. Trunk vertebrae ten to 15 of CAPPA/UFSM 0035. A, right lateral view. B, left lateral view. C, ventral view. Abbreviations: f, foramen; hy, hyposphene; ncs, neurocentral suture; ns, neural spine; poz, postzygapophysis; prz, prezygapohypsis; t, trunk vertebra; tr, trunk rib.

the parapophysis. The paradiapophyseal lamina is restricted to the cranial (second and third) trunk vertebrae. All well-preserved vertebrae bear the caudal centrodiapophyseal lamina, in addition to the postzygodiapophyseal and spinopostzygapophyseal laminae. The cranial (from first to fifth) elements have three (cranial, middle and caudal) infradiapophyseal fossae bounded by the laminae. However, after the rearrangement of the parapophysis, the subsequent vertebrae lack the cranial infradiapophyseal fossa.

In the second trunk element, the neural spine is taller than long (Fig. 23C), whereas from middle to caudal (sixth to 16nth trunk vertebrae), the neural spine is subequal in those dimensions. For instance, the dorsal margin of the neural spine of the second trunk vertebra is 5 mm long and 6.5 mm high, whereas in the seventh it is respectively ~12 and 11 mm. The spines of the entire trunk series are transversely compressed (~0.5 mm broad in the tenth element) and subrectangular in lateral view. They lack any lateromedial expansion (spine tables) on their dorsal margins. The caudodorsal portion of the neural spine of the sixth element projects in a slightly caudal direction. The lateral surface close to the dorsal margin is rugose in the better-preserved neural spines.

Sacral vertebrae and ribs

There are two preserved vertebrae attached to the ilia, corresponding to the primordial sacral vertebrae (Fig. 25). The 16nth trunk vertebra rests between

the preacetabular iliac alae, but (although the tip is fractured) its transverse processes do not contact the ilium. Indeed, there is no sign of any contact area in the ilium. It resembles the condition of the putative first sacral vertebra of *E. lunensis* (PVSJ 512; Sereno *et al.*, 2013), which also does not contact the ilium.

The centra of the sacral vertebrae are not co-ossified and are subequal in length, at 18.5 mm (Fig. 25B). They are longer than tall, as the cranial height of the first element is 12 mm and the caudal height of the second element is 12.5 mm. The cranial articular facet of the first sacral centrum and the caudal articular facet of the second are concave. Their ventral surfaces are smooth, lacking keels or grooves. The transverse processes and ribs are partly hidden by both matrix and ilia, but it is possible to observe that the transverse processes are craniocaudally expanded. The height of the transverse process/rib of the first primordial sacral vertebra is inaccessible, but it forms, ventrally, an inclined platform. The transverse process/rib of the second element is 20.5 mm in height. In addition, the ventral margin of the structure reaches the

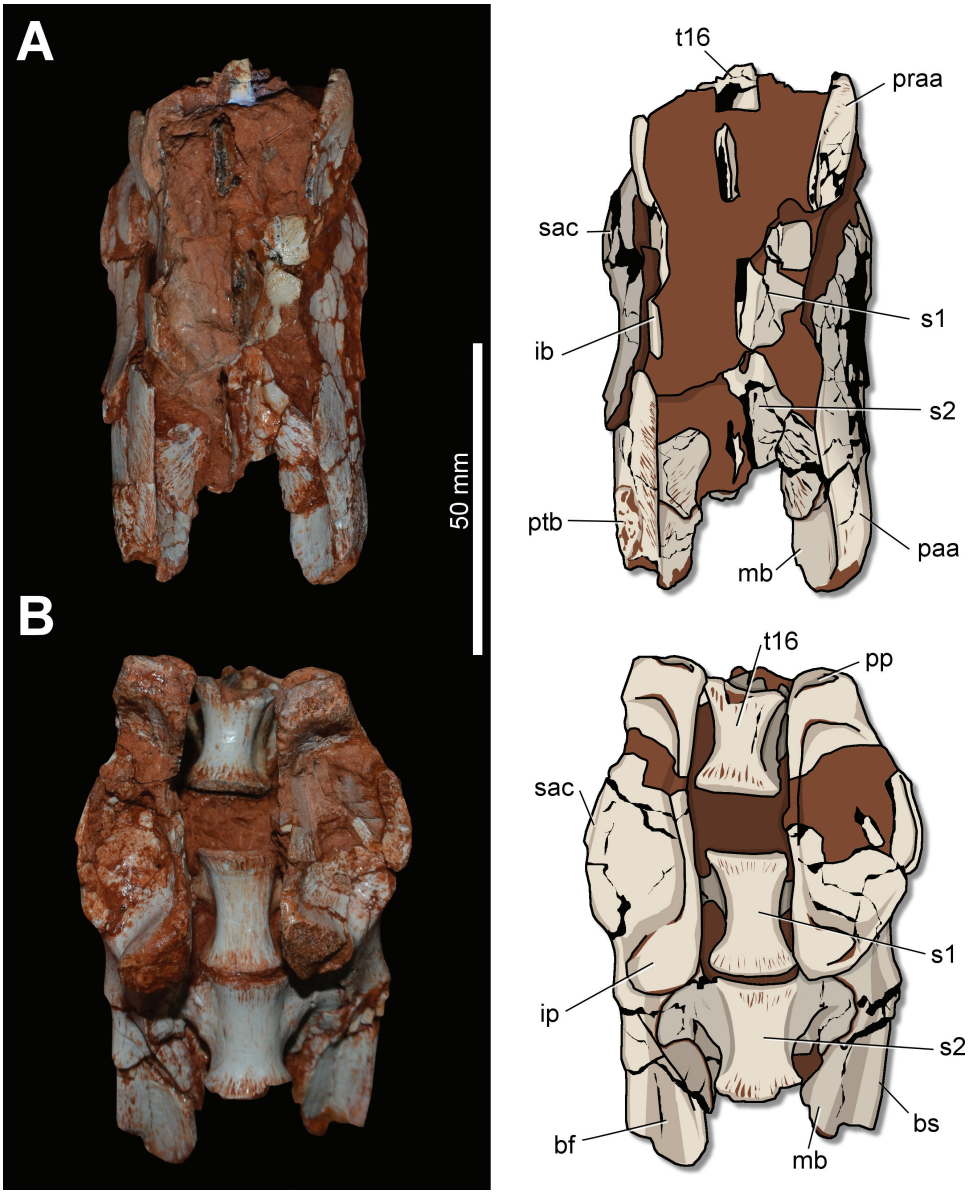

Figure 25. Sacrum of CAPPA/UFSM 0035. A, photograph and interpretative drawing in dorsal view. B, photograph and interpretative drawing in ventral view. Abbreviations: bf, brevis fossa; bs, brevis shelf; ib, iliac blade; ip, ichiadic peduncle; mb, medial blade; paa, postacetabular ala; pp, pubic peduncle; praa, preacetabular ala; ptb, protuberance; s, sacral vertebra; sac, supra-acetabular crest; t, trunk vertebra.

level of the ventral margin of its respective centrum, whereas in the first sacral vertebra the ventral margin of the transverse process/rib is slightly dorsal to the ventral margin of its centrum. The transverse process/rib of the first sacral vertebra does not contact the cranial portion of the transverse process/rib of the second element dorsally (Fig. 25A). The dorsal portion of the transverse process/rib of the second sacral vertebra is caudolaterally directed and rests on the dorsal surface of the medially deflected ventral margin of the postacetabular ala of the ilium. However, the transverse process/rib does not reach the caudal end of that structure. That area probably hosts the contact of the additional caudosacral vertebra. From that point, the transverse process/rib extends cranioventrally and continues cranially as a ventral horizontal shelf, which contacts the ventral portion of the transverse process/rib of the previous vertebra. The neural spine of the first primordial sacral vertebra is almost entirely preserved. It is transversely compressed, following the shape of the trunk series spines. In addition, spine tables are absent on the dorsal end of the neural spines. Only the basal portion of the spine of the second element is preserved.

Cervical ribs

Only the left side has preserved elements, probably owing to taphonomic processes. Except for the rib of the ninth cervical vertebra, all other preserved elements are articulated with their respective vertebrae. In addition, there is no evidence of fusion between them. The ribs are generally tetraradiate, because they are formed by three processes (capitulum, tuberculum and spinous) and by a slender shaft. The capitulum is medially oriented and articulates to the parapophysis. The tuberculum rests on the diapophysis, whereas the shaft of the previous rib lies close to the medial surface of the spinous process. Both the tuberculum and the capitulum of the rib of the third cervical vertebra are short, and the spinous process is also poorly developed (Fig. 26A). The shaft is broken, but part of it reaches the middle of the centrum of the fourth cervical vertebra. Therefore, the shaft is ≥ 30 mm in length.

The rib of fourth cervical vertebra bears more developed processes than the previous one (Fig. 26A). The total length of the preserved portion is 27.5 mm. The spinous process is long (4.5 mm in length), with its pointed tip exceeding cranially the caudal margin of the third cervical centrum. The slender, rod-like shaft follows the craniocaudal orientation of the previous rib, but is partly broken, so that its total length cannot be confirmed. The fifth cervical vertebra does not have its associated rib preserved. The rib of the sixth cervical element is more robust than that of the third one, but their tuberculi are similar in size (Fig. 26B). The preserved portion is 35.5 mm long. The spinous process is longer (5.5 mm) than the previous one and slightly curved dorsally. The preserved portion of the shaft extends along the ventral surface of the rib associated with the seventh cervical element and reaches its midlength (Fig. 26C). The subsequent cervical rib lacks, almost entirely, its shaft. Its morphology resembles that of the previous elements, but the spinous process is 8 mm in length.

The rib of the ninth cervical vertebra is almost completely preserved (Fig. 26D). It is 51 mm long, with the tuberculum more developed than those from the remaining cervical ribs, but smaller than the capitulum. The medial surface between both articulations is concave, and a spinous process is absent, with no indication that this could have been broken. The shaft is about three times longer than its respective centrum. In contrast to the slender and straight shaft of the previous ribs, this is more robust and curved ventrally along its length. In its medial surface, a shallow sulcus extends along the entire length of the shaft.

Trunk ribs

Trunk ribs are preserved on both sides. The left ribs are articulated with their respective vertebrae, whereas those from the right side are disarticulated. No trunk rib is entirely preserved, so their total length is unknown. The first trunk rib (Fig. 27) is longer and more robust than the last cervical one, and its capitulum is longer (8 mm) than the tuberculum (3.5 mm). There is a gap separating both processes in the cranial (visible in the first two trunk ribs) elements, but it reduces in size along with the upward displacement of the parapophysis throughout the trunk series. Unlike the cervical ribs, the elements from the trunk series completely lack a spinous process. Also, whereas the shafts of the cervical ribs are almost entirely directed caudally, they are more ventrally directed in the trunk series. In addition, the cranial surface of the trunk ribs is transversely convex, whereas a longitudinal groove extending from the region between the tuberculum and capitulum excavates their caudal surface.

Pectoral girdle and forelimb

The pectoral girdle and forelimb elements were found disarticulated in the field, but closely associated with the specimen. Only the left side has preserved elements, including a partial scapula, coracoid and humerus (Fig. 28). The scapula lacks the cranial part of its basal portion, including the acromion and the distal end of the blade. Only the caudal half of the coracoid is preserved. The lateral half of the proximal portion of the humerus is preserved. Despite their incompleteness, these bones have well-preserved surfaces.

Scapula

The scapula is lateromedially flattened and laterally arched in cranial/caudal views (Fig. 28C, D). As

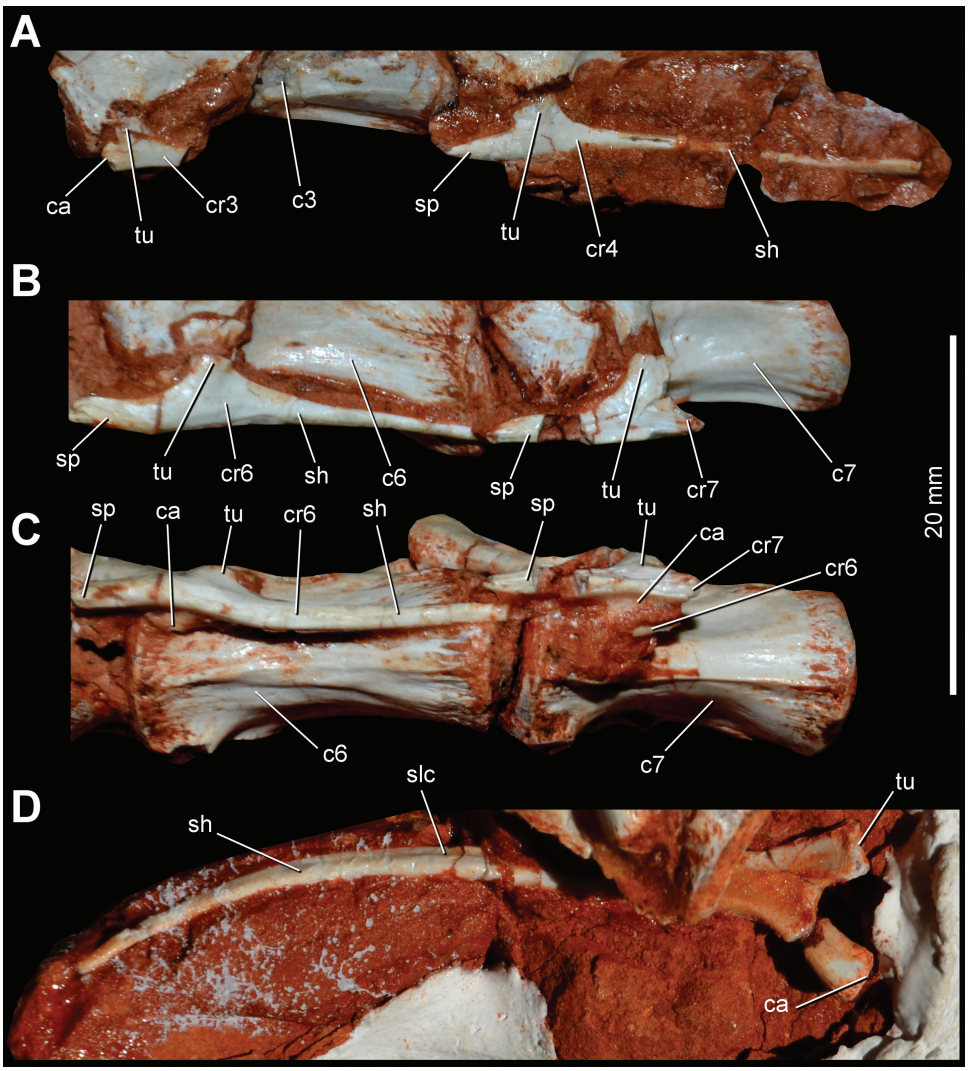

Figure 26. Cervical ribs of CAPPA/UFSM 0035. A, ribs associated with the cervical vertebrae three and four in left lateral view. B, ribs associated with the cervical vertebrae six and seven in left lateral view. C, ribs associated with the cervical vertebrae six and seven in ventral view. D, rib associated with ninth cervical vertebra in medial view. Abbreviations: c, cervical vertebra; ca, capitulum; cr, cervical rib; sh, shaft; slc, sulcus; sp, spinous process; tu, tuberculum.

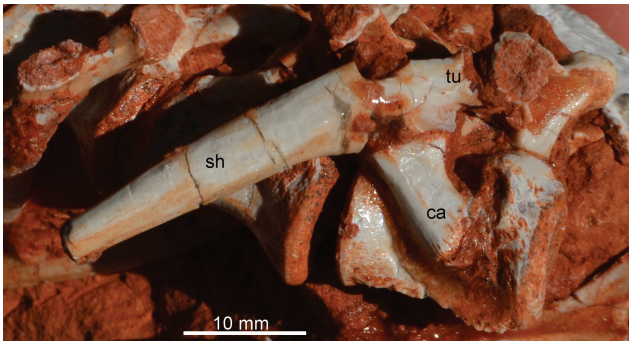

Figure 27. First trunk rib of CAPPA/UFSM 0035 in lateral view. Abbreviations: ca, capitulum; sh, shaft; tu, tuberculum.

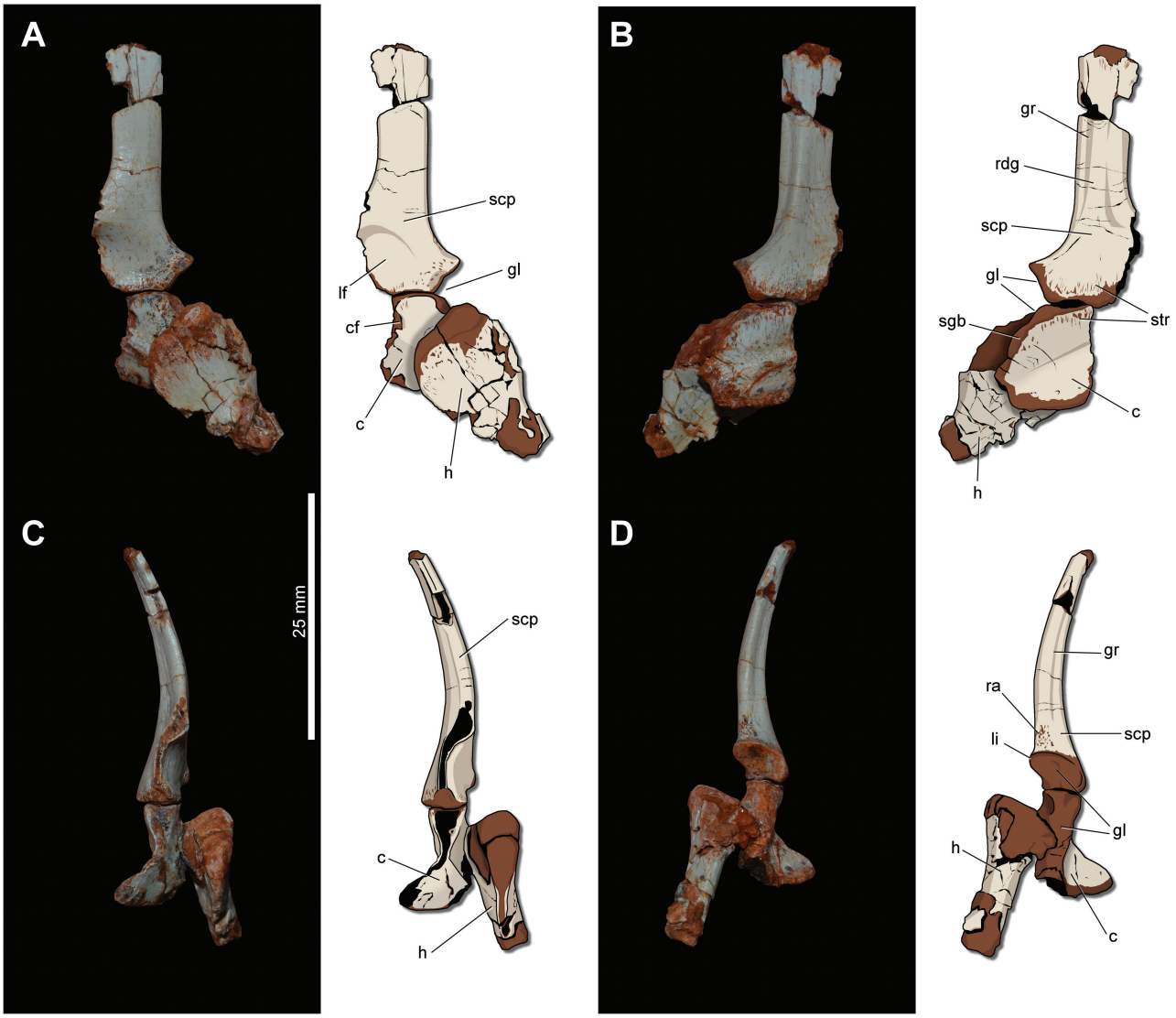

Figure 28. Left pectoral girdle and forelimb of CAPPA/UFSM 0035. A, photograph and interpretative drawing in lateral view. B, photograph and interpretative drawing in medial view. C, photograph and interpretative drawing in cranial view. D, photograph and interpretative drawing in caudal view. Abbreviations: c, coracoid; cf, coracoid foramen; gl, glenoid; gr, groove; h, humerus; lf, lateral fossa; li, lip; ra, rugose area; rdg, ridge; scp, scapula; sgb, subglenoid buttress; str, striations.

indicated by the preserved portion of its cranial margin, the blade expands gradually from the neck. The thinnest part is 10 mm in craniocaudal breadth, reaching 12 mm more distally. The lateral surface of the scapular blade is mainly smooth (Fig. 28A), but there are some longitudinal scars generally associated with the m. deltoideus scapularis (e.g. Langer, França & Gabriel, 2007; Remes, 2008). In contrast to the lateral surface, the medial surface bears a long longitudinal ridge located in the caudal half of the craniocaudal breadth (Fig. 28B). Caudal to the ridge, there is a parallel longitudinal groove for either m. serratus superficialis or m. scapulohumeralis posterior (Remes, 2008; Burch, 2014). Cranial to the ridge, a gentle depression is occupied by longitudinal muscle scars from the m. scapularis. Towards the scapular body, the cranial margin of the scapular blade starts to expand more distally than the caudal, but the cranial expansion is more gradual. This cranial expansion culminates in the acromion, not preserved in the specimen.

The body of the scapula rests on the dorsal surface of the coracoid, and the bones are clearly unfused. The preserved portion of the coracoid articulation forms a straight ventral margin. The lateral and medial surfaces near the coracoid articulation are densely marked with dorsoventrally oriented striations, a

pattern also present in the adjacent portion of the coracoid. The cranial half of the scapular body is craniomedially compressed and bears a wide fossa on its lateral surface for the m. supracoracoideus (Fig. 28A). In contrast, the caudal half is transversely broad, forming the scapular part of the glenoid. The scapular body is laterally depressed immediately cranial to the ventral margin of the glenoid; therefore, the dorsal part of the scapular glenoid expands more laterally than the ventral, forming a lip (Fig. 26D). Together with its coracoid portion, this forms a C-shaped glenoid, with the convexity facing slightly lateral. The scapular part of the glenoid is flat, except for a shallow groove that extends from the dorsal to the lateroventral margin. A rugose area (6 mm in length) for the attachment of the m. triceps brachii scapularis is present on the lateral surface of the scapular body neighbouring the glenoid (Fig. 28D), where a pit is present in *Saturnalia tupiniquim* (Langer *et al.*, 2007).

Coracoid

The dorsal half of the preserved portion of the coracoid is dorsoventrally oriented and thicker than the ventral half (Fig. 28C). The maximal transverse breadth (7 mm) occurs at the articulation with the scapula. The caudal tip of the coracoid is more caudally placed than the maximal caudal extension of the scapula, but they have similar participation in the glenoid (Fig. 28B). The caudal border of the glenoid forms a gently subglenoid buttress, ventral to which there is a lateromedially oriented groove that does not reach the medial margin of the coracoid; hence, no marked notch ventral to the glenoid is observed in medial view. The caudal half of the coracoid foramen is preserved and visible in lateral view, close to the dorsal margin of the coracoid (Fig. 28A). The contact of the dorsal portion of the coracoid with its plate-like (2-mm-thick) ventral portion is marked by a wide fossa in medial view, because the ventral part is medially inflected. This fossa is probably related to the m. subcoracoideus (Remes, 2008). This arrangement makes the medial surface of the coracoid markedly concave, with the opposite configuration occurring on the lateral surface.

Humerus

The recovered part of the humerus is 32 mm long (Fig. 29). The proximal end expands craniocaudally when compared with the preserved part of the shaft. Its caudal margin expands caudally and forms a convex edge in proximal view (Fig. 29D), which is more evident in its central part, where the projection forms a lip. On the caudal surface of the humerus, this lip probably separated the proximal portions of the insertions of m. scapulohumeralis cranialis and m. scapulohumeralis caudalis (Remes, 2008). In addition, the proximal portion of the lateral surface

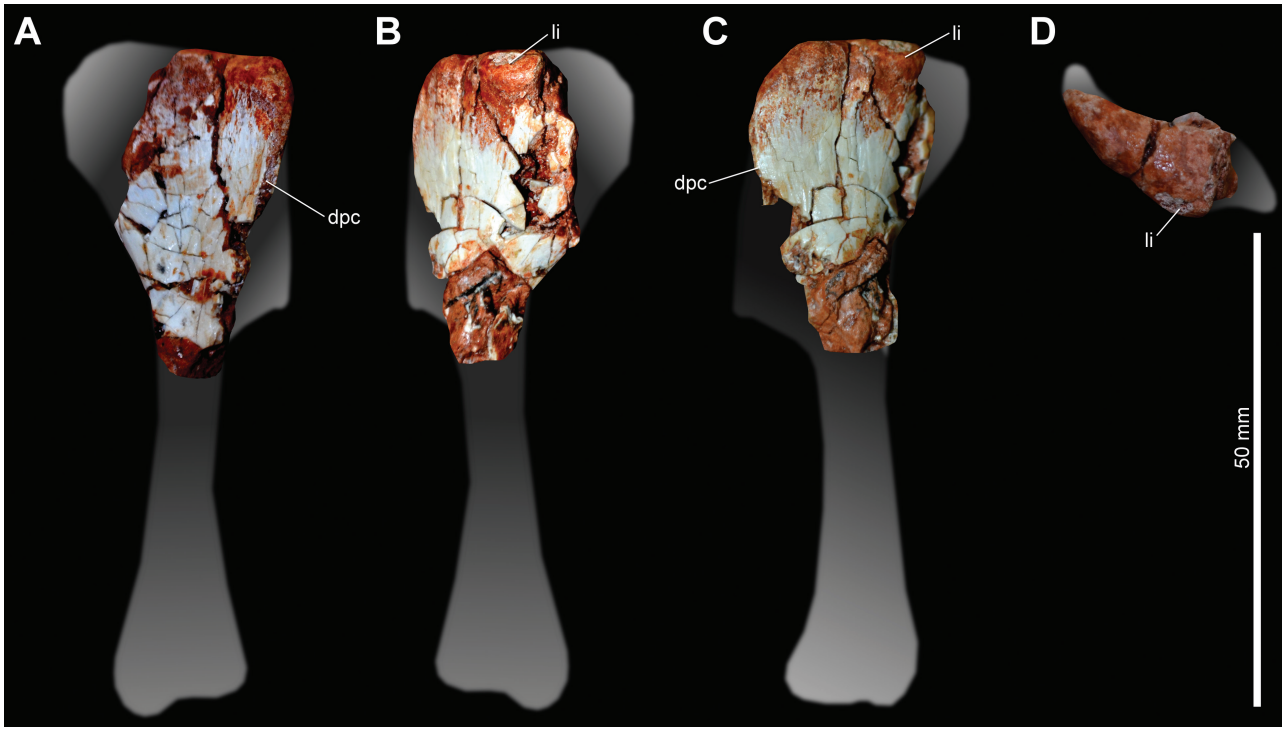

Figure 29. Left humerus of CAPPA/UFSM 0035. A, cranial view. B, caudal view. C, lateral view. D, dorsal view. Abbreviations: dpc, deltopectoral crest; li, lip.

of the humerus is rugose, which could be associated with m. scapulohumeralis cranialis and m. deltoideus scapularis.

The cranial surface of the proximal portion of the humerus is slightly concave and striated at the proximalmost region, which is generally associated with m. coracobranchialis (e.g. Langer *et al.*, 2007; Remes, 2008; Burch, 2014). Only a proximal portion of the deltopectoral crest is preserved (Fig. 29A–C). The cranial folding of the proximal articular surface of the humerus forms the proximal portion of the crest, which expands craniolaterally and is lateromedially compressed. The transition from the humeral head to the crest is smooth (Fig. 29C). The proximal half of the humerus also expands medially, as observable on its concave medial margin. The medial portion that includes the internal tuberosity is not preserved in the specimen. The distalmost preserved portion probably corresponds to part of the attachment area of m. triceps brachii medialis.

Pelvic girdle and hindlimb

Both pelvic girdle and hindlimb elements were preserved in articulation on both sides, but the right elements are more complete. Both ilia are complete, but some portions are fractured and displaced. A portion of the iliac peduncle of the left pubis is preserved. The right element is better preserved, but also composed of the proximal part only. The ischia are represented by only one fragment corresponding to the iliac peduncle of the right element. The right femur is almost completely preserved, whereas the left is represented by only a fragment of the proximal portion and part of the shaft. The left tibia is unknown, but a partial right tibia was recovered, although poorly preserved and lacking its distal end. A partial right fibula is also preserved, the distal portion of which was lost. Right pedal digits III and IV are partly preserved. The ungual phalanx of digit III is incomplete. In contrast, digit IV preserves the ungual, but lacks phalanx 1 and part of phalanx 2.

Ilium

The ilium is 76 mm in total length (Figs 30, 31). The acetabulum is 16 mm deep and the upper iliac blade 30 mm deep. The entire dorsal margin of the blade is covered with muscle insertion striations (Fig. 30). The lateral surface of the cranial half of the blade is concave, probably corresponding to the attachment area of m. iliofemoralis. In lateral view, the dorsal margin of the iliac blade is nearly straight, but the cranial tip folds down, forming the rounded dorsocranial margin of the preacetabular ala. The cranioventral surface of the preacetabular ala is also rounded. The whole structure is short, because its cranial tip does not reach the cranial margin of the pubic peduncle. The transition from the preacetabular ala to the pubic peduncle is concave in lateral view, although the medial surface is gently excavated for the attachment of the m. puboischiofemoralis 1.

The postacetabular ala is longer than the preacetabular and tapers caudally. On the lateral surface of its caudal end, a rugose protuberance (subtriangular and 12 mm long) is present in the left ilium (Fig. 30B). The homologous surface of the opposite bone is densely marked by muscle scars (Fig. 30A), but no similar protuberance is seen. This might be related to recent weathering, given that this portion was exposed in the outcrop when the specimen was discovered. In any case, this protuberance could be related to either m. flexor tibialis externus or m. iliofibularis. The brevis shelf expands lateroventrally and does not merge cranially with the supra-acetabular crest. Laterodorsally, the shelf set the limits of the brevis fossa, whereas its medial border is set by the medially deflected ventral margin of the postacetabular ala, forming the point of attachment to the m. caudofemoralis brevis. The medial blade is ~9 mm in width at its widest transverse point, whereas the brevis shelf is ~7.5 mm, resulting in an asymmetrical brevis fossa in caudal view. The arrangement of these two blades, associated with the dorsal iliac blade, forms an inverted Y in caudal view (Fig. 31B).

The supra-acetabular crest forms the roof of the acetabulum. It is lateroventrally oriented and reaches its maximal lateromedial extension above the centre of the acetabulum. The crest extends along the pubic peduncle, merging cranially with the iliac surface slightly before (4 mm) the distal margin of the peduncle. The lateral margin of the supra-acetabular crest is convex when observed in dorsal or ventral views. The acetabulum is craniocaudally longer (26 mm) than dorsoventrally deep (13 mm) and has a semilunate shape in ventral view (Fig. 25B). A transversely compressed bone extension that corresponds to the acetabular wall connects the iliac and pubic peduncles, closing the acetabulum medially. It extends caudally from the medial surface of the pubic peduncle and reaches the cranial margin of the ischiatic peduncle medially. The ventral margin of the wall is almost straight, although there is a gentle concavity near the cranial margin, close to the pubic peduncle.

The pubic peduncle is cranioventrally oriented and forms the cranialmost tip of the ilium. In cranial view (Fig. 31A), it is almost as high as broad. It bears two distinctly oriented surfaces for articulation with the pubis. One is cranially oriented and bears a central depression, whereas the other is ventrally oriented and C shaped in ventral view. Those surfaces are separated by a cranioventrally directed convex protuberance that rests in a

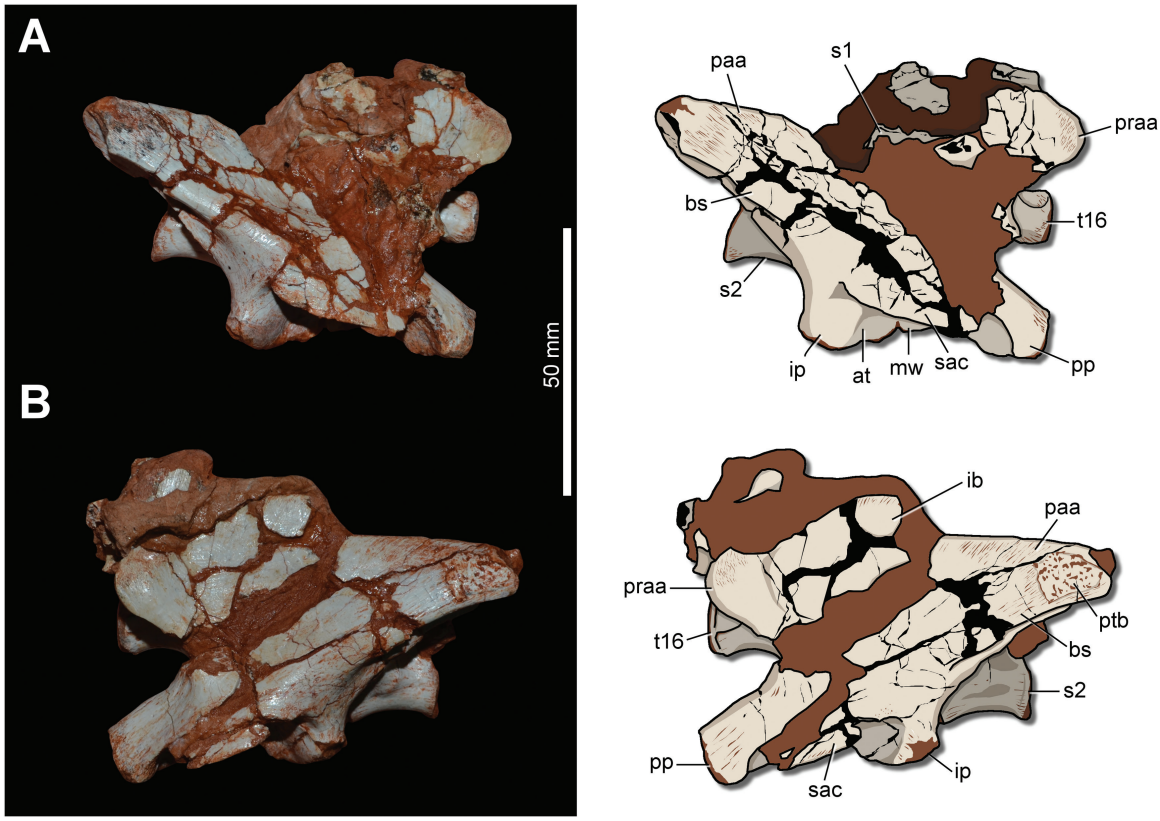

Figure 30. Sacrum of CAPPA/UFSM 0035. A, photograph and interpretative drawing in right lateral view. B, photograph and interpretative drawing in left lateral view. Abbreviations: at, antitrochanter; bs, brevis shelft; ib, iliac blade; ip, ischiatic peduncle; mw, medial wall; paa, postacetabular ala; pp, pubic peduncle; praa, preacetabular ala; ptb, protuberance; s, sacral vertebra; sac, supra-acetabular crest; t, trunk vertebra.

depression on the iliac articulation of the pubis. The dorsal surface of the pubic peduncle is lateromedially rounded and lacks crests or ridges. The lateral surface is also rounded, whereas the medial is flat. The ischiatic peduncle projects ventrocaudally. It is ovoid in cross-section, with a ventrocaudally convex articular surface. The cranioventral surface of the peduncle is convex, corresponding to the antitrochanter.

Pubis

The pubis (Fig. 32) is cranioventrally projected from the acetabulum. In proximal view, its iliac articulation is ovoid (Fig. 32D), with a 20 mm long axis and 9 mm transverse axis. It is formed by two main surfaces that form an angle of ~110° to one another. In addition, a bony wall bounds the medial margin of the articulation, resulting in a transversely concave articular surface. The preserved lateral surface of the pubis is covered by muscle scars and has a protuberance related to the m. ambiens (Fig. 32B). The obturator process expands from the medioventral surface of the pubis, in the dorsal portion of which a foramen pierces the bone (Fig. 32C). The pubic shaft is more craniocaudally flattened in its medial portion, where it forms the medial lamina. This starts proximally as a medioventrally expanding lamina and becomes limited to the medial surface along the preserved remnant of the bone, becoming progressively more expanded distally (Fig. 32A).

Ischium

The iliac peduncle is ovoid in proximal view (Fig. 33C), with the medial margin almost straight and the lateral margin convex. The preserved portion is ~20 mm in dorsoventral height and is 11 mm transversely. The proximal articulation is divided into dorsal and lateroventral surfaces. The former is concave, meets the ischial peduncle of the ilium, and is laterally bounded by a bump. Lateroventrally, the antitrochanteric surface is ventrally descending, with the medial margin more expanded than the lateral. Yet, its lateral margin also shows a slight expansion, forming the acetabular margin and resulting in a lateral ridge (Fig. 33A). A thin bone wall expands ventrally and forms the medioventral edge of the antitrochanter (Fig. 33B). This indicates the medial closure of the concavity between the iliac and pubic peduncles.

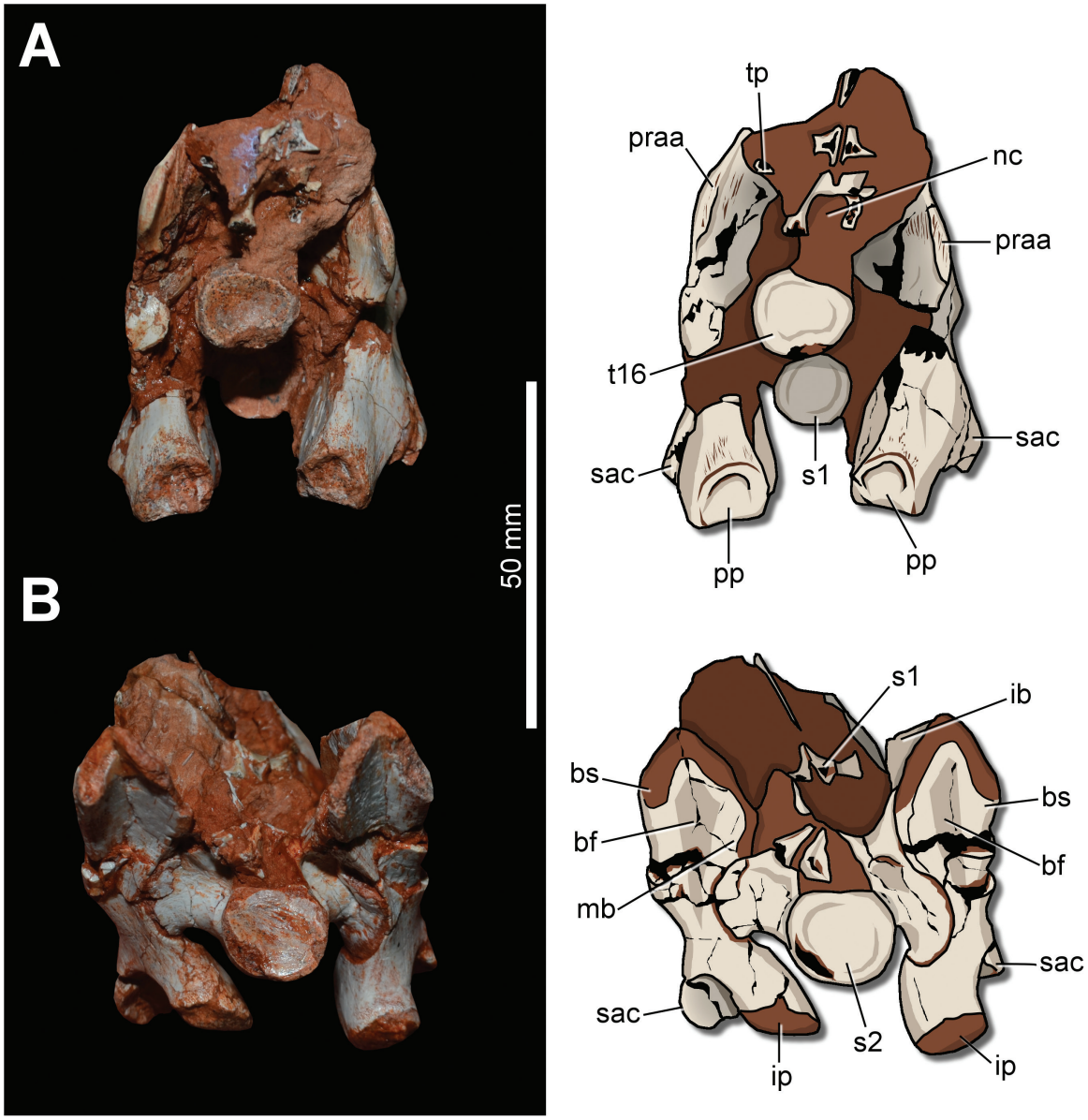

Figure 31. Sacrum of CAPPA/UFSM 0035. A, photograph and interpretative drawing in cranial view. B, photograph and interpretative drawing in caudal view. Abbreviations: bf, brevis fossa; bs, brevis shelf; ip, ischiatic peduncle; mb, medial blade; nc, neural canal; pp, pubic peduncle; praa, preacetabular ala; s, sacral vertebra; sac, supra-acetabular crest; t, trunk vertebra; tp, transverse process.

Femur

The left femur is 136 mm long (Fig. 34), with the long axes of the proximal and distal ends measuring, respectively, 24 and 22 mm. The femoral head is craniomedially directed in proximal view, and the shaft is sigmoid in cranial/caudal and lateral/medial views. A straight, shallow groove extends along the proximal surface (Fig. 35A), from the level of the caudomedial tuber to the craniolateral tuber. The proximal surface is gently convex in caudolateral/craniomedial views. The craniolateral tuber is poorly developed and distally connected to a descendant ridge (craniomedial crest of Bittencourt & Kellner, 2009) that reaches the proximal tip of the cranial trochanter. The craniomedial tuber is rounded and separated from the caudomedial tuber by the sulcus for the ligamentum capitis femoris. Although both tuberi are equivalent in size, the craniomedial is more expanded distally. Lateral to the caudomedial tuber, a distally descended surface corresponds to the facies articularis antitrochanterica.

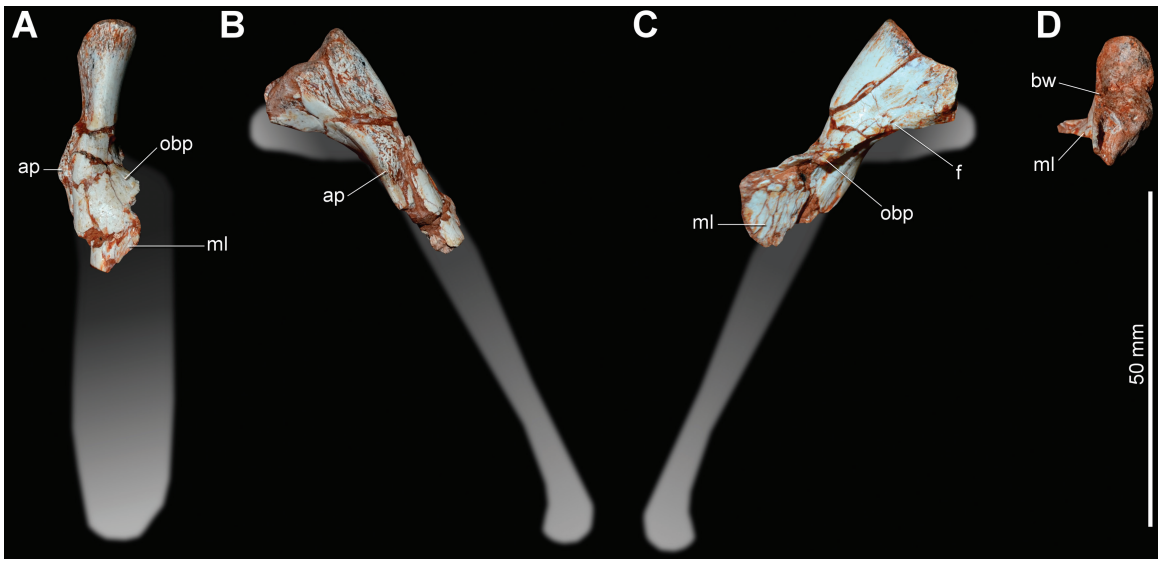

Figure 32. Right pubis of CAPPA/UFSM 0035. A, cranial view. B, lateral view. C, medial view. D, proximal view. Abbreviations: ap, ambiens process; bw, bone wall; f, foramen; ml, medial lamina; opb, obturator process.

The femoral head bears several muscle and soft tissue scars (Fig. 35C). Between the craniomedial crest and the dorsolateral trochanter, a rounded bone protuberance is present, which is possibly equivalent to a scar found in some individuals of *Asilisaurus kongwe* (NMT RB159, NMT RB216, NMT RB221; Griffin & Nesbitt, 2016) and *Silesaurus opolensis* (ZPAL AbIII/361/21, ZPAL AbIII/411/4R; Piechowski, Tałanda & Dzik, 2014). The cranially convex dorsolateral trochanter is protuberant, but merges smoothly to the femoral shaft proximally, completely disappearing at the ventral surface of the femoral head. Some dorsolateral trochanter scars reach the caudal portion of the bone, at the level of the trochanteric shelf (Fig. 35D). The cranial trochanter is knob like and bears an extremely striated surface (Fig. 35C). The proximal tip is distal to the tip of the dorsolateral trochanter and separated from the femoral shaft by a cleft. However, the cleft possibly resulted from taphonomic processes, which is suggested by the presence of a fracture between the dorsal tip of the trochanter and the femoral shaft. The distal portion of the cranial trochanter is associated with a well-developed trochanteric shelf, which is also marked by a striated surface and reaches the caudolateral margin of the femoral shaft. The caudolateral portion of the trochanteric shelf extends distally, reaching the level of the proximal tip of the fourth trochanter. At the same level of the trochanteric shelf, the medial surface of the femoral head bears striations that correspond to muscle insertions.

The fourth trochanter is located at the caudomedial surface of the proximal half of femoral shaft (Fig. 34C). It corresponds to a large (20 mm) proximodistally oriented crest, densely covered by muscle scars. The proximal portion of the trochanter merges with the shaft smoothly, whereas the distal forms a more acute angle, so that the structure has an asymmetrical shape. The lateral surface of the fourth trochanter possesses a longitudinal rugose margin probably related to the m. caudofemoralis brevis. In contrast, the medial surface bears a concavity with a rough surface (Fig. 34D), which extends onto the femoral shaft. A faint ridge bounds the distal margin of this concavity, and the entire region has been suggested as an insertion point for the m. caudofemoralis longus (Langer, 2003; Grillo & Azevedo, 2011; Müller *et al.*, 2016). Distal to the fourth trochanter, the femoral shaft is ovoid in cross-section. In addition, two intermuscular lines extend longitudinally along the shaft. The cranial intermuscular line extends from the distal end of the cranial trochanter to the distal quarter of the bone (Fig. 34A). The proximal portion of the caudolateral intermuscular line rises approximately on the middle point of the shaft and extends distally until the distal quarter of the bone (Fig. 34C). The femoral shaft expands gradually from its middle point to the distal margin.

The cranial surface of the distal portion of the femur is strongly marked by longitudinal muscle scars, mostly grouped densely in the craniomedial margin (Fig. 34A). Muscle scars extend to the craniolateral surface, but no concavity or depression, as found in *Herrerasaurus ischigualastensis* (PVS J373; Novas, 1994), is present in that area. The distal surface of the femur bears three condyles (Fig. 35B). The medial one is subequal in size to the crista tibiofibularis, and both are caudally separated by a craniocaudally broad (6.5 mm), but proximodistally short (13 mm) popliteal fossa. The lateral condyle is ventrally larger than the crista tibiofibularis,

and both are separated distally by a groove. The cranial edge of the distal femoral end is convex in distal view.

Tibia

The preserved length of the partial tibia (Fig. 36) is 109 mm. Its proximal end is craniocaudally expanded (~33 mm long) and subtriangular in proximal view (Fig. 36D), with a slightly convex proximal surface in lateral or medial view. On the cranial margin of the proximal end, there is a craniolaterally arched cnemial crest, which projects proximally relative to the caudal edge of the proximal end of the bone. Both cranial and lateral margins of the crest are rounded in proximal view. However, its caudomedial portion is separated from the main body of the tibia by a concavity, which forms a depression in proximal view. Also in that view, the caudal continuation of the medial margin is convex. The lateral margin bears the fibular (or lateral) condyle (Fig. 36A), which is located in the middle of its caudal half. The proximal part of this structure is missing, but it is possible to observe that it is as laterally expanded as the cnemial crest. The medial condyle is subequal in size relative to the lateral condyle, but it is more caudally located, forming the caudomedial edge of the proximal end of the tibia.

The transition from the proximal end to the tibial shaft is relatively smooth, with the caudal margin narrowing distally, slightly more abruptly (in lateral/medial views) than the cranial. A craniocaudally oriented striated zone occurs on the medial surface of the proximal part of the tibia (Fig. 36B), probably related to m. gastrocnemius medialis. On the lateral surface of the proximal portion, rising from the distal edge of the fibular condyle, a proximodistally oriented and rugose fibular crest is present, which is sigmoid in lateral view and ~21 mm long. Probably, this crest received ligamentum tibiofibularis (Langer, 2003). The tibial shaft is almost equal in width (craniocaudal breadth of ~10 mm) along

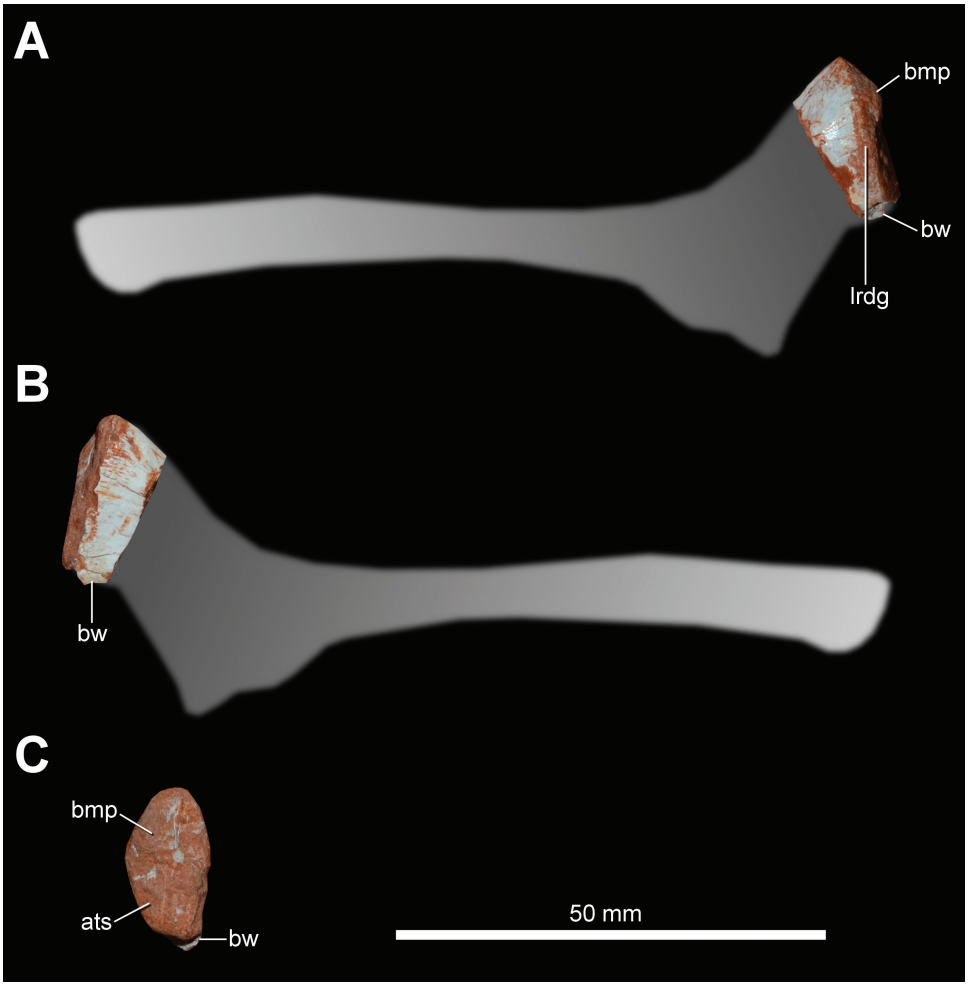

Figure 33. Right ischium of CAPPA/UFSM 0035. A, lateral view. B, medial view. C, proxiaml view. Abbreviations: ats, atitrochanteric surface; bmp, bump; bw, bone wall; lrdg, lateral ridge.

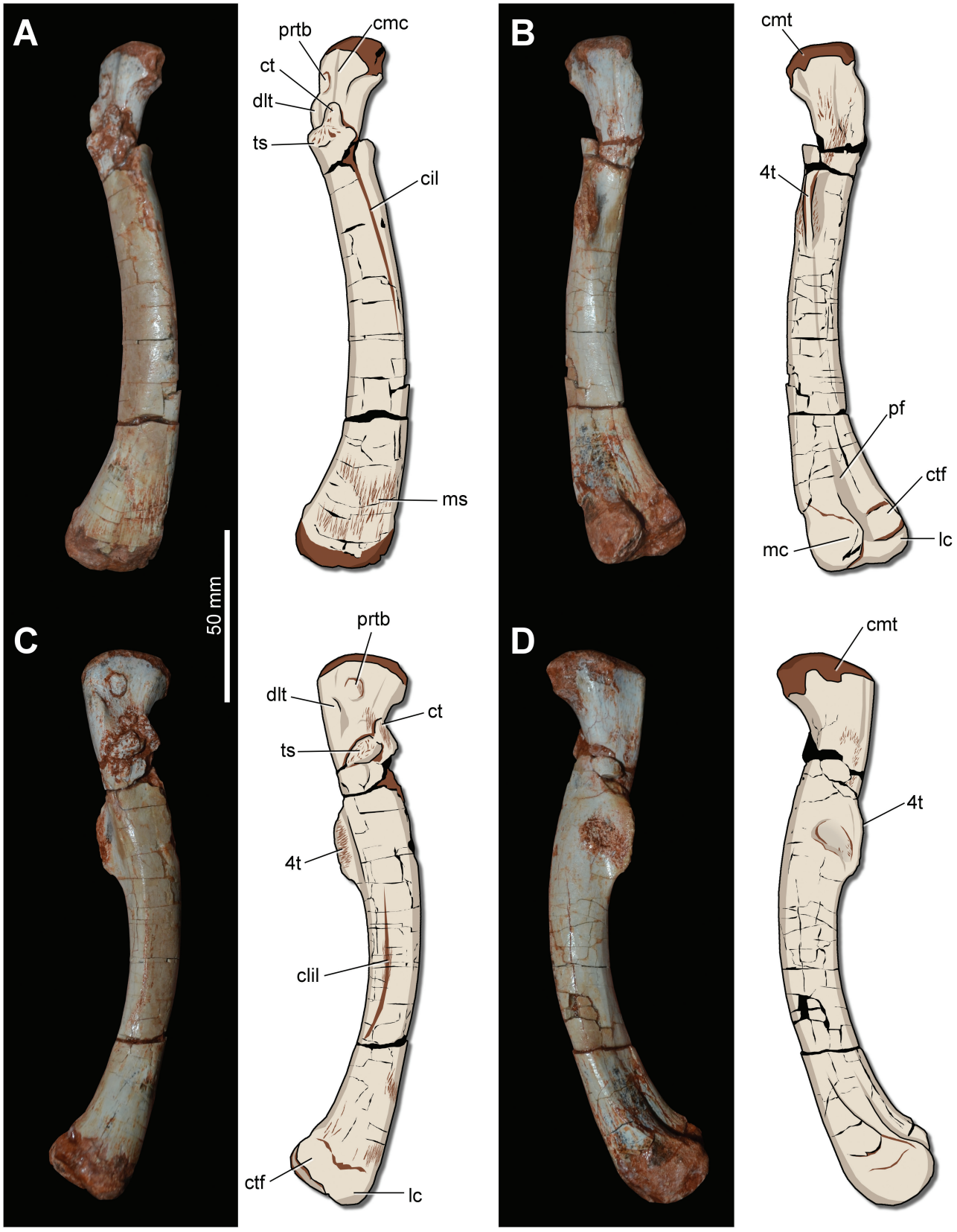

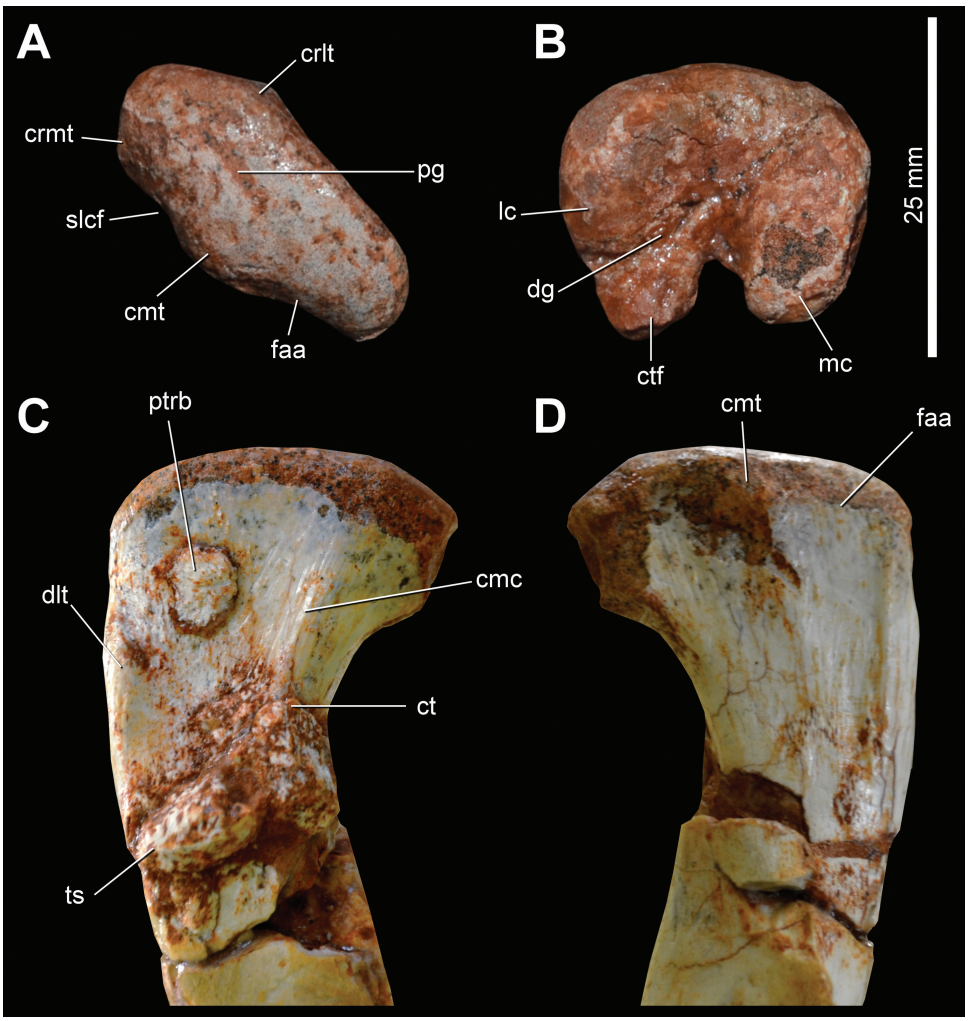

Figure 35. Right femur of CAPPA/UFSM 0035. A, proximal view. B, distal view. C, proximal portion in lateral view. D, proximal portion in medial view. Abbreviations: cmc, craniomedial crest; cmt, caudomedial tuber; crlt, craniolateral tuber; crmt, craniomedial tuber; ct, cranial trochanter; ctf, crista tibiofibularis; dg, distal groove; dlt, dorsolateral trochanter; faa, facies articularis antitrochanterica; lc, lateral condyle; mc, medial condyle; pg, proximal groove; ptrb, protuberance; slcf, sulcus for ligamentum capitis femoris; ts, trochanteric shelf.

its length. The preserved portion is proximodistally straight and subcircular in cross-section.

Fibula

The fibula (Fig. 37) is gracile and possesses a straight shaft. It is 121 mm long as preserved. The proximal portion is craniocaudally expanded (with a 21 mm long axis) and transversely narrow. The cranial margin of the proximal portion is more proximally expanded than the caudal. In contrast, the caudal margin is far more caudally projected from the shaft. Therefore, the caudal margin of the bone depicts a concave transition between the shaft and the proximal end, in lateral view. The lateral margin of the proximal end is convex in proximal view, whereas the medial is concave and articulates against the tibia. In lateral or medial view, there is a gentle concavity on the caudal half of the proximal end, whereas the cranial half is convex.

Figure 34. Right femur of CAPPA/UFSM 0035. A, photograph and interpretative drawing in cranial view. B, photograph and interpretative drawing in caudal view. C, photograph and interpretative drawing in lateral view. D, photograph and interpretative drawing in medial view. Abbreviations: 4t, fourth trochanter; cil, cranial intermuscular line; clil, caudolateral intermuscular line; cmc, craniomedial crest; cmt, caudomedial tuber; ct, cranial trochanter; ctf, crista tibiofibularis; dlt, dorsolateral trochanter; lc, lateral condyle; mc, medial condyle; ms, muscle scars; pf, popliteal fossa; prtb, protuberance; ts, trochanteric shelf.

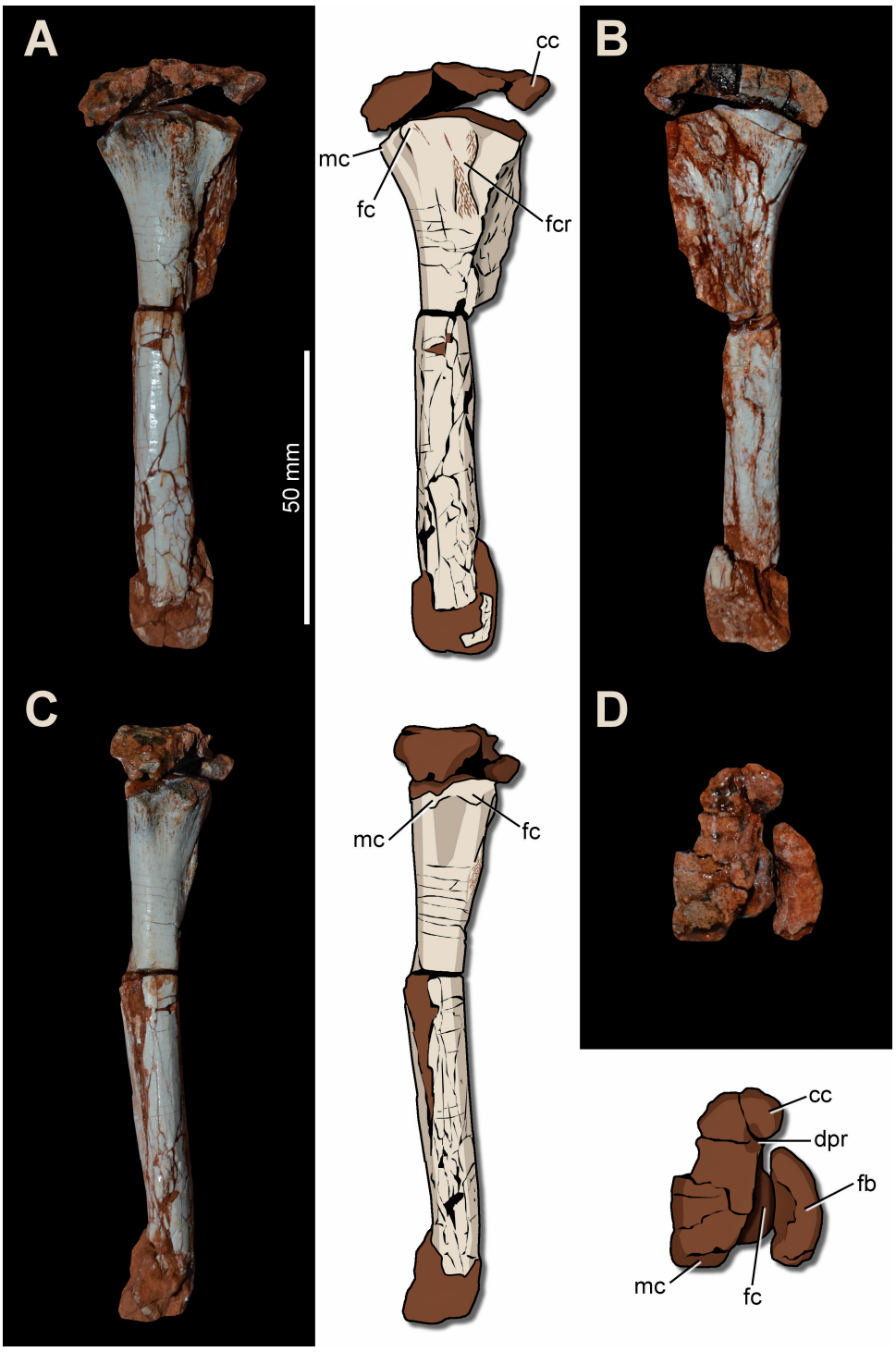

Figure 36. Right tibia of CAPPA/UFSM 0035. A, photograph and interpretative drawing in lateral view. B, photograph in medial view. C, photograph and interpretative drawing in caudal view. D, photograph and interpretative drawing of tibia and fibula in proximal view. Abbreviations: cc, cnemial crest; dpr, depression; fb, fibula; fc, fibular condyle; fcr, fibular crest; mc, medial condyle.

On the medial surface of the proximal part of the fibula, a 20-mm-long rugose faint ridge is visible (Fig. 37C), rising from the caudal edge of the proximal end and extending craniodistally along the medial surface of the bone, reaching the cranial edge of the shaft. This structure is related to the fibular crest of the tibia, as it should also support the ligamentum tibiofibularis. The lateral surface of the fibular proximal portion is almost flat, but bears some faint scattered longitudinal scars. More distally, a proximodistally oriented ridge extends along the lateral surface of the shaft (Fig. 37A), probably corresponding to an attachment point of m. iliofibularis. This 18-mm-long ridge has its proximal tip rising from the cranial margin of the shaft, whereas its distal portion merges to the lateral surface of the shaft. It is, therefore, slightly oblique to the fibular shaft. The rough surface texture of this structure differs from that surrounding it, which is smooth. This distinct rough surface extends craniomedially from the ridge until a protruding tubercle on the craniomedial surface of the shaft (Fig. 37B, C).

The long and slender fibular shaft has a fairly constant diameter, 8 mm in craniocaudal width. The entire lateral surface is craniocaudally convex, whereas the medial surface is flat. This gives a semilunar shape to the shaft in cross-section. A foramen pierces the medial surface of the shaft slightly distal to the middle point of the preserved length of the bone (Fig. 37C). Close to the foramen, on the caudomedial margin of the shaft, a small bony salience is visible.

Pedal phalanges

Pedal digit III has four preserved phalanges (Fig. 38A, B), including a partial ungual. The phalanges are proportionally larger than those preserved for digit IV. Their sizes decrease from the proximal to the distal elements (not considering the incompletely preserved ungual). Phalanx 1 is 20 mm long, phalanx 2 is 16.5 mm, and phalanx 3 is 13 mm. All non-terminal phalanges of this digit are longer than lateromedially wide. Their midshaft is constricted, and both extremities are equally broad transversely. The dorsal margin of the proximal portion of phalanx 1 is poorly preserved where the other phalanges bear a dorsal intercondylar process. The dorsal surface of the distal portion of the non-terminal phalanges has a marked depression for the insertion of m. extensor digitorum brevis. In addition, the sides of both distal condyles bear deep collateral ligament pits. A flexor tubercle is absent or poorly developed on the ventral margin of the articular surface of the ungual phalanx of digit III. That phalanx is triangular in cross-section, with lateral and medial surfaces gently convex.

Following the phalangeal formula of several other early dinosaurs (Sereno *et al.*, 2013), we presume that digit IV of CAPPA/UFSM 0035 has phalanges 2–5 preserved, with phalanx 5 being the ungual (Fig. 38C, D). Phalanx 2 is heavily fractured. Phalanges 3 and 4 are subequal in length, ~8 mm. Together, they are only slightly longer than the ungual of that digit, which is 14 mm long. Only phalanx 4 has the dorsal intercondylar process preserved. All non-terminal phalanges bear a deep dorsal extensor depression and collateral ligament pits. The medial and lateral surfaces of the ventral margin of the proximal portion of phalanges 3 and 4 bear a rugose bump with irregular striations. The ungual phalanx is pointed at the distal extremity, but does not significantly curve ventrally, because the margin between its distal tip and the ventral surface of the proximal half is straight to slightly concave. The lateral and medial surfaces of the ungual bear a sharp ridge, which should have been covered by a keratinous sheath. Below those ridges, a longitudinal groove extends until the distal tip of the phalanx. The ventral surface is flat, except for the most proximal portion, which is convex in lateral view and densely striated, probably for m. flexor digitalis longus. The ungual is triangular in cross-section.

RESULTS

Phylogenetic analysis

The first analysis recovered 54 MPTs of 853 steps each (consistency index [CI] = 0.345; retention index [RI] = 0.639). CAPPA/UFSM 0035 forms a clade with *B. schultzi*, with both forming the sister group to all other Sauropodomorpha in all MPTs (Fig. 39A). The CAPPA/UFSM 0035 plus *B. schultzi* clade is supported by the presence of a pedicel caudally projecting the forking part of the caudal process of the jugal. The rest of the strict consensus topology is the same as that recovered by Cabreira *et al.* (2016).

The second analysis also recovered 54 MPTs, but of 851 steps (CI = 0.347; RI = 0.637). The combined *B. schultzi* nests as the sister group of all other sauropodomorphs in all MPTs (Fig. 39B), similar to the results of Cabreira *et al.* (2016). In addition to the ten originally proposed character states, three additional conditions support the clade Sauropodomorpha, all of which are related to the cervical vertebrae: the absence of deep recesses on the cranial face of the neural arch, lateral to the neural canal [80(0)]; absence of pleurocoels in the cranial portion of the centra [86(0)]; and neural arches higher than caudal articular facets of the centra [87(0)]. The rest of the strict consensus tree is also the same as the former analysis.

The third analysis recovered 32 MPTs of 854 steps (CI = 0.349; RI = 0.636), with *B. schultzi* still as the sister taxon of all other sauropodomorphs in all the MPTs (Fig. 39C). Character states that support this position are the same as those found in the second analysis, except for an additional character related to the acute angle

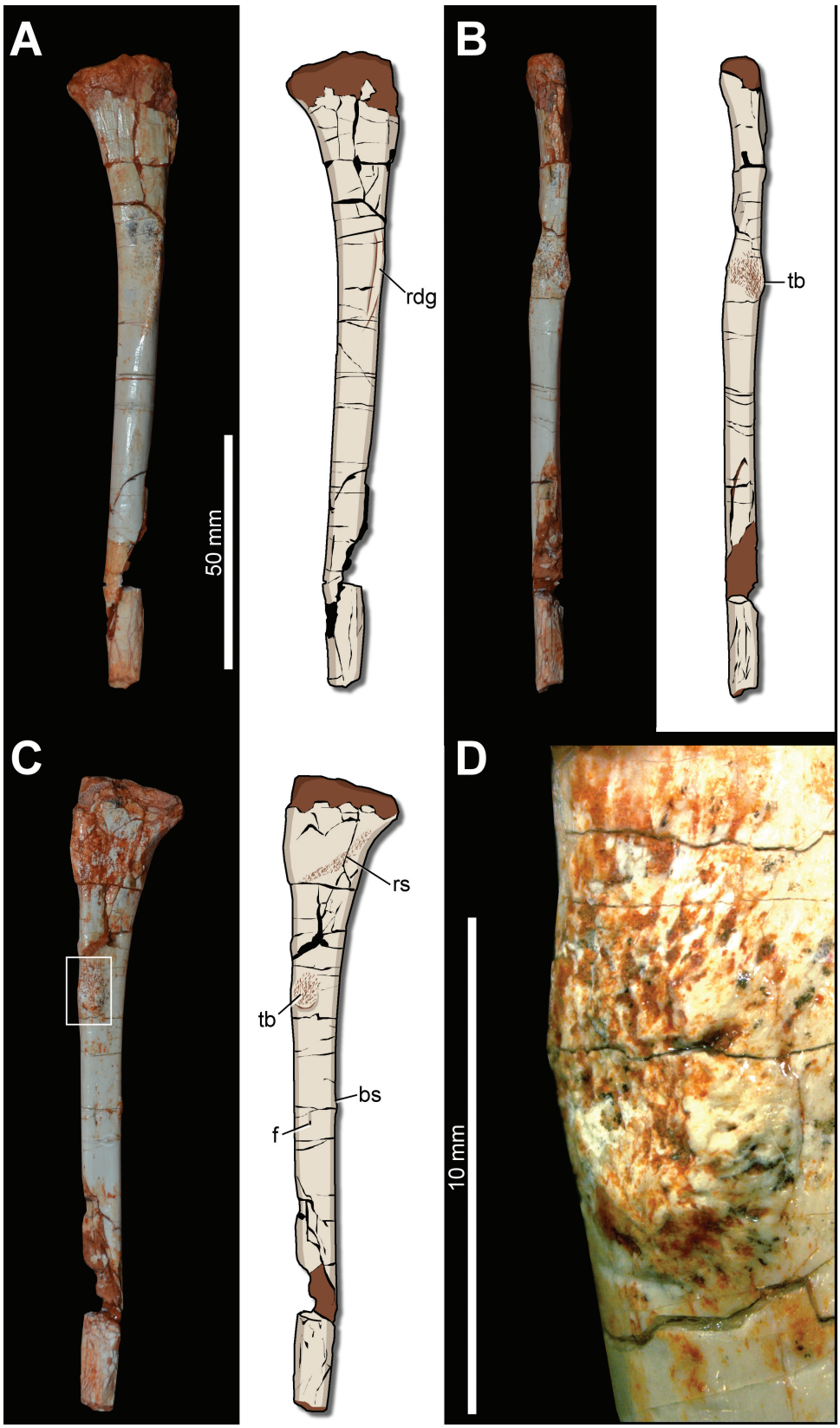

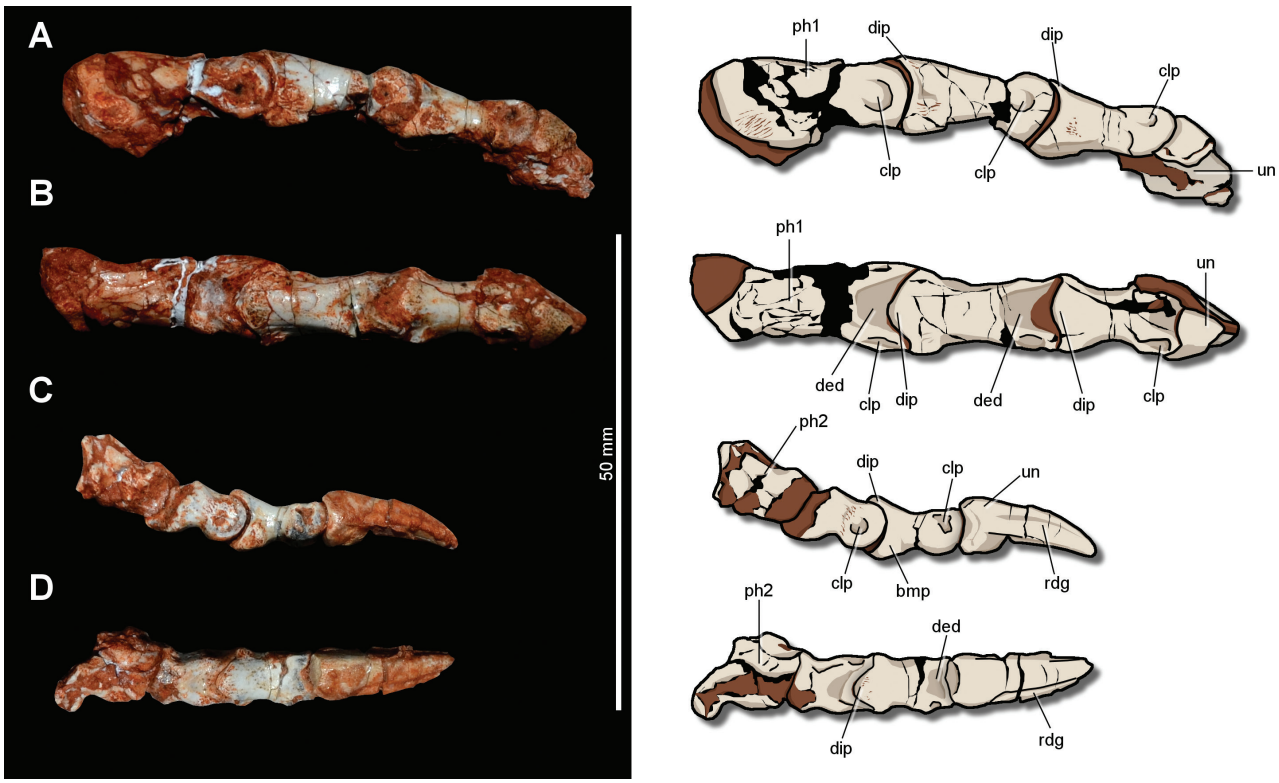

Figure 38. Pedal digits of CAPPA/UFSM 0035. A, photograph and interpretative drawing of digit III in lateral view. B, photograph and interpretative drawing of digit III in dorsal view. C, photograph and interpretative drawing of digit IV in lateral view. D, photograph and interpretative drawing of digit IV in dorsal view. Abbreviations: bmp, bump; clp, collateral ligament pit; ded, dorsal extensor depression; dip, dorsal intercondylar process; ph, phalanx; rdg, ridge; un, ungual phalanx.

formed between the ascending and caudal processes of the jugal [259(1)]. Unlike the results of Cabreira *et al.* (2016), *Pampadromaeus barberenai* and *P. protos* are sister taxa, supported by the absence of a sheet of bone between the rostral and ventral processes of the prefrontal [258(1)]. This node is sister to a clade including Saturnaliinae (*S. tupiniquim* and *C. novasi*) and other sauropodormohps. There are no other differences relative to the strict consensus trees of the previous analyses.

In the analysis with implied weighting (*k* value = 3–4), *B. schultzi* still nests within Sauropodomorpha in all the three MPTs (Fig. 39D), but as the sister taxon of *E. lunensis*, both forming the sister group of the clade including *P. barberenai* and *P. protos*. Those four species form a clade in a sister-group relationship with a large clade that includes Saturnaliinae and other sauropodomorphs. The clade comprising *B. schultzi*, *E. lunensis*, *P. barberenai* and *P. protos* is supported by the following synapomorphies: presence of a caudomedial process in the premaxilla (character 8, state 1); presence of a sharp longitudinal ridge on the ventral margin of the antorbital fossa of the maxilla [12(1)]; long axis of the jugal body nearly horizontal to the alveolar margin of the maxilla [26(0)]; presence of pterygoid teeth on palatal process [75(0)]; absence of a caudal groove on the astragalus [217(1)]; and the acute angle between the ascending and caudal processes of jugal [259(1)]. Another difference from the previous analyses performed here is the position of *T. hallae*, *Chindesaurus briansmalli*, *E. murphi* and *Guaibasaurus candelariensis* nested within Theropoda, because they were previously placed outside the clade formed by Theropoda plus Sauropodomorpha. The sister-group relationship between *T. hallae* and *C. briansmalli* remains supported in this analysis. Further increase of *k* recovers the same topology as the third analysis.

The fifth analysis recovered 40 320 MPTs of 1922 steps (CI = 0.274; RI = 0.621), seven steps shorter than the analysis by Langer *et al.* (2017). *Buriolestes schultzi* lies within Sauropodomorpha in all the MPTs

Figure 37. Right fibula of CAPPA/UFSM 0035. A, photograph and interpretative drawing in lateral view. B, photograph and interpretative drawing in cranial view. C, photograph and interpretative drawing in medial view. D, magnification of the rectangle in C. Abbreviations: bs, bone salience; f, foramen; rdg, ridge; rs, rough surface; tb, tuberosity.

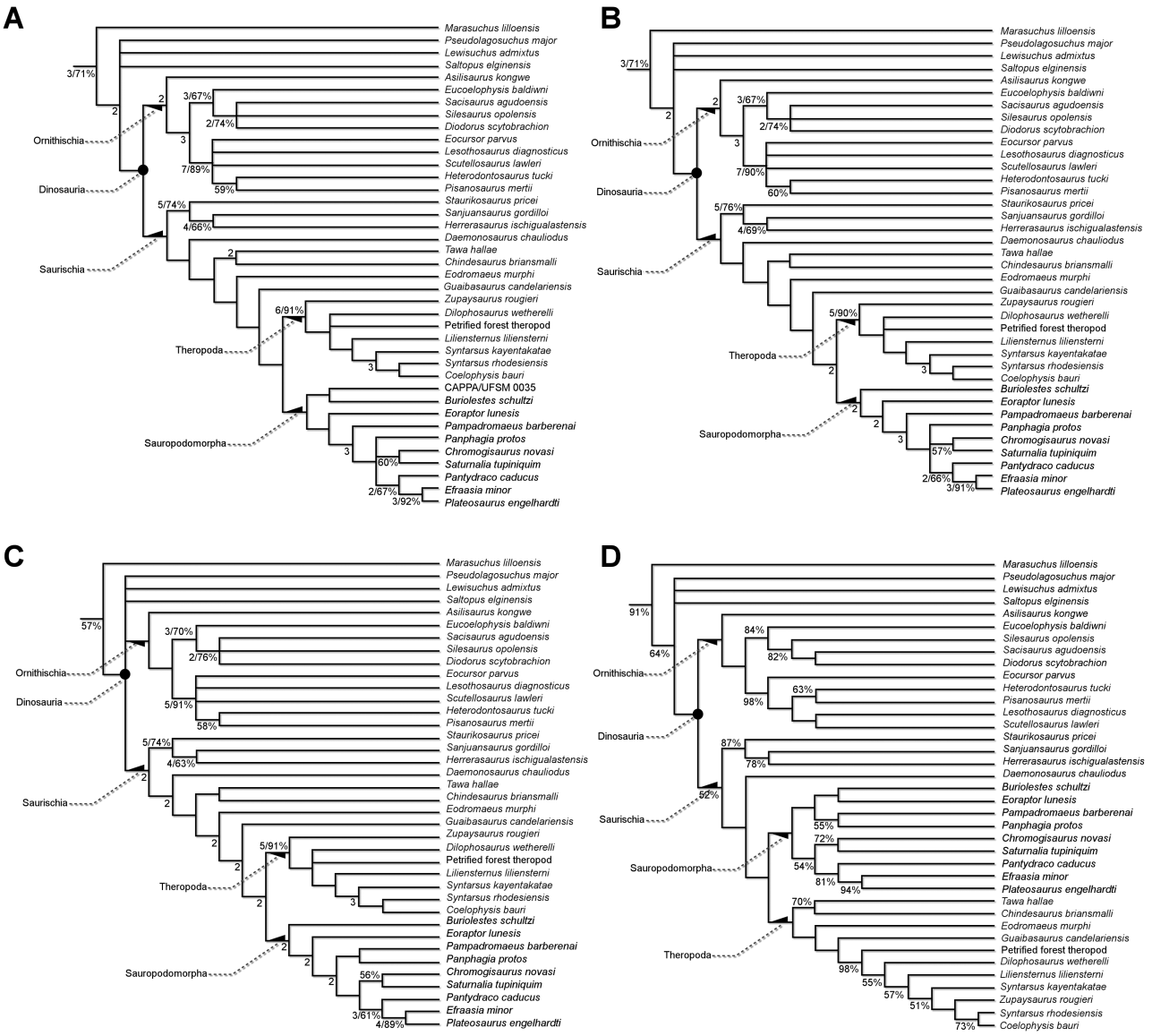

Figure 39. Results of the phylogenetic analyses (first to fourth). A, abbreviated strict consensus tree of the first analysis depicting the phylogenetic position of CAPPA/UFSM 0035. B, abbreviated strict consensus tree of the second analysis depicting the phylogenetic position of the combined *Buriolestes schultzi*. C, abbreviated strict consensus tree of the third analysis depicting the phylogenetic position of the combined *B. schultzi* using the modified data matrix. D, abbreviated strict consensus tree of the fourth analysis using implied character weighting with $k = 3$. Numbers below nodes represent Bremer support values (left) higher than one and Bootstrap values (right) higher than 50% (in A, B, C) and symmetric resampling values > 50% (in D).

(Fig. 40). In contrast with the first three analyses, the taxon is not recovered as the sister to all other members of the group, but as a member of a clade composed exclusively by all coeval South American forms. This group is supported by 13 synapomorphies, but none is exclusively shared by their members among the OTUs of the analysis. This clade has a sister-group relationship to a clade formed by *Pantydraco caducus* and all other sauropodomorphs. The Carnian South American clade has a pectinate structure, starting with *E. lunensis*, followed by *B. schultzi* and by *P. protos* as the sister group to a clade formed by *P. barberenai* and *S. tupiniquim*.

MORPHOLOGICAL DISPARITY ANALYSIS

As expected, the analysis using all characters recovered *B. schultzi* within the morphospace occupied by

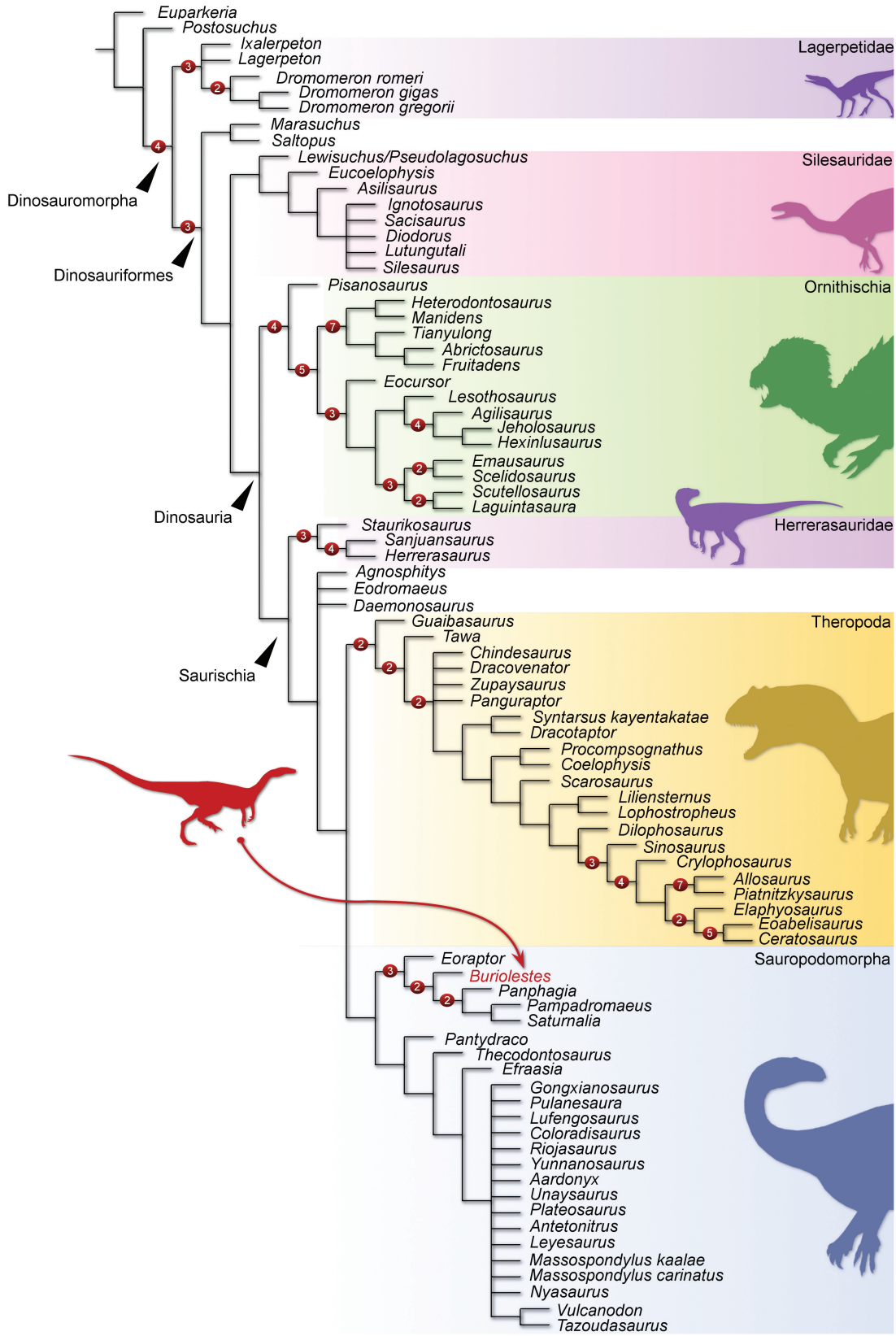

Figure 40. Strict consensus tree of the fifth phylogenetic analysis depicting the phylogenetic position of *Buriolestes schultzi* (ULBRA-PVT280 plus CAPPA/UFSM 0035). Numbers represent Bremer support values higher than one.

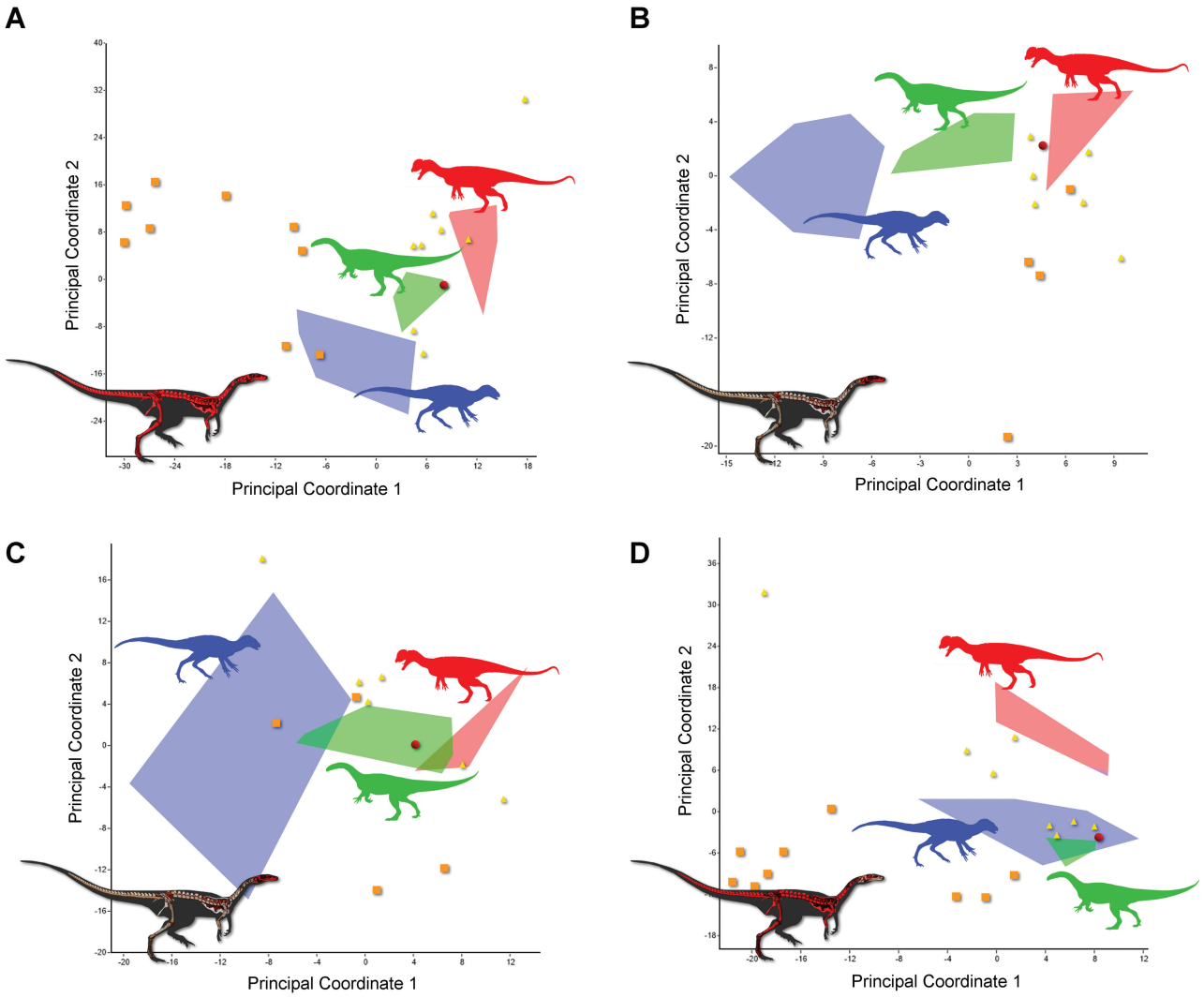

Figure 41. Bivariate plots showing the results of the morphospace occupation analysis. A, using all the characters. B, using cranial characters. C, using non-dentary cranial characters. D, using postcranial characters. Green convex hull corresponds to morphospace of sauropodomorphs, blue convex hull corresponds to morphospace of ornithischians, and red convex hull corresponds to morphospace of theropods. Squares correspond to non-dinosaur archosaurs, triangles correspond to basal saurischians outside the theropod–sauropodomorph dichotomy, and the red dot corresponds to *Buriolestes schultzi*.

sauropodomorphs (Fig. 41A). Morphospaces of ornithischians, sauropodomorphs and theropods are well defined, without overlap among convex hulls. In the analysis using solely cranial characters (Fig. 41B), these three groups also do not overlap, but *B. schultzi* lies outside their respective morphospaces, instead occupying a region occupied by other faunivorous dinosauriforms, such as *H. ischigualastensis*, *T. hallae* and *Daemonosaurus chauliodus*. It is clear that dentition influences this result, because *B. schultzi* lies deeply in the morphospace of sauropodomorphs when the analysis is run only with non-dentary cranial characters (Fig. 41C). In this analysis, although there is some degree of overlap among the morphospaces of sauropodomorphs, theropods and ornithischians, the area occupied by *B. schultzi* is restricted to sauropodomorphs.

The PCoA of postcranial characters (Fig. 41D) shows overlap between the convex hulls of Sauropodomorpha and Ornithischia. *Buriolestes schultzi* lies slightly outside the morphospace of sauropodomorphs, but within the morphospace of ornithischians. On the contrary, the three main dinosaur groups are well separated in the analysis with characters from the axial skeleton alone (Fig. 42A), with *B. schultzi* found within the morphospace occupied by sauropodomorphs. In the analysis of the pectoral girdle and forelimb characters (Fig. 42B), a common area occupied by ornithischians

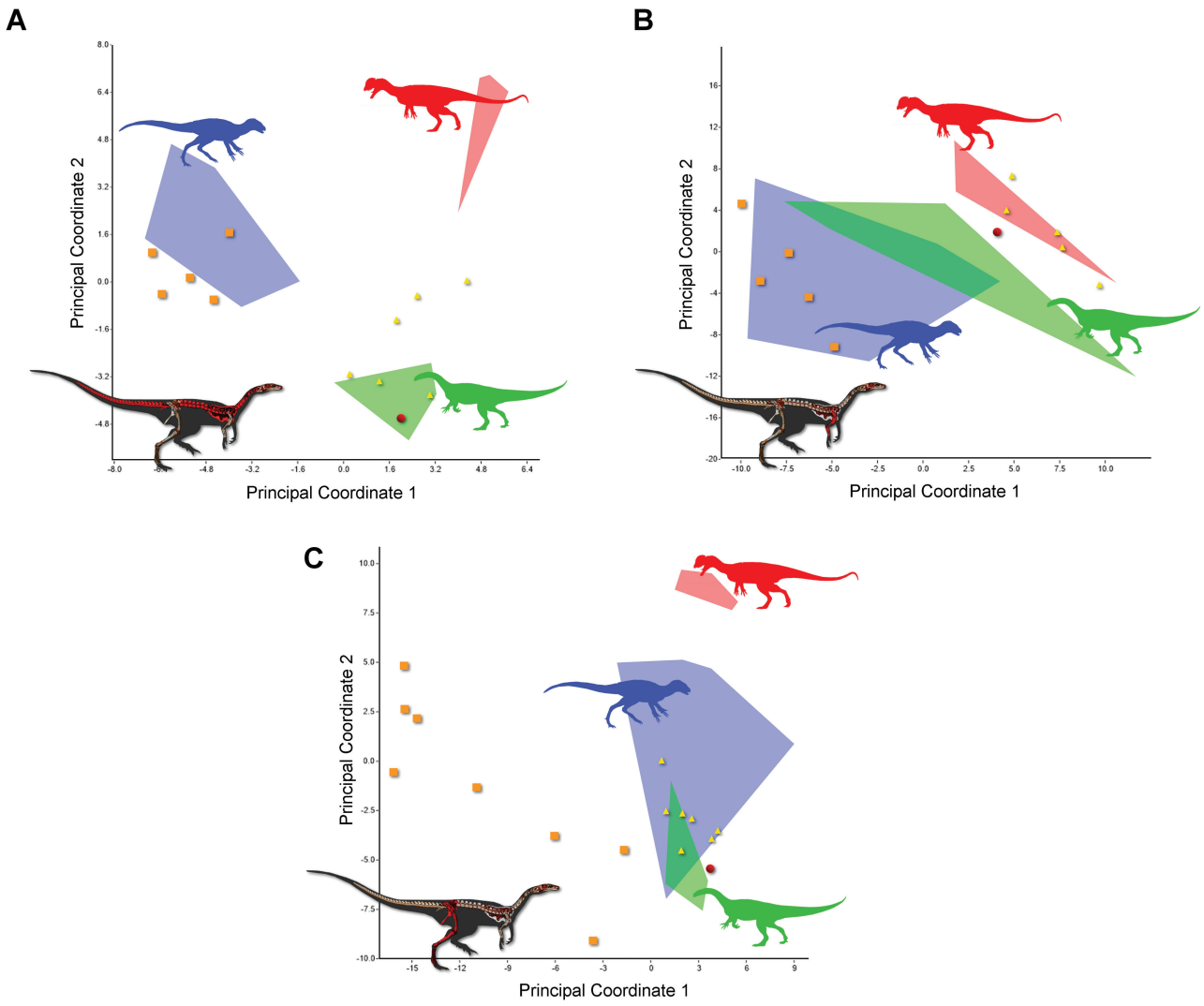

Figure 42. Bivariate plots showing the results of the morphospace occupation analysis. A, using axial characters. B, using pectoral and forelimb characters. C, using pelvic and hindlimb characters. Green convex hull corresponds to morphospace of sauropodomorphs, blue convex hull corresponds to morphospace of ornithischians, and red convex hull corresponds to morphospace of theropods. Squares correspond to non-dinosaur archosaurs, triangles correspond to basal saurischians outside the theropod–sauropodomorph dichotomy, and the red dot corresponds to *Buriolestes schultzi*.

and sauropodomorphs is found. However, *B. schultzi* lies outside any of the convex hulls of the three main groups. *Buriolestes schultzi* also lies outside the different morphospace areas of sauropodomorphs and ornithischians in the PCoA of pelvic girdle and hindlimb (Fig. 42C) but is close to both areas.

DISCUSSION

BURIOLESTES SCHULTZI INCLUSIVITY AND DISTINCTION FROM COEVAL SAUROPODOMORPHS

Sauropodomorphs are significantly less numerous in Carnian strata when compared with other vertebrates (Martínez *et al.*, 2011). The group was, however, apparently taxonomically diverse, with at least six coeval species in Argentina and Brazil (Sereno *et al.*, 1993; Langer *et al.*, 1999; Martínez & Alcober, 2009; Ezcurra, 2010; Cabreira *et al.*, 2011, 2016). Therefore, the assignation of CAPPA/UFSM 0035 to *B. schultzi* should not rely solely upon topotypic principles. Indeed, even the sister-group relationship between the new specimen and the holotype of *B. schultzi* brings ambiguous evidence regarding its taxonomic affinity, because a close phylogenetic affinity does not necessarily indicate alpha taxonomy inferences. Cabreira *et al.* (2016) proposed that the caudal projection of the medial condyle of the tibia, medial to the intercondylar notch,

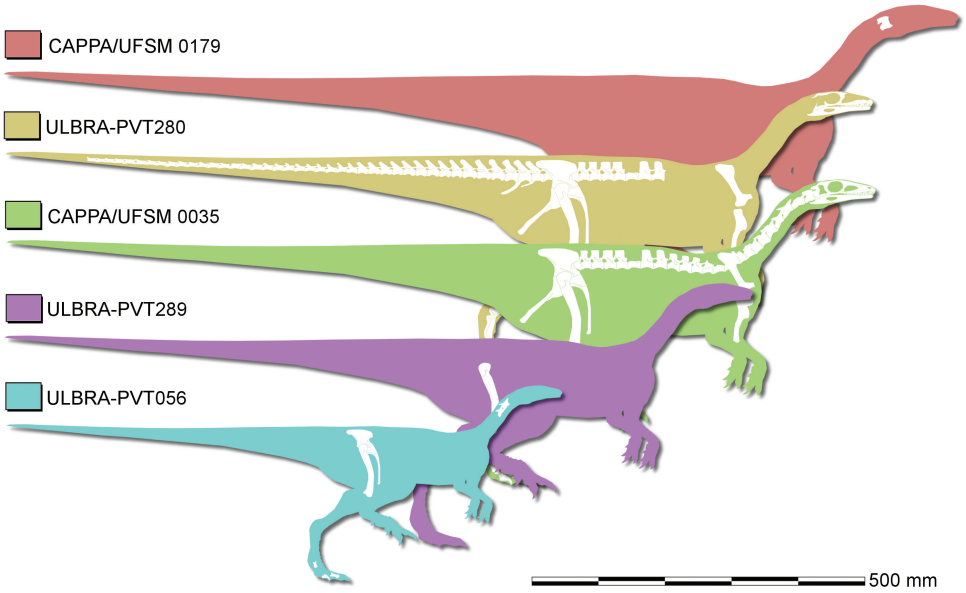

Figure 43. Specimens ascribed to Dinosauria from the Buriol outcrop.

is an autapomorphic trace of *B. schultzi*, but CAPPA/UFSM 0035 unfortunately does not have that part of the tibia preserved. Nonetheless, several skeletal parts preserved in both ULBRA-PVT280 and CAPPA/UFSM 0035 are similar and, together, they reveal a unique combination of features among coeval sauropodomorph taxa. These include the following: (1) a skull very slightly shorter than the femur; (2) short caudodorsal process of premaxilla; (3) lack of promaxillary fossa on the medial maxillary wall; (4) marked subnarial gap; (5) forking part of the caudal process of the jugal projected from a pedicel; (6) zyphodont dentition; (7) craniocaudally short, raised rugose process on the dorsocaudal margin of the iliac blade; (8) marked protuberance between the craniomedial crest and the dorsolateral trochanter of the femur; and (9) ovoid striated tuberosity on the craniomedial margin of the proximal third of the fibula.

In addition to CAPPA/UFSM 0035, there are at least three other dinosaur specimens (Fig. 43) excavated from the same layer/site that yielded the holotype of *B. schultzi*. ULBRA-PVT289 corresponds to an isolated right femur ~118 mm in length. Its morphology matches those of the femora of CAPPA/UFSM 0035 and ULBRA-PVT280, including the presence of a marked protuberance between the craniomedial crest and the dorsolateral trochanter of the femur. ULBRA-PVT056 includes two cervical vertebrae, ilium, proximal portion of the pubis, and femur from the right side, plus some phalanges. This individual is the smallest known dinosaur specimen from the site, with an 89-mm-long femur. Indeed, it lacks several muscle attachment structures that are present in the femora of both ULBRA-PVT280 and CAPPA/UFSM 0035, suggesting that it represents a less mature individual than the others. CAPPA/UFSM 0179 corresponds to an isolated axis (Müller *et al.*, 2017). Its morphology resembles that of CAPPA/UFSM 0035, but it is 12% larger, corresponding to the largest dinosaur from the Buriol outcrop. The attribution of these three additional specimens to *B. schultzi* is uncertain, but plausible for topotypic reasons. In paleoecological terms, if all specimens correspond to *B. schultzi*, this taxon was relatively abundant in comparison to other taxa from the Buriol outcrop and surrounding localities, such as *Polesinesuchus aurelioi* and *Prozostrodon brasiliensis*, which are recorded in the area based on a single specimen each (Roberto-da-Silva *et al.*, 2014; Pacheco *et al.*, 2017). On the contrary, *Hyperodapedon* sp. is widely sampled.

Corroborating its affinity to *B. schultzi*, it is possible to differentiate CAPPA/UFSM 0035 from all the other coeval sauropodomorphs as discussed below. Compared with *E. lunensis* (Sereno *et al.*, 1993; PVSJ 512, 559, 745, 852, 855, 860, 862, 876), the preorbital region of CAPPA/UFSM 0035 is longer than that of PVSJ 512. The rostral process of the maxilla of PVSJ 512 tapers rostrally to form a triangular portion, whereas the rostral margin of the maxilla of CAPPA/UFSM 0035 is delimited by a concavity. CAPPA/UFSM 0035 possesses more maxillary teeth than PVSJ 512. The rostroventral process of the nasal overlaps the caudodorsal process of the premaxilla in CAPPA/UFSM 0035, whereas the inverse condition occurs in PVSJ 512. Unlike that specimen, CAPPA/UFSM 0035 lacks a ventral notch on the caudalmost portion of the

quadratojugal. CAPPA/UFSM 0035 bears a parasagittal tooth row on the pterygoid, but lacks the diagonal row seen in PVSJ 512 (Sereno *et al.*, 2013). A mylohyoid foramen is absent in the splenial of PVSJ 512 (Sereno *et al.*, 2013) but present in CAPPA/UFSM 0035. On the lateral surface of the surangular, CAPPA/UFSM 0035 has a longitudinal ridge that is absent in PVSJ 512. Unlike PVSJ 512, CAPPA/UFSM 0035 lacks an accessory articular process on the medial side of the base of the prezygapophysis of the fifth and sixth cervical vertebrae. The coracoid foramen is slightly more ventrally located in CAPPA/UFSM 0035 than in PVSJ 512. The articular surface of the pubic penducle of the ilium is triangular in PVSJ 512 (Sereno *et al.*, 2013) but subovoid in CAPPA/UFSM 0035.

CAPPA/UFSM 0035 also differs from *S. tupiniquim* (Langer *et al.*, 1999; MCP 3844-PV, 3845-PV, 3846-PV). The ridge between the slot for the postorbital and the supratemporal fossa in the frontal of MCP 3845-PV is more slender than in CAPPA/UFSM 0035. The humerus of CAPPA/UFSM 0035 lacks the ligament ridge that is present on the caudolateral surface of the proximal portion of the humerus of MCP 3844-PV (Langer *et al.*, 2007). The craniodorsal corner of the ischium of MCP 3844-PV is fairly expanded, embracing the caudal surface of the ischiatic peduncle of the ilium. In CAPPA/UFSM 0035, this portion is less developed, so the contact occurs with only the ventral surface of the ischiatic peduncle. Another difference in the ischium is the lateral extension of the acetabular margin, which is more developed in MCP 3844-PV than in CAPPA/UFSM 0035. The scar on the craniolateral surface of the distal portion of the femur of MCP 3844-PV is circular, but forms an inverted U in CAPPA/UFSM 0035. Unlike CAPPA/UFSM 0035, MCP 3844-PV lacks a circular bone protuberance between the craniomedial crest and the dorsolateral trochanter. The dorsalmost extension of the tibia occurs in the centre of the proximal surface in MCP 3844-PV, whereas in CAPPA/UFSM 0035 this is located on the proximal portion of the cnemial crest.

As for *P. protos* (Martínez & Alcober, 2009; PVSJ 874), its prefrontal lacks a bony sheet between the rostral and ventral processes (Cabreira *et al.*, 2011), seen in CAPPA/UFSM 0035. The slot for articulation with the postorbital of the frontal is straight in PVSJ 874 and sinuous in CAPPA/UFSM 0035. The longitudinal ridge on the dorsal surface of the parietal is more marked in PVSJ 874, whereas the nuchal crest of the occipital is broader in CAPPA/UFSM 0035. The articular region that receives the medial condyle of the quadrate projects more dorsally in PVSJ 874. Unlike PVSJ 874, CAPPA/UFSM 0035 lacks an oval scar on the lateral surface of the centra of the cervical vertebrae. The scapular blade of PVSJ 874 is craniocaudally broader than that of CAPPA/UFSM 0035. The iliac peduncle of the ischium is slightly wider in PVSJ 874.

Chromogisaurus novasi (Ezcurra, 2010; Martínez, Apaldetti & Abelin, 2013; PVSJ 845) has the glenoid lip of the scapula less laterally expanded than in CAPPA/UFSM 0035. In addition, the fossa on the caudal surface of the scapular blade of PVSJ 845 almost reaches the glenoid rim on the scapular body, whereas in CAPPA/UFSM 0035 an equivalent sulcus merges with the scapular blade and disappears distant from the dorsal margin of the glenoid rim. The dorsoventral height of the iliac acetabulum is proportionally larger in PVSJ 845 than in CAPPA/UFSM 0035, and the dorsocaudal margin of the iliac blade bears a raised rugose process along its entire length that expands caudally. In CAPPA/UFSM 0035, the homologous surface is marked by striations and bears a raised process only at the caudalmost portion of the postacetabular ala. The femora of PVSJ 845 possess a lateral fossa (Ezcurra, 2010) that is absent in CAPPA/UFSM 0035, but the PVSJ 845 condition might be related to preservational biases (Martínez *et al.*, 2013). Likewise, the proximal articular surface of the tibia of PVSJ 845 has a deep concavity that, according to Martínez *et al.* (2013), has been exaggerated by sedimentary compression. On the contrary, the same surface of CAPPA/UFSM 0035 is convex to smooth. Also, unlike CAPPA/UFSM 0035, PVSJ 845 lacks the ovoid tuberosity on the craniomedial margin of the proximal third of the fibula.

CAPPA/UFSM 0035 also differs from *P. barberenai* (Cabreira *et al.*, 2011; Müller *et al.*, 2016; ULBRA-PVT016; CAPPA/UFSM 0027). The alveoli from the rostral portion of the maxilla are concave in lateral view in ULBRA-PVT016 but straight in CAPPA/UFSM 0027. The medial wall of the antorbital fossa of the maxilla projects more caudally in CAPPA/UFSM 0035 than in ULBRA-PVT016. Unlike CAPPA/UFSM 0035, the dentary of ULBRA-PVT016 lacks a rostralmost edentulous surface. According to Cabreira *et al.* (2011), the prefrontal of ULBRA-PVT016 lacks a sheet of bone covering the lacrimal. This differs from the condition of CAPPA/UFSM 0035, in which the prefrontal covers part of the caudolateral surface of the lacrimal. The caudal process of the postorbital of CAPPA/UFSM 0035 is proportionally longer and slender. In CAPPA/UFSM 0035, the bifurcation of the caudal process of the jugal does not occur as rostrally as in ULBRA-PVT016. The scapular blade of ULBRA-PVT016 is slightly more caudally oriented in comparison to CAPPA/UFSM 0035. The sulcus for the ligamentum capitis femoris is narrower in ULBRA-PVT016. The crista tibiofibularis of the femur of CAPPA/UFSM 0035 is transversely wider than in ULBRA-PVT016 and CAPPA/UFSM 0027. Unlike CAPPA/UFSM 0027, the craniolateral surface of the distal portion of the femur of CAPPA/UFSM 0035 lacks an ovoid depression.

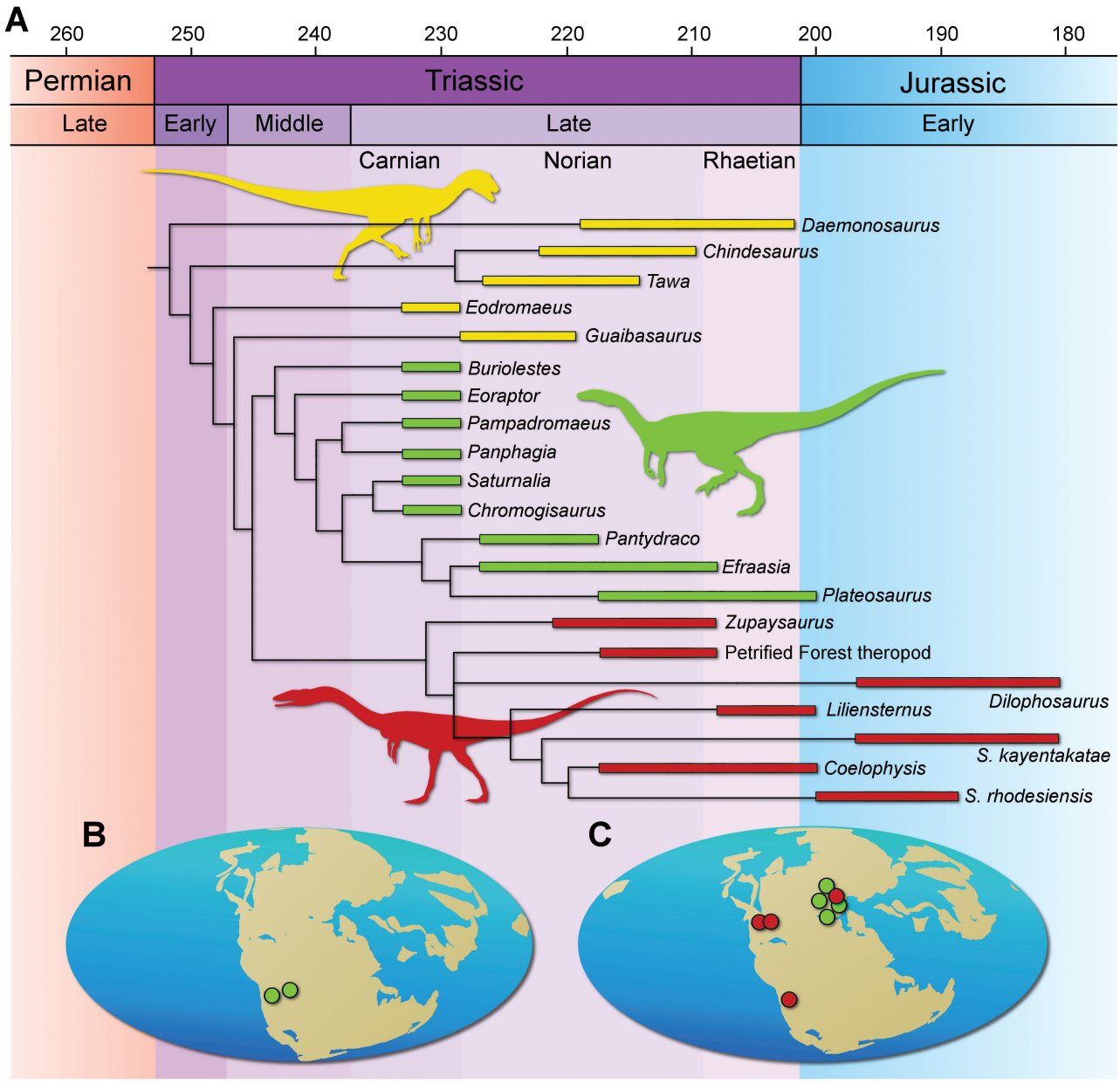

Figure 44. Reduced strict consensus tree of the third phylogenetic analysis within geographical distribution of the major groups. A, time-calibrated phylogeny. B, geographical distribution of theropods (red dot) and sauropodomorphs (green dot) of the analysis along the Carnian. C, geographical distribution of post-Carnian theropods (red dot) and sauropodomorphs (green dot) of the analysis.

THE FIRST STEPS FROM DISTINCT POINTS OF VIEW

The differences seen in the strict consensus topologies of the analyses indicate that the phylogeny of early dinosaurs can be affected by the choice of different weighting schemes and taxon samples. Discussions regarding the usefulness of implied weighting over unweighted analyses are still ongoing (Congreve & Lamsdel, 2016), and our discussion here attempts only to evaluate alternative evolutionary scenarios, rather than to provide additional arguments for one or other scheme.

In the first scenario (i.e. based on the results from the third analysis), the Carnian sauropodomorphs are arranged in low-diversity groups along the stem leading to latter sauropodomorphs (Fig. 44). In this scheme, the anatomical features characterizing sauropodomorphs as a whole are not related to the dentition, suggesting that herbivorous feeding habits were not

the main drive in the origin of the group. In this scenario, the acquisition of a dental morphology related to herbivore/omnivore diets occurred in a second step, as seen in forms nested in the clade including *E. lunensis* and other sauropodomorphs, but not *B. schultzi*. These have maxillary and dentary tooth crowns that are labiolingually expanded in distal/medial view and have fewer denticles per millimetre, contrasting with the blade-like morphology present in faunivorous forms, such as *T. hallae*, *Coelophysis bauri* and *B. schultzi*. In the sister clade to *E. lunensis*, the distal margin of the maxillary/dentary tooth crowns is markedly expanded at the base, as in typically herbivorous forms, such as *P. mertii*, *S. opolensis* and *Unaysaurus tolentinoi*. Finally, the clade including *P. caducus*, *Efraasia minor* and *Plateosaurus engerlhardi* acquires maxillary/dentary teeth with large serrations forming oblique angles with the margin of the teeth. In sum, this first scenario

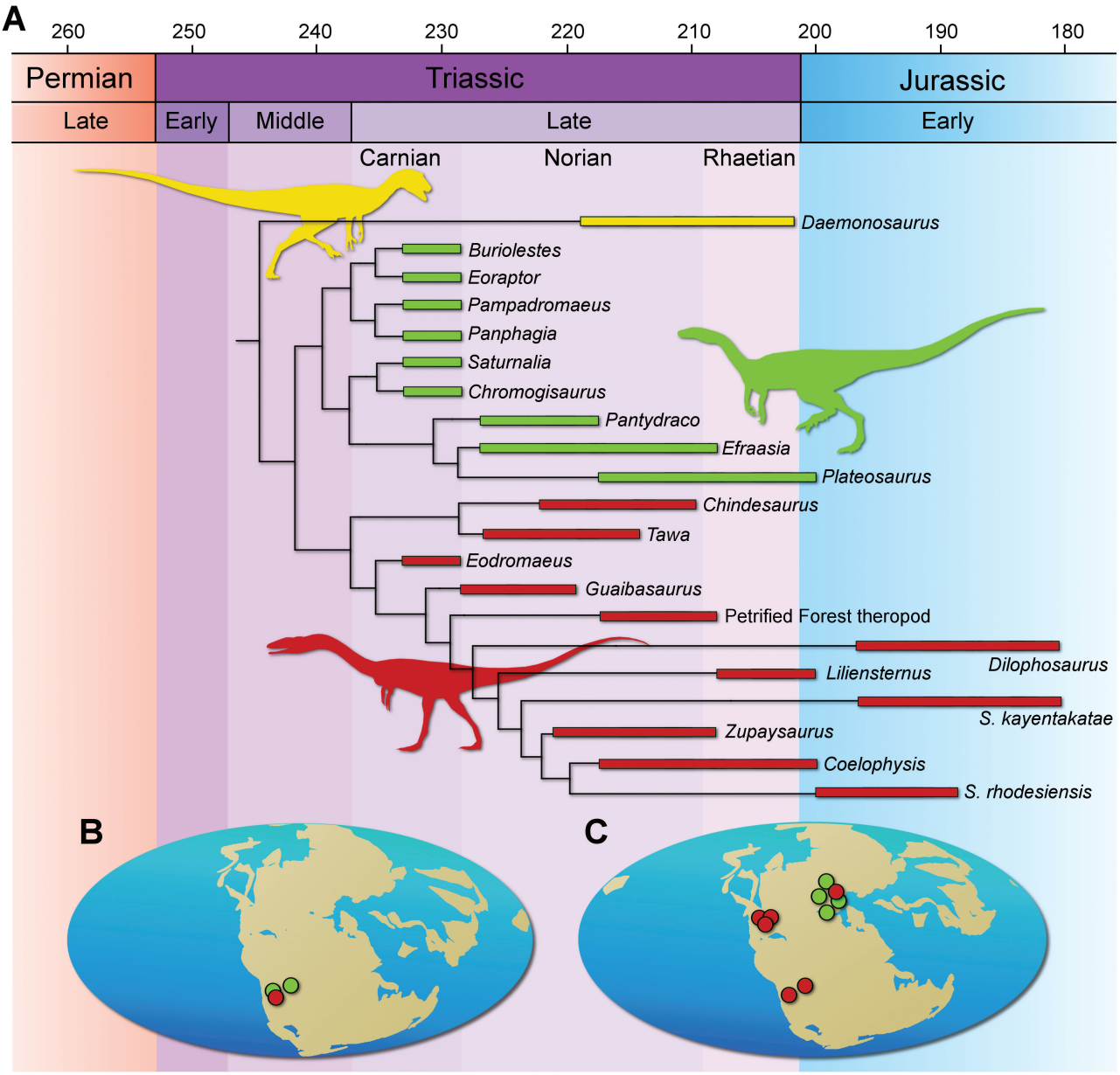

Figure 45. Reduced strict consensus tree of the fourth phylogenetic analysis (using implied character weighting with $k = 3$) within geographical distribution of the major groups. A, time-calibrated phylogeny. B, geographical distribution of theropods (red dot) and sauropodomorphs (green dot) of the analysis along the Carnian. C, geographical distribution of post-Carnian theropods (red dot) and sauropodomorphs (green dot) of the analysis.

indicates that faunivory was the ancestral condition for Sauropodomorpha (Cabreira *et al.*, 2016) and that taxa such as *E. lunensis*, *Pampadromaeus barbarenai* and *S. tupiniquim* represent the first steps of a stepwise acquisition of traits related to a more herbivorous diet. As such, the high diversity of Carnian sauropodomorphs might be related to the adoption of slightly different feeding strategies (also true for the next scenario).

In the alternative scenario, based on the analysis with implied weighting, the sauropodomorphs *B. schultzi*, *E. lunensis*, *P. barberenai* and *P. protos* form a clade (Fig. 45). Indeed, early South American sauropodomorphs share a particular set of traits, so the recovery of a clade including some of these forms is not unexpected. Although weakly supported, this arrangement leads to distinct interpretations regarding character evolution. For instance, some features related to herbivorous/omnivorous feeding habits, such as the reduction in the number of serrations per millimetre in middle maxillay/dentary teeth, are reconstructed for the node including all sauropodomorphs, and reverted to the plesiomorphic condition in *B. schultzi*. Overall, in this scenario, dentition plays an important role in the initial evolution of the group. However, most character states that support the Carnian sauropodomorph clade are ambiguous, because their condition in *S. tupiniquim* and *C. novasi* is unknown. One exception is character 217, related to the apomorphic absence of a caudal groove on the astragalus of *P. protos*, *E. lunensis* and *B. schultzi*, which is present in *S. tupiniquim* and *Plateosaurus engelhardti*. Besides, although the set of character states that supports Sauropodomorpha is slightly distinct from that of the previous analysis, some features, such as the ventrally inclined dorsal surface of the rostral tip of the dentary, still characterize the group. Also synapomorphic for Sauropodomorpha, a low mandibular articulation occurs convergently in Ornithischians. Finally, another outcome of the implied weighting analysis is the reinterpretation of *T. hallae*, *C. briansmalli*, *E. murphi* and *G. candelariensis* as theropods.

The scenario derived from the analysis using the data matrix by Baron *et al.* (2017a) modified by Langer *et al.* (2017) differs from that based on the analysis with implied weighting because a more inclusive clade of sauropodomorphs from the Carnian of South America was recovered. Nevertheless, it supports the existence of this clade, in contrast with the first three analyses. In that hypothesis, *S. tupiniquim* is recovered within the group, as the sister taxon to *P. barberenai* (Fig. 40), based on the sharing of the first dentary tooth inserted in the extreme rostral end of the dentary [(0)149] and the slightly concave dorsal margin of the ilium in lateral view [(1)301]. The clade composed by Carnian forms lacks synapomorphies related to a herbivorous diet, whereas the clade supporting *P. caducus* plus other sauropodomorphs is supported by several characters related to a herbivorous feeding behaviour: crown of the premaxillary teeth is at least moderately expanded above root [(1)152]; large and coarse denticles on maxillary and dentary teeth [(2)169]; majority of maxillary and dentary teeth weakly recurved [(1)174]; and caudal cutting edge of the caudal maxillary teeth convex [(1)175]. The placement of *E. murphi* as a saurischian basal to the Theropoda–Sauropodomorpha dichotomy implies, in the absence of theropods in the Carnian, agreement with the first scenario discussed here.

Regardless of the parameters applied in the phylogenetic analysis, *B. schultzi* is consistently nested within Sauropodomorpha, reinforcing the taxonomic assignation of Cabreira *et al.* (2016). Yet, and perhaps even more interesting, none of the disparity morphological analyses places *B. schultzi* in an area occupied by theropods, suggesting that its skeleton does not comprise a marked mosaic of theropod and sauropodomorph traits, but instead a combination of sauropodomorph and common saurischian traits. Our partitioned data matrix with characters from the axial skeleton also reveals well-delimited groups in the morphological disparity analysis. In contrast, other portions of the skeleton are generally less delimited, as indicated by the overlapped morphospace of the groups. These results suggest that axial traits played a relevant role in the evolution of the first dinosaurs. Indeed, sauropodomorphs are known for their peculiar axial skeleton, which in later members developed to conciliate feeding behaviours and their extremely large bodies (Wedel, 2003; Fronimos & Wilson, 2017; Ibiricu *et al.*, 2017). The neural arches of the sauropodomorphs' neck vertebrae become tall, a feature already observed in the new specimen of *B. schultzi*. This condition, associated with the absence of pleurocoels, results in a unique morphology for the early members of the group, as already reported in the literature (e.g. Martínez, 2009; Apaldetti *et al.*, 2011; Wang, You & Wang, 2017). The increase in neck length typical of later sauropodomorphs has, however, not yet taken place in *B. schultzi* and other Carnian members of the group (e.g. *P. protos*).

CONCLUSIONS

The anatomy of the new specimen described here is consistent with that of *B. schultzi*, sharing with its holotype a unique combination of traits among coeval taxa. In addition, there is no significant difference in the repeated elements of both specimens. Accordingly,

we identify CAPPA/UFSM 0035 as a second individual of *B. schultzi*, substantially expanding our knowledge of the anatomy of this dinosaur. As such, *B. schultzi* is now as complete as the best-known early dinosaurs, such as *E. lunensis* and *H. ischigualastensis*.

The phylogenetic analyses performed fully support *B. schultzi* as a member of Sauropodomorpha, corroborating previous assignations. In fact, the morphological disparity analyses failed to find any indication of convergences with Theropoda in its skeletal parts. Indeed, such analyses demonstrate that the main dinosaur groups (Ornithischia, Sauropodomorpha, Theropoda) overlap in morphospace occupation for most skeletal parts, with a clear exception being the axial skeleton. We also propose an alternative evolutionary scenario for the first members of Sauropodomorpha, where some Carnian South American taxa are nested in a monophyletic group, rather than being arranged in low-diversity groups on the stem leading to later sauropodomorphs.

ACKNOWLEDGEMENTS

We are grateful to the Buriol family for allowing access to their property to excavate the specimen described herein. Reviews and comments by the Associate Editor, Matthew G. Baron, and an anonymous reviewer greatly improved the manuscript. We also extend our gratitude to Agustin G. Martinelli, Átila A. S. da Rosa, Jonathas S. Bittencourt and Flávio A. Pretto for comments and suggestions that also improved the quality of this manuscript. The authors thank Matthew Wills (University of Bath) for the software MATRIX. We also thank the Coordenação de Aperfeiçoamento de Pessoal de Nivel Superior (CAPES) for the scholarship to R.T.M. and C.P.P.; the Conselho Nacional de Desenvolvimento Científico e Tecnológico (CNPq) for the research grants to S.D.S. (process 306352/2016–8) and M.B. (Science Without Borders, process: 246610/2012–3); and Fundação de Amparo à Pesquisado Estado de São Paulo (FAPESP) for the grant to M.C.L. (number 2014/03825-3). We thank the Willi Henning Society for the gratuity of TNT software.

REFERENCES

Agnolín FL, Rozadilla S. 2017. Phylogenetic reassessment of *Pisanosaurus mertii* Casamiquela, 1967, a basal dinosauriform from the Late Triassic of Argentina. *Journal of Systematic Palaeontology*: 1–27. doi:10.1080/14772019.2017.1352623

Alcober OA, Martínez RN. 2010. A new herrerasaurid (Dinosauria, Saurischia) from the Upper Triassic Ischigualasto Formation of northwestern Argentina. *ZooKeys* **63:** 55–81.

Apaldetti C, Martinez RN, Alcober OA, Pol D. 2011. A new basal sauropodomorph (Dinosauria: Saurischia) from Quebrada del Barro Formation (Marayes-El Carrizal Basin), northwestern Argentina. *PLoS ONE* **6:** e26964.

Baron MG, Norman DB, Barrett PM. 2017a. A new hypothesis of dinosaur relationships and early dinosaur evolution. *Nature* **543:** 501–506.

Baron MG, Norman DB, Barrett PM. 2017b. Baron *et al*. reply. *Nature* **551:** E4–E5.

Bittencourt J, Kellner AWA. 2009. The anatomy and phylogenetic position of the Triassic dinosaur *Staurikosaurus pricei* Colbert, 1970. *Zootaxa* **2079:** 1–56.

Bouxin G. 2005. Ginkgo, a multivariate analysis package. *Journal of Vegetation Science* **16:** 355–359.

Bronzati M, Rauhut OWM. 2017. Braincase redescription of *Efraasia minor* (Huene, 1908) (Dinosauria, Sauropodomorpha) from the Late Triassic of Germany, with comments on the evolution of the sauropodomorph braincase. *Zoological Journal of the Linnean Society* **182:** 173–224.

Burch SH. 2014. Complete forelimb myology of the basal theropod dinosaur *Tawa hallae* based on a novel robust muscle reconstruction method. *Journal of Anatomy* **225:** 271–297.

Butler RJ, Brusatte SL, Andres B, Benson RB. 2012. How do geological sampling biases affect studies of morphological evolution in deep time? A case study of pterosaur (Reptilia: Archosauria) disparity. *Evolution; International Journal of Organic Evolution* **66:** 147–162.

Button DJ, Barrett PM, Rayfield EJ. 2016. Comparative cranial myology and biomechanics of *Plateosaurus* and *Camarasaurus* and evolution of the sauropod feeding apparatus. *Palaeontology* **59:** 887–913.

Cabreira SF, Kellner AWA, Dias-da-Silva S, Roberto da Silva L, Bronzati M, Marsola JCA, Müller RT, Bittencourt JS, Batista BJ, Raugust T, Carrilho R, Brodt A, Langer MC. 2016. A unique late Triassic dinosauromorph assemblage reveals dinosaur ancestral anatomy and diet. *Current Biology: CB* **26:** 3090–3095.

Cabreira SF, Schultz CL, Bittencourt JS, Soares MB, Fortier DC, Silva LR, Langer MC. 2011. New stem-sauropodomorph (Dinosauria, Saurischia) from the Triassic of Brazil. *Die Naturwissenschaften* **98:** 1035–1040.

Casamiquela RM. 1967. Un nuevo dinosaurio ornitischio Triásico (*Pisanosaurus mertii*; Ornithopoda) de la Formación Ischigualasto, Argentina. *Ameghiniana* **4:** 47–64.

Colbert EH. 1970. A saurischian dinosaur from the Triassic of Brazil. *American Museum Novitates* **2405:** 1–39.

Congreve CR, Lamsdel JC. 2016. Implied weighting and its utility in palaeontological datasets: a study using modelled phylogenetic matrices. *Palaeontology* **59:** 447–462.

Dias-da-Silva S, Cabreira SF, Roberto-da-Silva L. 2011. Occurrence of giant stereospondyl remains in the Santa Maria Formation (Middle/Upper Triassic of southern Brazil). *Alcheringa* **35:** 11–19.

Dias-da-Silva S, Sengupta DP, Cabreira SF, Roberto-da-Silva L. 2012. The presence of *Compsocerops* (Brachyopoidea: Chigutisauridae) (Late Triassic) in southern Brazil with comments on chigutisaurid palaeobiogeography. *Palaeontology* **55:** 163–172.

Dilkes DW, Hutchinson JR, Holliday CM, Witmer LM. 2012. Reconstructing the musculature of dinosaurs. In: Brett-Surman MK, Holtz TR, Farlow JO, eds. *The complete dinosaur*. Bloomington: Indiana University Press, 151–190.

Ezcurra MD. 2006. A review of the systematic position of the dinosauriform archosaur *Eucoelophysis baldwini* Sullivan & Lucas, 1999 from the Upper Triassic of New Mexico, USA. *Geodiversitas* **28:** 649–684.

Ezcurra MD. 2010. A new early dinosaur (Saurischia: Sauropodomorpha) from the Late Triassic of Argentina: a reassessment of dinosaur origin and phylogeny. *Journal of Systematic Palaeontology* **8:** 371–425.

Fronimos JA, Wilson JA. 2017. Neurocentral suture complexity and stress distribution in the vertebral column of a sauropod dinosaur. *Ameghiniana* **54:** 36–49.

Goloboff PA, Carpenter JM, Arias JS, Esquivel DRM. 2008. Weighting against homoplasy improves phylogenetic analysis of morphological data sets. *Cladistics* **24:** 758–773.

Goloboff PA, Farris JS, Källersjö M, Oxelman B, Szumik CA. 2003. Improvements to resampling measures of group support. *Cladistics* **19:** 324–332.

Goloboff PA, Farris JS, Nixon KC. 2008. TNT, a free program for phylogenetic analysis. *Cladistics* **24:** 774–786.

Gradstein F, Ogg J, Schmitz M, Ogg G. 2012. *The geological time scale 2012*. Amsterdam: Elsevier.

Griffin CT, Nesbitt SJ. 2016. The femoral ontogeny and long bone histology of the Middle Triassic (? late Anisian) dinosauriform *Asilisaurus kongwe* and implications for the growth of early dinosaurs. *Journal of Vertebrate Paleontology* **36:** e1111224.

Grillo ON, Azevedo SA. 2011. Pelvic and hind limb musculature of *Staurikosaurus pricei* (Dinosauria: Saurischia). *Anais da Academia Brasileira de Ciencias* **83:** 73–98.

Hammer Ø, Haper DAT, Ryan PD. 2001. PAST: paleontological statistics software package for education and data analysis. *Palaeontologica Electronica* **4:** 1–9.

Horn BLD, Melo TM, Schultz CL, Philipp RP, Kloss HP, Goldberg K. 2014. A new third-order sequence stratigraphic framework applied to the Triassic of the Paraná Basin, Rio Grande do Sul, Brazil, based on structural, stratigraphic and paleontological data. *Journal of South American Earth Sciences* **55:** 123–132.

Huene F. 1932. Die fossile Reptil-Ordnung Saurischia, ihre Entwicklung und Geschichte. *Monographien zur Geologie und Paläontologie* **4:** 1–361.

Ibiricu LM, Lamanna MC, Martínez RD, Casal GA, Cerda IA, Martínez G, Salgado L. 2017. A novel form of postcranial skeletal pneumaticity in a sauropod dinosaur: implications for the paleobiology of Rebbachisauridae. *Acta Palaeontologica Polonica* **62:** 221–236.

Irmis RB, Nesbitt SJ, Padian K, Smith ND, Turner AH, Woody D, Downs A. 2007. A Late Triassic dinosauromorph assemblage from New Mexico and the rise of dinosaurs. *Science (New York, N.Y.)* **317:** 358–361.

Langer MC. 2003. The pelvic and hind limb anatomy of the stem-sauropodomorph *Saturnalia tupiniquim* (Late Triassic, Brazil). *PaleoBios* **23:** 1–30.

Langer MC. 2014. The origins of Dinosauria: much ado about nothing. *Palaeontology* **57:** 469–478.

Langer MC, Abdala F, Richter M, Benton MJ. 1999. A sauropodomorph dinosaur from the Upper Triassic (Carnian) of Southern Brazil. *Comptes Rendus de l'Académie des Sciences-Series IIA-Earth and Planetary Science* **329:** 511–517.

Langer MC, Ezcurra MD, Rauhut OWM, Benton MJ, Knoll F, McPhee BW, Novas FE, Pol D, Brusatte SL. 2017. Untangling the dinosaur family tree. *Nature* **551:** E1–E3.

Langer MC, Ferigolo J. 2013. The late Triassic dinosauromorph *Sacisaurus agudoensis* (Caturrita Formation: Rio Grande do Sul, Brazil): anatomy and affinities. *Geological Society, London, Special Publications* **379:** 353–392.

Langer MC, França MA, Gabriel S. 2007. The pectoral girdle and forelimb anatomy of the stem-sauropodomorph *Saturnalia tupiniquim* (Upper Triassic, Brazil). *Special Papers in Palaeontology* **77:** 113–137.

Legg DA, Sutton MD, Edgecombe GD. 2013. Arthropod fossil data increase congruence of morphological and molecular phylogenies. *Nature Communications* **4:** 2485.

Marsicano CA, Irmis RB, Mancuso AC, Mundil R, Chemale F. 2016. The precise temporal calibration of dinosaur origins. *Proceedings of the National Academy of Sciences of the United States of America* **113:** 509–513.

Martínez RN. 2009. *Adeopapposaurus mognai*, gen. et sp. nov. (Dinosauria: Sauropodomorpha), with comments on adaptations of basal Sauropodomorpha. *Journal of Vertebrate Paleontology* **29:** 142–164.

Martinez RN, Alcober OA. 2009. A basal sauropodomorph (Dinosauria: Saurischia) from the Ischigualasto Formation (Triassic, Carnian) and the early evolution of Sauropodomorpha. *PLoS ONE* **4:** e4397.

Martínez RN, Apaldetti C, Abelin D. 2013. Basal sauropodomorphs from the Ischigualasto Formation. *Journal of Vertebrate Paleontology* **32:** 51–69.

Martínez RN, Apaldetti C, Correa GA, Abelín D. 2016. A Norian Lagerpetid Dinosauromorph from the Quebrada Del Barro Formation, Northwestern Argentina. *Ameghiniana* **53:** 1–13.

Martínez RN, Sereno PC, Alcober OA, Colombi CE, Renne PR, Montañez IP, Currie BS. 2011. A basal dinosaur from the dawn of the dinosaur era in southwestern Pangaea. *Science* **331:** 201–210.

Müller RT, Langer MC, Cabreira SF, Dias-da-Silva S. 2016. The femoral anatomy of *Pampadromaeus barberenai* based on a new specimen from the Upper Triassic of Brazil. *Historical Biology* **28:** 656–665.

Müller RT, Pretto FA, Stefanello M, Silva-Neves E, Dias-da-Silva S. 2017. On a dinosaur axis from one of the oldest dinosaur-bearing sites worldwide. *Acta Palaeontologica Polonica* **62:** 543–548.

Nesbitt SJ. 2011. The early evolution of archosaurs: relationships and the origin of major clades. *Bulletin of the American Museum of Natural History* **352:** 1–292.

Nesbitt SJ, Barrett PM, Werning S, Sidor CA, Charig AJ. 2012. The oldest dinosaur? A Middle Triassic dinosauriform from Tanzania. *Biology Letters* **9:** 20120949.

Nesbitt SJ, Butler RJ, Ezcurra MD, Barrett PM, Stocker MR, Angielczyk KD, Smith RMH, Sidor CA, Niedźwiedzki G, Sennikov AG, Charig AJ. 2017. The earliest bird-line archosaurs and the assembly of the dinosaur body plan. *Nature* **544:** 484–487.

Nesbitt SJ, Smith ND, Irmis RB, Turner AH, Downs A, Norell MA. 2009. A complete skeleton of a Late Triassic saurischian and the early evolution of dinosaurs. *Science (New York, N.Y.)* **326:** 1530–1533.

Novas FE. 1994. New information on the systematics and postcranial skeleton of *Herrerasaurus ischigualastensis* (Theropoda: Herrerasauridae) from the Ischigualasto Formation (Upper Triassic) of Argentina. *Journal of Vertebrate Paleontology* **13:** 400–423.

Novas FE, Salgado L, Suárez M, Agnolín FL, Ezcurra MD, Chimento NR, de la Cruz R, Isasi MP, Vargas AO, Rubilar-Rogers D. 2015. An enigmatic plant-eating theropod from the Late Jurassic period of Chile. *Nature* **522:** 331–334.

Owen R. 1842. Report on British fossil reptiles. Part II. *Reports of the British Association for the Advancement of Science* **11:** 60–204.

Pacheco CP, Martinelli AG, Pavanatto AE, Soares MB, Dias-da-Silva S. 2017. *Prozostrodon brasiliensis*, a probainognathian cynodont from the Late Triassic of Brazil: second record and improvements on its dental anatomy. *Historical Biology* 1–11. doi:10.1080/08912963.2017.1292423

Perez PA, Malabarba MCSL. 2002. A Triassic freshwater fish fauna from the Paraná Basin, in southern Brazil. *Revista Brasileira de Paleontologia* **4:** 33–54.

Piechowski R, Tałanda M, Dzik J. 2014. Skeletal variation and ontogeny of the Late Triassic dinosauriform *Silesaurus opolensis*. *Journal of Vertebrate Paleontology* **34:** 1383–1393.

Rauhut OWM. 2004. Braincase structure of the Middle Jurassic theropod dinosaur *Piatnitzkysaurus*. *Canadian Journal of Earth Sciences* **41:** 1109–1122.

Reig OA. 1963. La presencia de dinosaurios saurisquios en los "Estratos de Ischigualasto" (Mesotriásico Superior) de las provincias de San Juan y La Rioja (Republica Argentina). *Ameghiniana* **3:** 3–20.

Remes K. 2008. *Evolution of the pectoral girdle and forelimb in Sauropodomorpha (Dinosauria, Saurischia): osteology, myology and function*. Unpublished PhD Thesis, Fakultät für Geowissenschaften, Ludwig-Maximilians-Universität.

Richter M, Toledo CEV. 2008. The first Triassic lungfish from South America (Santa Maria Formation, Paraná Basin) and its bearing on geological correlations within Pangaea. *Geological Society, London, Special Publications* **295:** 43–54.

Roberto-Da-Silva L, Desojo JB, Cabriera SF, Aires AS, Müller RT, Pacheco CP, Dias-Da-Silva S. 2014. A new aetosaur from the Upper Triassic of the Santa Maria Formation, southern Brazil. *Zootaxa* **3764:** 240–278.

Sampson SD, Witmer LM. 2007. Craniofacial anatomy of *Majungasaurus crenatissimus* (Theropoda: Abelisauridae) from the Late Cretaceous of Madagascar. *Journal of Vertebrate Paleontology* **27:** 32–102.

Seeley HG. 1887. On the classification of the fossil animals commonly named Dinosauria. *Proceedings of the Royal Society of London* **43:** 165–171.

Sereno PC. 2012. Taxonomy, morphology, masticatory function and phylogeny of heterodontosaurid dinosaurs. *ZooKeys* **226:** 1–225.

Sereno PC, Forster CA, Rogers RR, Monetta AM. 1993. Primitive dinosaur skeleton from Argentina and the early evolution of the Dinosauria. *Nature* **361:** 64–66.

Sereno PC, Martínez RN, Alcober OA. 2013. Osteology of *Eoraptor lunensis* (Dinosauria, Sauropodomorpha). *Journal of Vertebrate Paleontology* **32:** 83–179.

Sereno PC, Novas FE. 1994. The skull and neck of the basal theropod *Herrerasaurus ischigualastensis*. *Journal of Vertebrate Paleontology* **13:** 451–476.

Snively E, Russell AP. 2007. Functional variation of neck muscles and their relation to feeding style in Tyrannosauridae and other large theropod dinosaurs. *Anatomical Record (Hoboken, N.J.: 2007)* **290:** 934–957.

Toledo CEV, Bertini RJ. 2005. Occurrences of the fossil Dipnoiformes in Brazil and its stratigraphic and chronological distributions. *Revista Brasileira de Paleontologia* **8:** 47–56.

Wang YM, You HL, Wang T. 2017. A new basal sauropodiform dinosaur from the Lower Jurassic of Yunnan Province, China. *Scientific Reports* **7:** 41881.

Wedel MJ. 2003. The evolution of vertebral pneumaticity in sauropod dinosaurs. *Journal of Vertebrate Paleontology* **23:** 344–357.

Will MA. 1998. Cambrian and recent disparity: the picture from priapulids. *Paleobiology* **24:** 177–199.

Witmer LM. 1997. Craniofacial air sinus systems. In: Currie PJ, Padian K, eds. *Encyclopedia of dinosaurs*. San Diego: Academic Press, 151–159.

Zerfass H, Lavina EL, Schultz CL, Garcia AJV, Faccini UF, Chemale F. 2003. Sequence stratigraphy of continental Triassic strata of Southernmost Brazil: a contribution to Southwestern Gondwana palaeogeography and palaeoclimate. *Sedimentary Geology* **161:** 85–105.

APPENDIX

FULL CODING TO CAPPA/UFSM 0035 IN THE FIRST PHYLOGENETIC ANALYSIS

0?21?11?00?100111?1101?11??01?11?101100100??0?1
0001?0011100?020 0000000?00?01011011111000001011101001001?01?????1???12??????????????????????????1
00111011001001?0???1?1???????11110210110011111
1?00001?0201?????????????????????????????????????0?
0??1111100111

FULL CODING TO *BURIOLESTES SCHULTZI* (ULBRA-PVT280 PLUS CAPPA/UFSM 0035) IN THE SECOND PHYLOGENETIC ANALYSIS

0?2101110011001111?1101?11010111101011001000?00
110001?0011100102000000000?0010101101111100000
1011101001001101000101?111120110????0???01?????
?????10011101100100l?0110111?11111111110210110

01111111?0000110201001001 1?10???110????0001 00?
??001111111010001111100111

DATA MATRIX PROCESSED IN THE THIRD AND FOURTH PHYLOGENETIC ANALYSES

Euparkeria capensis

00100?000000?0100000001000 00[01]?1011000000[01]
0000000000?0001000001000000000000000000010000
000?0100101000000000??0100000100000???0000010
0??0???0??0010000?00?0101000?00000000000001000
0000000000?000000[01]0000000000000000000?00?000
?0000000000000000000010?00010000?000000

Lagerpeton chanarensis

??
????????????????????????????????????1?000000000000??
????????????????????????????????????0001000?0000010000
?0000000000000000001000101000 10?0010010110000
010000100?[012]11100?0110100001100000101 0????0
20??????????

Dromomeron gregorii

??
??
??
????0000000?01010100?0010121010100000 0?000010?
??

Dromomeron romeri

??
??
??
?????000000010001010000?10121010110000010000 1
00?011100?011010????? ????????0?????????????????

Ixalerpeton polesinensis

0????????????????????????????????????1??11????0???
????????????????????????????????0?1??0010?0???01000
00000000???00????00000?????????????????????00
01001?00000?0?0???0?0?0000000000000010001010
00010?00200101101000100 00?????????????????????
??????????????0000001100???

Marasuchus lilloensis

????????????????????????????????????01?1?0?????????0???
????????0?000010?????01?0?00000000?0000010000000
000?000101000020000?????????????????????[01]0101[0
1]0?10000110000110110000111010001 0[01]10011001
10?0000110100000 0?0100001?0010001?00?00100110
00000110???0000???01000??

Saltopus elginenis

??
??000??????0?
10??10??00?10???????????0?1??0????0?????????0???000?
????01??1???????????1??1??????? ?????1?????????????????
????????00???????1?1???1?1?????????????????0??

Lewisuchus admixtus

????????0000101?????011?000?0100010111111???0????
???????????200000000????01001?1?000000?0?100?01???
?????????1011?002??0????????????????????????????????
??0110??10011
0?????????????????????????????1?000????101101??1

Pseudolagosuchus major

??
??
??10000?110
?????00000100?11??111110?????11?10???100?1?10?1?
0???????0????????????????????????????????

Asilisaurus kongwe

??01??
????????????00??111?0????0??0?1000000??1010101
0???10?????01?11?002?????????????????????????000
?00?101???1?00??1?1?1?11??111101?01110[01]111?1
01?0001?020000100010000 1?100001200000??????
?0?????0???10???????????

Diodorus scytobrachion

????????????????????????0????????????????????????????
???? ????10?0111?11????????????????????????????????
??????00??00??
????????101111?01[12]10?0111[01]0?10001??????????
????????????????????????????????????1?????????????

Eucoelophysis baldwini

??
??
??1001011111?
?????111101?01211011?001?0001??11000????????????
????????????????????1?1?????????????????????

Silesaurus opolensis

0?00000?0010000??0???101?110?0101001101111000?0
1010?0000010020011001111 00[01]?10001001100010
10101010101011100100[01]1111000000000?????????
??????????10002[01]0110100111001010111110 1[12
]111101210[01]01110011000100[12]11002000101011
0010?001100 010????1010010?10000102 1?100110?0

Sacisaurus agudoensis

????????0000101?????????0?????????????????????01?
????????????1101111101 1??????????????????????????
???????0??11??????????0?????????????????????000[12-
]0??101???1100??1?1?11????1[01][12]1111012100011
100?10001101110021101 01?????????????????????????
???????102???????????

Pisanosaurus mertii

?????????1?0????????????????????????????????????1?111
?0111???1?1111110????????0????010?????0??0????????
??0?
??????????2????????????????????0001?011010?0011?1
0?1?111?110?11011????1??1?1???0???1?????????????

Scutellosaurus lawleri
????0????1?0??1???????????0???0???????????????1?0?1?
10????2??120111101?????00??0??0?0??0?101000???1
0???0001?000011000?0?????00???????0?????01??????00
?????11?????1?01??11110002201310[01]0111110000
011020010211110100102 11?000001111?????????11
0?1???1???????????00

Lesothosaurus diagnosticus
000000001100001000001001 10000?00111010?00
000101110?0110011120012011111010010 10?00?0
100?0??001?????111?000????100010110001 0????00
00000??000?0000111111?000010?1100?111?01002
110200220130001101110000011020 01020?1101??1??
1???????1?1?0??0101001 1??000010101110 11?0?0

Eocursor parvus
0????????????????????????????????????01???0????????1?
1110011 0????201?1110???????????0?00?1??0??0??00
1?1?0?0????11???01??01?????????????????????????01002
2000000100?1???111?010?2?1110022013 1001111111?
000011020?102011101??1?????????????????1????????
0???1010???1111???

Heterodontosaurus tucki
000011001100121000001001110001?001?001100000
101111?1110111100012100101000110000000010000
00011?1001111?000?000110001120001110001110 01
1001100000011?22100000100110 0?111?101021?????
?2??30?0110111?0000110201???0?1????????1??????11?
?10000101101??1011010001110110001

Herrerasaurus ischigualastensis
0000101?000010000010001101000111000?00?0?000
0100100000100010100000000000?1001?01?111011?0
111?0010100011101110 1?1111[12]10101[01 2]101111
000010010211020102 0?1010001101011111112011 11
1102101100111011 1?000010021000100110101111101?
002 0000100110101011010000001011 0?????00

Staurikosaurus pricei
0??0010?00
??0?0????000000000?????00?011?010?0?01?00100100
1110111?????????????????????????????????1010120?101
000110111111111?1??1111102101[01]00?111?10?0000
110210001000101?????????????????????????????0???00
10??????????

Sanjuansaurus gordilloi
????????0000100?????????????????????????????????????
????100000000?????00?11??111011001110 0?1010101110
1??01111???????1?????????????????????????????????0?20
11111?????102102101100111 1?1000?000002000010001
?10?11101?00?01??10?????????????????0????????????

Panphagia protos
0?????????????1?0????????????????????????0????100010001
1100???[01]10000 10000??????0?11110000?1011?010????
110?01010?????????????????????????????????0021011 00??
11??000???0111111?????????????1???????????020000100
1101001111 1?00200????????0????????????1020?1??????1?

Eoraptor lunensis
0110111?001101111011011110001110 0100?????1000
10001?000010?101[01]100000000000???1??001100000
11111010100??1??0?000101212101 10??100010111100
0020101001210111 01?0110000111011[12]121???1??1
011??1?1?111?000011020100100110100111111?002000
0101110101011111 0111111111?????101

Pampadromaeus barberenai
002[12]11?100111[01]1??0?10101100 1?1????????????
?0???00000?0???0010201000010000000?????????????????
10111010??001?01?1?10??????0?100?????????????????
?100?2101??0???1?0 ???1?1???????11110[12]1011?0111
11111??00?10[12]0????0???????????????? ????????????
??????11?10101??????11

Buriolestes schultzi
0?2101110011001 11?1101?1101011110100100 10??00
110001?001110010200 000000?001010110111110000
0101110100100110100010 1?111201 10????0???01????
??????100111011001001?0110111?1111111111021011
001111111?00001102 010010011?10???110?????00010
0???001111111010001111100111101

Saturnalia tupiniquim
1?????????????????11?1?????????????010???0?????00?1?
??????????1100001000?????10?1?1100000101010100
100110101010101212011 11?????????????????????100[0
1]21011001?1110100111011[12]111111102101101111
1111?000010020100110110100111 01?002[01]00010?1
10101111111 10???1021?1?0101???

Chromogisaurus novasi
??
??1???
??????????1?????????????????????012101?0?1??????????
?????????????????1????111????1?020100110110 1????
??????????????????????????????020??????????

Pantydraco caducus
????101??0?????????????0??????????101??????0??10
011??0?????10?12?000100100 1????01111?000??10
??????????????00??00??11?????????????????????
?0111???1?1?0010?0???????11[12]1?????????????
????1??00001??200???00?1?1?0?????????????????
00101112 10???100111?0110000

Efraasia minor
1?2110100020101?111101???1?00????100100001?1??1
0011101101?01?2120?00110000????10?111100???101
01010?0?0?1101010101012120111001 1?0101111?1101
[12]0000010220110 01?11100001110121111111021 0
1100011111100000100200001101101001121 1?????00?
100110001011120 0???101011?01100??

Plateosaurus engelhardti
1121101000201011111010011[01]00?0111001000011
1001001110110100202120100111000101110111110100
1101110100110110101010100212011100110010111
1110000000010220111011?111010011101121[12]111[01
]10210110001111110000000200001[01]11101001120
1?00200001011100010110200 010010101101110100

Chindesaurus briansmalli
??
??0??10?1????0???
????????????????????????????????1[12][12]??1??????1????
??????????10110210110011011O?0?001???1?0120001[0
1]10111111?112[01]0??????????????????????????????????

Guaibasaurus candelariensis
??
????????????????????????????????????1?1111100001110
?0???0??111?10110???111111110011?1??100121[01]
1101??11100?0111[01]11?111??????1?11?00?1?11[01
]10000?012100020011110111101?012000110111000
11111110????020??????????

Tawa hallae
012211?00020100???1000?001010?0100?01000001000
10000000?00?001000000000?001????1111211111?10
111?10?000??0?0?001??111[12]1010000010111000100
1011?1?010120?101??011020?1011?1??2?1021022111
1101111001000011021101200010101111111?11210001
1011000111110101110000 11?111100?

Eodromaeus murphi
0?1??0??0011010???????1??0????1?00????????0????0000
100???0?1?000000000000?0?0011?1???110?0?01?1110
?0??????010111?111210111111010?1?0100?110[12]100
10102101101001[12]1011?10?111??11???1?21?11001?
1?????000010122100100111O?111?0?00200001 1?????
0???????0???0020???0101???

Coelophysis bauri
012212?10021001110010111 1[01]0110100111101000
010110000100?10001120000000010011111111121111
01?10101111111001010011011 1?1?101102111111101
11111121?12100221111O1?121021?10111111212?000
22112001111100 10000[01]1122200????1101101 11?0
0201101100101111011010100010111 10????01

Liliensternus liliensterni
??????????0?1?????????????????1??1?????????????????0000?
00?????????000?00?0?00?????11?121?110?11010111?1
1100?0?????????11110?10??????????1?????????2100220-
11111?121021?10111111212111022112110111110?00
0010022200201111100101 11?0020110?1????1?1101??
?0???0121??????????

Syntarsus rhodesiensis
01221211?011000110010?101?????10011111??00?1??
?0000000?????112000000?010011???11112111101?10
1?11111110010100111111111210?11211111?1111101
1121?12101221111O1?1?100??10111111212111022 11
[12]01[01]111100?0000011222002011101001011 1?00
20111?1?0101111011010 11?0111?1101012??

Syntarsus kayentakatae
01221211?021010?10110110 1?10101110???00?0?0100
10000000?100011200000?00001????11112111101?10
1?111111100101??110111???1?????????????????????11?1
??????1??1???1?1021?101111??2?211102?11200111110
0100001112220 0?????10?1?????????111?1?0??111101?
??0100010 1111?1????0

Zupaysaurus rugeiri
?????2???011010?1011010111011000 11???00?????01100
?0100?1000??2000000?0000??1????????????????????????
??????????1????????????????????????????????11???????????
????????????????????????????????????0001???????2111111
0010101?0000010?1?????????????1100???1???????00

Daemonosaurus chauliodus
?00011???010100?0010???1100100 1001???00???11101
0010000?0000000?00000?0000??????10????????????????
??
??
????????????????????????????????????0110???1????????0

Petrified forest theropod
??
??
????????????????????????????????00221111?1??11021?1?
111?112?211102?11210111110??0001?021200211111
1001010??0??0110?100101?11?1????????111??????????

Dilophosaurus wetherelli
012[12]?2?10010010???11?0101101100101?111100111
00100100001 10?0111000000?000111110111111210?
11010111011101101001101 1121[12]10110???1111111
01100121?12100220111O1?121021?111111112121110
2211210[01]1111101000000021200211111100101 01?
00210111100101111011010011012111101?0??0

FULL CODING TO *BURIOLESTES SCHULTZI* (ULBRA-PVT280 PLUS CAPPA/UFSM 0035) IN THE FIFTH PHYLOGENETIC ANALYSIS

0001?00110110?0111101?110??0000?1010002011010
0100????00101000300011?1?000000???111110111O1?
111011?00??1100000100 1???1?00???000??00111 0100
00210012001102000000000??0003100?0000100001
010?10??11?1000001?0100001?0110?1000000001100
0?1000?????0000???1??1111011 1?0001100?1?????????
??????????????????10000001100 201200000020101101 22
101110210020 0?0???00???000010110000201010100 10
0100001111010100002 0?00?1000100000100000 10?1
1???1??000010110101030100110211010000 0??????

7 ARTIGO V

Título: An exceptionally preserved association of complete dinosaur skeletons reveals the oldest long-necked sauropodomorphs

Autores: Rodrigo Temp Müller, Max Cardoso Langer e Sérgio Dias da Silva

Periódico: Biology Letters

Volume: 14

Páginas: 1-5

Ano: 2018

DOI: 10.1098/rsbl.2018.0633

BIOLOGY LETTERS

rsbl.royalsocietypublishing.org

Research

Cite this article: Müller RT, Langer MC, Dias-da-Silva S. 2018 An exceptionally preserved association of complete dinosaur skeletons reveals the oldest long-necked sauropodomorphs. *Biol. Lett.* **14**: 20180633. http://dx.doi.org/10.1098/rsbl.2018.0633

Received: 6 September 2018
Accepted: 22 October 2018

Subject Areas:
palaeontology

Keywords:
Brazil, Dinosauria, evolution, Norian, Saurischia, Triassic

Author for correspondence:
Rodrigo Temp Müller
e-mail: rodrigotmuller@hotmail.com

Electronic supplementary material is available online at https://dx.doi.org/10.6084/m9.figshare.c.4285781.

THE ROYAL SOCIETY PUBLISHING

Palaeontology

An exceptionally preserved association of complete dinosaur skeletons reveals the oldest long-necked sauropodomorphs

Rodrigo Temp Müller[1,2], Max Cardoso Langer[3] and Sérgio Dias-da-Silva[2]

[1]Programa de Pós Graduação em Biodiversidade Animal, Universidade Federal de Santa Maria, Santa Maria, RS 97105-900, Brazil
[2]Centro de Apoio à Pesquisa Paleontológica da Quarta Colônia, Universidade Federal de Santa Maria, São João do Polêsine, RS 598, 97230-000, Brazil
[3]Laboratório de Paleontologia, Universidade de São Paulo, Ribeirão Preto, SP 14040-901, Brazil

RTM, 0000-0001-8894-9875

The rise of sauropodomorphs is still poorly understood due to the scarcity of well-preserved fossils in early Norian rocks. Here, we present an association of complete and exceptionally well-preserved dinosaur skeletons that helps fill that gap. They represent a new species, which is recovered as a member of a clade solely composed of Gondwanan Triassic taxa. The new species allows the definition of a set of anatomical changes that shaped sauropodomorph evolution along a period from 233 to 225 Ma, as recorded in the well dated Late Triassic beds of Brazil. In that time span, apart from achieving a more herbivorous diet, sauropodomorph dinosaurs increased their size in a ratio of 230% and their typical long neck was also established, becoming proportionally twice longer than those of basal taxa. Indeed, the new dinosaur is the oldest-known sauropodomorph with such an elongated neck, suggesting that the ability to feed on high vegetation was a key trait achieved along the early Norian. Finally, the clustered preservation mode of the skeletons represents the oldest evidence of gregarious behaviour among sauropodomorphs.

1. Introduction

The oldest sauropodomorph dinosaurs are represented by relatively rare, small-bodied forms from Carnian strata in southwestern Pangaea [1–5]. Soon after, approaching the end of the Triassic, larger members of the group became dominant faunal components in land ecosystems, with representatives from almost the entire supercontinent [6]. However, this transition is still poorly understood, given the scarce sauropodomorph record from early Norian strata [6,7]. Light was more recently shed on understanding the shift from small faunivorous to large herbivorous sauropodomorphs, with the discovery of new specimens from Brazil [5,8,9]. Nevertheless, well-preserved skeletons of early Norian sauropodomorphs are still lacking, hampering the identification of traits that possibly constrained their evolutionary trajectories along the Mesozoic. Here, we partially fill this gap with the description of an association of three skeletons from Brazil (see electronic supplementary material, figure S1).

2. Systematic palaeontology

Dinosauria Owen, 1842
Saurischia Seeley, 1887
Sauropodomorpha Huene, 1932
Unaysauridae clade nov.

(a) Type genus

Unaysaurus tolentinoi Leal *et al.*, 2004.

(b) Definition

Most inclusive clade including *Unaysaurus tolentinoi* Leal *et al.*, 2004, but not *Plateosaurus engelhardti* von Meyer, 1837 nor *Saltasaurus loricatus* Bonaparte & Powel, 1980.

(c) Diagnosis

Unaysauridae differs from all other sauropodomorphs by a substantial cranial expansion of the medial condyle of the astragalus. In addition, a promaxillary fenestra is also unique for the group of sauropodomorphs, although cranial elements are still unknown for *Jaklapallisaurus asymmetrica*.

Macrocollum itaquii gen. et sp. nov.

(d) Etymology

The generic name combines the Greek word μακρο (= long) and the Latin word 'collum' (= neck), referring to the elongated neck of the new taxon. The specific epithet honours Mr José Jerundino Machado Itaqui, one of the main actors behind the creation of CAPPA/UFSM.

(e) Holotype

CAPPA/UFSM (Centro de Apoio à Pesquisa Paleontológica da Quarta Colônia) 0001a. An almost complete and articulated skeleton.

(f) Paratypes

CAPPA/UFSM 0001b. An almost complete and partially articulated skeleton. CAPPA/UFSM 0001c. An articulated skeleton lacking skull and cervical series.

(g) Locality and horizon

The specimens were collected at the Wachholz site (29°36′46.42″ S; 53°15′54.06″ W), Agudo, Rio Grande do Sul, Brazil; upper portion of the Candelária Sequence, Paraná Basin [10]. Stratigraphically correlated beds from a nearby site were dated as early Norian (*ca* 225.42 ± 0.37), Late Triassic [11].

(h) Diagnosis

Macrocollum itaquii differs from all other known sauropodomorphs based on a unique combination of characters: antorbital fossa perforated by a promaxillary fenestra; medial margin of the supratemporal fossa with a simple smooth curve at the frontal/parietal suture; proximal articular surface of metacarpal I transversely narrow; acetabulum not fully open; ischiadic longitudinal groove not reaching the caudal half of the ischium; absence of trochanteric shelf on the femur; medial condyle of distal femoral articulation subrectangular in distal view; proximal end of metatarsal II with a straight medial margin (see electronic supplementary material, figure S2 for further details).

3. Description

The skull (figure 1*a–c*) is gracile and about half the femoral length, which is a usual trait in post-Carnian sauropodomorphs. The snout is slightly elongated, with the internarial fossa bounding a large external naris. It resembles *Plateosaurus engelhardti*, whereas in *Buriolestes schultzi* the external naris is narrow. The rostrocaudal length of the antorbital fenestra is subequal to the maximal orbital length. The caudodorsal process of the premaxilla does not contact the rostroventral process of the nasal. A well-developed wall, mediodorsally projecting from the maxilla, forms the extensive antorbital fossa, which is perforated by a promaxillary fenestra. An internarial fenestra is visible in dorsal view and the prefrontal does not contribute to the dorsal orbital rim. There is no marked rostrolateral projection from the frontal/parietal contact at the medial margin of the supratemporal fossa. The craniomandibular articulation is slightly below the tooth line. The rostral tip of the dentary is downturned. The retroarticular process is caudally elongated, but does not strongly fold at its tip. There are four premaxillary, about 23 maxillary, and about 21 dentary teeth. Except for those in the premaxilla, tooth crowns are constricted at their base and bear large denticles forming oblique angles with the main axis of the tooth. In contrast to Carnian sauropodomorphs, there is no evidence of pterygoid teeth.

The cervical vertebrae are remarkably elongated (figure 1*d*). For instance, the centrum of the fourth cervical vertebra is about six times longer than its cranial height, whereas that ratio is only 2.5 in *B. schultzi*. The neural spine is craniocaudally short in the cranial trunk vertebrae, but more elongated in the remaining elements (figure 1*e*). Three vertebrae compose the sacrum: the two primordial elements and one extra added from the trunk series. The chevrons from the cranial half of the tail are quite elongated (more than twice the length of their respective centra). Scapula and coracoid are unfused in all specimens (figure 1*h*). The proximal articular surface of the humerus is flat, with its distal end just moderately expanded transversely. A deep radial fossa is absent from the proximal end of the ulna and the olecranon is poorly developed. The twisted digit I (figure 1*i*) is somewhat more robust, but shorter than digits II and III, whereas digits IV and V are reduced, lacking ungual phalanges. The medial acetabular wall of the ilium is well developed (figure 1*f*), resembling the plesiomorphic condition also present in *Jaklapallisaurus asymmetrica*. On the other hand, plateosaurian sauropodomorphs, like *P. engelhardti* and *Coloradisaurus brevis* have a fully open acetabulum. The supracetabular crest is pronounced and the preacetabular ala is short and triangular. The ischium (figure 1*g*) is about 80% of the total length of the pubis. Its shaft has a triangular section at midlength, but expands dorsoventrally at the distal end, forming a semicircular outline. The femur is sigmoid in cranial view (figure 1*k*), but almost straight in lateral view. The proximal articular surface bears a well-developed caudomedial tuber. All the specimens lack a trochanteric shelf. The asymmetrical fourth trochanter is located at the proximal half of the bone. The tibia is nearly 90% the length of the femur. As in *J. asymmetrica*, the medial condyle of the astragalus is remarkably expanded cranially (figure 1*j*), whereas this is less pronounced in other sauropodomorphs. The foot is

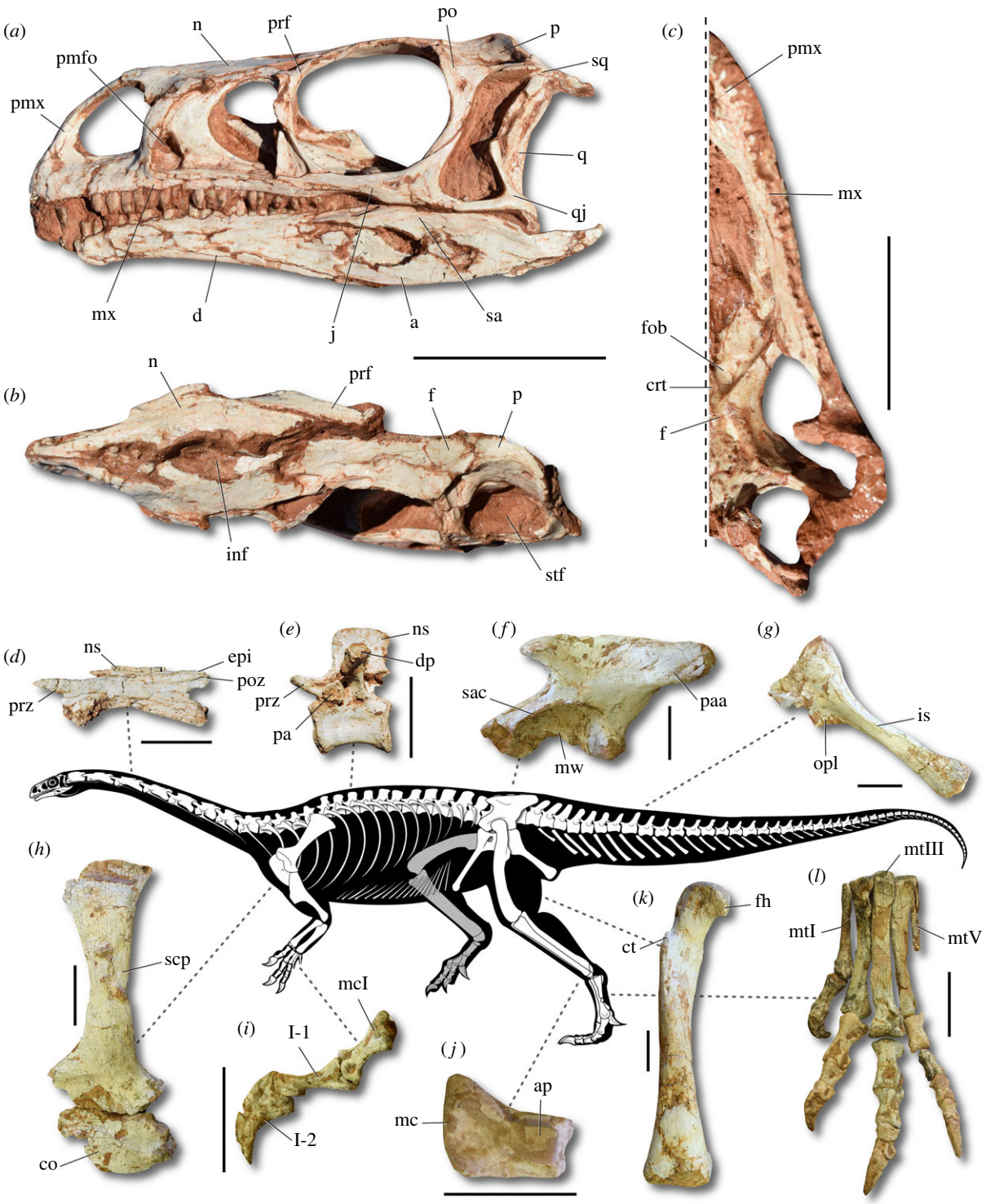

Figure 1. Reconstructed skeleton and representative elements of *Macrocollum itaquii*. (*a*) Skull in left lateral view (CAPPA/UFSM 0001a). (*b*) Skull in dorsal view (CAPPA/UFSM 0001a). (*c*) Skull in ventral view (CAPPA/UFSM 0001b). (*d*) Fourth cervical vertebra in left lateral view (CAPPA/UFSM 0001b). (*e*) Mid-truncal vertebra in left lateral view (CAPPA/UFSM 0001b). (*f*) Left ilium in lateral view (CAPPA/UFSM 0001b). (*g*) Left ischium in lateral view (CAPPA/UFSM 0001b). (*h*) Right pectoral girdle in lateral view (reversed - CAPPA/UFSM 0001b). (*i*) Right manual digit I in medial view (CAPPA/UFSM 0001b). (*j*) Right astragalus in dorsal view (CAPPA/UFSM 0001c). (*k*) Right femur in cranial view (CAPPA/UFSM 0001b). (*l*) Left pes in cranial view (CAPPA/UFSM 0001a). I-1, phalanx one of the digit I; I-2, phalanx two of the digit I; a, angular; ap, ascending process; co, coracoid; crt, crest; ct, cranial trochanter; d, dentary; dp, diapophysis; epi, epipophysis; f, frontral; fh, femoral head; fob, fossa for the olfactoy bulbus; inf, internarial fenestra; is, ischium shaft; j, jugal; mc, medial condyle; mcI, metacarpal I; mtI, metatarsal I; mtIII, metatarsal III; mtV, metatarsal V; mw, medial wall; mx, maxilla; n, nasal; ns, neural spine; opl, obturador plate; p, parietal; pa, parapophysis; paa, postacetabular ala; pmfo, promaxillary fenestra; pmx, premaxilla; po, postorbital; poz, postzygapophysis; prf, prefrontal; prz, prezygapophysis; q, quadrate; qj, quadratojugal; sa, surangular; sac, supracetabular crest; scp, scapula; sq, squamosal; stf, supratemporal fenestra. Scale bar = 50 mm. (Online version in colour.)

slender (figure 1*l*), with elongated phalanges, resembling early diverging sauropodomorphs like *B. schultzi* and *Eoraptor lunensis*. In contrast, *P. engelhardti* and massopodans have robust phalanges.

4. Phylogenetic analysis

Macrocollum itaquii was scored in a new data matrix constructed from previous studies on Triassic/Jurassic sauropodomorphs,

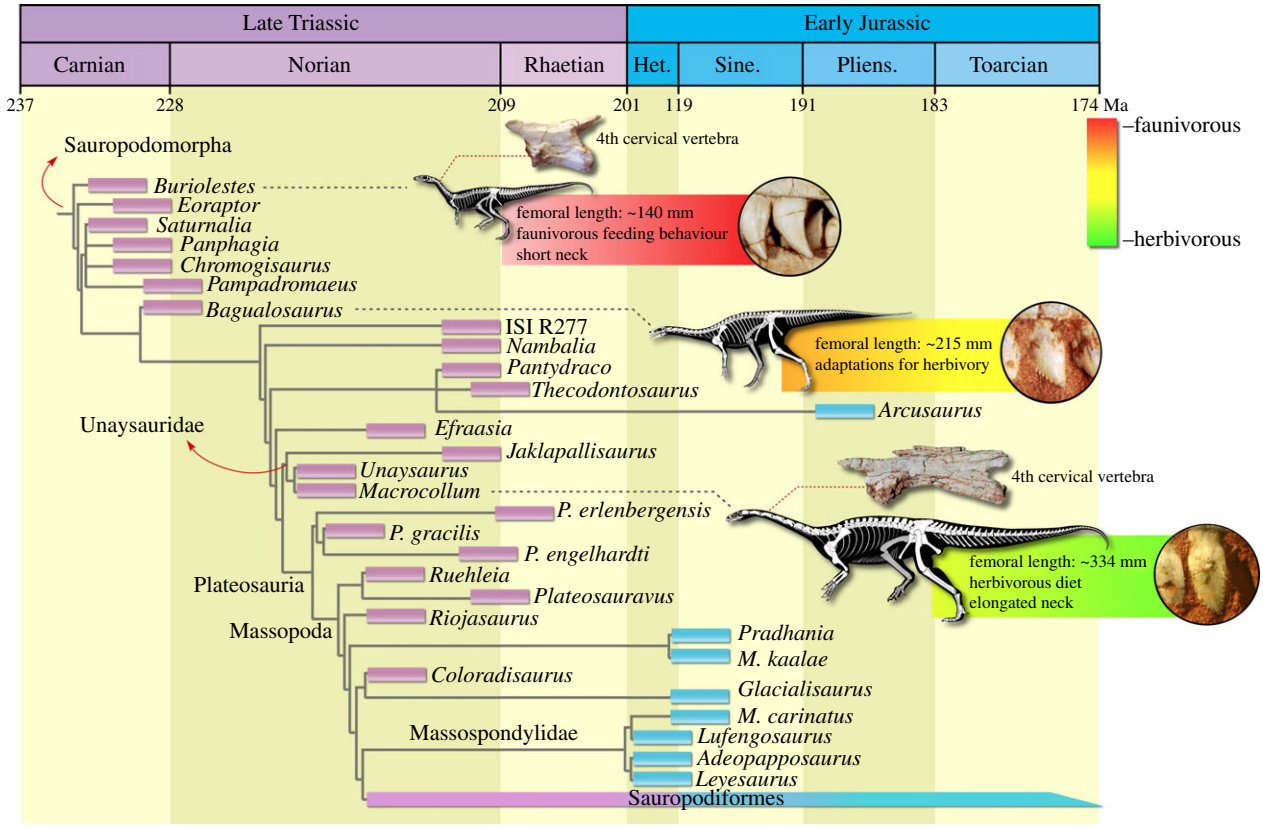

Figure 2. Time-calibrated reduced strict consensus tree depicting the phylogenetic position of *Macrocollum itaquii* and some evolutionary trends along the lineage. (Online version in colour.)

which was the subject of an equally weighted parsimony analysis in TNT v. 1.1 [12] (see electronic supplementary material). The analysis recovered 648 MPTs of 1507 steps each, which reveal a rich (and poorly understood) diversity of non-plateosaurian sauropodomorphs (figure 2). In opposition to previous proposals [13], *Unaysaurus tolentinoi* does not lie within Plateosauridae. Rather, it is nested in a new clade that encompasses the Indian *Jaklapallisaurus asymmetrica* [14] as the sister taxon of *M. itaquii* plus *U. tolentinoi*. Members of this new clade, Unaysauridae, share a medial condyle of the astragalus 1.6 times the craniocaudal length of the lateral condyle, whereas the sister taxon relationship between *M. itaquii* and *U. tolentinoi* is supported by the presence of a longitudinal ventral sulcus in the proximal and middle caudal vertebrae. Unaysauridae is the sister group of Plateosauria, which is composed of Plateosauridae plus Massopoda.

5. Discussion

The proposed phylogenetic hypothesis, associated with the precise time calibration of Triassic strata from Brazil [11], allows investigation of the timeline involved in the acquisition of some crucial sauropodomorph traits. *Buriolestes schultzi*, the sister taxon to all other sauropodomorphs [5,9], was exhumed from beds of about 233 Ma [11], whereas *Bagualosaurus agudoensis* comes from beds that overlap those yielding *Bu. schultzi* [8]. Finally, *M. itaquii* was recovered from rocks belonging to the upper part of the Candelária Sequence [10], constrained as about 225 Ma [11]. This framework allows changes in the sauropodomorph bauplan to be tracked along a *ca* 8 Ma time interval in Brazil. Indeed, these Brazilian taxa represent stages of early sauropodomorph evolution also recognized in the Ischigualato Formation in Argentina and in Norian deposits of various parts of the world, thus corresponding to general trends within the group. For instance, in contrast to most Carnian members of the group, the teeth of *M. itaquii* and other Norian taxa are fully adapted to an omnivore/herbivore diet, with coarse tooth serrations, mesiodistally expanded crowns above the root in cheek teeth, and overlap of adjacent crowns [15]. A gradual increase in size accompanies this shift, with femoral length increasing from about 135 mm in *Bu. schultzi* [9] to 215 in *Ba. agudoensis* [8], and to over 335 mm in *M. itaquii* and most mid-late Norian taxa. However, skull proportions reduce from about to 85% of the femoral length in *Bu. schultzi*, to *ca* 60% in *Ba. agudoensis*, and *ca* 45% in *M. itaquii* and mid-late Norian taxa, highlighting the presence of allometric processes in the size increase seen in the lineage. Likewise, the neck becomes proportionally two times longer in *M. itaquii* in comparison to *Bu. schultzi*. Not only representing one of the most important diagnostic traits of sauropodomorphs, neck elongation may also have provided a competitive advantage for gathering food resources, allowing members of the group to reach higher vegetation [16] compared to other early Norian vertebrates.

The hindlimb of *M. itaquii* also carries modifications that could be related to the progressive loss of cursorial habits. Its femur is longer than the tibia, whereas earlier forms have the inverse condition [1]. The straight femur of *M. itaquii* in lateral view also differs from those of older sauropodomorphs, which have a sigmoidal outline, and the absence of a trochanteric shelf also in contrast to the condition in Carnian forms. On the other hand, the gracile construction of the foot (with slender phalanges) resembles the plesiomorphic condition for sauropodomorphs, differing from the robust foot of

plateosaurians. Hence, the skeleton of the new dinosaur demonstrates a gradual abandonment of cursoriality combined with the acquisition of traits related to herbivorous feeding strategies.

Finally, the clustered preservation of the three skeletons of *Macrocollum itaquii* represents the oldest evidence of gregarious behaviour in sauropodomorphs. These corroborate the pattern seen in other Triassic associations, such as the '*Plateosaurus* bonebed' from Central Europe [17] and the *Mussaurus* remains from the Laguna Colorada Formation, Argentina [18,19]. Putative older evidences are not so compelling, relying on the skeletons of *Bu. schultzi* recovered from the same layer in a small area [5,9], as also reported for the coeval *Saturnalia tupiniquim*, from southern Brazil [2].

Data accessibility. Data are available from the Dryad Digital Repository: http://doi.dx.org/10.5061/dryad.gh4p57r [20].

Authors' contributions. R.T.M. and S.D.-d.-S. conducted the fieldwork. R.T.M. performed the mechanical preparation of specimens and carried out the analyses. R.T.M., M.C.L. and S.D.-d.-S. analysed and discussed the results. R.T.M., M.C.L. and S.D.-d.-S. wrote the paper. All authors approved the final version of the paper and agreed to be accountable for all aspects of the work.

Competing interests. We have no competing interests.

Funding. This work was supported by the Conselho Nacional de Desenvolvimento Científco e Tecnológico (CNPq; research grant to S.D.-d.-S., process number 306352/2016-8).

Acknowledgements. We thank the following people who played a role in the discovery of the specimens presented here: Mr Dilo Wachholz, Mr Olímpio Neu, Mrs Cladis Müller Kobs, Mrs Mariana Kobs, Mr Gercides Müller, and Mrs Estefânia Temp Müller. Handling Editor of Biology Letters, Dr Diego Pol, Dr Fernando Novas, and an anonymous reviewer provided valuable comments that greatly improved this manuscript. We also thank the Willi Henning Society, for the gratuity of TNT software.

References

1. Sereno PC, Forster CA, Rogers RR, Monetta AM. 1993 Primitive dinosaur skeleton from Argentina and the early evolution of Dinosauria. *Nature* **361**, 64–66. (doi:10.1038/361064a0)
2. Langer MC, Abdala F, Richter M, Benton MJ. 1999 A sauropodomorph dinosaur from the Upper Triassic (Carnian) of Southern Brazil. *Acad. Sci. Paris Sci. Terre et Planetnèt.* **329**, 511–517.
3. Martinez RN, Alcober OA. 2009 A basal sauropodomorph (Dinosauria: Saurischia) from the Ischigualasto Formation (Triassic, Carnian) and the early evolution of Sauropodomorpha. *PLoS ONE* **4**, e4397. (doi:10.1371/journal.pone.0004397)
4. Ezcurra MD. 2010 A new early dinosaur (Saurischia: Sauropodomorpha) from the Late Triassic of Argentina: a reassessment of dinosaur origin and phylogeny. *J. Syst. Palaeontol.* **8**, 371–425. (doi:10.1080/14772019.2010.484650)
5. Cabreira SF *et al*. 2016 A unique Late Triassic dinosauromorph assemblage reveals dinosaur ancestral anatomy and diet. *Curr. Biol.* **26**, 3090–3095. (doi:10.1016/j.cub.2016.09.040)
6. Müller RT, Langer MC, Dias-da-Silva S. 2017 Biostratigraphic significance of a new early sauropodomorph specimen from the Upper Triassic of southern Brazil. *Hist. Biol.* **29**, 187–202. (doi:10.1080/08912963.2016.1144749)
7. Mannion PD, Upchurch P, Carrano MT, Barrett PM. 2011 Testing the effect of the rock record on diversity: a multidisciplinary approach to elucidating the generic richness of sauropodomorph dinosaurs through time. *Biol. Rev.* **86**, 157–181. (doi:10.1111/j.1469-185X.2010.00139.x)
8. Pretto FA, Langer MC, Schultz CL. 2018 A new dinosaur (Saurischia: Sauropodomorpha) from the Late Triassic of Brazil provides insights on the evolution of sauropodomorph body plan. *Zool. J. Linn. Soc.*, zly028. (doi:10.1093/zoolinnean/zly028)
9. Müller RT *et al*. 2018 Early evolution of sauropodomorphs: anatomy and phylogenetic relationships of a remarkably well preserved dinosaur from the Upper Triassic of southern Brazil. *Zool. J. Linn. Soc.*, zly009. (doi:10.1093/zoolinnean/zly009)
10. Müller RT, Da-Rosa AAS, Silva LR, Aires ASS, Pacheco CP, Pavanatto AEB, Dias-da-Silva S. 2015 Wachholz, a new exquisite dinosaur-bearing fossiliferous site from the Upper Triassic of southern Brazil. *J. South Am. Earth Sci.* **61**, 120–128. (doi:10.1016/j.jsames.2014.10.009)
11. Langer MC, Ramezani J, Da Rosa AA. 2018 U-Pb age constraints on dinosaur rise from south Brazil. *Gondwana Res.* **57**, 133–140. (doi:10.1016/j.gr.2018.01.005)
12. Goloboff PA, Farris JS, Nixon KC. 2008 TNT, a free program for phylogenetic analysis. *Cladistics* **24**, 1–13. (doi:10.1111/j.1096-0031.2007.00173.x)
13. Leal LA, Azevedo SA, Kellner AW, Da Rosa ÁA. 2004 A new early dinosaur (Sauropodomorpha) from the Caturrita Formation (Late Triassic), Paraná Basin, Brazil. *Zootaxa* **690**, 1–24.
14. Novas FE, Ezcurra MD, Chatterjee S, Kutty TS. 2011 New dinosaur species from the Upper Triassic Upper Maleri and Lower Dharmaram formations of Central India. *Earth Environ. Sci. Trans. R. Soc. Edinb.* **101**, 333–349.
15. Nesbitt SJ, Sidor CA, Irmis RB, Angielczyk KD, Smith RM, Tsuji LA. 2010 Ecologically distinct dinosaurian sister group shows early diversification of Ornithodira. *Nature* **464**, 95–98. (doi:10.1038/nature08718)
16. Galton PM. 1985 Diet of prosauropod dinosaurs from the late Triassic and early Jurassic. *Lethaia* **18**, 105–123. (doi:10.1111/j.1502-3931.1985.tb00690.x)
17. Sander PM. 1992 The Norian *Plateosaurus* bonebeds of central Europe and their taphonomy. *Palaeogeogr. Palaeoclimatol. Palaeoecol.* **93**, 255–299. (doi:10.1016/0031-0182(92)90100-J)
18. Pol D, Powell JE. 2007 Skull anatomy of *Mussaurus patagonicus* (Dinosauria: Sauropodomorpha) from the late Triassic of Patagonia. *Hist. Biol.* **19**, 125–144. (doi:10.1080/08912960601140085)
19. Otero A, Pol D. 2013 Postcranial anatomy and phylogenetic relationships of *Mussaurus patagonicus* (Dinosauria, Sauropodomorpha). *J. Vertebr. Paleontol.* **33**, 1138–1168. (doi:10.1080/02724634.2013.769444)
20. Müller RT, Langer MC, Dias-da-Silva S. 2018 Data from: An exceptionally preserved association of complete dinosaur skeletons reveals the oldest long-necked sauropodomorphs. Dryad Digital Repository. (https://doi.org/10.5061/dryad.gh4p57r)

SUPPLEMENTARY INFORMATION

An exceptionally preserved association of complete dinosaur skeletons reveals the oldest long-necked sauropodomorphs

Rodrigo Temp Müller, Max Cardoso Langer & Sérgio Dias-da-Silva

Corresponding author email: rodrigotmuller@hotmail.com

Outline of contents

(a) Supplementary figure 1

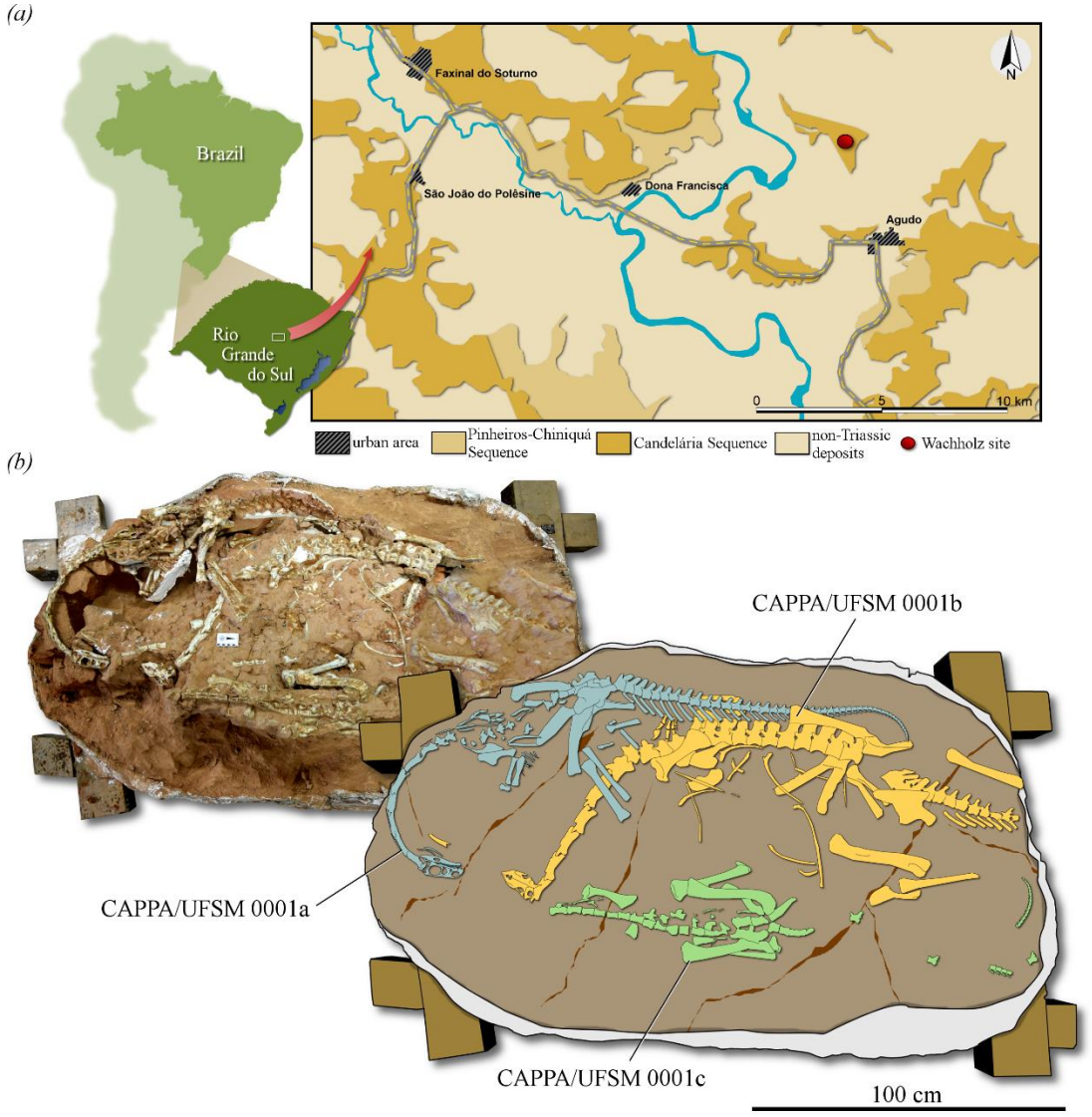

Caption: *Macrocollum itaquii* (CAPPA/UFSM 00001) and the location of the study area. (*a*) map of the Agudo area, Rio Grande do Sul, Brazil, showing the location of the Wachholz site. (*b*) CAPPA/UFSM 0001 in the rock block before its final preparation.

(b) Supplementary figure 2

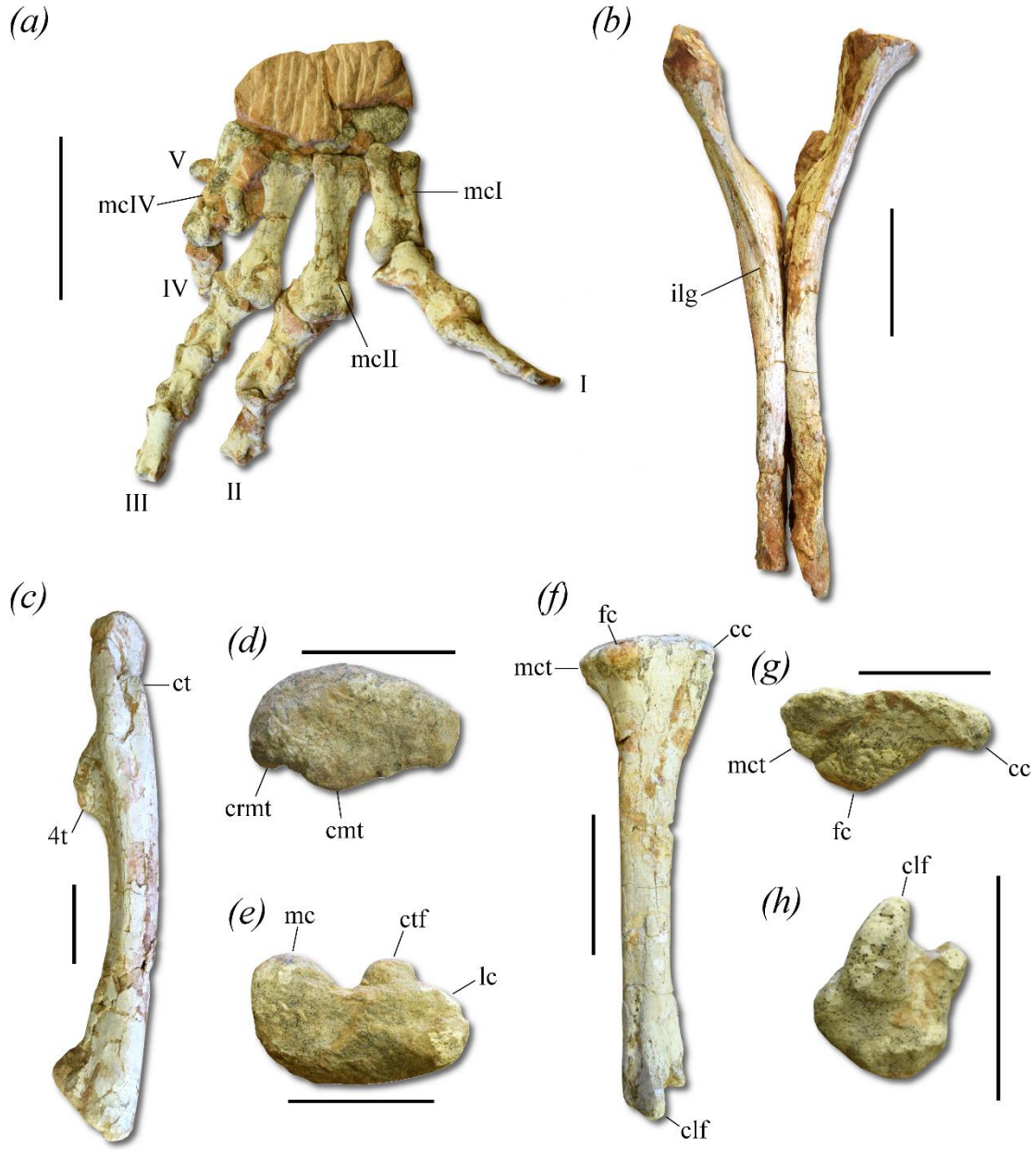

Caption: Selected skeletal parts of *Macrocollum itaquii*. (*a*) right manus in dorsal view (CAPPA/UFSM 0001b). *(b)* pair of ischia in dorsal view (CAPPA/UFSM 0001b). *(c)* right femur in lateral view (CAPPA/UFSM 0001b). *(d)* right femur in proximal view (CAPPA/UFSM 0001b). *(e)* right femur in distal view (CAPPA/UFSM 0001b). *(f)* right tibia in lateral view. *(g)* right tibia in proximal view. *(h)* right tibia in distal view. I-V, digits I to V, 4t, fourth trochanter; cc, cnemial crest; clf, caudolateral flange; cmt, caudomedial tuber; crmt, craniomedial tuber; ct, cranial trochanter; fc, fibular condyle; ilg, ischiadic longitudinal groove; lc, lateral condyle; mc, medial condyle; mcI, metacarpal I; mcII, metacarpal II; mcIV, metacarpal IV; mct, medial condyle of the tibia. Scale bar = 50 mm.

(c) Comparison between *Macrocollum itaquii* and *Unaysaurus tolentinoi*

Although the bioestratigraphic correlation of the type-localities of *Macrocollum itaquii* and *Unaysaurus tolentinoi* have been proposed (Müller et al. 2017), the contemporaneity of these taxa remains elusive. However, as this is a possibility, we pinpoint here a set of anatomical differences between them:

● *Macrocollum* lacks an additional fossa caudal to the premaxillary fenestra on the antorbital fossa.

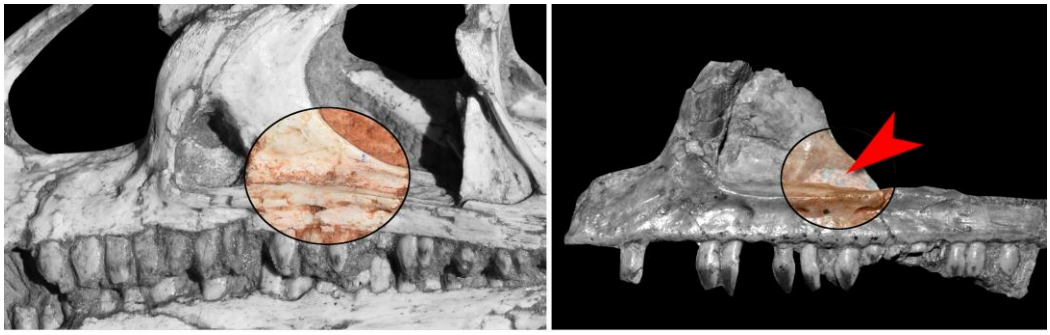

Lateral view of the skull of *Macrocollum* (left) and *Unaysaurus* (right): arrow indicates additional fossa

● *Unaysaurus* lacks a well-developed medial crest on the ventral margin of the frontal, medially bounding the fossa for the olfactory bulb.

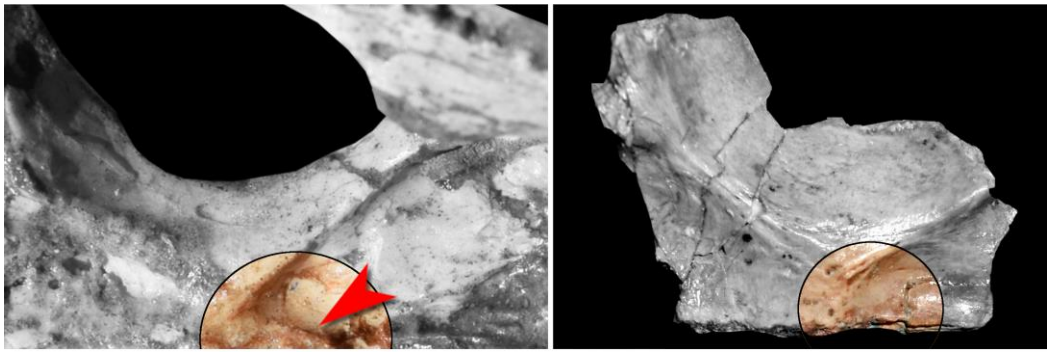

Ventral view of the skull of *Macrocollum* (left) and *Unaysaurus* (right): arrow indicates medial crest

● The medial margin of the supratemporal fossa of *Unaysaurus* bears a projection at the frontal/postorbital-parietal suture producing a scalloped margin. In *Macrocollum* the homologous surface forms a simple smooth curve.

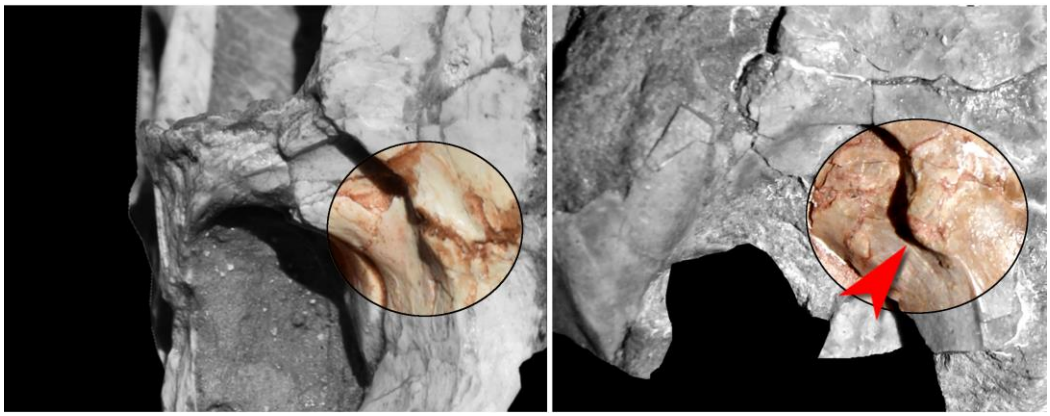

Dorsal view of the skull of *Macrocollum* (left) and *Unaysaurus* (right): arrow indicates scalloped margin

● The proximal articular surface of metacarpal I is proportionally wider in *Unaysaurus*.

Dorsal view of metacarpal I of *Macrocollum* (left) and *Unaysaurus* (right): bar indicates proximal width

● The medial margin of the proximal end of the metatarsal II is straight in *Macrocollum*, but concave in *Unaysaurus*.

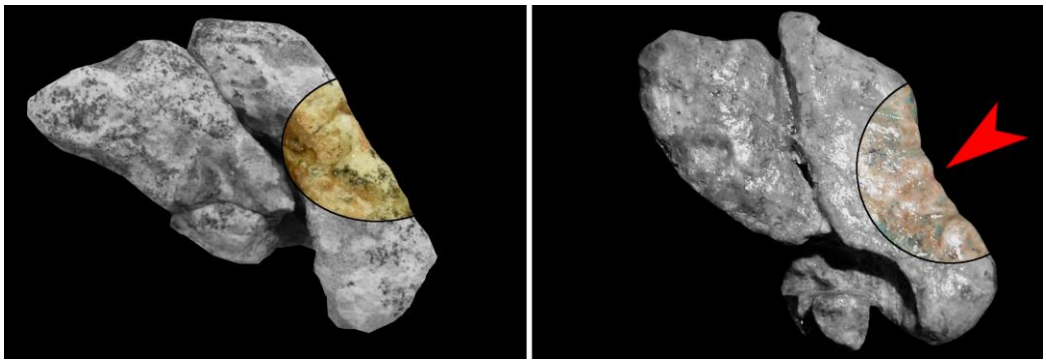

Proximal view of metacarpasl II and III of *Macrocollum* (left) and *Unaysaurus* (right): arrow indicates medial concavity

(d) Details of the phylogenetic analysis

In order to test its phylogenetic affinities and potential implications for the understanding of early sauropodomorph evolution, *Macrocollum itaquiii* was scored in a new data matrix constructed from previous studies on Triassic/Jurassic sauropodomorphs. The data matrix was based on that of McPhee & Choiniere (2017), with the addition of operational taxonomic units (OTUs) and characters from recent studies: Nesbitt 2011; Novas et al. (2011), Yates et al. (2011), Apaldetti et al. (2012), Otero & Pol (2013), Otero et al. (2015), Cabreira et al. (2016), Müller et al. (2016; 2018), Peyre de Fabrègues & Allain (2016), Cerda et al. (2017), Bronzati et al. (2017, 2018), Apaldetti et al. (2018), Chapelle & Choiniere (2018), Pretto et al. (2018). The added OTUs are: *Arcusaurus*, *Bagualosaurus*, *Buriolestes*, *Eodromaeus*, *Ingentia*, ISI R277, *Jaklapallisaurus*, *Massospondylus kaalae*, *Meroktenus*, *Nambalia*, *Pampadromaeus*, *Plateosaurus erlenbergensis*, *Pradhania*, *Sefapanosaurus*, and *Tawa*. The final data matrix includes 401 characters and 75 OTUs.

The data matrix was subject of an equally weighted parsimony analysis in TNT v. 1.1 (Goloboff et al. 2008). Characters 8, 14, 22, 26, 43, 63, 75, 108, 118, 135, 141, 151, 154, 167, 170, 172, 173, 180, 185, 190, 193, 200, 207, 231, 234, 241, 251, 256, 264, 273, 282, 285, 299, 312, 334, 340, 348, 372, 385, 388, 391, and 396 were treated as ordered. *Euparkeria* was used to root the most parsimonious trees (MPTs), which were recovered with a 'Traditional search' (random addition sequence + tree bisection reconnection) with 1000 replicates of Wagner trees (with random seed = 1), tree bisection reconnection and branch swapping (holding 10 trees save per replicate).

(e) List of characters

1. Skull to femur ratio: greater than 0.6 (0); less than 0.6 (1). (Yates 2007).

2. Lateral plates appressed to the labial side of the premaxillary, maxillary and dentary teeth: absent (0); present (1). (Yates 2007).

3. Relative height of the rostrum at the posterior margin of the naris: more than 0.6 the height of the skull at the middle of the orbit (0); less than 0.6 the height of the skull at the middle of the orbit (1). (Yates 2007).

4. Foramen on the lateral surface of the premaxillary body: absent (0); present (1). (Yates 2007).

5. Distal end of the dorsal premaxillary process: tapered (0); transversely expanded (1). (Yates 2007).

6. Profile of premaxilla: convex (0); with an inflection at the base of the dorsal process (1). (Yates 2007).

7. Size and position of the posterolateral process of premaxilla: large and lateral to the anterior process of the maxilla (0); small and medial to the anterior process of the maxilla (1). (Yates 2007).

8. Relationship between posterolateral process of the premaxilla and the anteroventral process of the nasal: broad sutured contact (0); point contact (1); separated by maxilla (2). Ordered. (Yates 2007).

9. Posteromedial process of the premaxilla: absent (0); present (1). (Yates 2007).

10. Shape of the anteromedial process of the maxilla: narrow, elongated and projecting anterior to lateral premaxilla-maxilla suture (0); short, broad and level with lateral premaxilla-maxilla suture (1). (Yates 2007).

11. Premaxilla, position of the first tooth: adjacent to rostral tip (0); retreated (1). (Pretto et al. 2018)

12. Development of external narial fossa: absent to weak (0); well-developed with sharp posterior and anteroventral rims (1). (Yates 2007).

13. Development of narial fossa on the anterior ramus of the maxilla: weak and orientated laterally to dorsolaterally (0); well-developed and forming a horizontal shelf (1). (Yates 2007).

14. Size and position of subnarial foramen: absent (0); small (no larger than adjacent maxillary neurovascular foramina) and positioned outside of narial fossa (1); large and on the rim of, or inside, the narial fossa (2). Ordered. (Yates 2007).

15. Shape of subnarial foramen: rounded (0); slot-shaped (1). (Yates 2007).

16. Maxillary contribution to the margin of the narial fossa: absent (0); present (1). (Yates 2007).

17. Maxilla, dorsally open neurovascular canal on the floor of the antorbital fossa: absent (0); present (1). (Witmer 1997; Yates & Kitching 2003; Pretto et al. 2018).

18. Maxilla, promaxillary fenestra: (0) absent; (1) present. (Martínez et al. 2011).

19. Diameter of external naris: less than 0.5 of the orbital diameter (0); greater than 0.5 of the orbital diameter. (Yates 2007).

20. Shape of the external naris (in adults): rounded (0); subtriangular with an acute posteroventral corner (1). (Yates 2007).

21. Level of the anterior margin of the external naris: anterior to the midlength of the premaxillary body (0); posterior to the midlength of the premaxillary body (1). (Yates 2007).

22. Level of the posterior margin of external naris: anterior to, or level with the premaxillamaxilla suture (0); posterior to the first maxillary alveolus (1); posterior to the midlength of the maxillary tooth row and the anterior margin of the antorbital fenestra (2). Ordered. (Yates 2007).

23. Dorsal profile of the snout: straight to gently convex (0); with a depression behind the naris (2). (Yates 2007).

24. Elongate median nasal depression: absent (0); present (1). (Yates 2007).

25. Width of anteroventral process of nasal at its base: less than the width of the anterodorsal process at its base (0); greater than the width of the anterodorsal process at its base (1). (Yates 2007).

26. Nasal relationship with dorsal margin of antorbital fossa: not contributing to the margin of the antorbital fossa (0); lateral margin overhangs the antorbital fossa and forms its dorsal margin (1); overhang extensive, obscuring the dorsal lachrymal-maxilla contact in lateral view (2). Ordered. (Yates 2007).

27. Pointed caudolateral process of the nasal overlapping the lachrymal: absent (0); present (1). (Yates 2007).

28. Anterior profile of the maxilla: slopes continuously towards the rostral tip (0); with a strong inflection at the base of the ascending ramus, creating a rostral ramus with parallel dorsal and ventral margins (1). (Yates 2007).

29. Length of rostral ramus of the maxilla: less than its dorsoventral depth (0); greater than its dorsoventral depth (1). (Yates 2007).

30. Shape of the main body of the maxilla: tapering posteriorly (0); dorsal and ventral margins parallel for most of their length (1). (Yates 2007).

31. Shape of the ascending ramus of the maxilla in lateral view: tapering dorsally (0); with an anteroposterior expansion at the dorsal end (1). (Yates 2007).

32. Rostrocaudal length of the antorbital fossa: greater than that of the orbit (0); less than that of the orbit (1). (Yates 2007).

33. Posteroventral extent of medial wall of antorbital fossa: reaching the anterior tip of the jugal (0); terminating anterior to the anterior tip of the jugal (1).

34. Development of the antorbital fossa on the ascending ramus of the maxilla: deeply impressed and delimited by a sharp, scarp-like rim (0); weakly impressed and delimited by a rounded rim or a change in slope (1). (Yates 2007).

35. Shape of the antorbital fossa: crescentic with a strongly concave posterior margin that is roughly parallel to the anterior margin of the antorbital fossa (0); subtriangular with a straight to gently concave posterior margin (1); antorbital fossa absent (2). (Yates 2007).

36. Size of the neurovascular foramen at the posterior end of the lateral maxillary row: not larger than the others (0); distinctly larger than the others in the row (1). (Yates 2007).

37. Direction that the neurovascular foramen at the posterior end of the lateral maxillary row opens: posteriorly (0); anteriorly, ventrally, or laterally (1). (Yates 2007).

38. Arrangement of lateral maxillary neurovascular foramina: linear (0); irregular (1). (Yates 2007).

39. Longitudinal ridge on the posterior lateral surface of the maxilla: absent (0); present (1). (Yates 2007).

40. Dorsal exposure of the lachrymal: present (0); absent (1). (Yates 2007).

41. Shape of the lachrymal: dorsoventrally short and blockshaped (0); dorsoventrally elongate and shaped like an inverted L (1). (Yates 2007).

42. Orientation of the lachrymal orbital margin: strongly sloping anterodorsally (0); erect and close to vertical (1). (Yates 2007).

43. Length of the anterior ramus of the lachrymal: greater than half the length of the ventral ramus (0); less than half the length of the ventral ramus (1); absent altogether (2). Ordered. (Yates 2007).

44. Web of bone spanning junction between anterior and ventral rami of lachrymal: absent and antorbital fossa laterally exposed (0); present, obscuring posterodorsal corner of antorbital fossa (1). (Yates 2007).

45. Extension of the antorbital fossa onto the ventral end of the lachrymal: present (0); absent (1). (Yates 2007).

46. Length of the posterior process of the prefrontal: short (0); elongated, so that total prefrontal length is equal to the anteroposterior diameter of the orbit (1). (Yates 2007).

47. Bone sheet between the rostral and ventral processes of the prefrontal: (0) absent; (1) present. (Müller et al. 2018).

48. Ventral process of prefrontal extending down the posteromedial side of the lachrymal: present (0); absent (1). (Yates 2007).

49. Maximum transverse width of the prefrontal: less than 0.25 of the skull width at that level (0); more than 0.25 of the skull width at that level (1). (Yates 2007).

50. Shape of the orbit: subcircular (0); ventrally constricted making the orbit subtriangular (1). (Yates 2007).

51. Slender anterior process of the frontal intruding between the prefrontal and the nasal: absent (0); present (1). (Yates 2007).

52. Jugal-lachrymal relationship: lachrymal overlapping lateral surface of jugal or abutting it dorsally (0); jugal overlapping lachrymal laterally (1). (Yates 2007).

53. Shape of the suborbital region of the jugal: an anteroposteriorly elongate bar (0); an anteroposteriorly shortened plate (1). (Yates 2007).

54. Jugal contribution to the antorbital fenestra: absent (0); present (1). (Yates 2007).

55. Angle between ascending process and caudal process of jugal: right or obtuse (0); acute, with an ascending process strongly dorsocaudally oriented (1). (Ezcurra 2006).

56. Dorsal process of the anterior jugal: present (0); absent (1). (Yates 2007).

57. Ratio of the minimum depth of the jugal below the orbit to the distance between the anterior end of the jugal and the anteroventral corner of the infratemporal fenestra: less than 0.2 (0); greater than 0.2 (1). (Yates 2007).

58. Transverse width of the ventral ramus of the postorbital: less than its anteroposterior width at midshaft (0); greater than its anteroposterior width at midshaft (1). (Yates 2007).

59. Postorbital, distal end of frontal ramus, distinct concave notch between parietal and frontal facets: (0) absent; (1) present. (Chapelle & Choiniere 2018).

60. Shape of the dorsal margin of postorbital in lateral view: straight to gently curved (0); with a distinct embayment between the anterior and posterior dorsal processes (1). (Yates 2007).

61. Height of the postorbital rim of the orbit: flush with the posterior lateral process of the postorbital (0); raised so that it projects laterally to the posterior dorsal process (1). (Yates 2007).

62. Postfrontal bone: present (0); absent (1). (Yates 2007).

63. Position of the anterior margin of the infratemporal fenestra: behind the orbit (0); extends under the rear half of the orbit (1); extends as far forward as the midlength of the orbit (2). Ordered. (Yates 2007).

64. Frontal contribution to the supratemporal fenestra: present (0); absent (1). (Yates 2007).

65. Orientation of the long axis of the supratemporal fenestra: longitudinal (0); transverse (1). (Yates 2007).

66. Medial margin of supratemporal fossa: simple smooth curve (0); with a projection at the frontal/postorbital-parietal suture producing a scalloped margin (1). (Yates 2007).

67. Length of the quadratojugal ramus of the squamosal relative to the width at its base: less than four times its width (0); greater than four times its width (1). (Yates 2007).

68. Proportion of infratemporal fenestra bordered by squamosal: more than 0.5 of the depth of the infratemporal fenestra (0); less than 0.5 of the depth of the infratemporal fenestra (1). (Yates 2007).

69. Squamosal-quadratojugal contact: present (0); absent (1). (Yates 2007).

70. Angle of divergence between jugal and squamosal rami of quadratojugal: close to 90 degrees (0); close to parallel (1). (Yates 2007).

71. Length of jugal ramus of quadratojugal: no longer than the squamosal ramus (0); longer than the squamosal ramus (1). (Yates 2007).

72. Shape of the rostral end of the jugal ramus of the quadratojugal: tapered (0); dorsoventrally expanded (1). (Yates 2007).

73. Relationship of quadratojugal to jugal: jugal overlaps the lateral surface of the quadratojugal (0); quadratojugal overlaps the lateral surface of the jugal (1); quadratojugal sutures along the ventrolateral margin of the jugal (2). (Yates 2007).

74. Position of the quadrate foramen: on the quadrate-quadratojugal suture (0); deeply incised into, and partly encircled by, the quadrate (1); on the quadrate-squamosal suture, just below the quadrate head (2). (Yates 2007).

75. Shape of posterolateral margin of quadrate: sloping anterolaterally from posteromedial ridge (0); everted posteriorly creating a posteriorly facing fossa (1); posterior fossa deeply excavated, invading quadrate body (2). Ordered. (Yates 2007).

76. Exposure of the lateral surface of the quadrate head: absent, covered by lateral sheet of the squamosal (0); present (1). (Yates 2007).

77. Proportion of the length of the quadrate that is occupied by the pterygoid wing: at least 70 per cent (0); greater than 70 per cent (1). (Yates 2007).

78. Depth of the occipital wing of the parietal: less than 1.5 times the depth of the foramen magnum (0); more than 1.5 times the depth of the foramen magnum (1). (Yates 2007).

79. Position of foramina for mid-cerebral vein on occiput: between supraoccipital and parietal (0); on the supraoccipital (1). (Yates 2007).

80. Postparietal fenestra between supraoccipital and parietals: absent (0); present (1). (Yates 2007).

81. Shape of the supraoccipital: diamond-shaped, at least as high as wide (0); semilunate and wider than high (1). (Yates 2007).

82. Orientation of the supraoccipital plate: erect to gently sloping (0); strongly sloping forward so that the dorsal tip lies level with the basipterygoid processes (1). (Yates 2007).

83. Orientation of the paroccipital processes in occipital view: slightly dorsolaterally directed to horizontal (0); ventrolaterally directed (1). (Yates 2007).

84. Orientation of the paroccipital processes in dorsal view: posterolateral forming a Vshaped occiput (0); lateral forming a flat occiput (1) (Yates 2007).

85. Size of the post-temporal fenestra: large fenestra (0); a small hole that is much less than half the depth of the paroccipital process (1). (Yates 2007).

86. Exit of the mid-cerebral vein: through trigeminal foramen (0); through a separate foramen anterodorsal to trigeminal foramen (1). (Yates 2007).

87. Shape of the floor of the braincase in lateral view: relatively straight with the basal tuberae, basipterygoid processes and parasphenoid rostrum roughly aligned (0); bent with the basipterygoid processes and the parasphenoid rostrum below the level of the basioccipital condyle and the basal tuberae (1); bent with the basal tuberae lowered below the level of the basioccipital and the parasphenoid rostrum raised above it (2). (Yates 2007).

88. Basioccipital component of th basal tubera, medial component in relation to the parabasisphenoidal component: (0) present; (1) absent. (Yates 2007).

89. Length of the basipterygoid processes (from the top of the parasphenoid to the tip of the process): less than the height of the braincase (from the top of the parasphenoid to the top of the supraoccipital) (0); greater than the height of the

braincase (from the top of the parasphenoid to the top of the supraoccipital) (1). (Yates 2007).

90. Basioccipital – basisphenoid junction on the ventral surface of the bones: (0) straight line; U/V shaped (1). (Bronzati & Rauhut 2017).

91. Subsellar recess: (0) maximum width equal or greater than the dorsoventral height; (1) maximum width smaller than the dorsoventral height. (Bronzati & Rauhut 2017).

92. Laminae/ridges extending from the basipterygoid process onto the parasphenoid rostrum: extend parallel untill they fade into the ventral margin of the cultriform process (0); converge anteromedially on the ventral surface of the cultriform process (1). (Bronzati & Rauhut 2017).

93. Angle between basipterygoid process and cultriform process of the parabasisphenoid: < 90 degress (0); 90 degress (1); > 90 degrees (2). (Bronzati et al. 2018)

94. Length of the basisphenoid (from the basipterygoid process to the basisphenoidal component of the basal tubera) in relation to the length of the basioccipital (from the basioccipital component of the basal tubera to posterior limit of the condyle): longer or equal (0); shorter (1). (Bronzati & Rauhut 2017).

95. Notch in the posterodorsal margin of the lateral portion of the parabasisphenoid: absent (0); present (1). (Bronzati & Rauhut 2017).

96. Number of foramina in the otoccipital between the exoccipital pillar (excluding the foramina for the hypoglossal nerve) posteriorly and fenestra ovalis anteriorly: one (0), two (1). (Bronzati & Rauhut 2017).

97. Unossified gap between the basioccipital and basisphenoidal component of the basal tubera and ventral ramus of the opistothic: absent (0); present (1). (Bronzati & Rauhut 2017).

98. Otosphenoidal crest: low and not projecting posterolaterally (i.e. does not cover the fenestra ovalis with the braincase in lateral view) (0); developed as a lamina projecting posterolaterally (i.e. cover the fenestra ovalis with the braincase in lateral view) (1). (Bronzati et al. 2018).

99. Frontal, anteroposterior length: approximately twice (0); or less than minimum transverse breadth (1). (Wilson 2002).

100. Parietal, distance separating supratemporal fenestrae: less than (0); or twice the long axis of supratemporal fenestra (1). (Wilson 2002).

101. Supratemporal region, anteroposterior length: temporal bar longer (0); or shorter anteroposteriorly than transversely (1). (Wilson 2002).

102. Dorsoventral depth of the parasphenoid rostrum: much less than the transverse width (0); about equal to the transverse width (1). (Yates 2007).

103. Shape of jugal process of ectopterygoid: gently curved (0); strongly recurved and hooklike (1). (Yates 2007).

104. Pneumatic fossa on the ventral surface of the ectopterygoid: present (0); absent (1). (Yates 2007).

105. Relationship of the ectopterygoid to the pterygoid: ectopterygoid overlapping the ventral surface of the pterygoid (0); ectopterygoid overlapping the dorsal surface of the pterygoid (1). (Yates 2007).

106. Position of the maxillary articular surface of the palatine: along the lateral margin of the bone (0); at the end of a narrow anterolateral process due to the absence of the posterolateral process (1). (Yates 2007).

107. Centrally located tubercle on the ventral surface of palatine: absent (0); present (1). (Yates 2007).

108. Medial process of the pterygoid forming a hook around the basipterygoid process: absent (0); flat and blunt-ended (1); bent upward and pointed (2). Ordered. (Yates 2007).

109. Length of the vomers: less than 0.25 of the total skull length (0); more than 0.25 of the total skull length (1). (Yates 2007).

110. Position of jaw joint: no lower than the level of the dorsal margin of the dentary (0); depressed, well below this level (1). (Yates 2007).

111. Shape of upper jaws in ventral view: narrow with an acute rostral apex (0); broad and U-shaped (1). (Yates 2007).

112. Length of the external mandibular fenestra: more than 0.1 of the length of the mandible (0); less than 0.1 of the length of the mandible (1). (Yates 2007).

113. Caudal end of dentary tooth row medially inset with a thick lateral ridge on the dentary forming a buccal emargination : absent (0); present (1). (Yates 2007).

114. Height : length ratio of the dentary: less than 0.2; greater than 0.2 (1). (Yates 2007).

115. Orientation of the symphyseal end of the dentary: in line with the long axis of the dentary (0); strongly curved ventrally (1). (Yates 2007).

116. Position of first dentary tooth: adjacent to symphysis (0); inset one tooth's width from the symphysis (1). (Yates 2007).

117. Dorsoventral expansion at the symphyseal end of the dentary: absent (0); present (1). (Yates 2007).

118. Splenial foramen: absent (0); present and enclosed (1); present and open anteriorly (2). Ordered. (Yates 2007).

119. Splenial-angular joint: flattened sutured contact (0); synovial joint surface between tongue-like process of angular fitting in groove of the splenial (1). (Yates 2007).

120. A stout, triangular, medial process of the articular, behind the glenoid : present (0); absent (1). (Yates 2007).

121. Length of the retroarticular process: less than the depth of the mandible below the glenoid (0); greater than the depth of the mandible below the glenoid (2). (Yates 2007).

122. Strong medial embayment behind glenoid of the articular in dorsal view: absent (0); present (1). (Yates 2007).

123. Number of premaxillary teeth: four (0); more than four (1). (Yates 2007).

124. Premaxilla, crown height of the first tooth: significantly lower than most teeth in the row (0); at least as high as the tallest maxillary tooth (1). (Pretto et al. 2018).

125. Premaxillary teeth, serration in the mesial margin: (0) present; (1) absent. (Rowe 1989).

126. Number of dentary teeth (in adults): less than 18 (0); 18 or more (1). (Yates 2007).

127. Arrangement of teeth within the jaws: linearly placed, crowns not overlapping (0); imbricated with distal side of tooth overlapping mesial side of the succeeding tooth (1).

128. Orientation of the maxillary tooth crowns: erect (0); procumbent (1). (Yates 2007).

129. Orientation of the dentary tooth crowns: erect (0); procumbent (1). (Yates 2007).

130. Teeth with basally constricted crowns: absent (0); present (1). (Yates 2007).

131. Tooth-tooth occlusal wear facets : absent (0); present (1). (Yates 2007).

132. Mesial and distal serrations of the teeth: fine and set at right angles to the margin of the tooth (0); coarse and angled upwards at an angle of 45 degrees to the margin of the tooth (1). (Yates 2007).

133. Distribution of serrations on the maxillary and dentary teeth: present on both the mesial and distal carinae (0); absent on the posterior carinae (1); absent on both carinae (2). (Yates 2007).

134. Long axis of the tooth crowns distally recurved: present (0); absent (1). (Yates 2007).

135. Texture of the enamel surface: entirely smooth (0); finely wrinkled in some patches (1); extensively and coarsely wrinkled (2). Ordered. (Yates 2007).

136. Lingual concavities of the teeth: absent (0); present (1). (Yates 2007).

137. Longitudinal labial grooves on the teeth: absent (0); present (1). (Yates 2007).

138. Distribution of the serrations along the mesial and distal carinae of the tooth: extend along most of the length of the crown (0); restricted to the upper half of the crown (1). (Yates 2007).

139. Pterygoid teeth on palatal process: (0) present; (1) absent. (Rauhut 2003).

140. Number of cervical vertebrae: eight or fewer (0); 9-10 (1); 12-13 (2); more than 13 (3). Ordered. (Yates 2007).

141. Shallow, dorsally facing fossa on the atlantal neurapophysis bordered by a dorsally everted lateral margin: absent (0); present (1). (Yates 2007).

142. Width of axial intercentrum: less than width of axial centrum (0); greater than width of axial centrum (1). (Yates 2007).

143. Position of axial prezygapophyses: on the anterolateral surface of the neural arch (0); mounted on anteriorly projecting pedicels (1). (Yates 2007).

144. Posterior margin of the axial postzygapophyses: overhang the axial centrum (0); flush with the caudal face of the axial centrum (1). (Yates 2007).

145. Length of the axial centrum: less than three times the height of the centrum (0); at least three times the height of the centrum (1). (Yates 2007).

146. Axis, dorsal margin of the neural spine: (0) expanded caudodorsally; (1) arcs dorsally where the cranial portion height is equivalent to the caudal height. (Nesbitt 2011).

147. Length of the anterior cervical centra (cervicals 3-5): no more than the length of the axial centrum (0); greater than the length of the axial centrum (1). (Yates 2007).

148. Length of middle to posterior cervical centra (cervical 6-8): no more than the length of the axial centrum (0); greater than the length of the axial centrum (1). (Yates 2007).

149. Dorsal excavation of the cervical parapophyses: absent (0); present (1). (Yates 2007).

150. Lateral compression of the anterior cervical vertebrae: centra are no higher than they are wide (0); are approximately 1.25 times higher than wide (1). (Yates 2007).

151. Relative elongation of the anterior cervical centra (cervical 3-5): lengths of the centra are less than 2.5 times the height of their anterior faces (0); lengths are 2.5-4

times the height of their anterior faces (1); the length of at least cervical 4 or 5 exceeds 4 times the anterior centrum height (2). Ordered. (Yates 2007).

152. Ventral keels on cranial cervical centra: present (0); absent (1). (Yates 2007).

153. Height of the mid cervical neural arches: no more than the height of the posterior centrum face (0); greater than the height of the posterior centrum face (1). (Yates 2007).

154. Orientation of the anterior-to-middle cervical postzygapophyses: (0) planar (minimally offset) with respect to the prezygapophyses; (1) dorsally raised roughly 20° relative to the coronal plane; (2) and dorsally raised at least 30° or more relative to the coronal plane. Ordered. (McPhee & Choiniere 2017).

155. Cervical epipophyses on the dorsal surface of the postzygapophyses: absent (0); present on at least some cervical vertebrae (1). (Yates 2007).

156. Posterior ends of the anterior, postaxial epipophyses: with a free pointed tip (0); joined to the postzygapophysis along their entire length (1). (Yates 2007).

157. Shape of the epipophyses: tall ridges (0); flattened, horizontal plates (1). (Yates 2007).

158. Epipophyses overhanging the rear margin of the postzygapophyses: absent (0); present in at least some postaxial cervical vertebrae (1). (Yates 2007).

159. Anterior spur-like projections on mid-cervical neural spines: absent (0); present (1). (Yates 2007).

160. Shape of mid-cervical neural spines: less than twice as long as high (0); at least twice as long as high (1). (Yates 2007).

161. Cervical vertebrae, deep recesses on the cranial face of the neural arch lateral to the neural canal: (0) absent; (1) present. (Nesbitt 2011).

162. Cervical vertebrae, pneumatic features (=pleurocoels) in the anterior portion of the centrum: absent (0); present (1). (Nesbitt 2011).

163. Shape of cervical rib shafts: short and posteroventrally directed (0); longer than the length of their centra and extending parallel to cervical column (1). (Yates 2007).

164. Position of the base of the cervical rib shaft: level with, or higher than the ventral margin of the cervical centrum (0); located below the ventral margin due to a ventrally extended parapophysis (1). (Yates 2007).

165. Postzygodiapophyseal lamina in cervical neural arches 4-8: present (0); absent (1).

166. Laminae of the cervical neural arches 4-8: well-developed tall laminae (0); weakly developed low ridges (1). (Yates 2007).

167. Shape of anterior centrum face in cervical centra: concave (0); flat (1); convex (2). Ordered. (Yates 2007).

168. Ventral surface of the centra in the cervicodorsal transition: transversely rounded (0); with longitudinal keels (1). (Yates 2007).

169. Number of vertebrae between cervicodorsal transition and primordial sacral vertebrae: 15-16 (0); no more than 14 (1). (Yates 2007).

170. Lateral surfaces of the dorsal centra: with at most vague, shallow depressions (0); with deep fossae that approach the midline (1); with invasive, sharp-rimmed pleurocoels (2). Ordered. (Yates 2007).

171. Oblique ridge dividing pleural fossa of cervical vertebrae: absent (0); present (1). (Yates 2007).

172. Laterally expanded tables at the midlength of the dorsal surface of the neural spines: absent in all vertebrae (0); present on the pectoral vertebrae (1); present on the pectoral and cervical vertebrae (2). Ordered. (Yates 2007).

173. Dorsal centra: entirely amphicoelous to amphiplatyan (1); first two dorsals are opisthocoelous (1); cranial half of dorsal column is opisthocoelous (2). Ordered. (Yates 2007).

174. Shape of the posterior dorsal centra: relatively elongated for their size (0); strongly axially compressed for their size (1). (Yates 2007).

175. Laminae bounding triangular infradiapophyseal fossae (chonae) on dorsal neural arches: absent (0); present (1). (Yates 2007).

176. Location of parapophysis in first two dorsals: at the anterior end of the centrum (0); located at the mid-length of the centrum, within the middle chonos (1). (Yates 2007).

177. Parapophyses of the dorsal column completely shift from the centrum to the neural arch: anterior to the thirteenth presacral vertebra (0); posterior to the thirteenth presacral vertebra (1). (Yates 2007).

178. Orientation of the transverse processes of the dorsal vertebrae: most horizontally directed (0); all upwardly directed (1). (Yates 2007).

179. Contribution of the paradiapophyseal lamina to the margin of the anterior chonos in mid-dorsal vertebrae: present (0); prevented by high placement of parapophysis (1). (Yates 2007).

180. Hyposphenes in the dorsal vertebrae: absent (0); present but less than the height of the neural canal (1); present and equal to the height of the neural canal (2). Ordered. (Yates 2007).

181. Prezygodiapophyseal lamina and associated anterior triangular fossa (anterior infradiapophyseal fossa): present on all dorsals (0); absent in mid-dorsals (1). (Yates 2007).

182. Anterior centroparapophyseal lamina in dorsal vertebrae: absent (0); present (1). (Yates 2007).

183. Prezygoparapophyseal lamina in dorsal vertebrae: absent (0); present (1). (Yates 2007).

184. Accessory lamina dividing posterior chonos from postzygapophysis: absent (0); present (1). (Yates 2007).

185. Pneumatic excavation of the dorsal neural arches: absent (0); equivocal (e.g., no more than depressions within the infradiapophyseal chambers) (1); sharp-rimmed subfossae or foramina clearly invading bone surface (2). Ordered. (Yates 2007).

186. Separation of lateral surfaces of anterior dorsal neural arches under transverse processes: widely spaced (0); only separated by a thin midline septum (1). (Yates 2007).

187. Height of dorsal neural arches, from neurocentral suture to level of zygapophyseal facets: much less than height of centrum (0); subequal to or greater than height of centrum (1). (Yates 2007).

188. Form of anterior surface of neural arch: simple centroprezygopophyseal ridge (0); broad anteriorly facing surface bounded laterally by centroprezygopophyseal lamina (1). (Yates 2007).

189. Shape of posterior dorsal neural canal: subcircular (0); slit-shaped (1). (Yates 2007).

190. Height of middle dorsal neural spines: less than the length of the base (0); higher than the length of the base but less than 1.5 times the length of the base (1); greater than 1.5 times the length of the base (2). Ordered. (Yates 2007).

191. Shape of anterior dorsal neural spines: lateral margins parallel in anterior view (0); transversely expanding towards dorsal end (2). (Yates 2007).

192. Cross-sectional shape of dorsal neural spines: transversely compressed (0); broad and triangular (1); square-shaped in posterior vertebrae (2). Ordered. (Yates 2007).

193. Spinodiapophyseal lamina on dorsal vertebrae: absent (0); present and separated from spinopostzygapophyseal lamina (1); present and joining spinopostzygapophyseal lamina to create a composite posterolateral spinal lamina (2). Ordered. (Yates 2007).

194. Well-developed, sheet-like suprapostzygapophyseal laminae: absent (0); present on at least the caudal dorsal vertebrae (2). (Yates 2007).

195. Shape of the spinopostzygapophyseal lamina in middle and posterior dorsal vertebrae: singular (0); bifurcated at its distal end. (Yates 2007).

196. Shape of posterior margin of middle dorsal neural spines in lateral view: approximately straight (0); concave with a projecting posterodorsal corner (1). (Yates 2007).

197. Transversely expanded plate-like summits of posterior dorsal neural spines: absent (0); present (1). (Yates 2007).

198. Last presacral rib: free (0); fused to vertebra (1). (Yates 2007).

199. Sacral rib much narrower than the transverse process of the first primordial sacral vertebra (and dorsosacral if present) in dorsal view: absent (0); present (1). (Yates 2007).

200. Number of dorsosacral vertebrae: none (0); one (1); two (2). Ordered. (Yates 2007).

201. Caudosacral vertebra: absent (0); present (1). (Yates 2007).

202. Shape of the iliac articular facets of the first primordial sacral rib: singular (0); divided into dorsal and ventral facets separated by a non-articulating gap (1). (Yates 2007).

203. Deep, medially-directed pit excavating the surface of the non-articulating gap of the first primordial sacral rib: absent (0); present (1). (Yates 2007).

204. Depth of the iliac articular surface of the primordial sacrals: less than 0.75 of the depth of the ilium (0); greater than 0.75 of the depth of the ilium (1). (Yates 2007).

205. Sacral ribs contributing to the rim of the acetabulum: absent (0); present (1). (Yates 2007).

206. Posterior and anterior expansion of the transverse processes of the first and second primordial sacral vertebrae, respectively, partly roofing the intercostal space: absent (0); present (1). (Yates 2007).

207. Length of first caudal centrum: longer anteroposteriorly than dorsoventrally tall (0); taller than long (1); highly compressed (dorsoventral height at least twice anteroposterior length). Ordered. (Yates 2007).

208. Position of postzygapophyses in proximal caudal vertebrae: protruding with an interpostzygapophyseal notch visible in dorsal view (0); placed on either side of the caudal end of the base of the neural spine without any interpostzygapophyseal notch (1). (Yates 2007).

209. A hyposphenal ridge on caudal vertebrae: absent (0); present (1). (Yates 2007).

210. Prezygadiapophyseal laminae on anterior caudals: absent (0); present (1). (McPhee et al. 2015).

211. Depth of the bases of the proximal caudal transverse processes: shallow, restricted to the neural arches (0); deep, extending from the centrum to the neural arch (1). (Yates 2007).

212. Position of last caudal vertebra with a protruding transverse process: distal to caudal 16 (0); proximal to caudal 16 (1). (Yates 2007).

213. Orientation of posterior margin of proximal caudal neural spines: sloping posterodorsally (0); vertical (1). (Yates 2007).

214. Longitudinal ventral sulcus on proximal and middle caudal vertebrae: present (0); absent (1). (Yates 2007).

215. Length of midcaudal centra: greater than twice the height of their anterior faces (0); less than twice the height of their anterior faces (1). (Yates 2007).

216. Cross-sectional shape of the distal caudal centra: oval with rounded lateral and ventral sides (0); square-shaped with flattened lateral and ventral sides (1). (Yates 2007).

217. Length of distal caudal prezygapophyses: short, not overlapping the preceding centrum by more than a quarter (0); long and overlapping the preceding the centrum by more than a quarter (1). (Yates 2007).

218. Shape of the terminal caudal vertebrae: unfused, size decreasing toward tip (0); expanded and fused to form a club-shaped tail (1). (Yates 2007).

219. 'Weaponized' dermal spikes on tail: absent (0); present (1). (McPhee et al. 2015).

220. Length of the longest chevron: less than twice the length of the preceding centrum (0); greater than twice the length of the preceding centrum (1). (Yates 2007).

221. Anteroventral process on distal chevrons: absent (0); present (1). (Yates 2007).

222. Mid-caudal chevrons with a ventral slit: absent (0); present (1). (Yates 2007).

223. Longitudinal ridge on the dorsal surface of the sterna plate: absent (0); present (1). (Yates 2007).

224. Craniocaudal length of the acromion process of the scapula: less than 1.5 times the minimum width of the scapula blade (0); greater than 1.5 times the minimum width of the scapula blade (1). (Yates 2007).

225. Minimum width of the scapula: greater than 20 per cent of its length (0); less than 20 per cent of its length (1). (Yates 2007).

226. Caudal margin of the acromion process of the scapula: rises from the blade at angle that is less than 65 degrees from the long axis of the scapula, at its steepest point

(0); rises from the blade at angle that is greater than 65 degrees from the long axis of the scapula, at its steepest point (1). (Yates 2007).

227. Ventromedial ridge of scapula: absent (0) or present (1). (Otero & Pol 2013).

228. Width of dorsal expansion of the scapula: less than the width of the ventral end of the scapula (0); equal to the width of the ventral end of the scapula (1). (Yates 2007).

229. Flat caudoventrally facing surface on the coracoids between glenoid and coracoid tubercle: absent (0); present (1). (Yates 2007).

230. Coracoid tubercle: present (0); absent (1). (Yates 2007).

231. Length of the humerus: less than 55 per cent of the length of the femur (0); 55-65 per cent of the length of the femur (1); 65-70 per cent of the length of the femur (2); more than 70 per cent of the length of the femur (3). Ordered. (Yates 2007).

232. Shape of the humeral head: weakly developed, rounded in anterior-posterior view but minimally expanded perpendicular to the latter axis (0); flat in anterior-posterior view with only a slightly expanded lateral component (1); domed, being convex/hemispherical in anterior-posterior view with a strong lateral incursion onto the humeral shaft (2). (McPhee et al. 2018).

233. Shape of the deltopectoral crest: subtriangular (0); subrectangular (1). (Yates 2007).

234. Length of the deltopectoral crest of the humerus: less than 30 per cent of the length of the humerus (0); 30-50 per cent of the length of the humerus (1); greater than 50 per cent of the length of the humerus (2). Ordered. (Yates 2007).

235. Shape of the anterolateral margin of the deltopectoral crest of the humerus: straight (0); strongly sinuous (1). (Yates 2007);

236. Rugose pit centrally located on the lateral surface of the deltopectoral crest: absent (0); present (1). (Yates 2007).

237. Well-defined fossa on the distal flexor surface of the humerus: present (0); absent (1). (Yates 2007).

238. Transverse width of the distal humerus: less than 33 per cent of the length of the humerus (0); greater than 33 per cent of the length of the humerus (1). (Yates 2007).

239. Shape of the entepicondyle of the distal humerus: rounded process (0): with a flat distomedially facing surface bounded by a sharp proximal margin (1). (Yates 2007).

240. Length of the radius: greater than 80 per cent of the humerus (0); less than 80 per cent of the humerus (1). (Yates 2007).

241. Radial fossa on the anterolateral corner of the proximal ulna: absent (0); present, but only shallowly defined (1); a well-defined recess, deeper than transverse width of the anterior end of the anterior process (2). Ordered (Yates 2007).

242. Caudodistal tubercle of the radius: absent (0) or present (1). (Otero et al. 2015).

243. Biceps tubercle of the radius: absent (0) or present (1). (Otero et al. 2015).

244. Olecranon process on proximal ulna: present (0); absent (1); greatly enlarged olecranon (2). (Yates 2007).

245. Maximum linear dimensions of the ulnare and radiale: exceed that of at least one of the first three distal carpals (0); less than any of the distal carpals (1). (Yates 2007).

246. Transverse width of the first distal carpal: less than 120 per cent of the transverse width of the second distal carpal (0); greater than 120 per cent of the transverse width of the second distal carpal (1). (Yates 2007).

247. Sulcus across the medial end of the first distal carpal: absent (0); present (1). (Yates 2007).

248. Lateral end of first distal carpal: abuts second distal carpal (0); overlaps second distal carpal (1). (Yates 2007).

249. Second distal carpal: completely covers the proximal end of the second metacarpal (0); does not completely cover the proximal end of the second metacarpal (1). (Yates 2007).

250. Ossification of the fifth distal carpal: present (0); absent (1). (Yates 2007).

251. Length of the manus: less than 38 per cent of the humerus + radius (0); 38-45 per cent of the humerus + radius (1); greater than 45 per cent of the humerus + radius (2). Ordered. (Yates 2007).

252. Shape of metacarpus: flattened to gently curved and spreading (0); a colonnade of subparallel metacarpals tightly curved into a U-shape (1). (Yates 2007).

253. Proximal width of first metacarpal: less than the proximal width of the second metacarpal (0); greater than the proximal width of the second metacarpal (1). (Yates 2007).

254. Minimum transverse shaft width of first metacarpal: less than twice the minimum transverse shaft width of second metacarpal (0); greater than twice the minimum transverse shaft width of second metacarpal (1). (Yates 2007).

255. Proximal end of first metacarpal: flush with other metacarpals (0); inset into the carpus (1). (Yates 2007).

256. Shape of the first metacarpal: proximal width less than 65 per cent of its length (0); proximal width 65-80 per cent of its length (1); proximal width 80-100 per cent of its length (2); greater than 100 per cent of its length (3). Ordered. (Yates 2007).

257. Ventromedial margin of first metacarpal: poorly concave (0) or deeply concave (1). (Otero et al. 2015).

258. Strong asymmetry in the lateral and medial distal condyles of the first metacarpal: absent (0); present (1). (Yates 2007).

259. Deep distal extensor pits on the second and third metacarpals: absent (0); present (1). (Yates 2007).

260. Shape of the distal ends of second and third metacarpals: subrectangular in distal view (0); trapezoidal with flexor rims of distal collateral ligament pits flaring beyond extensor rims (1). (Yates 2007).

261. Shape of the fifth metacarpal: longer than wide at the proximal end with a flat proximal surface (0); almost as wide as it is long with a strongly convex proximal articulation surface (1). (Yates 2007).

262. Length of the fifth metacarpal: less than 75 per cent of the length of the third metacarpal (0); greater than 75 per cent of the length of the third metacarpal (1). (Yates 2007).

263. Length of manual digit one: less than the length of manual digit two (0); greater than the length of manual digit two (1). (Yates 2007).

264. Ventrolateral twisting of the transverse axis of the distal end of the first phalanx of manual digit one relative to its proximal end: absent (0); present but much less than 60 degrees (1); 60 degrees (2). Ordered. (Yates 2007).

265. Length of the first phalanx of manual digit one: less than the length of the first metacarpal (0); greater than the length of the first metacarpal (1). (Yates 2007).

266. Length of first phalanx of manual digit 1: much greater than (0), subequal or equal to (1), or much less than (2), its mediolateral width at proximal end. (Otero et al. 2015).

267. Shape of the proximal articular surface of the first phalanx of manual digit one: rounded (0); with an embayment on the medial side (1). (Yates 2007).

268. Shape of the first phalanx of manual digit one: elongate and subcylindrical (0); strongly proximodistally compressed and wedge-shaped (1). (Yates 2007).

269. Length of the penultimate phalanx of manual digit two: less than the length of the second metacarpal (0); greater than the length of the second metacarpal (1). (Yates 2007).

270. Length of the penultimate phalanx of manual digit three: less than the length of the third metacarpal (0); greater than the length of the third metacarpal (1). (Yates 2007).

271. Shape of non-terminal phalanges of manual digits two and three: longer than wide (0); as long as wide (1). (Yates 2007).

272. Shape of the unguals of manual digits two and three: straight (0); strongly curved with tips projecting well below flexor margin of proximal articular surface (1). (Yates 2007).

273. Length of the ungual of manual digit two: greater than the length of the ungual of manual digit one (0); 75-100 per cent of the ungual of manual digit one (1); less than 75 per cent of the ungual of manual digit one (2); the ungual of manual digit two is absent (3). Ordered. (Yates 2007).

274. Phalangeal formula of manual digits two and three: three and four, respectively (0); with at least one phalanx missing from each digit (1). (Yates 2007).

275. Phalangeal formula of manual digits four and five: greater than 2-0, respectively (0); less than 2-0, respectively (1). (Yates 2007).

276. Strongly convex dorsal margin of the ilium: absent (0); present (1). (Yates 2007).

277. Cranial extent of preacetabular process of ilium: does not project further anterior than the anterior margin of the pubic peduncle (0); projects anterior to the cranial margin of the pubic peduncle (1). (Yates 2007).

278. Buttress between preacetabular process and the supraacetabular crest of the ilium: present (0); absent (1). (Yates 2007).

279. Shape of the preacetabular process: blunt and rectangular (0); with a pointed, projecting anteroventral corner and a rounded dorsum (1). (Yates 2007).

280. Depth of the preacetabular process of the ilium: much less than the depth of the ilium above the acetabulum (0); subequal to the depth of the ilium above the acetabulum (1). (Yates 2007).

281. Length of preacetabular process of the ilium: less than twice its depth (0); greater than twice its depth (1). (Yates 2007).

282. Medial wall of acetabulum: fully closing acetabulum with a triangular ventral process between the pubic and ischial peduncles (0); partially open acetabulum with a straight ventral margin between the peduncles (1); partially open acetabulum with a concave ventralmargin between the peduncles (2); fully open acetabulum with medial ventral margin closely approximating lateral rim of acetabulum (3). Ordered. (Yates 2007).

283. Length of the pubic peduncle of the ilium: less than twice the anteroposterior width of its distal end (0); greater than twice the anteroposterior width of its distal end (1). (Yates 2007).

284. Caudally projecting ‘heel’ at the distal end of the ischial peduncle: absent (0); present (1). (Yates 2007).

285. Length of the ischial peduncle of the ilium: similar to pubic peduncle (0); much shorter than pubic peduncle (1); virtually absent so that the chord connecting the distal end of the pubic peduncle with the ischial articular surface contacts the postacetabular process (2). Ordered. (Yates 2007).

286. Length of the postacetabular process of the ilium: between 40 and 100 per cent of the distance between the pubic and ischial peduncles (0); less than 40 per cent of the distance between the pubic and ischial peduncles (1); more than 100 per cent of the distance between the pubic and ischial peduncles (2). (Yates 2007).

287. Well-developed brevis fossa with sharp margins on the ventral surface of the postacetabular process of the ilium: absent (0); present, ventrally facing (1); present, lateroventrally facing (2). (Yates 2007).

288. Anterior end of ventrolateral ridge bounding brevis fossa: not connected to supracetabular crest (0); joining supracetabular crest (1). (Yates 2007).

289. Shape of the caudal margin of the postacetabular process of the ilium: rounded to bluntly pointed (0); square ended (1); with a pointed ventral corner and a rounded caudodorsal margin (2). (Yates 2007).

290. Width of the conjoined pubes: less than 75 per cent of their length (0); greater than 75 per cent of their length (1). (Yates 2007).

291. Pubic tubercle on the lateral surface of the proximal pubis: present (0); absent (1).

292. Proximal anterior profile of pubis: anterior margin of pubic apron smoothly confluent with anterior margin of iliac pedicel (0); iliac pedicel set anterior to the pubic apron creating a prominent inflection in the proximal anterior profile of the pubis (1). (Yates 2007).

293. Minimum transverse width of the pubic apron: much more than 40 per cent of the width across the iliac peduncles of the ilium (0); less than 40 per cent of the width across the iliac peduncles of the ilium (1). (Yates 2007).

294. Position of the obturator foramen of the pubis: at least partially occluded by the iliac pedicel in anterior view (0); completely visible in anterior view (1). (Yates 2007).

295. Lateral margins of the pubic apron in anterior view: straight (0); concave (1). (Yates 2007).

296. Anterior fossa on the proximal region of the pubic apron: absent (0) or present (1). (Apaldetti et al. 2013).

297. Orientation of distal third of the blades of the pubic apron: confluent with the proximal part of the pubic apron (0); twisted posterolaterally relative to proximal section so that the anterior surface turns to face laterally (1). (Yates 2007).

298. Orientation of the entire blades of the pubic apron: transverse (0); twisted posteromedially (1). (Yates 2007).

299. Anteroposterior expansion of the distal pubis: absent (0); less than 15 per cent of the length of the pubis (1); greater than 15 per cent of the length of the pubis (2). Ordered. (Yates 2007).

300. Elongate interischial fenestra: absent (0); present (1). (Yates 2007).

301. Longitudinal dorsolateral sulcus on proximal ischium: absent (0); present (1). (Yates 2007).

302. Shape of distal ischium: broad and plate-like, not distinct from obturator region (0); with a discrete rod-like distal shaft (1). (Yates 2007).

303. Length of ischium: less than that of the pubis (0); greater than that of the pubis (1). (Yates 2007).

304. Notch separating posteroventral end of the ischial obturator plate from the ischial shaft: present (0); absent (1). (Yates 2007).

305. Ischial component of acetabular rim: larger than the pubic component (0); equal to the pubic component (1) (Yates 2007).

306. Shape of the transverse section of the ischial shaft: ovoid to subrectangular (0); triangular (1). (Yates 2007).

307. Orientation of the long axes of the transverse section of the distal ischia: meet at an angle (0); are coplanar (1). (Yates 2007).

308. Depth of the transverse section of the ischial shaft: much less than the transverse width of the section (0); at least as great as the transverse width of the section (1). (Yates 2007).

309. Distal ischial expansion: absent (0); present (1). (Yates 2007).

310. Transverse width of the conjoined distal ischial expansions: greater than their sagittal depth (0); less than their sagittal depth (1). (Yates 2007).

311. Length of the hindlimb: greater than the length of the trunk (0); less than the length of the trunk (1). (Yates 2007).

312. Longitudinal axis of the femur in lateral view: strongly bent with an offset between the proximal and distal axes greater than 15 degrees (0); weakly bent with an offset of less than 10 degrees (1); straight (2). Ordered. (Yates 2007).

313. Shape of the cross-section of the mid-shaft of the femur: subcircular (0); strongly elliptical with the long axis orientated mediolaterally (1). (Yates 2007).

314. Angle between the long axis of the femoral head and the transverse axis of the distal femur: about 30 degrees (0); close to 0 degrees (1). (Yates 2007).

315. Shape of femoral head: roughly rectangular in profile with a sharp medial distal corner (0); roughly hemispherical with no sharp medial distal corner (1). This character only applies to taxa with a medially, or anteromedially protruding femoral head. It does not apply tooutgroup taxa (*Euparkeria* or Crurotarsi) with proximally directed femoral heads and is coded as unknown in these taxa. (Yates 2007).

316. Posterior proximal tubercle on femur: well-developed (0); indistinct to absent (1). (Yates 2007).

317. Shape of the lesser trochanter: small rounded tubercle (0); proximodistally orientated, elongate ridge (1); absent (2). (Yates 2007).

318. Position of proximal tip of lesser trochanter: level with the femoral head (0); distal to the femoral head (1). (Yates 2007).

319. Projection of the lesser trochanter: just a scar upon the femoral surface (0); a raised process (1). (Yates 2007).

320. Transverse ridge extending laterally from the lesser trochanter: absent (0); present (1). (Yates 2007).

321. Height of the lesser trochanter in cross section: less than its basal width (0); at least as high as its basal width (1). (Yates 2007).

322. Position of the lesser trochanter in anterior view: near the centre of the anterior face of the femoral shaft (0); close to the lateral margin of the femoral shaft (1). (Yates 2007).

323. Visibility of the lesser trochanter in posterior view: not visible (0); visible (1). (Yates 2007).

324. Height of the fourth trochanter: a low rugose ridge (0); a tall crest (1). (Yates 2007).

325. Position of the fourth trochanter along the length of the femur: in the proximal half (0); straddling the midpoint (1). (Yates 2007).

326. Symmetry of the profile of the fourth trochanter of the femur: subsymmetrical without a sharp distal corner (0); asymmetrical with a steeper distal slope than the proximal slope and a distinct distal corner (1). (Yates 2007).

327. Shape of the profile of the fourth trochanter of the femur: rounded (0); subrectangular (1). (Yates 2007).

328. Position of fourth trochanter along the mediolateral axis of the femur: centrally located (0); on the medial margin (1). (Yates 2007).

329. Extensor depression on anterior surface of the distal end of the femur: absent (0); present (1). (Yates 2007).

330. Size of the medial condyle of the distal femur: subequal to the fibular + lateral condyles (0); larger than the fibular + lateral condyles (1). (Yates 2007).

331. Femoral distal transverse width: equal or lesser (0); greater (1) than 1·4 times its largest anteroposterior depth across the fibular condyle. (Novas et al. 2011).

332. Well-developed tibiofibular crest on distal femur: absent (0); present (1). (Smith & Pol 2007).

333. Distal surface of tibiofibular crest: as deep anteroposteriorly as wide mediolaterally or deeper (0); wider mediolaterally than deep anteroposteriorly (1). (Smith & Pol 2007).

334. Tibia:femur length ratio: greater than 1.0 (0); between 0.6 and 1.0 (1); less than 0.6 (2). Ordered. (Yates 2007).

335. Orientation of cnemial crest: projects anteriorly to anterolaterally (0); projecting laterally (1). (Yates 2007).

336. Paramarginal ridge on lateral surface of cnemial crest: absent (0); present (1). (Yates 2007).

337. Position of the tallest point of the cnemial crest: close to the proximal end of the crest (0); about half-way along the length of the crest, creating an anterodorsally sloping proximal margin of the crest (1). (Yates 2007).

338. Proximal end of tibia with a flange of bone that contacts the fibula: absent (0): present (1). (Yates 2007).

339. Position of the posterior end of the fibular condyle on the proximal articular surface tibia: anterior to the posterior margin of the proximal articular surface (0); level with the posterior margin of the proximal articularsurface (1). (Yates 2007).

340. Shape of the proximal articular surface of the tibia: transverse width subequal to anteroposterior length (0); transverse width between 0.6 and 0.9 times anteroposterior length (1); anteroposterior length twice the transverse width or higher (2). Ordered. (Yates 2007).

341. Transverse width of the distal tibia: subequal to its craniocaudal length (0); greater than its craniocaudal length (1). (Yates 2007).

342. Anteroposterior width of the lateral side of the distal articular surface of the tibia: as wide as the anteroposterior width of the medial side (0); narrower than the anteroposterior width of the medial side (1). (Yates 2007).

343. Relationship of the posterolateral process of the distal end of the tibia with the fibula: not flaring laterally and not making significant contact with the fibula (0); flaring laterally and backing the fibula (1). (Yates 2007).

344. Shape of the distal articular end of the tibia in distal view: ovoid (0); subrectangular (1). (Yates 2007).

345. Shape of the anteromedial corner of the distal articular surface of the tibia: forming a right angle (0); forming an acute angle (1). (Yates 2007).

346. Position of the lateral margin of descending caudoventral process of the distal end of the tibia: protrudes laterally at least as far as the anterolateral corner of the distal tibia (0); set well back from the anterolateralcorner of the distal tibia (1). (Yates 2007).

347. A triangular rugose area on the medial side of the fibula: absent (0); present (1). (Yates 2007).

348. Transverse width of the midshaft of the fibula: greater than 0.75 of the transverse width of the midshaft of the tibia (0); between 0.5 and 0.75 of the transverse width of the midshaft of the tibia (1); less than 0.5 of thetransverse width of the midshaft of the tibia (2). Ordered. (Yates 2007).

349. Proximal end of the tibia with a transverse/anteroposterior length ratio: narrow (ratio less than 0.7) (0) or broad (more than 0.7) (1) (Apaldetti et al. 2013).

350. Position of fibula trochanter: on anterior surface of fibula (0); laterally facing (1); anteriorly facing but with strong lateral bulge (2). (Yates 2007).

351. Depth of the medial end of the astragalar body in cranial view: roughly equal to the lateral end (0); much shallower creating a wedge-shaped astragalar body (1). (Yates 2007).

352. Shape of the posteromedial margin of the astragalus in dorsal view: forming a moderately sharp corner of a subrectangular astragalus (0); evenly rounded without formation of a caudomedial corner (1). (Yates 2007).

353. Dorsally facing horizontal shelf forming part of the fibular facet of the astragalus: present (0); absent with a largely vertical fibular facet (1). (Yates 2007).

354. Pyramidal dorsal process on the posteromedial corner of the astragalus: absent (0); present (1). (Yates 2007).

355. Shape of the ascending process of the astragalus: anteroposteriorly deeper than transversely wide (0); transversely wider than anteroposteriorly deep (1). (Yates 2007).

356. Astragalus with medial condyle anteroposterior depth: less (0); equal or more (1) than 1·6 times the depth of the lateral condyle. (Novas et al. 2011).

357. Posterior margin of astragalus: straight (0) or convex (1). (Otero & Pol 2013).

358. Mediolateral surface of distal astragalus straight (0), concave (1), or convex (0). (Otero & Pol 2013).

359. Posterior extent of ascending process of the astragalus: positioned anteriorly upon the astragalus (0); close to the posterior margin of the astragalus (1). (Yates 2007).

360. Sharp medial margin around the depression posterior to the ascending process of the astragalus: absent (0); present (1). (Yates 2007).

361. Buttress dividing posterior fossa of astragalus and supporting ascending process: absent (0); present (1). (Yates 2007).

362. Vascular foramina set in a fossa at the base of the ascending process of the astragalus: present (0); absent (1). (Yates 2007).

363. Distal articular surface of astragalus: relatively flat or weakly convex (0); extremely convex and roller-shaped (1). (Smith & Pol 2007).

364. Transverse width of the calcaneum: greater than 30 per cent of the transverse width of the astragalus (0); less than 30 per cent of the transverse width of the astragalus (1). (Yates 2007).

365. Lateral surface of calcaneum: simple (0); with a fossa (1). (Yates 2007).

366. Medial peg of calcaneum fitting into astragalus: present, even if rudimentary (0); absent (1). (Yates 2007).

367. Calcaneal tuber: large and well developed (0); highly reduced to absent (1). (Yates 2007).

368. Shape of posteromedial heel of distal tarsal four (lateral distal tarsal): proximodistally deepest part of the bone (0); no deeper than the rest of the bone (1). (Yates 2007).

369. Shape of posteromedial process of distal tarsal four in proximal view: rounded (0); pointed (1). (Yates 2007).

370. Ossified distal tarsals: present (0); absent (1). (Yates 2007).

371. Proximal width of the first metatarsal: less than the proximal width of the second metatarsal (0); at least as great as the proximal width of the second metatarsal (1). (Yates 2007).

372. Size of first metatarsal: maximum proximal breadth less than 0.4 times its proximodistal length (0); maximum proximal breadth between 0.4 and 0.7 times its proximodistal length (1); maximum proximal breadth greater than 0.7times its proximodistal length (2). Ordered. (Yates 2007).

373. Orientation of proximal articular surface of metatarsal one: horizontal (0); sloping proximolaterally relative to the long axis of the bone (1). (Yates 2007).

374. Shaft of metatarsal I: closely appressed to metatarsal II throughout its length (0); only closely appressed proximally, with a space between metatarsals I and II distally (1). (Smith & Pol 2007).

375. Orientation of the transverse axis of the distal end of metatarsal one: horizontal (0); angled proximomedially (1). (Yates 2007).

376. Shape of the medial margin of the proximal surface of the second metatarsal: straight (0); concave (1). (Yates 2007).

377. Shape of the lateral margin of the proximal surface of the second metatarsal: straight (0); concave (1). (Yates 2007).

378. Projection of ventral flange on proximal surface of second metatarsal: neither corner appreciably more developed than the other (0); laterally flaring (1); medially flaring (2). (Smith & Pol 2007).

379. Well-developed facet on proximolateral corner of plantar ventrolateral flange of mt II for articulation with medial distal tarsal: absent (0); present (1). (Smith & Pol 2007).

380. Length of the third metatarsal: greater than 40 per cent of the length of the tibia (0); less than 40 per cent of the length of the tibia (1). (Yates 2007).

381. Proximal outline of metatarsal III: subtriangular with acute or rounded posterior border (0); subtrapezoidal, with posterior border broadly exposed in plantar view (1). (Smith & Pol 2007).

382. Minimum transverse shaft diameters of third and fourth metatarsals: greater than 60 per cent of the minimum transverse shaft diameter of the second metatarsal (0); less than 60 per cent of the minimum transverse shaft diameter ofthe second metatarsal (1). (Yates 2007).

383. Transverse width of the proximal end of the fourth metatarsal: less than twice the anteroposterior depth of the proximal end (0); at least twice the anteroposterior depth of the proximal end (1). (Yates 2007).

384. Angle formed by the anterior and anteromedial borders of metatarsal IV: obtuse (0); right angle, or acute (1). (Smith & Pol 2007).

385. Transverse width of the proximal end of the fifth metatarsal: less than 25 percent of the length of the fifth metatarsal (0); between 30 and 49 percent of the length of the fifth metatarsa (1); greater than 50 percent of the length of the fifth metatarsal(2). Ordered. (Yates 2007).

386. Transverse width of distal articular surface of metatarsal four in distal view: greater than the anteroposterior depth (0); less than the anteroposterior depth (1) (Yates 2007).

387. Pedal digit five: reduced, non-weight bearing (0); large (fifth metatarsal at least 70 per cent of fourth metatarsal), robust and weight bearing (1). (Yates 2007).

388. Length of non-terminal pedal phalanges: all longer than wide (0); proximalmost phalanges longer than wide while more distal phalanges are as wide as long (1); all nonterminal phalanges are as wide, if not wider, than long (2). Ordered. (Yates 2007).

389. Division of the length of the first phalanx of the digit I of the foot (at the midpoint) by the maximum height of the proximal end: 2.4 or more (0); 2.3 or less (1). (Müller et al. 2017).

390. Length of the first phalanx of pedal digit one: greater than the length of the ungual of pedal digit one (0); less than the length of the ungual of pedal digit one (1). (Yates 2007).

391. Length of the ungual of pedal digit one: less than at least some non-terminal phalanges (0); longer than all non-terminal phalanges but shorter than first metatarsal (1); longer than the first metatarsal (2). Ordered. (Yates 2007).

392. Shape of the ungual of pedal digit one: shallow, pointed, with convex sides and a broad ventral surface (0); deep, abruptly tapering, with flattened sides and a narrow ventral surface (1). (Yates 2007).

393. Shape of proximal articular surface of pedal unguals: proximally facing, visible on medial and lateral sides (0); proximomedially facing and visible only in medial view, causing medial deflection of pedal unguals in articulation (1). (Yates 2007).

394. Penultimate phalanges of pedal digits two and three: well-developed (0); reduced discshaped elements if they are ossified at all (1). (Yates 2007).

395. Shape of the unguals of pedal digits two and three: dorsoventrally deep with a proximal articulating surface that is at least as deep as it is wide (0); dorsoventrally flattened with a proximal articulating surface that iswider than deep (1). (Yates 2007).

396. Length of the ungual of pedal digit two: greater than the length of the ungual of pedal digit one (0); between 90 and 100 per cent of the length of the ungual of pedal digit one (1); less than 90 per cent of the length of the ungual of pedal digit one (2). Ordered. (Yates 2007).

397. Size of the ungual of pedal digit three: greater than 85 per cent of the ungual of pedal digit two in all linear dimensions (0); less than 85 per cent of the ungual of pedal digit two in all linear dimensions (1). (Yates 2007).

398. Number of phalanges in pedal digit four: four (0); fewer than four (1). (Yates 2007).

399. Phalanges of pedal digit five: present (0); absent (1). (Yates 2007).

400. Presence of growth marks (LAGs and/or annuli) in the cortical bone: growth marks in the whole cortex (0); growth marks absent or only formed in the outer cortex (1). (Cerda et al. 2017).

401. Relative abundance of woven fibered (WFB) or parallel fibered bone (PFB) in the primary compact bone: (0) PFB>WFB; (1) WFB>PFB. (Cerda et al. 2017).

(f) Data matrix

Euparkeria
00000000?00000?000000000?000?10010000000000000000?000000000000010000
000000000100?000000??00?010000?00?000?000000000?10000000000000000000?
0000000000000???000000??000000000?00?0?00??000000000000000000000000?00?0?
????0????0000?00200000000000000??????000000000001?0??0?0000???001?000?0000
?0110000000000010000000000?02?000??01000000??1?000?100000?00000000?0???
0?0?0010??0000?0????0?00?1?10?0000000?00[01]0
Aardonyx
1101?00210?002?1?01?11?????1110?1011000??????1?010??0??110110???0?1???????
?1?0?????????0?????????????????????1??0?0?1?0?????1??1?00101011001??1???????00
10?0110100??101101?0000011?00110001000020000010?1100??0110000?01110?0?00
??????11??????????1110??00??????131101???1??10??10?????????????????111010?00
1011?0?10110?101?1111000011111000?1????????1101110??0???01?????????????012
01111[0 2]0?0010?0?2???00?0???0??
Adeopapposaurus
1001100210?00211?01?11?1101101111101000010110100001l0[01]11110111100010
00102001[01]00110101100011l001?1000010110100000l011[01]1010100111111110[
01]10011110011?1100200010010100101101100[01]00111001100000000000001001
10100010000000100000000000101010[12]211000101000011011110111101011002001
000001000[01]01003100000[02]0110110001?1100010110010001101000010[12]1010?
10000000111011001100l111?000100001110100001111000001020001110000110000
Anchisaurus
10???00??00102?1?0??11?????111011?010?001010?1?0001100?111?101100?10?????
?01?001101?1??0011?10????00010??????10?10?000?10001?0000101?11?01?11?001?
1???100?100111??1011?10000?010?001100?000??0000000??01000?0???000?00?10?0
????11[01]?0???2?1100101100?0??0??1101011010010020110000020000[01]010131000
00?1111100001011?000101001010110100001O[01]11101?0100000111011O?1??01?01
00?0???010111?0?0011????0?01?1?00?1000001001??
Antetonitrus
??
??0?[01]0???
???????????00?00?001??00[12]10002010121001000???1?????1??00?01100?0??0?000
01??3211000[01]011110??????0011?31100???10?10???????0001003???000201001000
01????????????[12]1101111001111111O??1100000210010101O0?????????????????
?121111120100?????[12]?1200?0??????
Arcusaurus
?0?1??0[12]1??0????????0?010?1????????????????????????0???????0?00?????????????
??????????????????????????????????0????0?01010?????0??11?0101010000?????????????
??00?????????????
?????0?0??0????????????????????????
??[1
2]????0?0??????
Bagualosaurus
10?1?00[12]??11?1[01]?100?1??????101?010?1000?10?10????0?100?10?????????????
??????????????????????????????????????0?0000010?????01110001010O0?00????????
?????????????????????????0??001??0?1???10?0?0000000?0??01??001???????0?0???0??
??0100011000202?00?00??0?

????????????000??0111000101110????100000?0?01??01?0?????????????????????0???1
????0?0??0110?????????????
Barapasaurus
??
??1?111211?????????????1?1????
?00????002??100101??00201102111120121100?0[12]10001?1?1?1??1????0????1010?
00?21???????2001????????????0?????????????????1111103101100011111000 11??11
?110010?????????????????????1????1?1?????????1??1?????000??1??????????20???????
??????????2?1????????
Blikanasaurus
??
??
??
??
????????????????????0000?1110111?10?0100101001111101110012011110 01?1112102?
120000100???
Buriolestes
0001?001??0100?110001110?1100100100100001001000000?10?1100110100001?000
01?01?00110101????1?100????0?0?0?????000000010100100001000000000000111?0
011100001010011?001011010000001000111011000000000000??01??0010???0???0?
0???????1?1?1121110000??0??0?????????????????????????????0010001100210 1?0?
??????1?11?00?0?1?10000101110001011000010000000 1??0????1000????0???????0??
?????000?????0??1?0??00???0????0???
Camelotia
??
??1??????
????????0??0??001??002100000000??00?0???????????1???0??011?????????????????
??1??????????1???00111?1
11011110111?1??1101???00000??[1
2]????000??????
Cetiosaurus
1??
??2??001?1110111011
0100??100020?2001?1??1020??1[12]11102010100???[12]??????20111?00100?0??011
11101032110010002 0?1???????1?????????????????????????1111103?0210?0110?1?001
1?110?1?00???211112??0???010?111???2101002100101110?????????????????????????
??????????????????????????
Chindesaurus
??
??0?????????
????????01?0??0?1??0?1??????000??00?????000????1?0?????1000?0?????????????????
??0???001??????00??????????????00
0010111000101110000??????11111100??0?01?110??0100?????????????????????????????
?????????????
Chromogisaurus
??
??
??10000??10?0??11?????????????????????
????0????????????????????????????????????0?1???11002102?????????????????????????0?

?????1???10110?????[01]00000[12]01010001?0??????????????????????????????????0
??0????000??????
Coloradisaurus
?00?1002??010??1?011111?1??1110??011000?10??0?0?10?100?110111100001001007
10100111110101001111007100001?????1?1001011010011???1000101010001171?00
?1100200010010100?01100?00?001?1001100000000000000101?????00?11000?011??
?0????0100010121110011?????????????????????1?????????????????01?0?31100???011?
1110020110001011000000110100001021110?1110000011101100?1?011110010?001?
?????000011111101010200071[0 1]0000210000
Crurotarsi
0000000000?000?0??[01]000000000?0001000000[01]000000?0000000?000?0000?000
000000000000000000?00000???[01]?01[01]00??000000000000000000000??000000000
0000?0000000000000000???00??00??000002000?00?0?00??000020000000000000000
0000000000000[01]00?0[01]0??002?0000000000?000000000000000000000001000000[
01]000010000?0000?0[01]000000000000000000000000?00?000000000000000?1?0000
[01]00000?00?00000?0???0?0000000000?00000000?00?0010?0000000000??
Efraasia
100?1001?0010??1?0?111?112?1110?100???00100100?000??0??10???01?0??1??????10
?00???????100?1111001?00??00??????10010010??11?011110010101000071???1??1
10011001001010010110100000017??001?000000000000000001?00000100000?011000
00?0?010?011201200011100101101012010?10100000110101000100001100310001010
0000100000011000101101000011110000101100001000000011101?0010?011010010?
0??01?11100000171??0?0?01?1?0011[01]00001000??
Eodromaeus
00????????0?????1?10??1????0000?00?0?1?????????????????1?????????????????????
??????????????????????????????????0?000???0?0?000000000000001?????????????0
?1?????11??????000??01??011?????????0?????1???10?????????????1?1??1???01010?
?01110??0?10??2?????020?000??100?00001000??????0?0001000210[01]000?10?001?
1??????????0?00101110001017???0??000?11100?110??0??100100?010?????????????
?????????????0????????????
Eoraptor
00?1?00[01]?001010??000111001110100100100001101000000?100110011010??0110
000100111???1?1?????????????????????????????00000010???0?001?00?10000000017????
??110000101001???01011??000??01?00??100?000??00000011??10????10???001??0??
0000?010?0??10?10??0010010?????020?000011?000100100000[01]010010001000210
1??0??0?0?0??10??1011?10??0?011100010110000171?00?1?0111010??10?0?00????????
001????0?000?????0?0??00100000000??00??
Eucnemesaurus_entaxonis
??
??
???????????0?0?01??0????0???000??0000?00?1011?0?10?00?01????0??????????????
??0??1??3?000100??1??0??0??11??010110?
1?1?011101001010110?10?0?????110111?1??0??0?????????0??????1101111??001?[
1 2]?00?11000???????
Eucnemesaurus_fortis
??
??
???????????0???01??001100[01]10000??00?0???????????10000?01100???????????11?
??110????0???????????

??0110111010?1010110????000001110110??0??????????????????????????????????????
??????????????
Glacialisaurus
??
??
??
??0???
???????????00?11?????????????????0???1010010[01]0????1100?0111111?1010?????
???????????
Gongxianosaurus
1?????0?????????????12??
??????????????????????????????????????0??0???1??2121?????????????0??????
?????????1??0??001??0??????0?0??00000??????????????0?0?1?0??000?011????2?1
10????1????????????????????????????????????0??100???0??????????????????????????[
12]111?2??????0???110???1??????1?0??1????0?1?1????????1?11??01?0??????1?0??2
?11?1200002000??
Guaibasaurus
??
??
???????????0???01??011001000000??00000??0000000?00000?01?0??0[01]00??1?1???
??110????1?0?0???????0????0110??0?11?00??0?0?0010?0[12]1002101100100?00000
100?1011000000100100001011010???[01]00?0?111111001000?011?0?01?000101110
0000000000001?0110000000000001??
Herrerasaurus
00000000?0010100?00000000000?000000000000001000000010000100101000001000
011010000010 1?00?1???0??0?00000?1000?00000000?1000000000000000000011010
000100000001000000?000010000011??0010[01]1000000200000010000001011001 0
01110100100?111?0??001100000000120000012000000010000010101101001000200
0000000100000010??01??0101001000010111000101100000010000110001000100010
0100001000010011000001000000010001000000000?011
Ingentia
??
??11?1???
?0??1011?0??0??1100
01011110?1?10?001113110110????????????0??
??
????????01
Isanosaurus
??
??0??0??????
????????2??10??0??????????????2?011000????????????????????????101??0???????
??211
112??0???001?1?0111?????????????????????????????1?????????????0?????????????
???????11
ISI_R277
??
??0010??????
??00???1???????????0??????????????000??0?01???01????????????????????????????
??2?1??201?????????????????????0?

0101100001011O??????0??
??????????
Jaklapallisaurus
??
??
???????????0???0??1????????????????????
??1????????????????????????????????????
???????????001???000011110110??0?0110110?0??00???????0?0???1????0???1??0??
??????????
Jingshanosaurus
1001?002???10211??111100?0?11101110110O?102001???1?100?1101111O?001000??
??0110001010l?2?1????????????1000??1?10110010??1110??1100101211001?????11?
1??010???????1?????10100??0011100?1???000000000000??10???011000000010000
000?001?0??12120101110??0??00??0011?3?100100?011000102000011003100000201
10011002?110?010110?[12]0[01]011010000101111O???10100011101l0?1?201101???
0?00???????0120?1112?1?01?20001120000010???
Leonerasaurus
?0??
??????????????????????????????????0?0?????????1?1101011001?1???00?1??010?[0
1]1?????????1100?00?0?10000110000000??00000100?111?001?????????????????010
00????1100000?????????????????????????????????????101013100?????????0?????11?
??1?1????0??100111020??
???????????0??????00
Lessemsaurus
??
??0?011???01
00?????101?0000011?00[12]10000000111000000?????????????????????????000?1??
??110001011??0???????0???3110?????00?0??1????001100310000?0111100001??1??
?10110?111011?10???01111?01???0000011101?1??1?01101002100l1?????????????11
2????1?2101???00??0???01
Leyesaurus
?001?00?10?00211?0??11?????1010?1101000010110l0?00?100111111111?00100010
[02]0011?????????00?11?00??1?0?0?110??1?00?10110??1010?1?1111010[01]0001??1
???1?1100200010011100101l????0????????????????????????????????????0000?001??
??000??1?
00??010?????
?????0?1020001????0???0?00
Lufengosaurus
110???02????0211?0?1?11?111111110101001010110l?000010111100111l?0010?1??
??0110??1010??00011??0???????100?001010010????0111???1100101010001l1?00?1
?1100200?110111???011010002001110011000000000000001001101?0011000000[0
1]100000000011?0111212[01]101110?001101111011130100101200100010200001100
311000020110110002011010101100101011010000102111O?11101000111011001000
1111???0?00001?11100[0 1]011110101010200011100O0[12][01]00??
Macrocollum
100110021001021111111111121111001001000010010000001100010011010000100O
001101???????????0???????????0?0?0?10???1001011010?1?0??1100101010000111?01
1111002000100111001011010000001110111010000000000000100110??001000000001
0000100?0100011111200001100001101112010100101000210100000100001l002100

010200?0?0?0010110?0101110100000110000101100011010000[01]11101100100011
011010100001011100001101000001011000000000001000??
Mamenchisaurus
11000113?1?11201??10120000000101112??001112010?1010111?11111012?1000001
112210100101112?2?1?11?1?0??1010?????2?11[01]00001001000??111111112111?3?
0001?11012100100001??10002?11101010100201102011020121000001100111211111
011001?0111111?000322100100120001100110110000?100011?0??10?1?31?11111031
011?00111110001100110010010021111 2??0???010?011???21010?0??0???????10101?
??11111?????1120?1????2?1??2?12?1211102??0??
Marasuchus
00???????0??0?????????????0?00???????0????????????0?????????????????????????
???00???0?0?0?100100?????????????????????????0?00?00000000??1?100000000001
00???00?0?0??00?000000?00???00??000?00000000?000000000??00101000000000?000
??012?1000?00000?????????????0?????????????????000000000000?0100010000000
000000001000000011000100000000??000000100010001000100000000?0?0000000000
0?000??0?00?0?00??0??00???1??
Massospondylus_carinatus
10011002101002 11?011111112111101001100001011010000110011111111100010001
0200100011010110001[01]1001110000111100011001111010001 0[01]111001010110
0111100?10110020001001110010110100020011100110000000000000010111010001[
01]000000000000000?01[01]00111212010111000011011110111201001012111000000
20000110031000[01]000110110001011000101110[01]0101101000010[12]1010?10[01
]000001110110010001111?010100?011111000011111 00?0102000111000021 0000
Massospondylus_kaalae
?0???002???00211???101????110?10011000010010????0?10?1?10??01???????????1?
?0?????????????????????????0???????0??0101?????0??0100101000000?????????????
??
??
??
????????????
Meroktenos
??
??
??
????????????????????????????????????0???0?31?00001011?000001???????????111
111100?000111110???01?0????????????
?????????
Mussaurus
??????????????????0?????????????????????????????????????1????????0??????????????
??001000????
????10110??0000?1??00100000000?00000010??1?1??0111?00001110?0????01110??1
011000111111 0?1?11?00101201011012011000020 0??0?0?3100010?011??1?001011?
??10110?10101101000010111 10?1?100000[12]1101110100011 01?1010?????011
011110000011 2001?1100001100[0 1][0 1]
Nambalia
??
??
??000????????????????????
??????????????????????????????0?010??0?10????????2?0??20??0??????????1?????111?010

011010100101107?0000???????1101?0????0110100?0??000101???0?00101?0?0010111
00??00????00??
Neosauropoda
1100011311[01]11201?0101200000101011[02]11101112010?101011[01]?111?10121
100[01]10112221110010111112[01][01]0[01][01][012]1000[01]1010000102011100001
201000[01]1[01]111111[02]12[01]1112[01]0000?1110011?110100??11002012101010
1[01]020111[12]011020121100002100011201111[01]1000[01]0100111?0003?21001[
01]00200111000101000000000011002017?1?3001111103102100011111000110111100[
01]10[01]00211012??0???010?1111112101?010000111?110101002111111011??112
11100??2?10?20121121110211011
Neotheropoda
00[01]1[01]002[01]00102010100110000 1[01]000000000000110000000010[01][01]1
00?[01]01000001[01]0001[012]0100000101100001?[01]?0100000011100010000000
01?000000000000000000011011001110000010000[01]11100001020000101011001 0
000001000000000[12]10000110010000001001000010000 10?1100000100100100012 0
00000010?00010001100[12]0101101030002111010100000111101000110100001?011
000100000001000[01]011111111002000101100?000001111100 00??0?0000000?01000
0000000001[01][01]
NMQR1551
??
??
??????11???00?001??00210000000010000000?02?1100120000?0[01]11000????01010
???2?????00011110???????????2?1???????1?????????00?1003100000[01]0110100001?
??????????1110111100111 0[01]1110?1110000011101100 1000?101?0?010000??????
11011112?000?????1?120000??????
NMQR3314
1001?10310?00211?0111101?1110101111???10101011001011 00?1101101 1?0000001
022011011101 0??20011?????????10011011101?00111?1000??110?100211001?10?01
0?11001?00110100??1011[01]10000001??0??100??0?0?10000000?0111100 1?0100?0?
1??00?????1?????[23]01100?0?11??0??????0010?2?100101[12]0??0001020000?10031
000[01]0[12]????????????1???10110?????????????1???110?111000011?011?01??0??
0????0???10011100120111120100 1?2?01?1[1 2]00001100??
Omeisaurus
1100011311011201??10120000010101 1?20100111201 0?1010111?110?101211000001
12221110010111???0????????????0???1???11100001?0?0001?11101111121111?3??00
1?11012000110101??11002?12101010110201 10?01102012110 0?021???1?201111001
00??01111010000322100100020?1??????0100000100011 00?01001?310111110310110
00111110001100110110010021101 2??0???010?010???210100?1?0??111??01101???0?
11???1????121?110??2?10?2012?1211102?10??
Ornithischia
0010000000[01]000?000000000?000?101100010010 0?10000000100[01]100?0010000
00[01]000100100000000100001 0?[01]?01?000000010010[01]01[01]0000001001[01]1
11001110100001100000000000100100[01]000?00??010000000?00?0?00?0000000000
00000[12]10000000000001000001000010?0111[02]1100000100?0000000000000000
000000000000000011101310001000 1??0000?00110000000010000 1?01011110200000
?000000[01]101110002 0?01?[01]10??0000001111000 00?000?00?00?0[0
1]00?0000000001[01][01]
Pampadromaeus
00?1?00?10110??1100011?????1000?100100001????010????0?1100?1??????1?????1?
??????????????????????????????????????00??000???0?000100010100000000??????????

??1????????111???
??0010001100??0????????????????????
????000010111000101110001000??
????????????????????
Panphagia
????????????????????????0?1????????????????????10??1??????????1?0?????????10?1?
0?1????0???????????00??????????0?0?0?1010000???10?0101000000??????????00101
010011100?01101?000?01???01?10?00?000000000??0??0?00??0000?01100?0?0??011
?1??0?1?0?1[01]0021010?00?0?00??
11???0?110????????????????????????00100101010O??0?0100????010?0????????????
???0?????????????????????
Pantydraco
?0???0????0?????1????[01]00?0???1??1????000100100000010?0100000 1?00???????
?00?000?1?10??00?101100??00??011?000?00?01010??000011?10010101000011001??
?1100110010100100101101?00???1????1?????????????????????????0??1?0000100000
100??????11?01?00??00110021100001??????
????011?0?10110?00??????????1?1?00000??0000010?01?0010?????????????????????
000011100000101?00000000001001??
Patagosaurus
11??
????????????????????????????????1?00001????????0??01110121111????????110010121
00000??110020?2001010?00201?02111120121?00?02100011[12]0?01?0?100????0?11
1??00??2100100?2??1?????????????????????????????1111103101000011111000110
1110110010?211112??0???00111111???10100[01]??0????????????0?????????????????
?????????????????????????11
Plateosauravus
??
??10???00100
101???01101?00[12]0011?00110000000011000000??10???011??00??110??0??????0??
??[23]0111001110000?????????????1?????????????????00110031100001????????????1
1???10110?100?11?10000101100001?100000111011O??0????0?????????????????????
110???0?????0?????????????
Plateosaurus_engelhardti
100110011011020110 1[01]1111121111001011000010010100101100011010110001100
010011011011101011100110200010000000101111001011010111 11?1100101010000
111001101100110010 0[01]0100101101000200111001100000000000000010100100001
[01]000000010000000001000111 11[12]000011000011011110101101001001000000
100001100311001020010100001111010101111100011110000101100011010000[01]1
110110010001101011010000101110000111000000101100111000010000 1
1101100100011010110100001011100001110000001011001110000100001
????????????????
Plateosaurus_gracilis
?00??001?0?102?1?010111?1??1110?101??00?10?101?0?0??0??100?0110???10??????
???????????1?????????????????????????0??0110?????1?1110010101O?00?1??????1100
??001???01??101101?00?001?100110000000000000010?10100001000000010000?00

????0????11200?01100?0?1011?101010010000???010?????0?00110031100102001010
000111101010 11??[01]0001111000010110?01??10000?1??0110??0???????01????????
??????0??????????????01?0??????????
Pradhania
??????????????????????????????1???????00??
?10????????????????????????????0???1?1????????????1?1010?????????????????20?????
????????10??
??????????????????????0?1?????20??0??
??
???????
Pulanesaura
??
??10?012011??????????001?111?
0100????11?????0??1??00[12][01]?0010?0120001000?????????2?111?011???0?0?????
??????????10??[12]??11
?0?1?11?????????????????????????0?000021001 01?????????????????????????????
????????????1?????????
PVL_3808
??????????????????0??
??1?0?11?1100110011
110100?011[01]1?00100111001100000000000000101010 1?00110000?0110000??????
???10321210011 10??0????????????????????????????????00110031100102 0?10100001?
???1???????1?010101010010111?0?10100000111011001 10??????01????????????????
?????????????1?????????00
Ruehleia
??
??01?11001?00???
?01?????101?0020011?00110010000011000010??1000001?0?00?0110??????0100011
101200011100 10?0100??010110101000????0??00???00110031100002 0??1100001011
01?10110?10100101000010210000??10?00?111011001 0?0?001???0100?????????????
??????????????????????????
Sarahsaurus
10?1?00?10???201?0??11?????1110111???0?010?0110010010??110100100001 0?0???
001000111?01?0001??????????1011??1?10?10010?????0?111001010100 01?1?00110
110?100011111100101 1?1100200111001?00?000000000010?110??00110000000?00
00000001010101[02]121000110000110111101 1?1010?10121110000020000?100310[0
1]0002001011?0010110?0101110??101101000010010?0?10100000?1?011001?001101
?0001?0001111101[0 1]01?11200?0102000??[01]000?1100??
Saturnalia
?0????????????????????????????1??1????00?100?0????????????????????0??10?????1??0
0???0?0??0101?1?00?0000?0??????????00000?????????000100000000?????????0010
1010010?00?01101?000001000011001000000000000000001000010???0??1100???0??1
11001111110001010002??????????????????????????????00100011[01]021010000000
0010110001001000000101110001011000010000000101010001000100100001000010
0010000000000000100110?00?000?00?01
Sefapanosaurus
??
??00??0?110
0?????0?10??00?001????1?00000001??0000????1??????11?00??011?????0?0?01010??
1?00????1110?1011??0101311010??10110??

????0?111110000??11[01]??????000000??????0?0001101?010111?0001??0?????11?0?
?0??2?0??????????????
Seitaad
??
??
???????????00?[01]?1??00??00?001????0000??????????????????????????0010?011??
110001111?0011?111001113010?00?21110??0???0??????????????0?1000001???????
???????????????????????????0?00?11101?0????01101?0?010?00??11?00??11????0?0
10???1?1[01]0000010???
Shunosaurus
11000113?1?10201??1012000000001011?201001112010?1010100?1101101200001001
1121010001111?1200?????0??11?1???1102001100001201000??1111111212111?2??0
00?11?10012?1?100??10012?110000101102 1?0??01??201210000?11??00?101?11011
0011?111?1??0002221001100?0011000?10110010?0001100200??1?31011111031011
00011111?00110?1101100100211112??0???000?011???21010?[01]1?0????1?10?101?
?????1?1011??1121?110??2?00?2?12?121?102110??
Silesaurus
00?0??00?00000?0000100000??0?00?0?01010??????????0010?0?0?1???0??????????0
0?0?0?1000??0001111000000??0?????1?00?0?010???0?0?10000100010000110?000?0
00000000???00001000000000001010000110000000000000??100000100000?0?0????
????111??11100000100000000??????????????????????????????00100000000200100000
00000?0100100?0?10000110110001001000000100011110000000?0000001000??011
?1??002???00000000?0?10????000?0010[01]
Spinophorosaurus
1????1??????????????????????????????????2???????????????0??????1?????????0??1
00111111201???21?0?1?01?????????1???????????????100111012?11?2??????11?1101
01?0?01???0002?110??01????[12]?11???1?12?1010?0?????????[12]???11011?001?1??
111?0?03?2[12]0?10??[12]????1?1???
?01[12]?0110??001??211111110?1101??0?0???20?1002??0??11??10??0????0?01?????
??????????????????????????????????
Staurikosaurus
00??
??????????????????????????????000000000100 0???00?0000000000?????????00010??
???00???01001?000011?000?00000000020000001??010?101100?001100100????1?1??
???0000002001100001 10?0010?00100
?00000100001??000?0101?0000??00000110000000011????01???????????????????????
???????????????????????
Tawa
0?1?000??00100?100101100?11110?0?00?????10101000?0?101??1??1010???0[01]001
01??10????0????0?0????????????????????00000000???1??0010000000000??1??????
110?100???????11??????0????0?????[12]?????????00????00??00???????????0?0?10?1
00?000?0??1?010????1?????????020??0???1???0?0??00001000?0?0??20010110?1????
???2?????????????0?0?0?0110?1?1?0????0??10??01???????????0?1??????0?101?11??0?
?01?????0?0??0?10?????0???????
Tazoudasaurus
11???0?10????????????[02]01
1???1???1????????????????????????00?00000???0????10?1111012101????000???0010
120????????0002??100001??002001010110201 21000?????????21?11?111?????11????
??01?22100100?[12]10????????010?[01]0100001001?0001?310?10???3101??0?11100

0?002?11?0?1??1??2110111100111101?01???00100201010??1101010101111??01
1????1?????20????????1???10?1??????
Thecodontosaurus
?0?????????????????????????????1??1??1000??????0??0?0?0????0?00????????????10?0
?0?1010?10001??000?10???0???????00?11010????????1100101010000??1???????000
1001010?1???01101?000001??00110000000000000000?10000?0101000?01000?0?00?
010?01120110001010??011000120100001100001001000001010010002100000 1???0?
0?00?011???01010?[01]000111100001011000 00?[01]000001010110 0?1?011010??010
0?????1100?0?111??0??1??0000??00?0??????
Unaysaurus
1001100210010??111?1111?1??1110?10?1000????????????0?0?00??????01???000??
0?10??1?10??10?110?0??100??0???????10?10110?????0??1100101010000????0?1???
???0??1?0????????????0??0?11?00?10100?0??00000??????????????0???010000?00?0
100011?1120000110000???????????1010????2101???0??0?????????????????????????
??110110????01101101 0?00????????0???110
0?????????00???0????????
Vulcanodon
??
??
??????????????????????[12]?????????????????????1??????01?11?0?00??0?0???1????2?[
12]10?10?0[12]001?????????????????????????????????????310[12]?00?011110000101
110110010?111011110010011?1?????[12]0?10021?0???110?10101010101111011??11
1?10102?10010201111110?121?0??
Xingxiulong
??????????????????0????????1???1?1111???0?10?0??0??01100?110?0110000?000101?0
1?00110101?0??1???????????1???????0?????????001????000?????????110011?11001
000110?01???011010002001110011000000000?0000110011 0???1110000001?????00?
000?0????120?01111??0????1??????1?101?????????????????00?1003110000[12]0?1011
?002?11?0??0?10010101111000010110 10?00000[01]10?11001?001101???0?0?0?0
11?001101110000001?2100?1100002100??
Yunnanosaurus
100?1002???00??1??0011001??101?111????00101110??00??0??110?1111?001000001
?01?0?01010????????????????????????????000?0010???0?????00010?21000??1???11?11
00[01]100110100???011010000001100011000000000010000000?0101?10110000?00?0?
??0??001?00??121200?111[01]??0??01??0011?201011002011000[01]020?001100310
00000011010?001?110?010111?[01]0101101000010110 10?1?10100011001100 11?011
01???0100001111001?0?1110?0?011???111?0000110???

(g) References for supplementary information

Apaldetti C, Martínez RN, Cerda IA, Pol D, Alcober O. 2018. An early trend towards gigantism in Triassic sauropodomorph dinosaurs. *Nat. Ecol. Evol.* (doi:10.1038/s41559-018-0599-y).

Apaldetti C, Pol D, Yates A. 2013 The postcranial anatomy of *Coloradisaurus brevis* (Dinosauria: Sauropodomorpha) from the Late Triassic of Argentina and its phylogenetic implications. *Palaeontology* **56**, 277–301.

Bronzati M, Benson RB, Rauhut OW. 2018 Rapid transformation in the braincase of sauropod dinosaurs: integrated evolution of the braincase and neck in early sauropods?. *Palaeontology* **61**, 289–302.

Bronzati M, Rauhut OWM. 2017. Braincase redescription of *Efraasia minor* (Huene, 1908) (Dinosauria, Sauropodomorpha) from the Late Triassic of Germany, with comments on the evolution of the sauropodomorph braincase. *Zool. J. Linn. Soc.* **182**, 173–224.

Cabreira SF et al. 2016 A unique Late Triassic dinosauromorph assemblage reveals dinosaur ancestral anatomy and diet. *Curr. Biol.* **26**, 3090–3095.

Cerda IA, et al. 2017 Novel insight into the origin of the growth dynamics of sauropod dinosaurs. *PLoS One* (doi:10.1371/journal.pone.0179707).

Chapelle KEJ, Choiniere JN. 2018 *Massospondylus carinatus* Owen (Dinosauria: Sauropodomorpha) based on computed tomographic scans and a review of cranial characters for basal Sauropodomorpha. *PeerJ* (doi:10.7717/peerj.4224).

Ezcurra MD. 2006 A review of the systematic position of the dinosauriform archosaur *Eucoelophysis baldwini* Sullivan & Lucas, 1999 from the Upper Triassic of New Mexico, USA. Geodiversitas**28**, 649–684.

Goloboff PA, Farris JS, Nixon KC. 2008 TNT, a free program for phylogenetic analysis. *Cladistics* **24**, 1–13.

Martínez et al. 2011 A basal dinosaur from the dawn of the dinosaur era in southwestern Pangaea. *Science* **331**, 206–210.

McPhee et al. 2015 A new basal sauropod from the pre-Toarcian Jurassic of South Africa: evidence of niche-partitioning at the sauropodomorph-sauropod boundary? *Scientific Reports* **5**, 13224.

McPhee BW, Choiniere JN. 2018 The osteology of *Pulanesaura eocollum*: implications for the inclusivity of Sauropoda (Dinosauria). *Zool. J. Linn. Soc.* **182**, 830–861.

McPhee BW, Choiniere JN, Yates AM, Viglietti PA. 2015 A second species of *Eucnemesaurus* Van Hoepen, 1920 (Dinosauria, Sauropodomorpha): new information on the diversity and evolution of the sauropodomorph fauna of South Africa's lower Elliot Formation (latest Triassic). . *J. Vert. Paleontol.* **35**, e980504.

Müller RT, Langer MC, Dias-da-Silva S. 2017 Biostratigraphic significance of a new early sauropodomorph specimen from the Upper Triassic of southern Brazil. *Hist. Biol.* **29**, 187–202.

Müller RT, et al. 2018 Early evolution of sauropodomorphs: anatomy and phylogenetic relationships of a remarkably well preserved dinosaur from the Upper Triassic of southern Brazil. *Zool. J. Linn. Soc.* (doi:10.1093/zoolinnean/zly009).

Nesbitt SJ. 2011 The early evolution of Archosauria: relationships and the origin of major clades. *B. Am. Mus. Nat. Hist*. **352**, 1–292.

Novas FE, Ezcurra MD, Chatterjee S, Kutty TS. 2011 New dinosaur species from the Upper Triassic Upper Maleri and Lower Dharmaram formations of Central India. *Earth Env. Sci. T. R. So.* **101**, 333–349.

Otero A, Pol D. 2013 Postcranial anatomy and phylogenetic relationships of *Mussaurus patagonicus* (Dinosauria, Sauropodomorpha). *J. Vert. Paleontol.* **33**, 1138–1168.

Otero A, et al. 2015. A new basal sauropodiform from South Africa and the phylogenetic relationships of basal sauropodomorphs. *Zool. J. Linn. Soc.* **174**, 589–634.

Peyre de Fabrègues C, Allain R. 2016 New material and revision of *Melanorosaurus thabanensis*, a basal sauropodomorph from the Upper Triassic of Lesotho. *PeerJ* (doi:10.7717/peerj.1639).

Pretto FA, Langer MC, Schultz CL. 2018 A new dinosaur (Saurischia: Sauropodomorpha) from the Late Triassic of Brazil provides insights on the evolution of sauropodomorph body plan. *Zool. J. Linn. Soc.* (doi:10.1093/zoolinnean/zly028).

Rauhut OWM. 2003 The interrelationships and evolution of basal theropod dinosaurs. *Spec. Pap. Palaeontol.* **69**, 1–213.

Rowe T. 1989 A new species of the theropod dinosaur *Syntarsus* from the Early Jurassic Kayenta Formation of Arizona. *J. Vert. Paleontol.* **9**, 125–136.

Smith ND, Pol D. 2007 Anatomy of a basal sauropodomorph dinosaur from the Early Jurassic Hanson Formation of Antarctica. *Acta Palaeontol. Pol.* **52**, 657–674.

Wilson JA. 2002 Sauropod dinosaur phylogeny: critique and cladistic analysis. *Zool. J. Linn. Soc.* **136**, 217–276.

Witmer LM. 1997 The Evolution of the Antorbital Cavity of Archosaurs: A Study in Soft-Tissue Reconstruction in the Fossil Record with an Analysis of the Function of Pneumaticity. . *J. Vert. Paleontol.* **17**, 1–76.

Yates AM. 2007 The first complete skull of the Triassic dinosaur *Melanorosaurus Haughton* (Sauropodomorpha: Anchisauria). *Spec. Pap. Palaeontol*. **77**, 9–55.

Yates AM, Bonnan MF, Neveling J. 2011 A new basal sauropodomorph dinosaur from the Early Jurassic of South Africa. *J. Vert. Paleontol.* **31**, 610–625.

Yates AM, Kitching JW. 2003 The earliest known sauropod dinosaur and the first steps towards sauropod locomotion. *Proc. R. Soc. Lond. Ser. B. Biol. sci.* **270**, 1753–1758.

8 DISCUSSÃO

No primeiro artigo a análise comparativa da morfologia de CAPPA/UFSM 0179 revelou traços compartilhados unicamente com membros de Theropoda, apesar deste ter sido presumido como pertencendo a um sauropodomorfo na análise filogenética realizada. Entretanto, observou-se que nenhum dos sauropodomorfos coevos apresenta o áxis bem preservado, impedindo a codificação para determinados caracteres, especialmente aquele referente à forma da margem dorsal do processo espinhoso. Deste modo, é sugerido que a condição presente em certos membros de terópodes pode corresponder ao estado plesiomórfico, o que não descartaria a hipótese de CAPPA/UFSM 0179 corresponder a um sauropodomorfo. De fato, CAPPA/UFSM 0035, que corresponde a um esqueleto bastante completo e atribuído a *Buriolestes schultzi*, compartilha a morfologia de CAPPA/UFSM 0179, reforçando a hipótese de que a margem dorsal sem uma expansão posterior no espécime corresponde ao estado plesiomórfico para sauropodomorfos e terópodes. Esse caso exemplifica como as afinidades das formas mais basais destes dois clados podem ser afetadas pela incompletude do registro fóssil. Outros dois fatores responsáveis por gerar interpretações equívocas abordados na tese incluem a variação ontogenética e a compressão sedimentar. O segundo artigo, o qual lida com o primeiro fator, demonstrou que um indivíduo juvenil de sauropodomorfo é capaz de apresentar maior disparidade na codificação de caracteres em relação a um indivíduo ontogeneticamente mais desenvolvido da mesma espécie do que a dois animais adultos de espécies distintas, porém filogeneticamente próximas. O mesmo método de cálculo de disparidade foi aplicado pelo presente candidato em um estudo (MÜLLER, 2017) paralelo à tese, afim de quantificar a variação resultante de ontogenia em outros dinossauromorfos. Além disso, ao realizar uma análise filogenética experimental no primeiro artigo, onde foram aplicadas alterações em estados de caracteres que são afetados por processos ontogenéticos, notou-se que são resgatadas topologias distintas daquelas obtidas através da matriz original. Seguindo a mesma linha, o artigo que trata da variação morfológica nos ílios de sauropodomorfos em resposta da compressão sedimentar, demonstrou que certos estados de caracteres de matrizes de sauropodomorfos são afetados pelo modo de preservação do elemento ósseo. Porém, reconhecendo espécimes modelo é possível iniciar o levantamento de quais feições poderiam ter sido geradas por processos tafonômicos. Ambos os fatores mencionados, somam-se a outras causas que podem produzir topologias conflitantes, como a escolha de táxons na construção das matrizes e a adoção de determinados parâmetros de busca. Esses dois últimos tópicos são discutidos pelo presente candidato em outros dois estudos realizados em paralelo à tese (MÜLLER e DIAS-DA-SILVA, 2017; MÜLLER et al., 2018).

No quarto artigo, foi apresentada a anatomia de CAPPA/UFSM 0035 em detalhes. O espécime foi atribuído a *Buriolestes schultzi*. Em virtude do excelente grau de preservação deste espécime, foi possível levantar novos dados para o esqueleto de *B. schultzi*, especialmente para o crânio e esqueleto axial. Na verdade, o crânio de CAPPA/UFSM 0035 é um dos mais bem preservados dentre os dinossauros de sua idade, de modo que o espécime gerou um importante aporte anatômico também para Dinosauria. Certamente esse material tem potencial para servir como base para estudos futuros que venham a abordar a anatomia de dinossauros de idade Carniana. Além da anatomia, o estudo também explorou diferentes abordagens filogenéticas com o objetivo de testar o quanto elas podem afetar as topologias. Foi observado que adotando técnicas de pesagem de caracteres é possível recuperar diferentes topologias. Dentre elas, nota-se a variação de certos táxons (e.g. *Eodromaeus murphi*, *Guaibasaurus candelariensis*) que em certas árvores são recuperados como terópodes ou então como saurísquios basais a dicotomia Theropoda/Sauropodomorpha. Também se demonstraram sensíveis à pesagem formas mais basais de sauropodomorfos, incluindo *B. schultzi*, que formam um clado exclusivo de formas Sul Americanas, irmão de todos outros sauropodomorfos. Ainda no contexto filogenético, todas as análises realizadas suportaram o posicionamento de *B. schultzi* como um sauropodomorfo, corroborando a descrição original do táxon apresentada por Cabreira et al. (2016). No estudo também foram realizadas análises de disparidade morfológica com o objetivo de avaliar a ocupação de morfoespaço das diferentes regiões do esqueleto de *B. schultzi*. Observou-se que nenhuma região do esqueleto aponta possível convergência com terópodes. Esse resultado sugere que as características compartilhadas por *B. schultzi* e membros de Theropoda correspondam, na verdade, a plesiomorfias ao invés de terem origem através de convergência, como o caso dos dentes zifodontes, que devem ter estado presentes no ancestral de saurísquios e foi mantido nas formas mais basais de sauropodomorfos.

O quinto artigo trata da descrição de um novo gênero e espécie de sauropodomorfo baseado nos esqueletos que compõem CAPPA/UFSM 0001 (Figura 4). Para este estudo também foi construída uma nova matriz de dados de sauropodomorfos basais. Muitos estudos investigando as afinidades filogenéticas de sauropodomorfos basais foram publicados ao longo da última década, no entanto, muitas das informações apresentadas não foram agregados em um único conjunto nessas publicações. Deste modo, a proposta da nova matriz foi de agregar o máximo de informação referente aos sauropodomorfos do Triássico e do Jurássico Inferior. Assim, utilizou-se como base a matriz de McPhee e Choiniere (2017), que foi construída a partir da matriz de Yates (2007). Nela foram incluídas cerca de 15 novas unidades taxonômicas operacionais (UTOs) e quase 40 caracteres a partir de estudos prévios.

Detalhes das UTOs e da fonte dos caracteres são apresentados no material suplementar do artigo. A análise filogenética adotando a nova matriz revelou um cenário distinto do atual para muitos táxons. Primeiramente, observou-se uma elevada diversidade de formas basais a Plateosauria, incluindo um novo clado, nomeado no artigo. Esse clado foi recuperado como grupo-irmão de Plateosauria e é composto pelo novo gênero, *Unaysaurus* e *Jaklapallisaurus*. Esse arranjo diminui a diversidade de Plateosauridae (tornando o grupo restrito ao gênero *Plateosaurus*), uma vez que remove *Unaysaurus* do grupo. Massospondylidae também sofreu diminuição de diversidade, com membros recuperados fora do grupo, em clados de menor diversidade, como por exemplo, *Coloradisaurus* e *Glacialisaurus*. O resultado da análise concorda com estudos prévios (e.g. CABREIRA et al., 2016; MÜLLER et al., 2018) em relação a posição de *Buriolestes* como o membro mais basal de Sauropodomorpha.

Figura 4 – Representação do novo sauropodomorfo em vida. Fonte: Márcio L. Castro.

O arranjo filogenético recuperado no estudo, associado às datações (e.g. LANGER et al., 2018) dos depósitos Triássicos com restos de sauropodomorfos no Triássico do Rio Grande do Sul permitiu estabelecer padrões de tempo e modo em que certas estruturas surgiram ou mudaram no grupo. Essa abordagem permitiu traçar as mudanças ocorridas ao longo de um intervalo de cerca de oito milhões de anos, que abrange as formas mais antigas do grupo até o momento em que os sauropodomorfos passam a exercer um papel ecológico mais marcante nos ecossistemas terrestres. Assim, no artigo estão detalhadas mudanças que

ocorreram em relação a dieta e plano corpóreo, especialmente referente as mudanças do pescoço e proporções de certas estruturas. Constatou-se que o novo gênero corresponde ao mais antigo sauropodomorfo com pescoço longo. Também se observou que a associação de esqueletos agrupados e articulados parece corresponder a mais antiga evidencia de hábitos gregários em Sauropodomorpha.

9 CONCLUSÕES

Os resultados obtidos geraram um substancial aporte de informações relacionadas à origem e evolução inicial dos sauropodomorfos. Foi observado que a variação ontogenética desempenha um papel bastante forte sobre a forma dos sauropodomorfos mais basais, sendo capaz de afetar a codificação de caracteres morfológicos utilizados em análises filogenéticas. Da mesma forma, constatou-se que a compressão sedimentar também é capaz de produzir artefatos tafonômicos que podem ter papel na codificação de caracteres. Além disso, a presença de plesiomorfias em formas basais do grupo (como *Buriolestes*) também pode afetar interpretações. Assim, nota-se que a soma desses fatores exerce impacto sobre as topologias obtidas em estudos filogenéticos.

O excelente grau de preservação de CAPPA/UFSM 0035 possibilitou uma melhor compreensão a respeito da anatomia dos primeiros sauropodomorfos. Além disso, o espécime reforça a hipótese de que os sauropodomorfos tiveram origem a partir de um ancestral carnívoro e passaram a acumular traços dentários relacionados a uma dieta mais voltada a herbivoria apenas em um segundo momento da história evolutiva do grupo. A transição morfológica do clado pôde também ser acompanhada a partir das descobertas realizadas em estratos do Rio Grande do Sul, incluindo os esqueletos referentes à CAPPA/UFSM 0001. De fato, esses espécimes permitiram traçar alterações que ocorreram no plano corpóreo dos sauropodomorfos durante um intervalo de oito milhões de anos, revelando um cenário plausível de como o clado passou de formas pequenas e raras a animais gigantes e abundantes. Além de corresponder a um novo táxon, CAPPA/UFSM 0001 também trouxe novos dados referentes à biologia dos sauropodomorfos, sugerindo a mais antiga evidencia de gregarismo para o clado.

Por fim, uma análise filogenética adotando uma nova matriz de dados revelou uma rica diversidade de formas basais a Plateosauria que são ainda pouco investigadas. Essa nova hipótese ajuda a entender como foram os primeiros momentos de diversificação do grupo e como foi a dispersão dos sauropodomorfos durante sua fase inicial de irradiação. Os resultados sugerem que antes de alcançar o hemisfério norte, os sauropodomorfos espalharam-se e tornaram-se abundantes pelo Gonduana, iniciando sua história evolutiva no Oeste e depois chegando ao Leste, onde o grupo é representado em estratos da Índia.

REFERÊNCIAS

AGNOLÍN, F. L.; ROZADILLA, S. Phylogenetic reassessment of *Pisanosaurus mertii* Casamiquela, 1967, a basal dinosauriform from the Late Triassic of Argentina. **Journal of Systematic Palaeontology**, v. 16, p. 853-879, 2017.

APALDETTI, C.; MARTÍNEZ, R. N.; CERDA, I. A.; POL, D.; ALCOBER, O. An early trend towards gigantism in Triassic sauropodomorph dinosaurs. **Nature ecology & evolution**, v. 2 (1227), p. 1-9, 2018.

APALDETTI, C.; MARTINEZ, R. N.; POL, D.; SOUTER, T. Redescription of the skull of *Coloradisaurus brevis* (Dinosauria, Sauropodomorpha) from the Late Triassic Los Colorados Formation of the Ischigualasto-Villa Union Basin, northwestern Argentina. **Journal of Vertebrate Paleontology**, v. 34, p. 1113-1132, 2014.

ARCUCCI, A. Nuevos materiales y reinterpretacion de *Lagerpeton chanarensis* Romer (Thecodontia, Lagerpetonidae nov.) del Triasico Medio de La Rioja, Argentina. **Ameghiniana**, v. 23, p. 233-242, 1986.

BARRETT, P. M.; NESBITT, S. J.; PEECOOK, B. R. A large-bodied silesaurid from the Lifua Member of the Manda beds (Middle Triassic) of Tanzania and its implications for body-size evolution in Dinosauromorpha. **Gondwana Research**, v. 27, p. 925-931, 2015.

BENTON, M. J. Classification and phylogeny of diapsid reptiles. **Zoological Journal of the Linnean Society**, v. 84, p. 97-164, 1985.

BENTON, M. J. Dinosaur success in the Triassic: a noncompetitive ecological model. The **Quarterly Review of Biology,** v. 58, p. 29-55, 1983.

BITTENCOURT, J. S.; DA-ROSA, A. A. S.; SCHULTZ, C. Z.; LANGER, M. C. Dinosaur remains from the ‘Botucaraí Hill’ (Caturrita Formation), Late Triassic of south Brazil, and their stratigraphic context. **Historical Biology**, v. 25, p. 81-93, 2013.

BITTENCOURT, J. S.; LEAL, L. A.; LANGER, M. C.; AZEVEDO, S. A. K. An additional basal sauropodomorph specimen from the Upper Triassic Caturrita Formation, southern Brazil, with comments on the biogeography of plateosaurids. **Alcheringa**, v. 36, p. 269-278, 2012.

BRONZATI, M.; RAUHUT, O. W.; BITTENCOURT, J. S.; LANGER, M. C. Endocast of the Late Triassic (Carnian) dinosaur *Saturnalia tupiniquim*: implications for the evolution of brain tissue in Sauropodomorpha. **Scientific reports**, v. 7 (11931), p. 1-7, 2017.

BRUSATTE, S. L.; BENTON, M. J.; RUTA, M.; LLOYD, G. T. Superiority, competition, and opportunism in the evolutionary radiation of dinosaurs. **Science**, v. 321, p. 1485-1488, 2008.

BRUSATTE, S. L.; NIEDZWIEDZKI, G.; BUTLER, R. J. Footprints pull origin and diversification of dinosaur stem lineage deep into Early Triassic. **Proceedings of the Royal Society of London, Biological Sciences**, v. 278, p. 1107-1113, 2011.

CABREIRA, S. F.; KELLNER A. W.; DIAS-DA-SILVA, S.; ROBERTO-DA-SILVA, L.; BRONZATI, M.; MARSOLA, J. A. C.; MÜLLER, R. T.; BITTENCOURT, J. S.; BATISTA, B. J.; RAUGUST, T.; CARRILHO, R.; BRODT, A.; LANGER, M. C. A Unique Late Triassic

Dinosauromorph Assemblage Reveals Dinosaur Ancestral Anatomy and Diet. **Current Biology**, v. 26, p. 3090-3095, 2016.

CABREIRA, S. F.; SCHULTZ, C. L.; BITTENCOURT, J. S.; SOARES, M. B.; FORTIER, D. C.; SILVA, L. R.; LANGER, M. C. New stem-sauropodomorph (Dinosauria, Saurischia) from the Triassic of Brazil. **Naturwissenschaften**, v. 98, p. 1035-1040, 2011.

CASAMIQUELA, R. M. Un nuevo dinosaurio ornitischio Triásico (*Pisanosaurus mertii*; Ornithopoda) de la Formación Ischigualasto, Argentina. **Ameghiniana**, v. 4, p. 47-64, 1967.

DZIK, J. A beaked herbivorous archosaur with dinosaur affinities from the early Late Triassic of Poland. **Journal of Vertebrate Paleontology**, v. 23, p. 556-574, 2003.
EZCURRA, M. D. A new early coelophysoid neotheropod from the Late Triassic of Northwestern Argentina. **Ameghiniana**, v. 54, p. 506-538, 2017.

EZCURRA, M. D. Comments on the taxonomic diversity and paleobiogeography of the earliest known dinosaur assemblages (late Carnian – earliest Norian). **Revista de Historia Natural, Nueva Serie**, v. 2, p. 49-71, 2012.

FERIGOLO, J.; LANGER, M. C. A Late Triassic dinosauriform from south Brazil and the origin of the ornithischian predentary bone. **Historical Biology**, v. 19, p. 23-33, 2007.

GALTON, P. M.; UPCHURCH, P. Prosauropoda. In: WEISHAMPEL, D.B., DODSON, P., OSMÓLSKA, H. (Eds.). **The Dinosauria. 2nd ed**. University of California Press, Berkeley, p. 232-258, 2004.

HORN, B. L. D.; MELO, T. M.; SCHULTZ, C. L.; PHILIPP, R. P.; KLOSS, H. P.; GOLDBERG, K. A new third-order sequence stratigraphic framework applied to the Triassic of the Paraná Basin, Rio Grande do Sul, Brazil, based on structural, stratigraphic and paleontological data. **Journal of South American Earth Sciences**, v. 55, p. 123-132, 2014.

IRMIS, R. B.; NESBITT, S. J.; PADIAN, K.; SMITH, N. D.; TURNER, A. H.; WOODY, D.; DOWNS, A. A Late Triassic dinosauromorph assemblage from New Mexico and the rise of dinosaurs. **Science**, v. 317, p. 358-361, 2007.

LANGER, M. C.; ABDALA, F; RICHTER, M.; BENTON, M. J. A sauropodomorph dinosaur from the Upper Triassic (Carnian) of Southern Brazil. **Acad Sci Paris Sci Terre et Planetnét**, v. 329, p. 511-517, 1999.

LANGER, M. C.; EZCURRA, M. D.; BITTENCOURT, J. S.; NOVAS, F. E. The origin and early evolution of dinosaurs. **Biological Reviews**, v. 85, p. 55-110, 2010.

LANGER, M. C.; FERIGOLO, J. The Late Triassic dinosauromorph *Sacisaurus agudoensis* (Caturrita Formation; Rio Grande do Sul, Brazil): anatomy and affinities. **Geological Society London Special Publications**, v. 379, p. 353-392, 2013.

LANGER, M. C.; RAMEZANI, J.; DA ROSA, Á. A. U-Pb age constraints on dinosaur rise from south Brazil. **Gondwana Research**, v. 57, p. 133-140, 2018.

LANGER, M. C.; RIBEIRO, A.M.; SCHULTZ, C.L.; FERIGOLO, J. The continental tetrapod-bearing Triassic of South Brazil. **Bulletin of the American Museum of Natural History**, v. 41, p. 201-218, 2007.

LEAL, L. A.; AZEVEDO, S. A. K.; KELLNER, A. W.; DA-ROSA, Á. A. S. A new early dinosaur (Sauropodomorpha) from the Caturrita Formation (Late Triassic), Paraná Basin, Brazil. **Zootaxa**, v. 690, p. 1-24, 2004.

MARTÍNEZ, R. N.; APALDETTI, C. A Late Norian—Rhaetian Coelophysid Neotheropod (Dinosauria, Saurischia) from the Quebrada Del Barro Formation, Northwestern Argentina. **Ameghiniana**, v. 54, p. 488-505, 2017.

MARTÍNEZ, R. N.; APALDETTI, C.; ALCOBER, O. A.; COLOMBI, C. E.; SERENO, P. C.; FERNANDEZ, E.; SANTI MALNIS, P.; CORREA, G. A; ABELIN, D. Vertebrate succession in the Ischigualasto Formation. **Journal of Vertebrate Paleontology**, v. 31, p. 10-30, 2013.

MARTÍNEZ, R. N.; APALDETTI, C.; CORREA, G. A.; ABELÍN, D. A Norian lagerpetid dinosauromorph from the Quebrada del Barro Formation, northwestern Argentina. **Ameghiniana**, v. 53, p. 1-13, 2016.

MARTINEZ, R. N.; SERENO, P. C.; ALCOBER, O. A.; COLOMBI, C. E.; RENNE, P. R.; MONTAÑEZ, I. P; CURRIE, B. S. A basal dinosaur from the dawn of the dinosaur era in thwestern Pangaea. **Science**, v. 331, p. 206-210, 2011.

MCPHEE, B. W.; BENSON, R. B.; BOTHA-BRINK, J.; BORDY, E. M.; CHOINIERE, J. N. A giant dinosaur from the earliest Jurassic of South Africa and the transition to quadrupedality in early sauropodomorphs. **Current Biology**, v. 28, p. 3143-3151, 2018.

MCPHEE, B. W.; CHOINIERE, J. N. The osteology of *Pulanesaura eocollum*: implications for the inclusivity of Sauropoda (Dinosauria). **Zoological Journal of the Linnean Society**, v. 182, p. 830-861, 2017.

MÜLLER, R. T. Are the dinosauromorph femora from the Upper Triassic of Hayden Quarry (New Mexico) three stages in a growth series of a single taxon? **Anais da Academia Brasileira de Ciências**, v. 89, p. 835-839, 2017.

MÜLLER, R. T.; DA-ROSA, A. A.; SILVA, L. R.; AIRES, A. S. S.; PACHECO, C. P.; PAVANATTO, A. E. B.; DIAS-DA-SILVA, S. Wachholz, a new exquisite dinosaur bearing fossiliferous site from the Upper Triassic of southern Brazil. **Journal of South American Earth Sciences**, v. 62, p. 120-128, 2015.

MÜLLER, R. T.; DIAS-DA-SILVA, S. Taxon sample and character coding deeply impact unstable branches in phylogenetic trees of dinosaurs. **Historical Biology**, Online First, p. 1-4, 2017

MÜLLER, R. T.; LANGER, M. C.; BRONZATI, M.; PACHECO, C. P.; CABREIRA, S. F.; DIAS-DA-SILVA, S. Early evolution of sauropodomorphs: anatomy and phylogenetic relationships of a remarkably well-preserved dinosaur from the Upper Triassic of southern Brazil. **Zoological Journal of the Linnean Society**, Online First, p. 1-62, 2018.

MÜLLER, R. T.; LANGER, M. C.; DIAS-DA-SILVA, S. Biostratigraphic significance of a new early sauropodomorph specimen from the Upper Triassic of southern Brazil. **Historical Biology**, v. 29, p. 187-202, 2017.

MÜLLER, R. T.; Langer, M. C.; Dias-Da-Silva, S. Ingroup relationships of Lagerpetidae (Avemetatarsalia: Dinosauromorpha): a further phylogenetic investigation on the understanding of dinosaur relatives. **Zootaxa**, v. 4392, p. 149-158, 2018.

MÜLLER, R. T.; LANGER, M. C.; PACHECO, C. P.; DIAS-DA-SILVA, S. The role of ontogeny on character polarization in early dinosaurs: a new specimen from the Late Triassic of southern Brazil and its implications. **Historical Biology**, Online First, p. 1-12, 2018.

MÜLLER, R. T.; PRETTO, F. A.; KERBER, L.; SILVA-NEVES, E.; DIAS-DA-SILVA, S. Comment on 'A dinosaur missing-link? Chilesaurus and the early evolution of ornithischian dinosaurs'. **Biology letters**, v. 14(20170581), 2018.

NESBITT, S. J.; BUTLER, R. J.; EZCURRA, M. D.; BARRETT, P. M.; STOCKER, M. R.; ANGIELCZYK, K. D.; SMITH, R. M. H.; SIDOR, C. A.; NIEDZWIEDZKI, G.; SENNIKOV, A G.; CHARING, A. J. The earliest bird-line archosaurs and the assembly of the dinosaur body plan. **Nature**, v. 544, p. 484-487, 2017.

NESBITT, S. J.; IRMIS, R. B.; PARKER, W. G.; SMITH, N. D.; TURNER, A. H.; ROWE, T. Hindlimb osteology and distribution of basal dinosauromorphs from the Late Triassic of North America. **Journal of Vertebrate Paleontology**, v. 29, p. 498-516, 2009.

NESBITT, S. J.; SIDOR, C. A.; IRMIS, R. B.; ANGIELCZYK, K. D.; SMITH, R. M. H.; TSUJI, L. A. Ecologically distinct dinosaurian sister-group shows early diversification of Ornithodira. **Nature**, v. 464, p. 95-98, 2010.

NORMAN, D. B.; BARON, M. G.; BARRETT, P. M. A new hypothesis of dinosaur relationships and early dinosaur evolution. **Nature**, v. 543, p. 501-506, 2017.

NOVAS, F. E. La evolucioón de los dinosaurios carnívoros. In: SANZ, J. L.; BUSCALIONI, A. (Eds.). **Los dinosaurios y su entorno biotico**. Actas II Curso de Paleontologíca en Cuenca, Espanha, p. 125-163, 1992.

OWEN, R. Report on British fossil reptiles, Part II. **Reports of the British Association for the Advancement of Science**, p. 60-204, 1842.

PARRISH J. M. The origin of high browsing: the paleoecological significance of the sauropodomorph bauplan. **Journal of Vertebrate Paleontology**, v. 18, p. 69, 1998.

PINHEIRO, F. L. A fragmentary dinosaur femur and the presence of Neotheropoda in the upper Triassic of Brazil. **Revista Brasileira de Paleontologia**, v. 19, p. 211-216, 2017.

PRETTO, F. A.; LANGER, M. C.; SCHULTZ, C. L. A new dinosaur (Saurischia: Sauropodomorpha) from the Late Triassic of Brazil provides insights on the evolution of sauropodomorph body plan. **Zoological Journal of the Linnean Society**, Online First, p. 1-29, 2018.

ROBERTO-DA-SILVA, L.; DESOJO, J. B.; CABREIRA, S. F.; AIRES, A. S. S., MUELLER, R. T.; PACHECO, C. P.; DIAS-DA-SILVA, S. A new aetosaur from the Upper Triassic of the Santa Maria Formation, southern Brazil. **Zootaxa**, v. 3764, p. 240-278, 2014.

ROMER, A. S. The Chañares (Argentina) Triassic reptile fauna. X. Two new but incompletely known long-limbed pseudosuchians. **Breviora**, p. 378, v. 1-10, 1971.

ROWE, T.B.; SUES, H-D.; REISZ, R.R. Dispersal and diversity in the earliest North American sauropodomorph dinosaurs, with a description of a new taxon. **Proceedings of the Royal Society B: Biological Sciences**, v. 278, p. 1044-1053, 2010.

SALGADO, L.; CORIA, R. A.; CALVO, J. O. Evolution of titanosaurid sauropods. I. Phylogenetic analysis based on the postcranial evidence. **Ameghiniana**, v. 34, p. 3-32, 1997.

SARIGÜL, V. New basal dinosauromorph records from the Dockum Group of Texas, USA. **Palaeontologia Electronica**, v. 19, p. 1-13, 2016.

SEELEY, H. G. On the classification of the fossil animals commonly named Dinosauria. **Proceedings of the Royal Society of London**, v. 43, p. 165-171, 1887.
SERENO, P. C.; FORSTER, C. A.; ROGERS, R. R.; MONETTA, A. M. Primitive dinosaur skeleton from Argentina and the early evolution of the Dinosauria. **Nature**, v. 361, p. 64-66, 1993.

SERTICH, J. J.; LOEWEN, M. A. A new basal sauropodomorph dinosaur from the Lower Jurassic Navajo Sandstone of southern Utah. **PLoS One**, v. 5(3e9789), p. 1-17; 2010.

TAYLOR, M. P.; UPCHURCH, P.; YATES, A. M.; WEDEL, M. J.; NAISH, D. Sauropoda. In: DE QUEIROZ, K.; CANTINO, P. D.; GAUTHIER, J. A. (Eds.). **Phylonyms: a Companion to the PhyloCode**. University of California Press. Berkley, 2010.

UPCHURCH, P.; BARRETT, P. M.; GALTON, P. M. A phylogenetic analysis of basal Sauropodomorph relationships: implications for the origin of sauropod dinosaurs. **Special Papers in Palaeontology**, v. 77, p. 57-90, 2007.

YATES, A. M. The first complete skull of the Triassic dinosaur *Melanorosaurus* Haughton (Sauropodomorpha: Anchisauria). **Special Papers in Palaeontology**, v. 77, p. 9-5, 2007.

ZERFASS, H.; LAVINA, E. L.; SCHULTZ, C. L.; GARCIA, A. J. V.; FACCINI, U. F.; CHEMALE JR, F. Sequence stratigraphy of continental Triassic strata of Southernmost Brazil: a contribution to Southwestern Gondwana palaeogeography and palaeoclimate. **Sedimentary Geology**, v. 161, p. 85-105, 2003.